

Stony Brook University



OFFICIAL COPY

The official electronic file of this thesis or dissertation is maintained by the University Libraries on behalf of The Graduate School at Stony Brook University.

© All Rights Reserved by Author.

**Development of a Novel Bioassay Chamber to Optimize Autologous Endothelial Cell
Viability and Density on Topological and Topographical Substrates**

A Dissertation Presented

by

David Alan Rubenstein

to

The Graduate School

in Partial Fulfillment of the

Requirements

for the Degree of

Doctor of Philosophy

in

Biomedical Engineering

Stony Brook University

August 2007

Stony Brook University

The Graduate School

David Alan Rubenstein

We, the dissertation committee for the above candidate for the
Doctor of Philosophy degree, hereby recommend
acceptance of this dissertation.

Mary D. Frame Ph.D. – Dissertation Advisor

Associate Professor of Biomedical Engineering,

Helmut H. Strey Ph.D. – Chairperson of Defense

Assistant Professor of Biomedical Engineering

Michael Hadjiargyrou Ph.D.

Associate Professor of Biomedical Engineering

Pelagia-Irene Gouma Ph.D.

Associate Professor of Material Science and Engineering, Stony Brook University

This dissertation is accepted by the Graduate School

Lawrence Martin

Dean of the Graduate School

Abstract of the Dissertation

Development of a Novel Bioassay Chamber to Optimize Autologous Endothelial Cell

Viability and Density on Topological and Topographical Substrates

by

David Alan Rubenstein

Doctor of Philosophy

in

Biomedical Engineering

Stony Brook University

2007

Tissue engineering is an interdisciplinary field which focuses on scaffold design to aid in tissue replacement. One major difficulty involves the lack of vasculature within these scaffolds. This leads to replacement failure. Our lab uses the microvascular tissue engineering approach to fabricate a scaffold that directs endothelial cell (EC) migration to eventually form planar capillary networks. In vivo, a combination of topological, mechanical and chemical cues plays a role in EC migration. Here, scaffold composition, surface chemistry and shear stress were used to direct endothelial cell growth.

Cell culture experiments were designed to optimize fabrication of an electrospun cellulose acetate scaffold for ECs. Results indicated that ECs prefer to grow along fibers with a diameter in the range of 1-5 μ m. The addition of chitosan to electrospun fibers enhanced viability. Fibronectin addition increased EC density. Carbon nano-tubes and vascular endothelial growth factor were unsuitable additives.

A novel bioassay chamber was designed to optimize EC culture from an autologous tissue donor source. Murine aortas were dissected using an institutionally endorsed tissue sharing protocol. They were cannulated and perfused at low flow rates in my bioassay chamber. ECs preferred large diameter fibers enhanced with chitosan. Cell density was unrelated to perfusate flow rate in the bioassay chamber, but viability was enhanced with higher flow. Long term culture increased cell viability but did not affect density.

The directed growth of ECs was investigated on hydrophilic and hydrophobic glass substrates microstamped with extracellular matrix (ECM) proteins. ECM proteins playing key roles in cell migration and adhesion were investigated. Cell density on these proteins was significantly higher vs. the paired hydrophilic or hydrophobic substrates. Cell viability was significantly higher on stamped proteins vs. on hydrophobic glass.

In the bioassay chamber with low pulsatile flow ECs displayed a significantly higher density on microstamped ECM proteins vs. on both hydrophilic and hydrophobic glass. They grew with a significantly higher viability on ECM vs. hydrophobic glass substrates. This novel bioassay chamber can thus be used to test multiple factors promoting angiogenesis in a controlled system.

For Wei, My Parents and Everyone Else Who Has Helped Me to Get Here

TABLE OF CONTENTS

List of Abbreviations and Symbols	x
List of Figures	xii
List of Tables	xv
Acknowledgements	xvi
SECTION I: INTRODUCTION	1
SECTION II: BACKGROUND	3
2.1 Arteriolar Vascular Physiology	3
2.1.1 Endothelial Cells	3
2.1.2 Vascular Smooth Muscle Cells, Pericytes and Other Cell Types ...	4
2.2 Microcirculation	5
2.2.1 Microvascular Network Structure	5
2.2.2 Microvascular Network Function	8
2.2.3 Rheology within the Microcirculation	8
2.3 Biology of Angiogenesis	9
2.3.1 Angiogenesis Progression Overview	9
2.3.2 Extracellular Matrix Proteins and Endothelial Cell Adhesion	10
2.3.3 Angiogenic Growth Factors Cues	11
2.3.4 Endothelial Cell Migration	13
2.3.5 Endothelial Cells and Lumen Formation	13
2.3.6 Wall Shear Stress as a Mechanical Stimulus	14
2.4 Classical Means to Study Angiogenesis Progression	14
2.4.1 Animal Studies	14
2.4.1.a Dorsal Window Model	14
2.4.1.b Bat Wing Model	15
2.4.2 <i>In vitro</i> Studies	15
2.4.2.a Wound Healing Studies	15
2.4.2.b Flow Chamber Studies	16
2.5 Vascular Tissue Engineering	16
2.5.1 <i>In vivo</i> ECM and Electrospun Scaffolds – Topography	16
2.5.2 Directed Growth of Endothelial Cells – Topology	19
2.5.3 Tissue Engineering of Blood Vessels	20
2.5.4 Vascular Patches	20
2.6 Fabrication Techniques	20
2.6.1 Electrospinning	20
2.6.2 Photolithography and Soft-lithography	21
2.6.3 Microcontact Printing	25
SECTION III: METHODS AND MATERIALS	27
3.1 Fabrication Techniques	27
3.1.1 Scaffold Preparation	27
3.1.1.a Electrospun Scaffolds	27
3.1.1.b Sylgard® 184 Scaffolds	29

3.1.1.c Matrigel® Scaffolds	31
3.1.2 Lithography Techniques	31
3.1.2.a Photolithography	31
3.1.2.b Soft-lithography	32
3.1.3 Surface Modifications	34
3.1.3.a Microstamp	34
3.1.3.b Hydrophilic/Hydrophobic Glass Washing	36
3.1.3.c Contact Angle Measurements	36
3.1.4 Design Criteria and Fabrication of Bioassay Chamber	36
3.2 Endothelial Cell Culture	39
3.2.1 Culture of Human Umbilical Vein Endothelial Cells	39
3.2.2 Culture of Human Dermal Microvascular Endothelial Cells	39
3.2.3 Passage of Endothelial Cells	39
3.3 Bioassay Chamber	40
3.3.1 Dissection of Explanted Vessels	40
3.3.2 Cannulation and Perfusion	41
3.3.3 Characterization of Flow within the Bioassay Chamber	43
3.4 Data Collection – Endothelial Culture and Bioassay Chamber	43
3.4.1 Immunohistochemistry	43
3.4.1.a Live/Dead Viability Assay	43
3.4.1.b BS-1 Lectin	43
3.4.1.c DAPI	44
3.4.1.d Fibronectin Coating	44
3.4.2 Imaging	44
3.4.2.a Imaging of Cultured Endothelial Cells	44
3.4.2.b Imaging in the Bioassay Chamber	45
3.5 Data Processing and Statistical Analysis	45
3.5.1 Cell Viability	45
3.5.2 Cell Density	45
3.5.3 Percent Confluence	46
3.5.4 MATLAB® Programming	48
3.5.4.a Cell Morphology	48
3.5.4.b Video Image Acquisition	50
3.5.4.c Monte Carlo Simulation to Optimize Parameters	50
3.5.5 Statistical Analysis	53
3.5.5.a Cell Culture	53
3.5.5.b Bioassay Chamber	53
SECTION IV: RESULTS	54
4.1 Cell Culture	54
4.1.1 Effects of Electrospun Cellulose Acetate Scaffolds	54
4.1.1.a Effect of Electrospun Cellulose Acetate Fiber Diameter	54
4.1.1.b Effects of Additives to the Electrospun Cellulose Acetate Scaffolds	61
4.1.1.c HUVEC Morphology on Electrospun Scaffolds	66
4.1.1.d Migration onto Cellulose Acetate Scaffolds	69

4.1.2 Effects of Surface Modifications	80
4.1.2.a Effects of Hydrophilic vs. Hydrophobic Surfaces	80
4.1.2.b Effects of Microstamped ECM Proteins on Hydrophilic Surfaces	86
4.1.2.c Effects of Microstamped ECM Proteins on Hydrophobic Surfaces	90
4.2 Bioassay Chamber	94
4.2.1 Electrospun Cellulose Acetate Scaffolds	99
4.2.1.a Effects of Scaffold Composition and Flow Rate	99
4.2.1.b Cell Morphology on Electrospun Scaffolds	101
4.2.1.c Long Term Culture of Murine Aortas in Electrospun Scaffold	104
4.2.2 Effects of Surface Modifications	108
4.2.2.a Effects of Hydrophilic vs. Hydrophobic Surfaces	108
4.2.2.b Effects of Microstamped ECM Proteins on Hydrophilic Surfaces	113
4.2.2.c Effects of Microstamped ECM Proteins on Hydrophobic Surfaces	117
4.2.2.d Effects of Microstamped Fibronectin onto CA180 Scaffolds	121
SECTION V: DISCUSSION	124
5.1 Cell Culture	124
5.1.1 Electrospun Cellulose Acetate	124
5.1.1.a Effects of Scaffold Fiber Diameter on Viability and Density..	124
5.1.1.b Effects of Scaffold Additives on Viability and Density	125
5.1.1.c Effects of Scaffolds on Cell Morphology and Scaffolds	127
5.1.1.d Migration onto Cellulose Acetate Scaffolds	128
5.1.2 Effects of Surface Modifications	129
5.1.2.a Effects of Hydrophilic vs. Hydrophobic Surfaces on Viability and Density	130
5.1.2.b Effects of Microstamped ECM Proteins on Hydrophilic Surfaces on Viability, Density and Morphology	130
5.1.2.c Effects of Microstamped ECM Proteins on Hydrophobic Surfaces on Viability, Density and Morphology	131
5.2 Bioassay Chamber	132
5.2.1 Electrospun Cellulose Acetate Scaffolds	132
5.2.1.a Effects of Scaffold Composition and Flow Rate	133
5.2.1.b Cell Morphology on Electrospun Scaffolds	133
5.2.1.c Long Term Culture of Murine Aortas in Electrospun Scaffold	134
5.2.2 Effects of Surface Modifications	134
5.2.2.a Effects of Hydrophilic vs. Hydrophobic Surfaces	134
5.2.2.b Effects of Microstamped ECM Proteins on Hydrophilic Surfaces	135
5.2.2.c Effects of Microstamped ECM Proteins on Hydrophobic Surfaces	136

5.2.2.d Effects of Microstamped Fibronectin onto CA180 Scaffolds .	136
5.3 MATLAB® Programs Used to Facilitate Data Collection or Analysis ...	137
SECTION VI: SUMMARY AND FUTURE WORK	138
SECTION VII: REFERENCE LIST	140
Appendix A: MATLAB® m.files	163

LIST OF ABBREVIATIONS AND SYMBOLS

$\frac{dv}{dr}, \gamma$	Shear Rate (Blood or Perfusate)
α	Womersley Parameter
μ	Fluid Viscosity (Blood or Perfusate)
A	Acetone
bFGF	Basic Fibroblast Growth Factor
BS-1	<i>Bandeiraea simplicifolia</i> -1
BSA	Bovine Serum Albumin
CA	Cellulose Acetate
CAMs	Cellular Adhesion Molecules
Cx	Connexin
ECGS	Endothelial Cell Growth Serum
ECM	Extracellular Matrix
ECs	Endothelial Cells
EDTA	Ethylenediaminetetraacetic Acid
EGM-MV	Endothelial Growth Media – Microvascular
eNOS	Endothelial Nitrous Oxide Synthase
FBS	Fetal Bovine Serum
FCS	Fetal Calf Serum
Fn	Fibronectin
g	Gravity Constant (9.81 m/s ²)
HBS	Hepes Buffered Saline
HBSS	Hank's Buffered Salt Solution
hDMECs	Human Dermal Microvascular Endothelial Cells
HUVECs	Human Umbilical Vein Endothelial Cells
ICAMs	Intracellular Adhesion Molecules
IgG	Immunoglobulin G
K	Darcy's Effective Hydraulic Conductivity
MMPs	Matrix Metalloproteinases
mRNA	Messenger Ribonucleic Acid
P	Inline Pressure for Apparent Porosity Measurements
PBS	Phosphate Buffered Saline
PDGF	Platelet Derived Growth Factor
PDMS	Polydimethylsulfoxide
Pen	Penicillin
PLGA	Poly _{D,L} -Lactic-co-Glycolic Acid
PLLA	Poly _L -Lactic Acid
PLLA-CA	Poly _L -Lactide-co- ϵ -Caprolactone
Q	Flow Rate (Blood or Perfusate)
r, r_0	Radius of a Tube (Blood Vessel)
Re	Reynolds Number
RGD	Arginine – Glycine – Aspartic Acid (Amino Acid Sequence)
rpm	Revolutions per Minute
SD	Standard Deviation

sec	Second (unit of time)
S.E.M.	Standard Error of the Mean
SEM	Scanning Electron Microscopy
Strep	Streptomycin
U	Inline Flow Rate for Apparent Porosity Measurements
v	Velocity (Blood or Perfusate)
VEGF	Vascular Endothelial Growth Factor
VSMCs	Vascular Smooth Muscle Cells
WBCs	White Blood Cells
τ_w	Wall Shear Stress

LIST OF FIGURES

Figure 2.1: Schematic of Two Common Arterial Networks	7
Figure 2.2: Schematic of the Basal Lamina	18
Figure 2.3: Schematic of an Electrospinning Apparatus	22
Figure 2.4: Schematic of the Photolithography Process	24
Figure 2.5: Schematic of Soft-Lithography and Microcontact Printing	26
Figure 3.1: Schematic of Grooved PDMS Scaffolds used within the Bioassay Chamber	30
Figure 3.2: Scanning Electron Microscopy Image of Gold Sputtered PDMS Stamps	33
Figure 3.3: A Picture of the Stamping Apparatus	35
Figure 3.4: A Picture of a Cured Bioassay Chamber with our Modified P1 Platform	38
Figure 3.5: Schematic of the Bioassay Chamber with a Cannulated Aorta and Electrospun Scaffold	42
Figure 3.6: Schematic of Images Taken After Explant Perfusion in the Bioassay Chamber	47
Figure 3.7: Sample Steps Taken While Using Cellcounting.m Program	49
Figure 3.8: Endothelial Cell Boundary with Phase-Contrast and the Cellcounting.m MATLab® Program	52
Figure 4.1: Representative Scanning Electron Microscope Images of Electrospun Scaffolds	55
Figure 4.2: Verification of Fibronectin Coating of CA180 Scaffolds	56
Figure 4.3: Force vs. Displacement and Stress vs. Strain Curve for CA180 and CA+1.6% Chitosan	59
Figure 4.4: Endothelial Cell Density and Viability on our Base Cellulose Acetate Scaffolds	60
Figure 4.5: Endothelial Cell Density and Viability on Electrospun Scaffolds with Different Material Composition	62
Figure 4.6: Endothelial Cell Density and Viability on Substrates With or Without 3.4µg/mm ² Fibronectin	64
Figure 4.7: Control Experiments to Quantify the Effects of Cellulose Acetate or Chitosan Material on HUVECs	65
Figure 4.8: Digital Images of HUVECs Grown on Electrospun Scaffolds or Matrigel®	68
Figure 4.9: Cell Density and Viability for HUVECs that had Migrated onto CA180 Scaffolds	70
Figure 4.10: Digital Images of HUVECs that had Migrated onto CA180 Electrospun Scaffolds and Paired Bare Glass	72
Figure 4.11: Cell Density and Viability for HUVECs that had Migrated onto CA180 Electrospun Scaffolds with the Addition of 3.4µg/mm ² Fibronectin	74
Figure 4.12: Digital Images of HUVECs that had Migrated onto CA180 Electrospun Scaffolds with 3.4µg/mm ² Fibronectin and Paired Bare Glass	75

Figure 4.13: Cell Density and Viability for HUVECs that had Migrated onto CA180 + 1.6% Chitosan Electrospun Scaffold	77
Figure 4.14: Digital Images of HUVECs that had Migrated onto CA + 1.6% Chitosan Electrospun Scaffold	78
Figure 4.15: Verification of Fibronectin Coating of Hydrophilic and Hydrophobic Glass	81
Figure 4.16: hDMEC Density and Viability on Bare Hydrophilic or Hydrophobic Glass	82
Figure 4.17: hDMEC Percent Confluence for all Microstamp Experiments.....	84
Figure 4.18: Digital Image of hDMECs on Bare Hydrophilic or Hydrophobic Glass	85
Figure 4.19: hDMEC Density and Viability on ECM Microstamped Proteins on Hydrophilic Glass	87
Figure 4.20: Digital Images of hDMECs Cultured on Microstamped ECM Proteins on Hydrophilic Glass	89
Figure 4.21: hDMEC Density and Viability on ECM Microstamped Proteins on Hydrophobic Glass	91
Figure 4.22: Digital Images of hDMECs Cultured on Microstamped ECM Proteins on Hydrophobic Glass	93
Figure 4.23: Cannulated Isolated Murine Aorta	95
Figure 4.24: Time Lapse Images of a Perfused Murine Aorta	96
Figure 4.25: Sinusoidal Waveform Approximation of Perfused Vessel Diameter	97
Figure 4.26: Digital Images of Endothelial Cells Stained with the BS-1 Lectin and DAPI.....	98
Figure 4.27: Endothelial Cell Density and Viability in our Bioassay Chamber after Perfusion of the Explanted Artery	100
Figure 4.28: Digital Images of Endothelial Cells within Scaffolds after Perfusion in the Bioassay Chamber	103
Figure 4.29: Endothelial Cell Density and Viability after Long-Term Perfusion of an Explanted Murine Aorta in our Bioassay Chamber	105
Figure 4.30: Digital Images of Endothelial Cells within CA180 Electrospun Scaffolds after Long-Term Perfusion in the Bioassay Chamber	107
Figure 4.31: Endothelial Cell Density and Viability on Bare Hydrophilic or Hydrophobic Glass in the Bioassay Chamber	109
Figure 4.32: Endothelial Cell Percent Confluence for all Microstamp Experiments in the Bioassay Chamber	111
Figure 4.33: Digital Image of Endothelial on Bare Hydrophilic or Hydrophobic Glass in the Bioassay Chamber	112
Figure 4.34: Cell Density and Viability in the Bioassay Chamber on Microstamped ECM Proteins on Hydrophilic Glass	114
Figure 4.35: Digital Images of Endothelial Cells Grown on ECM Microstamped Proteins on Hydrophilic Glass in the Bioassay Chamber	116
Figure 4.36: Cell Density and Viability in the Bioassay Chamber on Microstamped ECM Proteins on Hydrophobic Glass	118

Figure 4.37: Digital Images of Endothelial Cells Grown on ECM Microstamped Proteins on Hydrophobic Glass in the Bioassay Chamber	120
Figure 4.38: Cell Density and Viability in the Bioassay Chamber on Microstamped Fibronectin onto CA180 Electrospun Scaffolds.....	122

LIST OF TABLES

Table 2.1: Highlighted Studies that Investigated Angiogenic Growth Factors	12
Table 3.1: Summary of Electrospun Scaffold Process Parameters and Composition	28
Table 3.2: Average Percent Error between Two Methods of Analyzing Cell Morphology	51
Table 4.1: Void Space and Surface Area to Volume Ratio for CA180, CA + 1.6% Chitosan and Other Common Electrospun Scaffolds	58
Table 4.2: HUVEC Area and Fraction Elongated Cells for Short Growth Durations	67
Table 4.3: Cell Area and Fraction Elongated Cells for HUVECs that had Migrated onto Electrospun Scaffolds	71
Table 4.4: Cell Density and Viability Relative to Bare Glass for HUVEC Migration onto Cellulose Acetate Based Electrospun Scaffolds	79
Table 4.5: hDMEC Area and Fraction Elongated Cells on Bare Hydrophilic or Hydrophobic Glass	83
Table 4.6: hDMEC Area and Fraction Elongated Cells on Stamped Proteins on Hydrophilic Glass	88
Table 4.7: hDMEC Area and Fraction Elongated Cells on Stamped Proteins on Hydrophobic Glass	92
Table 4.8: Endothelial Cell Area and Fraction Elongated Cells in the Bioassay Chamber After Perfusion	102
Table 4.9: Endothelial Cell Area and Fraction Elongated Cells in the Bioassay Chamber After Long-Term Perfusion	106
Table 4.10: Perimeter Based Cell Area and Fraction Elongated Cells on Bare Hydrophilic or Hydrophobic Glass in the Bioassay Chamber	110
Table 4.11: Perimeter Based Cell Area and Fraction Elongated Cells on Stamped ECM Proteins on Hydrophilic Glass within the Bioassay Chamber ...	115
Table 4.12: Perimeter Based Cell Area and Fraction Elongated Cells on Stamped ECM Proteins on Hydrophobic Glass within the Bioassay Chamber ..	119
Table 4.13: Perimeter Based Cell Area and Fraction Elongated Cells on Stamped Fibronectin onto CA180 within the Bioassay Chamber	123

ACKNOWLEDGEMENTS

First and foremost I must acknowledge my Ph.D. advisor, Dr. Molly Frame. Without her guidance and support this dissertation would not have been completed. She never held the reins too tightly on me and allowed me the freedom to pursue the research that I enjoyed. I have learned how to compose manuscripts and grants efficiently from Molly and have also been given a vast amount of insight into how a lab functions. I will not forget the time that I spent with Molly as my mentor and learning about the microcirculation.

Also, I need to take the time here to acknowledge all of the members of my dissertation committee for 1) taking the time to help me focus my project and for 2) letting me use their resources to further the aims of the project. Dr. Helmut Strey provided the equipment for photolithography and allowed me time to pick his brain about many things on the nano- to micro-scale. Dr. Michael Hadjiargyrou, provided me great insight into the biological realm than helped to elucidate many aspects discussed here. Dr. Pelagia-Irene Gouma provided facilities for electrospinning and has proven to be a great resource for the Frame lab. Many aspects of this project would not have come together without the combined help of my committee.

I have to thank all of the students in Dr. Frame's lab that have had a hand in this project. I could not have completed this study without your help and insightful question. Although I make it hard for you in the beginning, there is always a program in sight.

Lastly, I must thank the greatest resource of them all, my wife, Wei. Without the constant bi-directional flow of ideas and opinions, my sanity could not be maintained.

SECTION I: INTRODUCTION

Tissue engineering is a new discipline that combines both biological and engineering requirements to fabricate biological replacement for organs, tissues or cells. Successful replacements, could lead to cures and endless transplant supplies. Although, there is a great deal of research undertaken in this field, there are still many problems that need to be solved before many of these benefits become a reality. One of these problems is the development of vascularized tissue/organs for implantation. The first step for this problem is the fabrication of a patent vasculature in prescribed patterns. The major reasons that tissue engineered solutions fail today is because there is a lack of vasculature within the fabricated tissue. The vasculature provides the growing tissue with nutrients, waste removal, biological defense mechanisms and maintenance of homeostasis. Currently, the only successful tissue engineered substitutes stem from native tissue which already possess extensive vasculature; i.e. skin patches.

While it is currently possible to culture cells, tissues and organs *ex vivo*, it is not yet possible to start from a mixture of cells and culture them into a functioning organ or vasculature. To begin to address the vascular problem it is necessary to initiate the *de novo* growth of blood vessels to be later co-cultured with cells, tissues or organs to allow for the complete fabrication of a patent vasculature. In the Frame Laboratory, I began to address this problem by designing a novel bioassay chamber that could be used to test *in vitro* angiogenesis on to patterned substrates. Our bioassay chamber houses an explanted blood vessel which serves as the initial source of endothelial cells. Various tissue engineered scaffolds can be applied within the bioassay chamber. The onset of angiogenesis can be monitored hourly and daily. For this study, I investigated the onset of angiogenesis with control of one mechanical cue, flow rate, and one biological cue, scaffold composition (topology/topography).

To be able to design patent vascular networks, biological and engineering conditions that promote angiogenesis must be found, characterized and optimized. The conditions that were controlled in this study were the material composition of the scaffold, the topography of the scaffold, the flow rate and the hydrophobicity and topology of a scaffold. These conditions were examined using explanted aortas as the initial endothelial cell culture source in the bioassay chamber and passaged endothelial cells in cell culture studies. Optimal conditions were characterized by studying the endothelial cell viability and density, endothelial cell morphology and the ability to direct the culture of endothelial cells onto prescribed patterns. Currently, no group has combined these factors to characterize the angiogenic processes and fabricate vascular networks from an autologous blood vessel. Therefore, this dissertation initiated an inclusive study to determine if early angiogenesis can be guided via topological signals and angiogenic growth factors in a tissue engineered scaffold.

The major goal of this thesis was to test the **hypothesis that a combination of mechanical and chemical growth cues can be optimized for the growth of**

endothelial cells into potential vascular networks. The goal was divided into two sub-goals; one that focused on addressing engineering design and the other which focused on the biology. The thesis itself is divided into sections which described preliminary cell culture experiments and the bioassay chamber experiments. The **Specific Aims** are:

Engineering Design Problem

Specific Aim 1: To design a bioassay chamber to support a viable explanted vessel that would serve as the source of endothelial cells that could construct a vascular network using various topographical and/or mechanical cues.

Aim 1.1: To design a bioassay chamber that maintains the viability of the explanted vessel by use of low pulsatile flow.

Aim 1.2: To have endothelial cells from the open side branches migrate into the surrounding scaffolding.

Aim 1.3: To maintain the viability of the explanted vessel and endothelial cells originating from the vessel over 7 days.

Engineering/Biology Question

Specific Aim 2: To optimize the endothelial cell growth conditions in the bioassay chamber and cell culture studies by varying scaffold composition, scaffold topology and/or flow rate application.

Hypothesis 2.1: Endothelial cells will prefer to grow within electrospun cellulose acetate fibers to which additional material strengthening compounds have been added.

Hypothesis 2.2: The addition of ECM proteins to the formed scaffold will enhance cell density on the scaffold.

Hypothesis 2.3: The addition of microstamped ECM proteins to hydrophilic substrate will direct the growth of endothelial cells onto the patterned proteins. Endothelial cells will preferentially adhere to the microstamped ECM proteins instead of the hydrophilic glass substrate.

Aim 2.3.a: To reach confluence quickly on the microstamped ECM proteins.

Aim 2.3.b: To excluded endothelial cells from the hydrophilic (non-patterned) substrate.

Hypothesis 2.4: The addition of patterned ECM proteins to hydrophobic substrate will direct the growth of endothelial cells onto the patterned ECM proteins. Endothelial cells will preferentially adhere to the microstamped ECM proteins instead of the *hydrophobic* glass substrate.

Aim 2.4.a: To reach confluence quickly on the microstamped ECM proteins.

Aim 2.4.b: To exclude endothelial cells from the hydrophobic (non-patterned) substrate.

SECTION II: BACKGROUND

2.1 Arteriolar Vascular Physiology

The cardiovascular system is responsible for many diverse tasks within living organisms; including the delivery of oxygen/nutrients to all cells and the maintenance of core body temperature (Carmeliet, 2005). In adults the cardiovascular system has a well defined structure, which is not present during fetus development. During the formation of the nascent cardiovascular system, termed vasculogenesis, all blood vessels resemble capillary networks and there is no differentiation between blood vessel types (Bauer et al., 2005; Millauer et al., 1993). However, towards the later stages of vasculogenesis, three specialized blood vessels form into the classic adult network structure (Carmeliet, 2005). These three specialized types of blood vessels exhibit different structures, which partially determine their function. Muscular arteries carry oxygenated high pressure blood. Capillaries comprised mostly of a single cell type (endothelial cells), allow for material exchange. Veins collect the oxygen depleted blood and return it to the heart/lungs (Guyton and Hall, 2000). Further differentiation of the blood vessels is accomplished by their structures and the relationships with other cell types (i.e. smooth muscle cells, pericytes). Section 2.2 briefly describes blood vessels that are found throughout the microcirculation. Although blood vessel have a different anatomy, the interior lining of all blood vessels is composed of endothelial cells (ECs) (Guyton and Hall, 2000). Larger vessels can have multiple layers of ECs but smaller blood vessels, like capillaries, have a monolayer of ECs.

2.1.1 Endothelial Cells

The primary function of endothelial cells is to separate blood constituents from all other cells within the body. The shape and interaction of ECs with neighboring ECs partially determines their ability to restrict molecules from entering the interstitial space. EC shape is partially governed by location within the circulatory system, but there are some common features to all ECs. ECs are generally spindle shaped with an average length of 100 μ m and maximal width of approximately 20 μ m (Guyton and Hall, 2000). They form the intimal layer of the vessel wall. Normally they function to inhibit coagulation, hemolysis and inflammation, however, these functions can change drastically during cytokine or physical force stimulation (Nichol et al., 2005; Uttayarat et al., 2005; Yamaguchi et al., 2000) or when vessels become injured (Silverstein, 1999). Endothelial cells “activate” and play critical regulatory roles during these processes. The other major function that ECs accomplish is the regulation of oxygen/nutrients to other cells. They act as a diffusion barrier against oxygen, nutrients and wastes within the capillary structures (Guyton and Hall, 2000) (Section 2.2).

A wide array of molecules adhere to the EC surface forming the glycocalyx, including glycoproteins and proteoglycans (i.e. glycosaminoglycan, GAGs) (Pahakis et al., 2007). This surface extends into the lumen (~10 μ m) providing a surface for fluid

forces to interact with. In response to these forces, a number of reactions occur within ECs including the activation of tyrosine kinase (Chen et al., 1999), integrins (Liu et al., 2002) and G-proteins (Olesen et al., 1988). The activation of any of these molecules causes a signaling cascade within the cell, releasing signaling molecules, causing alignment of cells and/or redistribution of load-bearing fibers within the cell (Chien, 2007; Friedman et al., 2006). These reactions can be transmitted quickly to neighboring ECs via gap junctions, so that near-by cells can respond in a similar manner to physical forces. Human ECs express connexin (Cx) 37 and Cx40 (Sohl and Willecke, 2004). Endothelial cells also are connected to vascular smooth muscle cells (VSMCs) via gap junctions (Takano et al., 2005). In response to a shear stress signal along the EC membrane, signals pass to the VSMCs to help regulate vascular caliber (i.e. hyperpolarization via gap junctions between ECs and VSMCs partially regulates vasodilation) (Takano et al., 2005). Therefore, gap junction communication contributes to flow regulation in vascular networks by communicating signals to alter vessel caliber.

Many groups have studied EC function in relation to physiological and pathological processes including angiogenesis (Section 2.3), wound healing and cancer (Sections 2.4). One requirement for all of these studies was a means to identify ECs specifically. Currently, one of the most popular techniques used to specifically identify ECs is the immunohistochemical identification with the *Bandeiraea simplicifolia* (BS-1) lectin (Hayes and Goldstein, 1974; Jung et al., 2002; Wu et al., 2001). Lectins are receptor proteins which bind to particular carbohydrates. The EC membrane carbohydrate that the BS-1 lectin binds to is present on other cell types (i.e. microvilli of the intestines (Lee et al., 2003)) but it is not present on other cells that comprise blood vessels (i.e. VSMCs (Jung et al., 2002)). Therefore, by using this lectin, endothelial cells associated with blood vessels can be selectively identified.

2.1.2 Vascular Smooth Muscle Cells, Pericytes and Other Cells Types

Vascular smooth muscle cells (VSMCs) are partially responsible for controlling the diameter of blood vessels by responding to neuronal, hormonal, and local chemical agonists. Depending on the type of receptor that is activated and the agonist that activates that receptor, VSMCs can contract or dilate to vary blood vessel diameter. VSMCs comprise the media layer in all arteries and veins. They are generally longer than ECs and have the ability to wrap both circumferentially and longitudinally around blood vessels (Guyton and Hall, 2000). VSMCs are not present along capillaries (Guyton and Hall, 2000). In arteries, VSMCs act to regulate the tone of the vessel (diameter and responsiveness), which, by affecting resistance between branch points, can influence the blood flow direction, especially at the microvascular level. Therefore, these cells play a key role in the regulation of oxygen/nutrient delivery to cells throughout the body.

VSMCs are connected via gap junctions allowing for the fast communication of electric signals between muscle cells. One method to identify VSMCs is the use of molecules that target specific connexins not present on other cells (Takano et al., 2005). VSMCs have many load bearing fibers, such as actin filaments. α -actinin provides a second method which can further help to identify this cell type (Takano et al., 2005).

Pericytes make direct contact with the endothelium on blood vessels, especially capillaries. They are currently thought to be precursors of VSMCs and have been shown to have the ability to differentiate into VSMCs in culture (Armulik et al., 2005). These

cells have a similar shape and size to ECs covering approximately 50% of the vascular bed in the microcirculation (Armulik et al., 2005). These cells play important roles in the development, stabilization and maturation of new vascular networks and are therefore located in close proximity to capillaries and/or arterioles (Guyton and Hall, 2000). However, ECs that initially form capillaries do not interact with these cells. Instead, pericytes play a key role during the stabilization phase of angiogenesis by interacting with existing capillaries. Markers for pericytes are not specific but include smooth muscle α -actin and platelet derived growth factor receptor- β (Armulik et al., 2005). These markers are normally used in conjunction with other more specific markers for ECs (i.e. BS-1 lectin) to differentiate between these cells that are in close proximity.

White blood cells (WBCs) and fibroblasts are also important cells within the cardiovascular system. Some classes of WBCs (primarily monocytes) release signaling molecules that interact with ECs during inflammation (Schober and Weber, 2005). These molecules activate ECs and act as a chemoattractant molecule. WBCs can aid in the degradation of the extracellular matrix (ECM) during angiogenesis, facilitating EC migration. WBCs are normally identified via classical histology techniques and there is a standard stain for each WBC type. Fibroblasts function to remodel the ECM, although ECs can also perform this function. Fibroblasts have the ability to produce collagen, Fn and other ECM proteins; releasing them in a structured way. Fibroblasts are also very prominent in inflammation and interact with ECs during these processes (Chettibi and Ferguson, 1999; Ruoslahti, 1999). These cells can help to activate ECs and play a role in their migration. There are classic histology techniques for fibroblasts. Many other cell types can interact with ECs but these highlighted cells play prominent roles during angiogenesis; aiding in the activation, migration and proliferation of ECs.

2.2 Microcirculation

Biological and engineering principles differ for the microcirculation as compared to the macrocirculation. Large and medium sized blood vessels deliver blood to all regions of the body (Guyton and Hall, 2000). However, it is the blood vessels in the microcirculation, predominantly capillaries, that function in the delivery of oxygen and nutrients to individual cells (Guyton and Hall, 2000). Capillaries have the highest total vascular cross-sectional area ($\sim 2500\text{cm}^2$) (Guyton and Hall, 2000) due to the constant division of blood vessels. Therefore, the majority of oxygenated blood ($>20\%$) is within the microcirculation at rest (Fung, 1997). The macrovascular arterial circulation (large conduits) houses approximately 18% of oxygenated blood and the rest is divided between organs (Guyton and Hall, 2000). Approximately 65% of all blood in the body is within the venous macrocirculation; held here as a reservoir (Guyton and Hall, 2000).

2.2.1 Microvascular Network Structure

The geometry of the arteriolar network dictates where the blood flows through tissues and hence which locations deep within the tissue receive the most oxygen and nutrients. Blood arriving from the arterial side is distributed to terminal arterioles in a prescribed fashion (Frame and Sarelius, 1993), and then to spatially arranged capillary modules (Berg and Sarelius, 1995). Nutrients are then delivered to the tissue via the capillaries and the waste is removed. The oxygen depleted blood is passed into the venous circulation, where it returns to the lungs to become re-oxygenated. There are

specific repeating network structures based on the organ type, which will equally perform these tasks, however, in the simplest sense there are two types of capillary network structures. One common network structure is an artery which divides into many parallel capillaries, which converge onto one vein (Figure 2.1 A). A second common network structure is an arterial network in close proximity to a venous network. There are many connections between these two networks (Figure 2.1 B) thus blood flow paths are both in parallel and series. Which structure predominates within an organ is partially determined by the need of the tissue and the structure can change over time during remodeling.

The terminology for an arteriole network is as follows. An arteriole generally has a diameter that ranges from 10 to 125 μ m (Fox and Frame, 2002a; Guyton and Hall, 2000). Arterioles have more than one layer of VSMCs surrounding the EC layer and a nerve fiber is associated with the vessel. A terminal arteriole is the final arterial structure which has a continuous single layer of VSMCs (Guyton and Hall, 2000). These vessels typically range from 10-50 μ m in diameter (Fox and Frame, 2002a). A metarteriole does not have a continuous layer of VSMCs surrounding the endothelial layer (Guyton and Hall, 2000). The final smooth muscle cell before the capillary is sometimes called the precapillary sphincter (Fung, 1997). It is this cell that is associated with the control of blood flow through capillary networks.

Within microvascular networks, it has been seen that arteriolar bifurcation geometry influences the flow distribution to sequential terminal arterioles. During rest and during maximal dilation the first branch from a transverse arteriole has the largest bifurcation angle ($\sim 120^\circ$) (Frame and Sarelius, 1993). Subsequent branches along the transverse arteriole show that the bifurcation angle decreases; the last branch has the smallest angle ($\sim 60^\circ$) (Frame and Sarelius, 1993). Bifurcation angle is also related to the distance between entrance to the transverse arteriole and the first terminal arteriolar. Bifurcation angle decreases with an increasing entrance length (Frame and Sarelius, 1993). One explanation for this was that the vascular network geometry was governed by energy optimization (Frame and Sarelius, 1995b). With models designed to minimize wall surface area, total volume, wall shear stress or power loss, predicted geometries at individual bifurcations were not obtained (Frame and Sarelius, 1995b). However, the network as a whole was still optimally designed (Frame and Sarelius, 1995b).

Different types/classes of capillaries are defined by the blood flow through the vessel. Capillaries with a higher velocity which carry blood during the majority of time are termed thoroughfares (Fung, 1997). Shorter capillary like structures, that bypass the capillary networks are termed anastomoses (Fung, 1997). Both play important roles in the allocation of oxygenated blood. Most capillaries are organized as a module or network. Within a capillary network, there are arteriolar, true and venular capillaries. Arteriolar capillaries have flow divergence at both end points, true capillaries have divergent flow upstream and convergent flow downstream, while venular capillaries have flow convergence at both end points (Williams and Huxley, 1993).

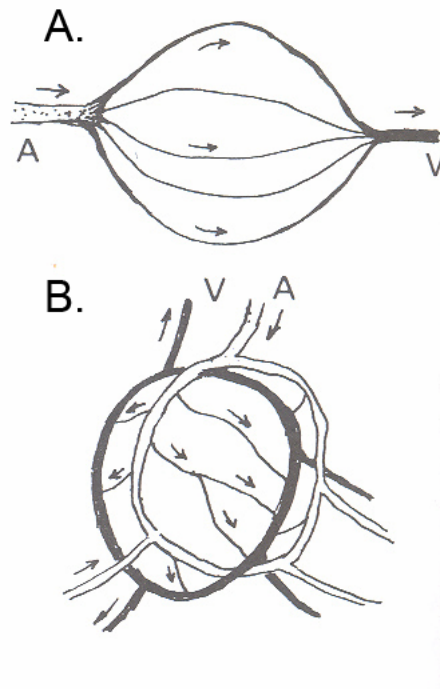


Figure 2.1: Schematic of Two Common Arterial Networks. (A) Capillaries that branch from a single terminal arteriole that converge into one collecting venule. (B) A capillary network that is in close proximity to a venous network. There are many connections between these networks. A: Arteriole, V: Venule, \rightarrow : Direction of flow. This figure has been taken from (Fung, 1997).

Capillaries are composed of a single layer of endothelial cells. A continuous basement membrane surrounds capillaries (Fung, 1997). The cell membrane of ECs within the capillary is in close proximity to neighboring EC membranes with a gap ranging between ~10 to 20nm (termed the intercell cleft) (Fung, 1997; Guyton and Hall, 2000). In some instances the gap is sealed by tight junctions (Guyton and Hall, 2000). Both the cleft and ensuing tight junctions regulate the diffusion of molecules around ECs playing a primary role in EC permeability. In the brain, the entire cleft is sealed by tight junctions, a molecule with a hydration radius larger than 2.5nm can not pass through the intercell cleft (Fung, 1997). The cleft size can be regulated by chemical agonists, especially during inflammation when it becomes “leaky” and enlarges. Small molecules, plasma proteins and WBCs can now infiltrate the EC gap. Therefore, a delicate balance is needed to regulate the diffusion of molecules/cells across the EC cleft.

2.2.2 Microvascular Network Function

One of the major functions of the arterial network is the exchange of nutrients to the surrounding tissue. The primary means for exchange to occur is through diffusion across the EC wall (Guyton and Hall, 2000). Diffusion is the random thermal motion of molecules from a region with higher concentration to a region with lower concentration and is governed by the concentration difference in molecules, the permeability of the molecules in a particular medium, the area over which diffusion can occur, the distance over which the molecules are diffusing and the temperature of the system (Giancoli, 2000). Compounds, such as oxygen and carbon dioxide, that are lipid-soluble can directly diffuse across the EC lipid bilayer (Guyton and Hall, 2000). Compounds that are not lipid-soluble but are water-soluble diffuse through the intercellular cleft (Guyton and Hall, 2000). Examples of these molecules are water, ions, albumin and glucose. The diffusion of these molecules is largely related to their hydration diameter. As the molecular weight increases, the hydration radius generally increases and its permeability (i.e. the diffusivity) through the intercellular cleft decreases (Pappenheimer, 1953). The hydration radius of water is ~20 times smaller than the diameter of the cleft (~10nm) (Guyton and Hall, 2000). The hydration radius of glucose is ~5 times smaller than the cleft, while plasma proteins have a hydration radius slightly larger than the cleft diameter (Guyton and Hall, 2000). Concentration difference determines in which direction there will be a greater net movement of molecules. In most cases, the permeability is so large that only a small concentration difference is needed. This is especially true for nutritional molecules such as glucose (Guyton and Hall, 2000); where a large amount of energy would be expended to maintain large concentration differences.

2.2.3 Rheology within the Microcirculation

Blood flow within the microcirculation is different than in the macrocirculation. Macrocirculation flow can be described by the fluid dynamic laws that govern laminar flow (treated as a continuum fluid, Newtonian flow). In laminar flow, the inertia of the fluid largely dictates the flow conditions. However, in the microcirculation, inertia of the fluid drops and its balance with the more prominent viscous forces and pressure gradients must be considered (Fung, 1997). Inertia drops, due to the large decrease in the average vessel diameter and slower blood flow. Vessel diameter decreases because of the constant division of the arterial network. Reynolds number (Re) is used to quantify the

inertia forces relative to the viscous forces. Re is the ratio of the inertial forces to the viscous forces and is $\ll 1$ within the microcirculation. The Womersley parameter (α) is also $\ll 1$. α is the ratio of the pulsation frequency (i.e. pressure pulse) to the kinematic viscosity (dynamic viscosity divided by the density). In the microcirculation, there is a low pulsation frequency (from the heart) causing the flow to be more steady (Fung, 1997). Blood cells must be categorized within the flow field using two-phase flow laws (Fung, 1997). This is ignored in the macrocirculation where the tube diameter is much larger in comparison to the particle diameter. In capillary circulation, blood cells (i.e. RBCs) continuously have variations in their velocity, direction, concentration and number of capillaries accessible to flow. Some capillaries see continuous flow (thoroughfares), while others are stagnant or even closed off (Fung, 1997).

Due to the constant changes in flow within the microcirculation, it is difficult to quantify many of the hemodynamic and physiological parameters. Estimates can be made but the accuracy of these estimates is dependent on the microvascular network in which the study was conducted in and the methods used to quantify parameters. For instance, temperature, humidity and time of the year can change parameter values. In the microcirculation, peak blood velocity is ~ 0.07 cm/s, the Re is ~ 0.001 and α is ~ 0.005 (Fung, 1997). The pressure gradient across a network is ~ 11 cmH₂O (Lipowsky and Zweifach, 1977). Rheological estimates have also been made on the microcirculation. Blood viscosity is estimated as 5cP (however, this depends on tube diameter) and the wall shear stress approaches 40 dyne/cm², in the cat mesentery (Lipowsky and Zweifach, 1977). The hematocrit is approximately 10% in the microcirculation but changes drastically with time and chemical exposure (Lipowsky et al., 1980).

In this dissertation, the characteristic microcirculation rheology was not mimicked. Explanted blood vessels were subjected to a low pulsatile flow to act as an endothelial cell stimulus not as a particular flow regime within the microcirculation.

2.3 Biology of Angiogenesis

Angiogenesis is the process by which new blood vessels form and mature from the existing vasculature. Numerous biochemical and physical factors can induce, promote and/or perpetuate angiogenesis *in vivo* and it is their interplay that allows for angiogenesis to function properly. There are two types of angiogenesis *in vivo*; sprouting and non-sprouting angiogenesis. Sprouting angiogenesis involves the degradation of ECM proteins, EC migration and tube formation. Non-sprouting angiogenesis, or intussusception, occurs when ECs proliferate within preexisting blood vessels and new vessels pinch off from the original (Risau, 1997). Both types of angiogenesis can occur at the same time, within the same tissue (Risau, 1997). Sprouting angiogenesis is the more applicable type of angiogenesis because we are studying endothelial cells derived from side branches of an explanted perfused blood vessel. These cells have the potential to elongate existing side branches; potentially forming new vascular networks. This phenomenon is categorized within sprouting angiogenesis (Arbiser, 1996).

2.3.1 Angiogenesis Progression Overview

Judah Folkman has been one of the leaders in the field of angiogenesis since the late 1970's. His group pioneered angiogenesis research and since the early 1980's his group has been the driving force behind numerous advances in the field (Ausprunk and

Folkman, 1977; Folkman et al., 1979; Folkman and Klagsbrun, 1987; Gimbrone et al., 1974). In a pivotal study from 1992 (Folkman and Shing, 1992), it was observed that angiogenesis is required for tumor growth. Many groups focused their research towards cancer angiogenesis, leading to many advances in understanding angiogenesis progression. Some of the crucial angiogenic factors include the release of angiogenic growth factors, local ECM interactions and the blood vessel wall shear stress. The natural progression of wound healing, arthritis and diabetes (Arbiser, 1996) also requires angiogenesis. However, in most normal non-diseased tissue, while vascular remodeling can occur, angiogenesis, per se, generally does not occur.

For angiogenesis to occur *in vivo*, specific EC signal transduction pathways must activate. The most common method for pathway activation is through the binding of growth factors (i.e. VEGF, PDGF etc.) to their respective cell membrane receptors (i.e. VEGFR1). Activation of receptors causes EC proliferation and migration towards the growth factor concentration gradient, within 48 hours (Ramos et al., 2007). Low pulsatile wall shear stress (3 dyne/cm²) enhances the growth factor induced signal by increasing second messenger signals within the EC (Ueda et al., 2004). Secondary angiogenic processes, include EC migration due matrix metalloproteinases (MMPs) degradation of the local ECM, within 7 days after the onset of angiogenesis (Arenberg and Strieter, 1999). EC membrane integrins activate; thus allowing for rapid binding/unbinding between ECs and ECM proteins (Arenberg and Strieter, 1999). EC integrins interaction with the ECM facilitates migration of ECs along the chemotactic gradient. Migrating ECs, release chemotactic signals which signal other unactivated ECs and nearby pericytes (Arenberg and Strieter, 1999) forming a positive feedback loop. Neighboring activated ECs, which had been migrating, then form lumen structures and release PDGF-BB to recruit pericytes to the maturing blood vessel between days 6-10 after angiogenesis onset (Defouw et al., 1989). Pericytes stabilize growing vessels (Arenberg and Strieter, 1999). Lastly, pericytes differentiate into VSMCs to make a stable mature vessel and classic network structures appear (Defouw et al., 1989). Sections 2.3.2-2.3.6 highlights key studies and parameters for angiogenesis progression. Although there is a large interplay between these factors, the following sections highlight major functions of each key-player.

2.3.2 Extracellular Matrix Proteins and Endothelial Cell Adhesion

The extracellular matrix surrounds and supports blood vessels providing a barrier against EC migration. The basement membrane is normally dense with proteins and therefore ECs can not migrate through it (Davis and Senger, 2005). Upon ECM degradation (and EC activation), ECs can begin to migrate through the ECM. Collagen, a ubiquitous protein, plays a crucial role during angiogenesis (Madri and Williams, 1983; Montesano et al., 1983; Montesano and Orci, 1985). Collagen aids in migration by providing ECs with attachment points for membrane bound integrins (Heilshorn et al., 2003; Simionescu et al., 2006). Different types of collagen support different EC functions. Collagen I and III, normally found in the interstitial space, enhance proliferation but had little effect on migration and tube formation (Madri and Williams, 1983). Collagen IV and V, normally found in the ECM, enhance EC migration and tube formation but did not support EC proliferation (Madri and Williams, 1983). Laminin also plays an important role during angiogenesis (Form et al., 1986; Sephel et al., 1996).

Laminin provides attachment points for ECs during migration and can enhance EC proliferation (Form et al., 1986; Sephel et al., 1996). With collagen IV, laminin can enhance the migration/tube formation of ECs (Herbst et al., 1988). Fibronectin, enhances EC migration and spreading during angiogenesis (Ingber, 1990; Iuliano et al., 1993).

The major type of adhesion molecule on the EC membrane that interact with the ECM is, the integrin super family. Integrins bind to collagens/fibronectin within the ECM (Aguzzi et al., 2004; Hotchkiss et al., 2005; Zisch et al., 2004). Without these interactions, ECs do not form tubes *in vitro* but can migrate minimally (Brooks et al., 1994; Luscinskas and Lawler, 1994). Integrins are directly involved with EC migration because with integrin blockage, EC migration is inhibited and angiogenesis does not progress (Aguzzi et al., 2004).

In late stages of angiogenesis, the ECM plays a key role in blood vessel stabilization. After a vascular network has been formed, new ECM proteins are produced to support the new blood networks. The job of producing new ECM proteins is primarily accomplished by fibroblasts (Chettibi and Ferguson, 1999; Ingber and Folkman, 1989; Velazquez et al., 2002). Initially, fibroblasts produce collagen I, to stabilize blood vessels (Chettibi and Ferguson, 1999). Later the collagen I can be converted into collagen IV for a more long term stability (Chettibi and Ferguson, 1999). Without the production of a new ECM, a new blood vessel can not fully stabilize or integrate into the native tissue. Therefore the ECs and ECM interaction is crucial for proper angiogenesis progression.

2.3.3 Angiogenic Growth Factors Cues

ECs activation does not occur without angiogenic growth factors. Three of the most common growth factors are; vascular endothelial growth factor (VEGF), platelet derived growth factor (PDGF) and basic fibroblast growth factor (bFGF) (Hughes et al., 2004; Papetti and Herman, 2002). While the secretion and localization of these growth factors is poorly understood, their interactions with ECs are clearer. These growth factors primarily act as EC mitogens, causing proliferation and migration towards the source of growth factor release only after they have bound to their respective EC receptor (Bauer et al., 2005; Offenber Sweeney et al., 2005).

VEGF induces proliferation, migration and survival of ECs (Stacker and Achen, 1999) during the early stages of angiogenesis (Westerband et al., 2001). It has been shown that blockage of the VEGF signal, after EC activation, causes apoptosis of immature ECs (Hunt, 2001). Without any VEGF signal, ECs remain quiescent (i.e. unactivated) (Hunt, 2001). bFGF acts as an EC mitogen inducing tube formation, migration and ECM protease production (Gospodarowicz, 1990). bFGF can be stored in the ECM and it is biologically active upon release (Folkman et al., 1988). bFGF functions optimally in close proximity to fibronectin (Ingber, 1990) during the mid to late stages of angiogenesis. bFGF is necessary for angiogenesis progression (Becker et al., 1989). PDGF acts as an EC mitogen causing migration during early angiogenesis and induces the formation of fibroblasts during late angiogenesis (Dardik et al., 2003; Dardik et al., 2005). PDGF is stored within the ECM and can be bound to collagen (Somasundaram and Schuppan, 1996). With PDGF signal inhibition, angiogenesis does not progress normally (Board and Jayson, 2005). Table 2.1 lists key angiogenic growth factor studies illustrating that that growth factors have similar functions and act synergistically with each other to enhance angiogenesis progression.

Growth Factor	Key Findings	Citation
bFGF + VEGF	↑ Capillary Density, Luminal Diameter <i>in vivo</i> , Growth Factors Function Better in Synergy	(Asahara et al., 1995)
PDGF	Enhance Endothelial Cell Tube Formation	(Battegay et al., 1994)
bFGF	Formation of Capillary Tubules in Collagen Matrices	(Montesano et al., 1986)
bFGF + VEGF	↑ Tube Formation in Fibrin Substrates, Growth Factors Function Better in Synergy with TNF - α	(Koolwijk et al., 1996)
bFGF + PDGF	↑ EC Migration, EC Proliferation and Tube Formation in Matrigel®, Growth Factors Function Better in Synergy	(De Marchis et al., 2002)
bFGF	↑ EC Proliferation, EC Survival, Production of MMP-1 mRNA and EC Motility, Tube Formation in Matrigel®	(Kumar et al., 1998)
VEGF	↑ EC Proliferation, EC Survival, EC Motility and EC Permeability, Induced Capillary Formation in Matrigel®	(Kumar et al., 1998)
bFGF + VEGF	↑ EC Proliferation and Cord Formation on Collagen Substrates, Growth Factors Function Better in Synergy	(Goto et al., 1993; Pepper et al., 1992)
VEGF	Induced the Release of bFGF from ECs	(Jonca et al., 1997)
bFGF	Induced the Release of VEGF from ECs	(Seghezzi et al., 1998)
bFGF	Induced Chemotaxis of EC in Culture	(Mignatti et al., 1989)
VEGF	↑ Number of Microvessels and Mean Vessel Length	(Nicosia et al., 1994)
PDGF	↑ Number of Microvessels and Mean Vessel Length	(Nicosia et al., 1994)
VEGF	↑ Vascularity in Cell Culture on PLG Scaffolds	(Peters et al., 2002)

Table 2.1: Highlighted Studies that Investigated Angiogenic Growth Factors. These studies are mentioned to highlight investigation towards the effects of VEGF, bFGF and/or PDGF on ECs and angiogenic processes. This is not an exhaustive list to all of the studies that have investigated these parameters. ↑ is an increase in the specified function, TNF- α is tumor necrosis factor- α .

2.3.4 Endothelial Cell Migration

Binding of adhesion molecules to the ECM induce signal transduction pathways within ECs causing proliferation, migration and/or tube formation. Mature ECs express various unactivated adhesion molecules (Brooks et al., 1994) and upon activation (by angiogenic growth factors), adhesion molecules activate also (Brooks et al., 1994; Davis and Camarillo, 1995; Huang et al., 2005; Liu et al., 2003; Luscinskas and Lawler, 1994). Without activation of adhesion molecules: 1) ECs do not adhere with the ECM and 2) angiogenesis does not occur. Endothelial cells mainly interact with ECM proteins via integrin molecules (Huang et al., 2005). When these molecules are knocked-out or competitively inhibited, ECs can not migrate through the degraded ECM and do not form tube-like structures (Huang et al., 2005). During patent tube formation, ECs proceed through a clear two step process which is regulated by ECM interactions. In the first stage, ECs activate, degrade the ECM and migrate through the degraded matrix (Davis and Senger, 2005). Here, endothelial cell integrins mainly interact with fibronectin and collagen in the ECM.

2.3.5 Endothelial Cells and Lumen Formation

The most prominent cell involved in angiogenesis is the endothelial cell. New blood vessel growth is initiated by the EC (Ausprunk and Folkman, 1977). It is essential for ECs to become activated for angiogenesis to progress (Arbiser, 1996). Activation normally occurs through the binding of growth factors (i.e. VEGF, PDGF, bFGF) to the EC membrane bound receptors (i.e. VEGFR1). Upon activation, ECs begin to proliferate within the blood vessel wall (Ando et al., 1987; Seghezzi et al., 1998; Yamaguchi et al., 2000). Without EC proliferation angiogenesis can not progress (Ando et al., 1987). The initiation of EC migration along the chemotactic gradient is also caused by growth factor binding. ECs (and other cells such as WBCs) begin to degrade the nearby basement membrane (Kalebic et al., 1983; Montesano et al., 1987; Montesano and Orci, 1985) via the release of MMPs (Bauer et al., 2005; Kumar et al., 1998). MMPs are released after growth factor induced EC activation (Kumar et al., 1998). Without degradation of the ECM, angiogenesis does not progress (Davis and Senger, 2005). “Scout” ECs lay down a pathway for migration (Offenberg Sweeney et al., 2005) by releasing chemical signals directed towards other ECs within the blood vessel to: 1) begin to migrate in the same direction as the “scout” ECs: 2) to form tube-like structures (lumens) that are contiguous with those of neighboring ECs (Davis and Senger, 2005).

During the end of this stage, vessel lumens begin to form via the fusion of intracellular vacuoles within one EC (Davis et al., 2002). These intracellular lumens, through exocytosis, fuse with neighboring EC intracellular lumens to form a continuous intercellular lumen. During the second stage of lumen formation, the vessel becomes stabilized and fully patent (Davis and Senger, 2005). Again the interactions of ECs with the local ECM play a crucial role; however, it is now laminin which interacts with ECs (Davis and Senger, 2005). Initially pericytes interact with nascent patent blood vessels to stabilize them (later VSMCs help to form mature networks). When tube-like structures begin to stabilize, signals that initiate the termination of angiogenesis are activated within the ECs (Armulik et al., 2005). Due to the important role that ECs play during every stage in angiogenesis they are the crucial cell to study.

2.3.6 Wall Shear Stress as a Mechanical Stimulus

Wall shear stress (τ_w), a natural biophysical force, enhances angiogenic functions *in vivo*. This force arises from the individual fluid laminas exerting forces on adjacent fluid laminas due to the internal viscous resistance (viscosity; μ) towards motion. In laminar flow, the shear stress (and shear rate; γ) is greatest along the blood vessel wall. This is where the ECs are located. Shear stress is a function of viscosity, fluid velocity (v) and radius (r) (Equation 2.1). In simple cases described by Newtonian flow, the wall shear stress can be approximated by using the Hagen-Poiseuille formulation (Equation 2.2) which assumes a constant μ , v and r at the cross-section of interest. This is a good approximation of the wall shear stress and will be used later in the study.

$$\tau_w = \mu \frac{dv}{dr} = \mu\gamma \quad \text{Equation 2.1}$$

$$\tau_w = \frac{4\mu Q}{r_o^3 \pi} \quad \text{Equation 2.2}$$

Shear stress does not normally initiate angiogenesis but it can perpetuate proangiogenic signals. τ_w , under laminar flow conditions, increases the production of VEGF mRNA after ECs have been activated (Gan et al., 2000; Milkiewicz et al., 2001). This VEGF is biologically active, causing quiescent ECs to proliferate and migrate (Gan et al., 2000). Shear stress (<10 dyne/cm²) increases the production and release of bioactive PDGF and bFGF in ECs (Mitsumata et al., 1993; Resnick et al., 1993; Sterpetti et al., 1994). Endothelial nitrous oxide synthase (eNOS), a vasodilator, has been found to be up-regulated in the presence of oscillating shear stress (Ziegler et al., 1998) and it is activated by PDGF (Fang et al., 1997). Shear stress (5-10 dyne/cm²) can also enhance the migration of ECs (Li et al., 2002a; Yamamoto et al., 2003). Thus, shear stress acts to increase angiogenic processes by perpetuating growth factor signals and EC functions (Ichioka et al., 1997; Silva-Azevedo et al., 2002; Ueda et al., 2004).

2.4 Classic Means to Study Angiogenesis Progression

Since J. Folkman and Y. Shing, made the observation that angiogenesis is required for cancer progression (Folkman and Shing, 1992), this became the gold standard to study angiogenesis (as reviewed in (Arbiser, 1996)). Initially, interest was focused on EC migration in response to growth factors or anti-angiogenic factors. A Boyden chamber chemotaxis assay was used to form chemotactic gradient to monitor cell migration (Mignatti et al., 1989). The Boyden chamber is comprised of two chambers which are separated by a cell permeable filter. A chemotactic gradient is placed across the filter and cell migration is observed. Since then others have found better methods to investigate migration. The chemoinvasive assay investigates the chemotaxis of cells into a basement membrane like structure (Albini, 1998; Albini et al., 2004). This assay benefits from a more natural substrate used to monitor cell migration. Similar techniques are used to study angiogenic processes during wound healing/repair.

2.4.1 Animal Studies

2.4.1.a Dorsal Window Model

In the dorsal window preparation, a skin flap is excised from an animal leaving some layers of skin and the underlying fascia intact (Shan et al., 2003). A window is then

placed over the wound so that various properties can be monitored. Many angiogenic processes that were investigated via *in vitro* preparations were verified with this model. Endothelial cell responsiveness is necessary for tumor angiogenesis to progress (Shan et al., 2003). Increased VEGF concentrations have been seen to directly increase the microvascular vessel density via angiogenesis (Peirce et al., 2004). The permeability and migration of ECs and the vessel density was dependent on the controlled temporal and spatial release of angiogenic growth factors (Yuan et al., 1996). One criticism of the dorsal window preparation is that the angiogenesis that is being investigated is related to wound healing, because a wound is inflicted to place the window in position (Gelaw and Levin, 2001; Menger et al., 2002). There is a potential that this type of angiogenesis is different than non-wound healing (i.e. cancer) angiogenesis.

2.4.1.b Bat Wing Model

A second common animal model used to study angiogenesis and vascular tissue remodeling is the bat wing. This method is used because vascular remodeling and angiogenesis can be investigated noninvasively. Capillary pressure, interstitial fluid pressure and vasomotor activity has been characterized with this model (Salathe, 1977). Other groups have investigated the geometry of the microvascular network, determining the relationships between blood vessels types (Chen, 1983; Chen et al., 1983). Blood velocity and pressure changes in the microcirculation were also investigated using the bat wing model both during angiogenesis and under normal conditions (Mayrovitz et al., 1977; Wiedeman, 1968). Others have shown that vascular remodeling during angiogenesis is shear stress dependent (Widmer et al., 2006). Growth factor stimulation and endothelial cell functions have not been studied as extensively with this model.

2.4.2 *In vitro* Studies

2.4.2.a Wound Healing Studies

A dermal wound is a classic pathological state to study angiogenesis. The simplest wound on the skin is a lesion through the outer epidermal layer. Since the epidermis is avascular (Roberts et al., 2004), repair of this type of wound does not require angiogenesis. However, a deeper wound damages the underlying dermis, which houses vasculature, nervous tissue and a large array of proteins requiring angiogenesis to heal properly (Clark, 1985). The initial step associated with wound healing is the movement of phagocytes into the damaged area. Their task is to prevent contamination of the site (Sido et al., 2004). Phagocytes localized in the wound release angiogenic growth factors that stimulate ECs (Maggelakis, 2003). The prominent growth factors here are VEGF and bFGF (Arenberg and Strieter, 1999; Bates and Jones, 2003; Gospodarowicz, 1990; Nissen et al., 1996; Nissen et al., 1998). In some cases, fibroblasts can move into the wound before ECs. These cells can help to remodel the ECM and aid in EC migration (Doherty et al., 1990). These growth factors have the same effect on ECs as previously discussed (Section 2.3.3), including migration and proliferation (Ausprunk and Folkman, 1977) and ECM remodeling (Gospodarowicz, 1990).

A more severe type of wound is a chronic wound, which does not heal because the damaged area remains avascular even though growth factors are released (Tonnesen et al., 2000). Damaged tissue is not supplied with oxygen and nutrients. Currently groups use Matrigel® and engineered scaffolds, to study wound healing progression and

to increase the vascularity of chronic wounds. Matrigel® has been shown to enhance angiogenesis (Benelli and Albini, 1999; Dye et al., 2004) supporting tube formation (Grant et al., 1989). Engineering scaffolds prepared from collagen support angiogenesis (Goto et al., 1993). Both of these scaffolds have been used in conjunction with growth factors and shear stress to quantify changes in angiogenic processes. These scaffolds may be applied to a chronic wound to help increase vascularity but further studies are needed to address the formation of patent vascular networks.

2.4.2.b Flow Chamber Studies

Shear stress is an important player in angiogenesis (Section 2.3.6). Studies have shown that shear stress can increase the release of angiogenic growth factors (Gan et al., 2000; Mitsumata et al., 1993), activate a shear stress magnitude dependent potassium current (Olesen et al., 1988) and reorganize the F-actin distribution within ECs (Frame and Sarelius, 2000). Using a cast of rabbit and mice arterial networks shear stress effects on ECs was investigated (Langille and Adamson, 1981). In cell culture studies blood flow through branches helps to orient ECs seeded in network structures (Langille and Adamson, 1981). Similarly, ECs were patterned onto PDMS molds and under laminar flow cells were restricted from certain locations based on the flow profile (Takayama et al., 1999). Other studies have used a hemodynamic shearing device to test EC responses to uniform shear. ECs proliferate faster at higher shear stresses as compared to static conditions (Ando et al., 1987; Dewey et al., 1981). Within 48 hours, ECs uniformly had an elongated morphology with their major axis oriented with the flow direction (Dewey et al., 1981). ECs had enhanced migration with fully-developed laminar flow (Ando et al., 1987). Endothelial progenitor cells have also been shown to respond to shear stress in hemodynamic shearing devices. These cells showed a marked increase in proliferation, differentiation and tube formation under constant shear (Yamamoto et al., 2003).

2.5 Vascular Tissue Engineering

One goal of tissue engineers is to fabricate replacement organs or tissues. It is beneficial to either make the tissue substitute mimic the native tissue or biodegrade so that native tissue can replace and/or invade the substitute. A substitute that mimics the native environment is beneficial because it replaces the damaged tissue. Further, cells that interact with the replacement will not recognize a foreign geometry. Some have had success with this approach (Ishii et al., 2005), however, the problem with this approach comes from the possible replacement foreign body rejection. Others have used substitutes that are biodegradable allowing for native tissue to replace the substitute reducing the chances of rejection. This method has also meet with mild success (Shin et al., 2004), but has a major disadvantage in inducing *in vivo* degradation products. The long term goal of this project is the design of a flexible degradable vascular patch. Initial studies aim to show that an explanted perfused blood vessel can be used as the initial source of ECs for tissue engineered vascular products.

2.5.1 *In vivo* ECM and Electrospun Scaffolds – Topography

Electrospinning can be used to fabricate scaffolds that mimic the native ECM. Normal *in vivo* ECM fiber diameters are in the range of 20-80nm (Alberts et al., 2001; Fawcett, 1986). Collagen molecules are the major constituent of extracellular matrix

proteins. They are generally long, helical chains with a very high stiffness of ~ 40 MPa (Alberts et al., 2001; Nalla et al., 2005). Collagens can form into fibrillar (i.e. collagen I) or mesh-like structures (i.e. collagen IV) (Alberts et al., 2001). Collagen IV can bind with other collagen IV molecules or laminin forming the basal lamina which surrounds blood vessels (Figure 2.2). Collagen IV interacts with cells through the integrin receptors on the cell membrane (i.e. $\alpha_1\beta_1$) (Alberts et al., 2001). Laminin is more flexible than collagen and organizes into a cross-like structure (Alberts et al., 2001). Laminin binds to other laminin molecules and interact with cells via integrins (i.e. $\alpha_3\beta_4$) (Alberts et al., 2001). Fibronectin (Fn) is an ECM protein that facilitates cell binding to the matrix via the RGD sequence. Fn proteins have binding sites for collagen, heparin (another ECM protein), cells (via integrins, $\alpha_5\beta_1$) and other Fn molecules (Alberts et al., 2001). It therefore acts to mesh the entire ECM together via cross-linking cells and proteins.

The basal lamina is a specialized ECM that acts to separate particular cell types from the underlying connective tissue and acts to exclude particular cells from each other, (i.e. fibroblasts and ECs) (Burns et al., 2003). In most quiescent tissue the basal lamina is predominantly formed from collagen IV and laminin (Alberts et al., 2001). The basal portion of ECs is attached directly to the basal lamina via integrins. During angiogenesis this layer is degraded to allow for EC migration along the angiogenic growth factor gradient (Section 2.3.3). Many try to mimic the basal lamina when electrospinning scaffold for tissue engineering purposes (Han and Gouma, 2006; Ji et al., 2006).

Current studies are focused on determining the bio-efficacy of electrospun scaffolds. EC proliferation and migration has been the initial focus of these studies. These scaffolds can be used as part of a vascular patch because they are biocompatible and biodegradable (Giavaresi et al., 2004; Hong et al., 2005; Ma et al., 2005a). However, they have largely been unable to induce the formation of tube-like structures. Electrospun scaffolds used in cell culture with ECs have been fabricated from collagen (Matthews et al., 2002), poly(L-lactide-co- ϵ -caprolactone) (PLLA-CA) (Mo et al., 2004), poly D,L-lactic-co-glycolic acid (PLGA) (Sung et al., 2004) and poly(L-lactic acid) (PLLA) (Xu et al., 2004b). Electrospun cellulose acetate (CA) scaffolds have also been investigated and show promising results with ECs and other cells types (Entcheva et al., 2004; Liu and Hsieh, 2002; Ma et al., 2005b; Son et al., 2004). All of these scaffolds can support EC migration and proliferation. Whether these scaffolds support angiogenesis, tube formation or capillary sprouting have largely been ignored.

Dr. P. Gouma's laboratory has previously optimized the electrospinning process parameters to fabricate cellulose acetate scaffolds in three broad diameter ranges (Han and Gouma, 2006). These three cellulose acetate based scaffolds were made by altering the flow rate and electrospinning solution viscosity (Han and Gouma, 2006; Rubenstein et al., 2007). Other groups have fabricated scaffolds with the addition of material strengthening compounds like carbon nano-tubes (Mahfuz et al., 2006; Moore et al., 2004) and chitosan (Khan et al., 2000). We added these compounds for their reported effects on material strength (Rubenstein et al., 2007). A third scaffold was made with the potent angiogenic growth factor VEGF-165 (Favot et al., 2003; Herve et al., 2005; Koolwijk et al., 1996). The effect of these scaffolds on ECs has been investigated here.

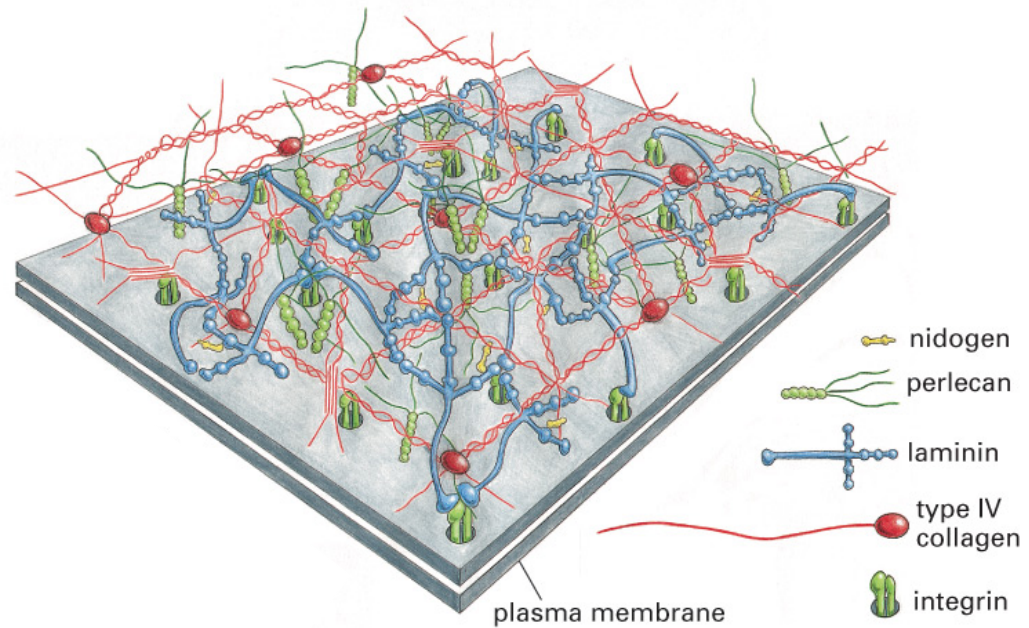


Figure 2.2: Schematic of the Basal Lamina. This figure shows the interactions of laminin and collagen IV within the extracellular matrix. Also, the binding of these proteins with the cell bound integrin receptors is also depicted. These molecules form a mesh-like structure that can inhibit the migration of cells. During angiogenesis this mesh must be broken down for EC migration to occur. This figure has been modified from (Alberts et al., 2001).

The apparent porosity of scaffolds that were within the fiber diameter range of 1-5 μ m was quantified (Rubenstein et al., 2007). This was evaluated by determining the effective hydraulic conductivity, \mathbf{K} , using Darcy's law, $U = -\mathbf{K} P$. U is the inline fluid velocity and P is the measured pressure across the scaffold. Steady state equilibration pressure was determined during constant flow across the scaffolding material over a range of pressures (Rubenstein et al., 2007). It was found that the addition of CNT or chitosan to the base cellulose acetate scaffold (1-5 μ m diameter) decreased the scaffold hydraulic conductivity (Rubenstein et al., 2007). This was attributed to the uneven distribution of CNT or chitosan throughout the scaffold. Apparent porosity was not measured for the other scaffolds because they did not perform well in culture conditions.

2.5.2 Directed Growth of Endothelial Cells – Topology

Directed growth of endothelial cells is a promising field in order to fabricate predetermined network structures, which can be incorporated into a vascular patch. Initial studies focused on guiding ECs using topographical features. These features were generally made through a combination of photolithography and soft-lithography. On silicone surfaces with micro- to nano-features EC actin filaments were seen to orient along the major axis of the features predominantly at focal adhesion sites (Uttayarat et al., 2005). Others have looked at the nature of the grooved topology to direct cell growth. Sinusoidal-like features, square features or triangular features on PDMS surfaces was used to study cell spreading and cytoskeleton arrangements (all features had a 10 μ m height) (Jiang et al., 2002). On all surfaces, ECs aligned along the major axis of the channel (Jiang et al., 2002). However, on square and triangular features more ECs were aligned than on the sinusoidal features (Jiang et al., 2002). Using PDMS molds (50 μ m feature size), controlled protein deposition was studied under laminar flow (Khademhosseini et al., 2004). They had the ability to control where polymers were deposited but they did not look into the extent of cell adhesion to the localized polymers (Khademhosseini et al., 2004). Similarly, angiogenic growth factors were used as a chemotactic molecule to direct the growth of ECs into 50 μ m channels (Kulkarni et al., 2004). ECs were found with a higher cell density within VEGF coated channels but they had not formed lumens (Kulkarni et al., 2004). Using physiological flow rates, within 10-30 μ m circular channels, HUVEC F-actin filaments align with the major direction of flow (Frame and Sarelius, 2000).

Other approaches used to direct the growth of ECs focus on modifying the surface of a particular substrate to enhance or inhibit cell adhesion. Using self-assembled monolayers of alkanethiolates that adhere to Fn, the attachment of ECs was guided to particular regions (Mrksich et al., 1996). With microcontact printing (Section 2.6.2) groups have been able to direct EC growth by using collagen I and IV (Falconnet et al., 2006; Jiang et al., 2002). Using these methods, cell adhesion and proliferation on microstamped proteins was investigated. Various cell types have been shown to have increased attachment to microstamped ECM proteins (den Braber et al., 1998; Matsuzawa et al., 1996). ECs also prefer 3-5 μ m Fn coated "islands" with hydrophilic glass intervening (Chen et al., 2003). EC proliferation is increased on larger patterns (Chen et al., 1997). This suggests that ECs would tend towards confluence on patterns of ECM proteins. Our aim was to exclude cells from the non-patterned region and obtain a high degree of confluent ECs on the microstamped pattern, during a short culture period.

Within grooved structures, ECs align with the groove axis, elongate with the groove, connect via gap junctions and begin to form tube-like structures (Britland et al., 1996; Clark et al., 1987; Clark et al., 1990; Craighead et al., 2001; Curtis and Wilkinson, 1997; Flemming et al., 1999; Jiang et al., 2002). In other studies, the changes in surface hardness on EC proliferation/migration were investigated. ECs prefer a softer substrates (Brown et al., 2005; Craighead et al., 2001). One group also investigated if surface charge effects the proliferation, orientation and shape of ECs in culture. They found that the cells did not have a preference towards positive, negative or neutral charges but they were more proliferative when the surface charge changed between positive and negative frequently (Brown et al., 2005). None of these studies investigated these properties with a tissue engineering/angiogenesis problem in mind.

2.5.3 Tissue Engineering of Blood Vessels

Some work has been done on the tissue engineering of blood vessels. In order to accomplish this ECs and VSMCs are cultured together to form patent blood vessels. Initial work focused on taking one cell and trying to induce tube formation (Buijtenhuijs et al., 2004; Neumann et al., 2003; Westerband et al., 2001; Xu et al., 2004c). Most of these groups had limited success with one cell type but upon introduction of the second cell type the vessel fails. These studies used cells that were taken from cell culture sources and not taken from a patient. This could lead to possible foreign body rejection. These studies did not investigate implantation biocompatibility. Our cells source is an autologous blood vessel and therefore there is the potential to form vascular networks without biocompatibility issues. However, one group has been able to tissue engineer a blood vessel from the patients own cells with limited success (L'Heureux et al., 1998). A critique of this method is that it takes a long amount of time (>3 months) to engineer the patent blood vessel.

2.5.4 Vascular Patches

Another approach to engineer replacement vascular networks is the fabrication of vascular patches. A vascular patch is defined as a patent vascular network within a biodegradable scaffold that can be directly implanted into the body. Vascular patches can possibly aid in the healing of chronic wounds. To date, the major shortcoming with this technique is the lack of a method to connect a fabricated patent vasculature to the native vascular network. Also a method to fabricate a patent vascular network within a biocompatible scaffold does not currently exist. Currently, scaffold based materials have been applied to chronic wounds to determine if vascular patches can aid in the formation of an *in vivo* vascular network healing a wound more efficiently (Iwai et al., 2005; Yang et al., 2006). The patch in these studies was avascular and the cells that had migrated into the patch typically die quickly. Therefore, the supply of oxygen and nutrients within the chronic wound is not enhanced and there is no added benefit to wound healing.

2.6 Fabrication Techniques

2.6.1 Electrospinning

Electrospinning is a process that takes a polymer in solution and through the application of a high voltage field, produces fibers from that polymer solution. This process was patented in the 1930's (Formhals, 1934; Formhals, 1939), but its application

to biology was much more recent. In order to electrospin a scaffold, first the polymer must be dissolved in a solvent. The polymer solution is placed into a syringe with a particular diameter metallic needle. The concentration of the polymer in solution governs the viscosity of the solution. A high voltage electric field is placed between the needle tip and a metallic collector. This voltage field needs to overcome the surface tension of droplets in order to make fibers. A syringe pump is used to generate a force on the polymer solution; expelling it out of the needle towards the collector. A schematic of an electrospinning apparatus (Figure 2.3), illustrates the critical parameters, the syringe pump flow rate, distance between the needle and the collector, viscosity of the polymer solution and the applied voltage fields. Variations in any of these parameters can change fiber characteristics (Liu and Hsieh, 2002) and these process parameters need to be carefully optimized. Electrospun fiber diameters normally increases with increasing flow rate, increasing needle diameter, decreasing voltage and decreasing distance between the tip and the collector (Liu and Hsieh, 2002). Generally an optimal polymer concentration exists, above and below which fibers do not form.

2.6.2 Photolithography and Soft-lithography

Photolithography is an optical technique to transfer geometric patterns onto a photosensitive substrate (Truskett and Watts, 2006). Standard photolithography uses six steps to fabricate a substrate; wafer cleaning, spin coating, soft bake, exposure, post-exposure bake and development. Wafer cleaning removes any dust, debris, proteins or any other molecules that may be on the surface of the silicone wafer (Qin and Li, 2003). The photosensitive substrate, photoresist, also adheres better to properly cleaned wafers (Qin and Li, 2003). There are four standard cleaning methods that could be used with silicone wafers; 1) Remote Chemical Analysis (R.C.A.), 2) Water-vapor Plasma, 3) *uv*/ozone and 4) Piranha Etch. All four methods clean wafers to similar extents and the resist can coat these cleaned wafers similarly (Donose et al., 2006).

There are two different types of photoresist that can be used in photolithography; positive and negative photoresists. For a positive photoresist, the combination of the incident *uv* light and the developer breaks molecular bonds in an exposed region (Kovarik and Jacobson, 2006). (The photoresist which is exposed to *uv* light is removed after development.) A negative photoresist is the opposite. The incident light cross-links molecules in the exposed region and the developer removes the uncross-linked resist (Kovarik and Jacobson, 2006). There is no advantage/disadvantage in using a positive or a negative photoresist. The choice of the resist is normal based on the mask that has been fabricated and which application suits the needs of the researcher best.

Here we choose to use the negative photoresist SU-8. It has been previously used to fabricate three dimensional structures on the micro- and nano-scale (Kovarik and Jacobson, 2006). Also, there is some precedence in the literature for this photoresist to be used in making microfluidic devices (Wu et al., 2005) that have been used for blood typing (Kim et al., 2006). In these two articles (Kim et al., 2006; Wu et al., 2005), flow was incorporated into the fabricated device to measure biological phenomena.

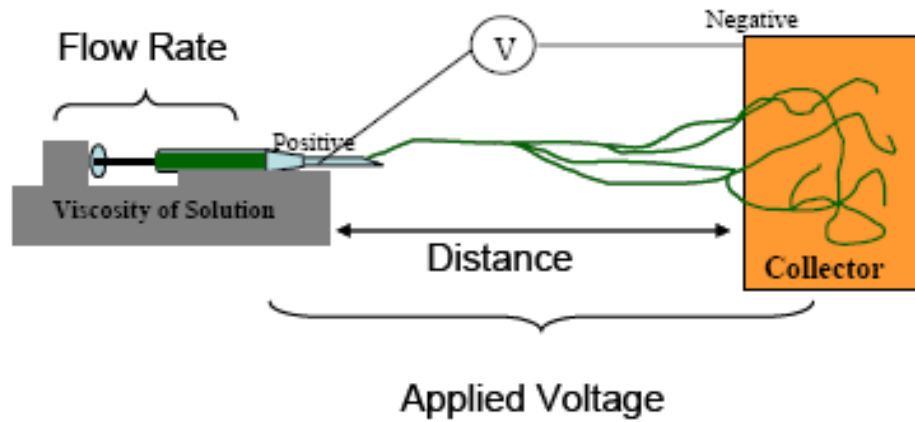


Figure 2.3: Schematic of an Electrospinning Apparatus. To make an electrospun scaffold a polymer solution is ejected from a syringe pump at a particular flow rate towards a metallic collector. The polymerized scaffold traverses through air across a high voltage field. Changing any of these process parameters will affect scaffold characteristics. We have fabricated three base polymers by changing the viscosity and the flow rate of the scaffold. Various materials were added to the electrospinning solution to test the effects of these materials. Original figure from M. Frame.

Spin coating is the process by which the photoresist is applied to the cleaned silicon wafer and is evenly distributed on the wafer. The resist is manually dispersed onto the wafer and is spread across the wafer at low revolutions per minute (rpm) (generally lower than 500rpm). A second spin cycle is used to make an even film thickness across the entire wafer (Microchem Corp., 2002). This is generally at higher rpm (>1000rpm). Next the wafer and the applied photoresist are soft baked to evaporate the solvent and increase the density of the photoresist film (Microchem Corp., 2002). SU-8 photoresist has been optimized for exposure at the near *uv* light wavelength range of 350-400nm. Within this range the resist can absorb the most energy from the light source (Microchem Corp., 2002). After exposure the wafer and resist are baked again to selectively cross-link the exposed portions of the SU-8 photoresist (Microchem Corp., 2002). The resist is developed to remove the unexposed and therefore uncross-linked resist (Microchem Corp., 2002). Figure 2.4 illustrates the steps during photolithography; highlighting the differences between a positive and a negative photoresist.

Soft-lithography is used to make the negative imprint of the photolithography end product. Polydimethylsiloxane (PDMS) has been used widely as the polymer to make these imprints. PDMS is relatively inexpensive, inert, non-immunogenic and easy to work with (Loesberg et al., 2005). PDMS can be molded into any shape or size, provided that the master has the features of interest (Jiang et al., 2002). Microfluidics has been studied extensively with PDMS molds (Hisamoto et al., 2004). To make a PDMS mold, the elastomer curing agent is mixed with the base elastomer. The curing agent cross-links the base elastomer forming a semi-rigid structure. After curing, the features of interest are transferred onto the PDMS mold.

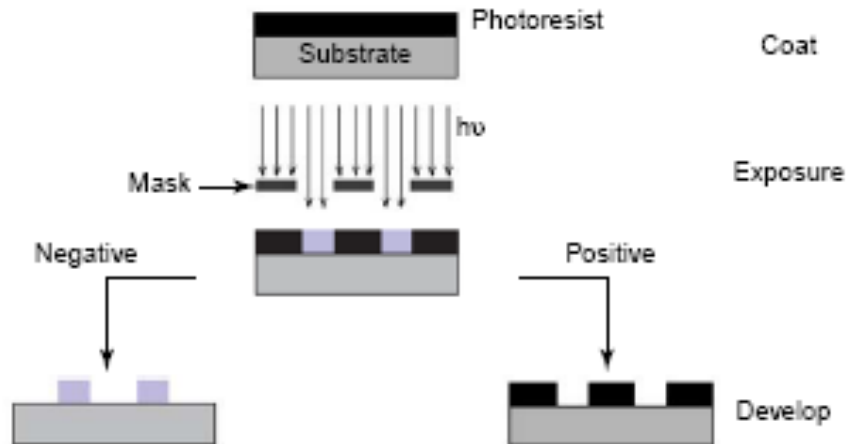


Figure 2.4: Schematic of the Photolithography Process. After spin coating the resist has a uniform thickness across the entire wafer. A mask is used to block certain areas from uv light exposure. The exposed resist and wafer are then developed and depending on the type of resist that is chosen there are two patterns that can be fabricated. The gray shaded area illustrates where the chemical properties of the resist have been altered. This figure has been modified from (Truskett and Watts, 2006).

2.6.3 Microcontact Printing

PDMS is the material of choice to make a stamp for microcontact printing. In microcontact printing a protein of interest is transferred from the stamp to a glass coverslip (Sharpe et al., 2006). The chemical (or protein (Rozkiewicz et al., 2006)) is allowed to partially dry on the stamp before transfer and then the substrate (normally glass) that the pattern will be transferred to is brought into contact with the stamp. This will transfer the chemical/protein onto the substrate (Figure 2.5). The geometry is retained during this transfer procedure (Wang et al., 2005) but the feature size may vary slightly due to surface interactions of the substrate and the stamped molecule. There are many examples of microcontact printing being used to direct migration or growth of particular cells. Proteins (Schmalenberg et al., 2004) have been used to guide the growth of neuronal (Thiebaud et al., 2002), endothelial (Jiang et al., 2002) or cancerous cells (Rozkiewicz et al., 2006). Others have shown that ECs can be partially excluded from hydrophobic surfaces (Iuliano et al., 1993). Cell adhesion and ECM formation was significantly reduced on these surfaces (Iuliano et al., 1993). Sigmacote® has been used in studies to rapidly produce hydrophobic glass surfaces with a contact angle of $\sim 100^\circ$ (Chapeau and Gagnon, 1987; Krylov and Dovichi, 2000). In the studies presented here, an ECM protein has been stamped onto hydrophilic or hydrophobic glass substrates in order to study the directed growth of ECs.

One of the major disadvantages of this technique is the choice of a material to use as a stamp. A material that is both rigid and soft is needed in order to accurately transfer the molecule in the geometry of interest (Falconnet et al., 2006). The material needs to be rigid to maintain the geometry but soft so that there is no voids when stamping (Falconnet et al., 2006). PDMS microstamps meet both of these requirements. Also, it is difficult to fabricate a stamp that has complex features in high density, using an elastomer such as PDMS because after curing it is likely that the PDMS is structurally weak and can break during peeling (Falconnet et al., 2006). Although there are some drawbacks to this method, we use it here because structures can be made rapidly and maintain the molded surface features. Also, a large quantity of substances can be applied to the stamp and transferred onto glass for use in cell culture.

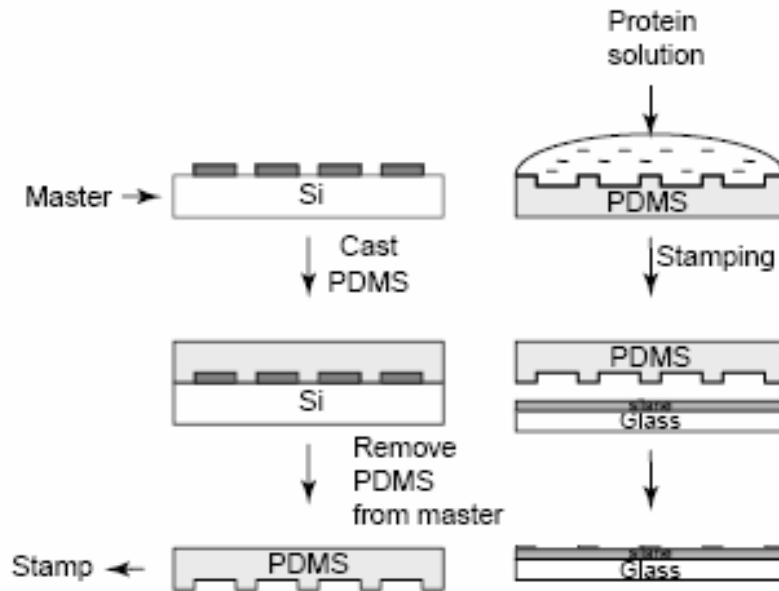


Figure 2.5: Schematic of Soft-Lithography and Microcontact Printing. After photolithography PDMS is cured over a master. The PDMS is removed from the master with the negative imprint of the master. A protein of interest is placed on the stamp and allowed to partially dry before printing onto a glass slide. For our studies, we used extracellular matrix proteins to guide the growth of endothelial cells. This figure is from (Truskett and Watts, 2006).

SECTION III: METHODS AND MATERIALS

3.1 Fabrication Techniques

3.1.1 Scaffold Preparation

3.1.1.a Electrospun Scaffolds

All electrospinning procedures were conducted by me in Dr. P. Gouma's Center for Nanomaterials and Sensor Development Lab under her training. Cellulose acetate (CA, average molecular weight of 29,000kD) with 40% substitution by acetyl groups was used as the base polymer (Sigma Aldrich, St. Louis, MO) for electrospinning. CA was dissolved in acetone (A, 99.5%, Sigma) 1 to 2 hours prior to electrospinning. The solution was mechanically stirred (for ~15 minutes) to ensure that the CA completely dissolved in the A. Previously, the process parameters for electrospinning were optimized to fabricate three base CA scaffolds (Han and Gouma, 2006). Each base scaffold had a characteristic fiber diameter which ranged from 0.01-0.2 μ m, 0.2 -1 μ m or 1-5 μ m (Han and Gouma, 2006). Two compounds were added to the electrospinning solution under the assumption that they would make the material stiffer; carbon nanotubes (Mahfuz et al., 2006; Moore et al., 2004) (CNTs, Carbon Solutions, Inc., 80-90% pure) and chitosan (Khan et al., 2000) (low molecular weight, 20-200cP viscosity, Sigma). VEGF (VEGF-165, Sigma), a potent angiogenic growth factor was also added prior to electrospinning. Electrospun solutions with additives were mechanically stirred for ~1 hour to ensure that CNT or chitosan dissolved completely. Also, chitosan can easily come out of solution therefore these scaffolds were electrospun within 5 minutes after mechanical stirring. Table 3.1 shows the electrospinning solutions and the process parameters used for each scaffold. For one electrospun scaffold composition, the material was fabricated and then fibronectin (Fn, 3.4 μ g/mm²) was added to the formed scaffold. This scaffold was made with the same process parameters to generate a CA180 scaffold and then in a laminar flow hood, Fn was allowed to dry on the scaffold for >30 minutes. The nomenclature that we use to describe our base scaffolds is CA (for cellulose acetate) followed by the flow rate that was used to fabricate the scaffold (i.e. 180) or the additive to the electrospun solution/formed scaffold (i.e. chitosan). The void space and the surface area to volume ratio for CA180 and CA+1.6% chitosan scaffolds were calculated using formulations from G. Bowlin's group (Boland et al., 2004). The effective hydraulic radius for our scaffolds (measured from SEM images) was used in these formulations. The effective hydraulic radius was 1.25 μ m and 1.02 μ m for CA180 and CA+1.6% chitosan, respectively.

Material composition	Composition	Flow Rate ($\mu\text{L}/\text{min}$)	Distance (cm)	Voltage (kV)
1-5μm Fiber Diameter Range				
CA*180	CA (1.65g) / A* (10ml)	180	15	12
CA + 3.3% CNT*	CA (1.5g)/ A (10ml) / 0.05g CNT	100	15	12
CA + 1.6% chitosan	CA (1.5g)/ A (10ml) / 0.025g chitosan	100	15	12
CA + 3.4 $\mu\text{g}/\text{mm}^2$ Fibronectin	Made as CA180 with the addition of 3.4 $\mu\text{g}/\text{mm}^2$ fibronectin after electrospinning.			
0.2-1μm Fiber Diameter Range				
CA80	CA (1.5g) / A (10ml)	80	15	12
CA + 1.7% CNT	CA (1.5g)/ A (10ml) / 0.025g CNT	100	15	12
0.01-0.2μm Fiber Diameter Range				
CA40	CA (1.0g) / A (10ml)	40	15	12
CA + 0.0013% VEGF*	CA (0.75g) / A (5ml) / VEGF (10 μg)	100	15	12

Table 3.1: Summary of Electrospun Scaffold Process Parameters and Composition. *CA, cellulose acetate; A, acetone; CNT, single-walled carbon nanotubes; VEGF, vascular endothelial cell growth factor (13ng/cm²); all % composition is by dry weight of minor component to CA. Nomenclature for scaffolds: CA180 = cellulose acetate with a flow rate of 180 $\mu\text{L}/\text{min}$, CA80 = cellulose acetate with a flow rate of 80 $\mu\text{L}/\text{min}$ and CA40 = cellulose acetate with a flow rate of 40 $\mu\text{L}/\text{min}$ or CA + the additive (i.e. chitosan). This table has been modified from (Rubenstein et al., 2007).

To electrospin our scaffolds, 1mL of the electrospinning solution was placed in a glass syringe with a 20 gauge metallic needle. The syringe and needle were attached to a syringe pump to force the solution out of the syringe at a calibrated flow rate. The tip of the needle was kept 15cm away from a metallic collector, covered with aluminum foil. The aluminum foil was finely coated with oil (WD-40 Company, San Diego, CA) to prevent the electrospun scaffold from adhering to the aluminum foil after electrospinning. (Prior to electrospinning, aluminum foil was wiped with a towel, to remove excess oil.) A positive electrode was placed at the tip of the metallic needle and a negative electrode was placed on the collector. At the same time, the syringe pump was started and a high voltage field (12kV) was placed across the tip and the metallic collector (Figure 2.3). The entire 1mL of the electrospun solution was expelled from the syringe to fabricate 1 scaffold. During electrospinning, occasionally a solid particle blocked the metallic needle. To remove the particle, the voltage field was turned off and the tip cleaned with an acetone coated towel. When cleaned the voltage field would be re-applied.

Scanning electron microscopy (SEM) was used to image scaffolds to determine the characteristic fiber morphology. SEM images were obtained by Dr. J. Quinn (Department of Materials Science and Engineering). Scaffolds were coated for 20 seconds (x2) with plasma phase gold. A LEO 1550 electron microscope (Zeiss, Germany) was used. 3-5 4cm² samples of each scaffold were imaged to obtain characteristic fiber diameter. Each sample was taken from a different location in order to determine if there were differences in scaffold morphology based on collector location. ProAnalyst, (V. 1.1.9.0, Xcitex Inc., Cambridge, MA) was used to obtain characteristic fiber diameter by measuring the long axis width of ~35 fibers per SEM image. The thickness of each scaffold fiber was also estimated. Characteristic fiber diameter for our base scaffolds was quantified elsewhere (Han and Gouma, 2006) and verified here.

Mechanical testing of electrospun scaffolds was conducted by IMR Test Labs (Lansing, NY). Scaffolds were cut to 1in x 1in square and placed on the platform for compression testing using a 2.795mm probe (TA Instruments Thermomechanical Analyzer model Q400, New Castle, DE). Due to the nature of the surface of electrospun scaffolds, the probe was lowered onto the scaffold until a preload of 0.001N was established. This point was considered as the zero displacement location. The compressive force was controlled at 0.1N/min, displacement is the output. Stiffness and the compressive modulus were calculated over the linear region.

3.1.1.b Sylgard® 184 Scaffolds

PDMS scaffolds were prepared using a mixture of 10 part silicone elastomer and 1 part curing agent (by weight) (Sylgard®, Dow Corning, Midland, MI). These solutions were manually mixed for 5 minutes. This was then degassed for >30 minutes and then poured onto our mold of interest. The PDMS scaffold was fabricated with triangular grooves on the surface (Figure 3.1, molds donated from Dr. E. Entcheva). The height of our grooves was 10µm with a base width of 46µm. The apex of each groove was 76µm apart. The template and the PDMS were placed in an isotherm incubator set at 50°C (VWR International, West Chester, PA). Curing at 50°C took place for 2 hours and then at room temperature (~25°C) for 48 hours. These scaffolds were soaked in ethanol; rinsed in water and placed under *uv* light prior to their use. PDMS scaffolds were not used for 7 days after curing to allow solvent release from the material.

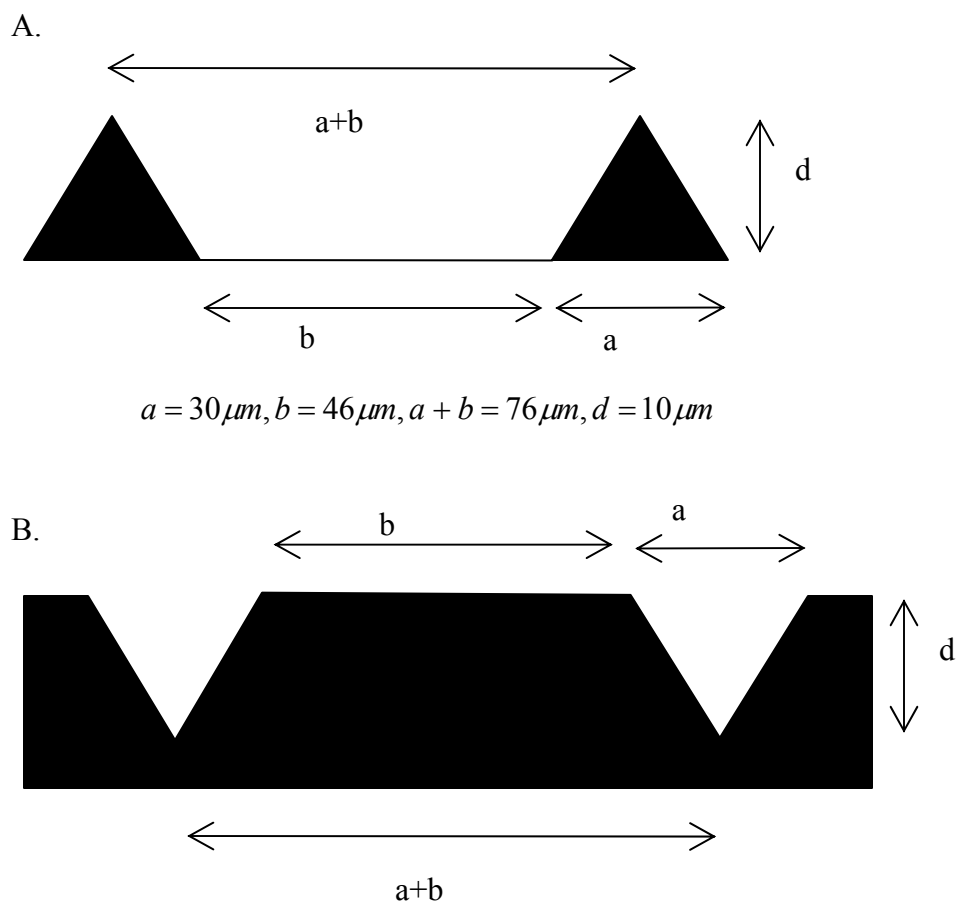


Figure 3.1: Schematic of Grooved PDMS Scaffolds used within the Bioassay Chamber. PDMS was cured around grooved templates (A) donated from Dr. E. Entcheva. Negatives of these templates (B) were used in cell culture experiments to investigate the addition of $3.4\mu g/mm^2$ fibronectin to formed scaffolds. Schematic is not drawn to scale.

3.1.1.c Matrigel® Scaffolds

ECM gel (Matrigel®, Sigma) was prepared from Engelbreth-Holm-Swarm sarcoma produced in mice. The extracellular matrix protein concentration was 8-12mg/mL in these preparations. Matrigel® is comprised of approximately 60% laminin and 30% collagen IV. Heparan sulfate proteoglycan and entactin make up the remaining portion of the preparation. Matrigel® was kept at -20°C, until 1 day prior to use where 1 aliquot would be placed at 4°C for ~12 hours. This allowed for the Matrigel® to thaw slowly. Once Matrigel® became a liquid, it was poured over a cannulated blood vessel (100µL) at 37°C and allowed to gel for 15 minutes. A second aliquot of Matrigel® (100-250µL, depending on the size of the vessel) was poured over the explant and allowed to gel at 37°C for 15 minutes prior to perfusion of the cannulated blood vessel (Section 3.3). In cell culture, liquid Matrigel® (100µL) was placed on a clean glass coverslip and allowed to gel at 37°C for 15 minutes. Cells were seeded within the well containing the Matrigel® coated coverslip (Section 3.2).

3.1.2 Lithography Techniques

3.1.2.a Photolithography

All photolithography techniques were conducted by me in Dr. Helmet Strey's Nanostructure and Biophysics Laboratory under his instruction. Silicone wafers (MEMC, St. Peters, MO) with a minimum resistivity of 2Ωm and a maximum resistivity of 20Ωm were used as the photoresist substrate. These wafers were chosen because they have a uniform thickness across the entire area. The thickness of individual silicone slices was between 19-21mm with a circular diameter between 75.7-76.7mm. Prior to photolithography, silicone wafers were cleaned separately using the RCA cleaning technique, developed at RCA laboratories. The first part of the cleaning procedure uses 5 parts deionized water (dH₂O), 1 part 27% ammonium hydroxide (NH₄OH, Fisher Scientific, Fairlawn, NJ) and 1 part 30% hydrogen peroxide (H₂O₂, Fisher). dH₂O and NH₄OH were warmed to 70°C on a contact hot plate (Fisher). H₂O₂ was added when the solution reaches 70°C, causing the solution to bubble. The silicone wafer was soaked in this solution for 15 minutes and then cleaned with dH₂O (5 minutes). The second cleaning solution consists of 6 parts of dH₂O, 1 part 27% Hydrochloric Acid (HCl, Fisher) and 1 part 30% H₂O₂. dH₂O and HCl were warmed to 70°C and H₂O₂ was added once the solution reaches 70°C. The silicone wafer was soaked in this solution for 15 minutes. The wafer was removed and rinsed for 5 minutes in dH₂O. Wafers were dried with a steady stream of argon gas and then kept in sterile Petri dishes at low humidity (23%; range 1-40%). Cleaned wafers were used within 2 hours.

Cleaned wafers were coated with SU-8 2100 negative photoresist (Microchem, Newton, MA). Silicone wafers were placed on a spin coater (Laurell Technologies Corp., North Wales, PA, Model: WS-400B-6NPP/Lite) under vacuum pressure. Approximately 5mL of SU-8 2100 was placed on the wafer. Photoresist was spread manually to cover the entire surface of the wafer; some bubbles formed due to the high viscosity of the SU-8. Wafers with photoresist were spun at 500rpm for 30 seconds (accelerated at 100rpm/sec). This spin cycle was used to spread the photoresist evenly over the entire surface of the wafer and remove bubbles. Wafers were then spun at 1000rpm for 30 seconds (accelerated at 300rpm/sec). This spin cycle was used to level the photoresist to a uniform thickness of ~260µm. The wafer was then baked on a

contact hot plate at 65°C for 7 minutes and then 90°C for 60 minutes. This “soft-bake” removes the organic solvents from the photoresist and increases the efficiency at which the photoresist can absorb *uv* light energy.

The “soft-baked” wafer/photoresist was placed on the vacuum assembly of a contact aligner (Newport, Irvine, CA). The mask of interest was placed in the mask aligner. Masks were chosen to expose the entire wafer except the area that had our geometry of interest (mask feature size was 50-150µm). The wafer and photoresist were placed in contact with the mask using a micromanipulator. The photoresist was exposed with a *uv* light source (Newport) for 5.2 seconds at 76mW/cm² (a total of 400mJ/cm² of energy was delivered to the photoresist). After exposure the wafer/resist was baked at 65°C for 1 minute and 95°C for 15 minutes on a contact hot plate. Following this post-exposure bake, resists were developed with SU-8 developer (Microchem) for 20 minutes. The wafer was gently agitated during development to facilitate the removal of the resist from the silicone wafer. After development the wafer was washed in isopropyl alcohol for 2 minutes. It was gently agitated during this wash. Wafers were dried with a gently stream of argon gas and placed in sterile Petri dishes.

3.1.2.b Soft-lithography

Polydimethylsiloxane (PDMS) positive molds were made from the negative photolithography end products. PDMS (Dow Corning, Sylgard 184) was mixed 10:1 by weight of the silicone elastomer base: silicone elastomer curing agent. This was mixed manually for 5-10 minutes to ensure the even disbursement of the curing agent throughout the base elastomer. The mixed PDMS was degassed for ~30 minutes and then poured over the wafer to a thickness of 0.5cm. PDMS was baked at 50°C for 2 hours and then allowed to finish curing at room temperature (22-25°C) for 48 hours. PDMS was pulled away from the wafer and kept in a sterile Petri dish. PDMS did not adhere well to silicone wafers or to photoresist. Therefore, each silicone wafer coated with photoresist (i.e. photolithography end-product) could be used multiple times.

SEM images of the positive PDMS molds were taken with a LEO 1550 electron microscope (Zeiss, Germany) using the services of Dr. J Quinn (Department of Materials Science and Engineering, Stony Brook University). PDMS molds were coated with gold for 20 seconds (x3) to make the surface electrically active. Images were obtained for each different mold that we fabricated with photolithography/soft-lithography (Figure 3.2). Feature sizes were measured using ProAnalyst (V1.1.9.0) and recorded to determine stamp widths.

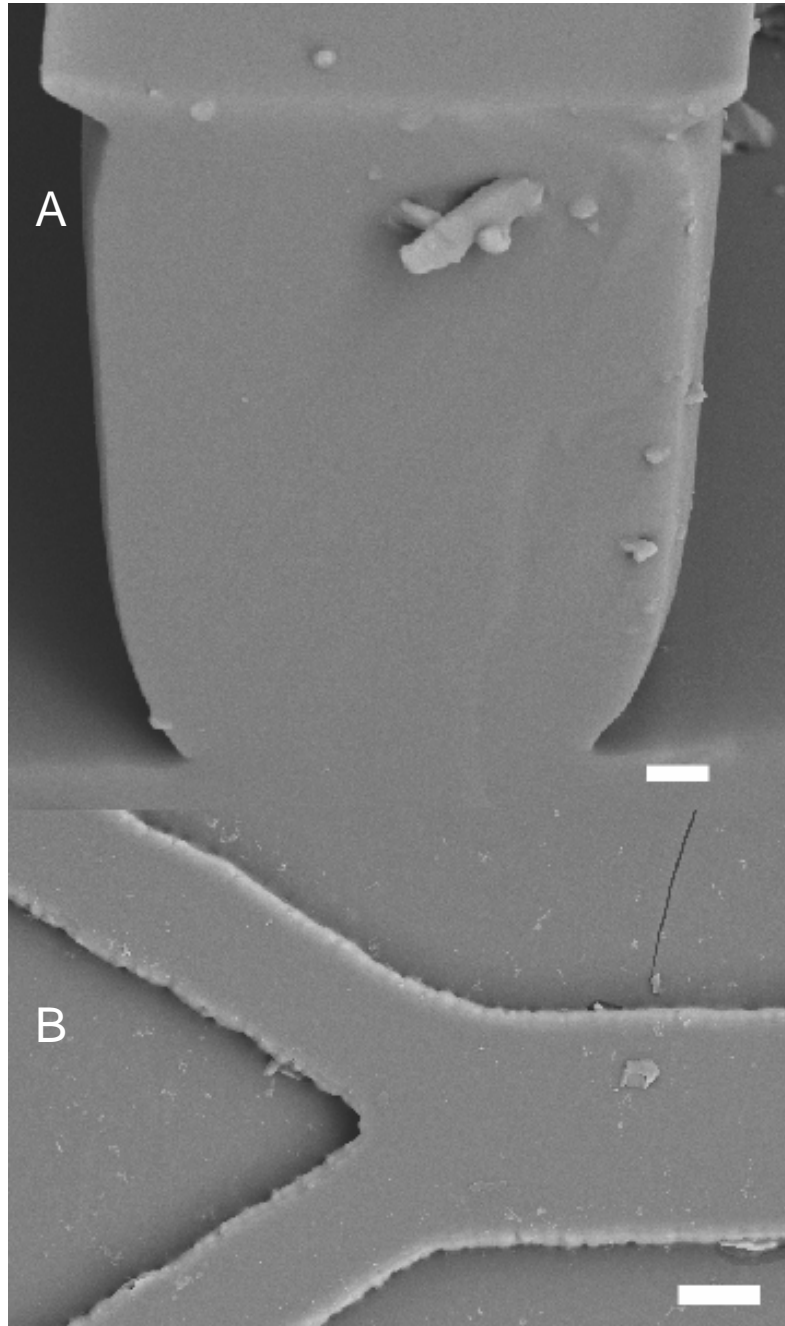


Figure 3.2: Scanning Electron Microscopy Image of Gold Sputtered PDMS Stamps. These images were used to measure the feature size of the PDMS stamps prior to microstamp methods. Pillars (A) or Y-branches (B) were molded to test directed growth of endothelial cells. Scale bars are 10 μ m (A) or 20 μ m (B). These images were taken by Dr. J. Quinn from the Department of Materials Science and Engineering at Stony Brook University.

3.1.3 Surface Modifications

3.1.3.a Microstamp

PDMS microstamps were cleaned in ethanol and allowed to dry prior to use. In a laminar flow hood, collagen I, IV, or laminin each at $5\mu\text{g}/\text{mm}^2$ or fibronectin at $3.4\mu\text{g}/\text{mm}^2$ was pipetted onto the positive features of the PDMS stamp. XRITC (substituted tetramethyl rhodamine isothiocyanate, 546MW, Molecular Probes, Eugene, OR) was mixed with each protein at a final concentration of 1×10^{-7} M. XRITC was used to determine the stamped feature size and to locate the stamped region after cell culture or bioassay chamber experiments. Proteins and XRITC were allowed to dry on the PDMS surface for ~ 10 minutes at room temperature (25°C) before attempts to stamp the solution. Excess solution was aspirated off the stamp prior to drying. Before the proteins and XRITC were completely dried on the PDMS surface, the PDMS stamp was placed onto the stamping apparatus. A cleaned glass coverslip (hydrophilic or hydrophobic) was brought into contact with the stamp using a KITE-R micromanipulator (WPI Inc., Sarasota, Florida) (Figure 3.3). Proteins were transferred, in the pattern of interest, onto the glass coverslip. The stamped protein and XRITC was allowed to dry completely on the glass coverslip at room temperature; typically within 10 minutes. Stamped patterns were marked on the glass for later verification (in conjunction with the XRITC). After drying, the average microstamp transfer width was determined using XRITC. The glass coverslips were then placed into a cell culture well or adhered to a bioassay chamber for studies investigating the directed growth of endothelial cells.

In one series of experiments, Fn at $3.4\mu\text{g}/\text{mm}^2$ was microstamped onto CA180 scaffolds, to investigate the combination of topological and topographical cues in the bioassay chamber. A *uv* light sterilized CA180 scaffold was placed under the microstamp and the stamp was then brought into contact with the scaffold. The scaffold was then draped over the cannulated blood vessel with the microstamped region being aligned with the open side branch of the vessel.

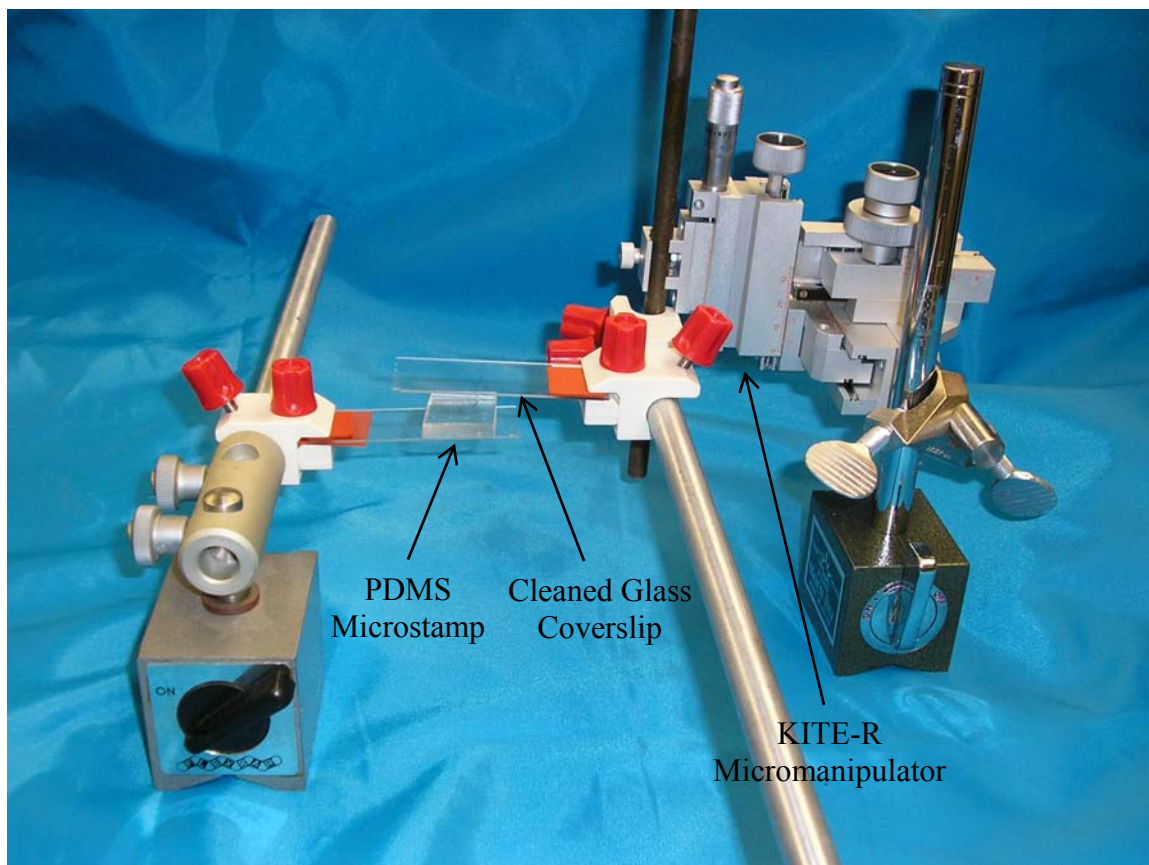


Figure 3.3: A Picture of the Stamping Apparatus. A combination of photolithography and soft-lithography was used to make stamps that tested the directed growth of endothelial cells. ECM proteins were allowed to partially dry on the PDMS microstamp. A KITE-R micromanipulator was used to bring a cleaned glass coverslip into contact with the “inked” stamp. The coverslip was removed from the stamp rapidly. The transferred protein was then allowed to fully dry on the glass before the experiment.

3.1.3.b Hydrophilic/Hydrophobic Glass Washing

Hydrophilic glass coverslips were prepared 1-2 weeks prior to use in cell culture or the bioassay chamber. Coverslips were cleaned with 70% ethanol containing 0.35M HCl for 30 minutes. These coverslips were immersed in sterile dH₂O three times (10 minutes for each cleaning cycle) and then kept in a clean Petri dish with sterile dH₂O (Yayapour and Nygren, 1999). Hydrophobic glass coverslips were prepared from hydrophilic coverslips ~1 week prior to the experiment. In a laminar flow hood, each coverslip was coated with ~2mL of Sigmacote® (Sigma) (Krylov and Dovichi, 2000; Vazquez et al., 2006). Sigmacote® is a chlorinated organopolysiloxane stored in heptane, which produces a thin hydrophobic film on glass. Water droplet contact angle has previously been measured between 90-100° for undiluted Sigmacote® (Chapeau and Gagnon, 1987; Elena Diaz and Cerro, 2004); however, we measure larger angles (Sections 3.1.3.c and 4.1.2). Coverslips were stored in a clean, dry dish within a laminar flow hood. Prior to cell seeding or cannulation (Sections 3.2.3 and 3.3.2) coverslips were cleaned with ethanol and then dH₂O. This removes any HCl from the coverslip that appears as a by-product of the silicization procedure. Coverslips were dried and placed on the stamping apparatus immediately.

3.1.3.c Contact Angle Measurements

The contact angle for a water droplet was measured by me for both hydrophilic and hydrophobic glass coverslips in Dr. M. Rafailovich's laboratory (Department of Materials Science and Engineering, Stony Brook University). A CAM 200 Optical Contact Angle and Surface Tension Meter (KSV Instruments Ltd., Finland) were used to measure the contact angle of a water droplet on each surface. Briefly, the stage of the meter was insured to be level by optical means. 1 glass sample was then placed on the stage and a 5µL drop of water was placed on the glass. Using the CAM software (KSV) the water droplet was focused on and a digital image of this drop was taken. Using a curve fitting method the contact angle on both the left and right side of the droplet was calculated. An error of more than 0.1% in the fit curve is considered unacceptable. A new digital image would be taken if this error rate was surpassed.

3.1.4 Design Criteria and Fabrication of Bioassay Chamber

My key design goal was to build a bioassay chamber that would be able to maintain the viability of a cannulated explanted blood vessel. One constraint was the ability to monitor angiogenic processes within the bioassay chamber. A calibrated flow rate to perfuse the cannulated blood vessel was necessary. Further, there were geometric constraints on the internal and external compartment (i.e. area) of the bioassay chamber, based on 1) the area of a modified PL1 platform (Warner Instruments, Inc., Hamden, CT) and 2) the dimensions of an explanted vessel. The PL1 platform was chosen to secure my bioassay chamber so that the external area was constrained to ~8cm x 4cm. Explanted vessels were ~0.3cm in diameter (with side branch length add ~0.3cm) and ~2cm in length. To include the access to inflow/outflow ports and scaffold area, the internal area of the bioassay chamber was constrained to ~3cm x 1.5cm. The perfused explant was required to be isolated from environmental/biological contamination but be in equilibrium with the surrounding atmosphere (air temperature, pressure and humidity). The bioassay chamber itself must be compatible with explanted blood vessels. The

ability to incorporate multiple tissue engineered scaffolds was also required. Our primary scaffolds were electrospun CA, PDMS or Matrigel® scaffolds. The scaffolds and the explant needed to be within the working distance of our inverted microscope (Diaphot 200, E400, Nikon, Japan) so that experimental end points can be quantified without altering the natural geometry of the scaffold and explant. This constrained the height of the inflow and outflow access points to the chamber.

A polydimethylsiloxane elastomer (Sylgard® 184, “PDMS”, Dow Corning,) was chosen as the material to fabricate the bioassay chamber. PDMS was chosen because it can be cured into any geometry and after curing the geometry can be easily modified to my constraints. Also, it does not elicit immune responses and is biocompatible (Yin et al., 2004). PDMS will rapidly become equilibrated with the surrounding environment (temperature, pressure and humidity) because the cured elastomer allows for air and heat to pass through it (De Coensel et al., 2006). However, contaminants in the atmosphere do not pass through the cured PDMS structure (De Coensel et al., 2006).

A mixture of 10 parts silicone elastomer with 1 part curing agent (by weight) was used to fabricate my bioassay chamber. The mixture was manually mixed for 5-10 minutes and was then degassed for 30 minutes. The degassed PDMS was poured into our mold (~0.5cm thickness) and allowed to cure for 48 hours (the first 2 hours was at 50°C and the remaining time was at room temperature). Molds were outlined with beeswax to our specified dimensions. Two 16G I.V. catheters (Medex, CA) were placed through the beeswax minimizing the distance between the bottom of the bioassay chamber and the catheter. Openings of the catheters were sealed with beeswax so PDMS would not cure within the catheter. After curing, catheters were imbedded within the PDMS bioassay chambers (a tight seal forms between the cured Sylgard® and the Teflon catheters). These catheters were used as inflow and outflow ports for the bioassay chamber. Leur locks manufactured on catheters protruded from the outside of the bioassay chamber to be used for quick external tight connections to the inflow perfusate and the outflow waste removal. After curing, chambers were removed from the mold and any remaining beeswax was removed with boiling water; water was also forced through the catheters to remove beeswax. The external area was cut to 4cm x 7cm x 0.5cm (width, length and thickness) and the internal area was cut to 1.5cm x 3cm x 0.5cm (± 0.2 cm on all dimension) (Figure 3.4). Cured chambers were not used for 7 days to allow for solvent removal. Chambers were soaked in ethanol overnight, cleaned with water and then placed under *uv* light in a laminar flow hood prior to cannulation. Chambers were used until the leur locks on catheters failed (~6 months) due from *uv* light exposure.

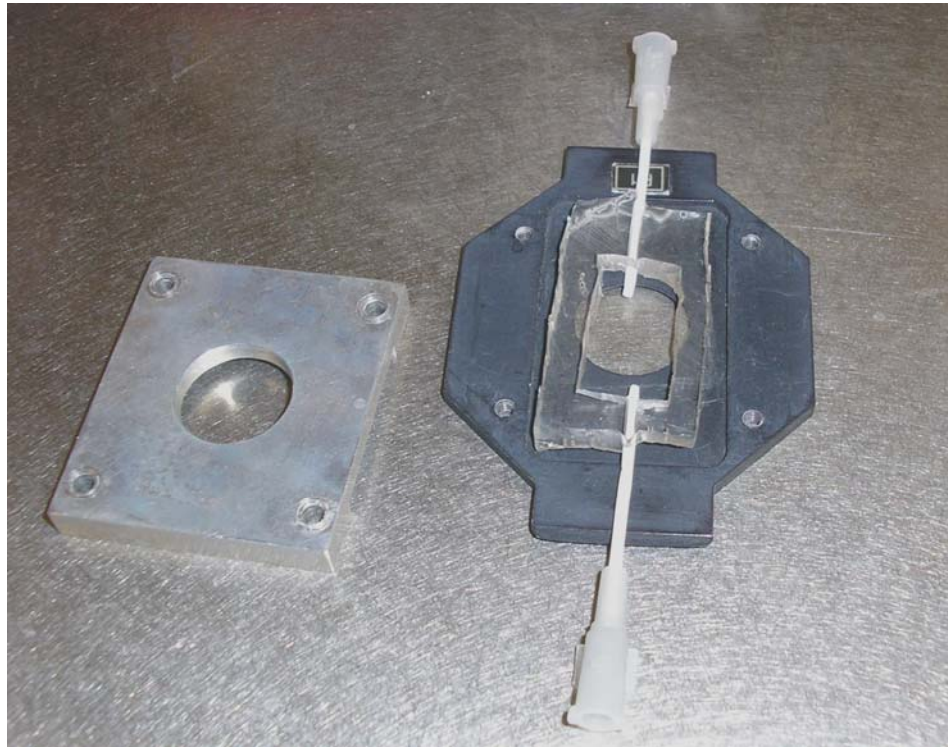


Figure 3.4: A Picture of a Cured Bioassay Chamber with our Modified P1 Platform. PDMS was used to fabricate a novel bioassay chamber that can be used to monitor the progression of angiogenesis. Catheters with leur locks were used for easy access to inflow perfusate and outflow waster removal. A modified P1 platform was used to firmly seal glass coverslips (not shown) to the bioassay chamber.

3.2. Endothelial Cell Culture

3.2.1 Culture of Human Umbilical Vein Endothelial Cells

HUVECs were obtained from Dr. M. Furie's lab at passage 1 or 2. These cells were isolated from healthy umbilical veins as described elsewhere (Furie et al., 2000; Sellati et al., 1996). HUVECs were used between passages 2 through 5 (cell passage is defined as population doubling) as a deliberate test of how cell passage can affect cell viability, density and morphology within our scaffolds. Immediately after cells were obtained, media was removed and exchanged with our HUVEC medium (McCoy's 5A Medium, 20% FCS, 100µg/mL Heparin, 50µg/mL Endothelial Cell Growth Supplement, 2mM L-glutamine 0.5U/mL Pen and 0.5µg/mL Strep, Sigma). These cells were maintained on T-25 culture flasks at 37°C and 5% CO₂ at all times except when cells were fed, passaged or imaged (room equilibrated air). Cell feeding and passaging took place within a sterile laminar flow hood. Cell media was changed 3 times a week (Monday, Wednesday and Friday) by gently tipping the culture flask to one side and aspirating the old media off. 4mL new media was immediately added and the cells were placed back at 37°C and 5% CO₂. Media was warmed to 37°C before feeding. Using transmitted light, it was determined if the cells were still attached to the flask.

3.2.2 Culture of Human Dermal Microvascular Endothelial Cells

Human dermal microvascular endothelial cells (hDMECs) were purchased from Cambrex Corporation (East Rutherford, NJ) or ScienCell Research Laboratories (San Diego, CA). Upon arrival, hDMECs were passaged 1:1 onto a new T-25 0.2% gelatin coated flask. Gelatin was coated on the flask for a minimum of 15 minutes prior to cell seeding. (cell passage was by trypsin digestion, Section 3.2.3). Cells arrived in basal Endothelial Growth Media – Microvascular (EGM-MV). This was exchanged upon arrival with our hDMEC media (EGM-MV, 5% FBS, 50µg/mL Endothelial Cell Growth Supplement, 0.5U/mL Pen and 0.5µg/mL Strep, Sigma). hDMECs were maintained at 37°C (with 5% CO₂) at all times except when feeding or passaging cells (when cells were within a sterile laminar flow hood) or imaged after experiments (37°C and room air). Media was exchanged 3 times a week (Monday, Wednesday and Friday) by gently tipping the culture flask to one side and aspirating the old media off. 4mL new hDMEC media, warmed to 37°C, was added to the cells. Using transmitted light, it was determined if the cells were still attached to the flask after feeding.

3.2.3 Passage of Endothelial Cells

HUVECs or hDMECs were passed at confluence to either 3 T-25 culture flasks or experimental 8 well chambers (Nalge Nunc, VWR Scientific). To passage confluent cells into new cell culture flasks, old media was aspirated off the cells and 1.5mL of Hank's Balanced Salt Solution (HBSS, Sigma) was immediately added to cells for 30 seconds. HBSS was aspirated off and 1.5mL trypsin-EDTA (Sigma) was added for 30 seconds. This initial trypsin digestion was used to remove loosely bound cells that may be undergoing apoptosis. After 30 seconds, trypsin was exchanged with fresh trypsin-EDTA (1.5mL). Trypsin digestion was stopped when most of the ECs have retracted from the culture flask (generally 90-95% cells retracted) occurring within 3-5 minutes. This was verified with transmitted light. To neutralize trypsin, 10.5mL of new medium was added to the culture flask (media type depended on the cell type as above). The total

volume of the cells and media is now 12mL. 4mL (x3) was removed and added to new T-25 culture flasks; making a 1:3 passage (by area). hDMECs would be passaged to new T-25 culture flasks that were previously coated with 0.2% gelatin (for at least 15 minutes). At this point cells would be considered to increase in passage number (i.e. passage 2 cells would now become passage 3). Media was exchanged the day following cell passage. Flasks are then placed on our normal M-W-F feeding schedule. At all times, HUVECs were maintained in HUVEC media and hDMECs were maintained in our hDMEC media.

To pass cells onto scaffolds, similar procedures were used as above. Electrospun and PDMS scaffolds were sterilized under *uv* light for 15 minutes prior to cell seeding. Matrigel® scaffolds were allowed to gel on clean coverslips prior to cell seeding. Hydrophilic or hydrophobic coverslips were cleaned and placed in the well prior to cell seeding. To pass cells to scaffolds, HBSS and trypsin-EDTA was applied as above. However, to neutralize trypsin, 6.5mL of our HUVEC media was added to the culture flask. This brings the total volume of cells to 8mL. 2mL (x4) was removed and placed into 8-well plates that already contained a cleaned coverslip with the sterilized scaffold. Approximately 100μL of cells would be removed to calculate the initial seeding density. After the addition of ECs and culture medium, the cell culture plate was placed at 37°C and 5% CO₂. Medium was changed the day after passing and then placed on the normal M-W-F feeding schedule until cells were imaged. For this cell passage, the passage number of the cells did not increase because the area that cells were passaged to is equal to 25cm² (i.e. passage 2 cells would remain passage 2). For microstamp experiments, hDMEC seeding density was measured and adjusted prior to cell seeding.

In one series of experiments, the apparent migration of HUVECs onto CA180, CA180 + 3.4μg/mm² Fn or CA + 1.6% chitosan scaffolds was investigated. HUVECs were passaged to cleaned glass coverslips as above on day zero. When exchanging media on the first day after passaging (day 1), a *uv* light sterilized scaffold was placed in the well with the cells. Fibronectin was allowed to dry onto some scaffolds for >30 minutes before it was placed into the well. All scaffolds investigated were sterilized under *uv* light for a minimum of 15 minutes prior to placing it into the well plate. Cells were then fed on the M-W-F feeding schedule. Scaffolds (and glass) were imaged on day 2, 4, 7 and 10 after cell seeding with the live/dead viability assay (Section 3.4.1.a).

3.3 Bioassay Chamber

3.3.1 Dissection of Explanted Vessels

Mice which have been used for live animal studies in Dr. Frame's lab, were euthanized with an overdose of sodium pentobarbital (100mg/kg, intraperitoneal) for dissection. These dissections were approved by an institution endorsed tissue sharing protocol (SUNY Stony Brook). A gross dissection through the abdominal wall was made removing organs (i.e. liver, stomach, small and large intestines) isolating the abdominal aorta. Connective tissue/fat surrounding the aorta was removed before the vessel was harvested. Aortas were approximately 2-3cm in length and ~0.3cm in diameter. These measurements were taken after the vessel has been removed and hence undergone relaxation. Dissected vessels generally have 1-3 existing side branches so that we can investigate cells in proximity to the branch. Explanted vessels were kept in 2mL sterile McCoy's 5A Medium (Sigma) that was supplemented with 80μL FCS, 0.5U/mL Pen and

0.5 μ g/mL Strep. Vessels were kept at 4°C for no more than 24 hours and generally used within 18 hours after dissection (Gamperl et al., 2002; Nagaoka et al., 2006). In some instances, vessels were cannulated immediately after harvesting. There were no measurable differences between these two techniques. The vasoactive response to adenosine, for some cannulated vessels that had been stored overnight and perfused for 24 hours (total time from dissection was ~42 hours), was measured. After perfusion, ~3 drops (~50 μ L) of 10⁻² adenosine was placed on the explant to measure the response.

3.3.2 Cannulation and Perfusion

Cannulation procedures were conducted within a sterile laminar flow hood. All bioassay chamber components were sterilized with ethanol before being placed within the flow hood and allowed to dry before cannulation takes place (~15 minutes). Glass coverslips and sterile 2-0 silk suture were kept within the flow hood. Dissection instruments were sterilized and placed within the flow hood. The explant to be cannulated was placed in the hood and cleaned of any remaining connective tissue/fat. One glass coverslip was attached to the bottom of the bioassay chamber. A glass cannula (maximum diameter of 1mm, tapered down to ~10 μ m using a pipette puller; Kopf Instruments, Tujunga, California) was placed through the inflow catheter embedded within in the Sylgard® (Figure 3.5). The cannula was placed into the lumen of the blood vessel which was then tied tightly to the cannulae with 2-0 silk suture. The second cannula was placed through the outflow catheter and into the lumen. It was also tied tightly. No perfusate was seen to leak between the vessel wall and the cannulae. The scaffold was placed within the bioassay chamber. Electrospun scaffolds were draped over the cannulated blood vessel and Matrigel® was allowed to gel over the vessel. PDMS scaffolds or microstamped glass was placed under the explant (prior to cannulation). Microstamped proteins were aligned with the open side branches of the explant during cannulation.

After cannulation, the bioassay chamber was covered with a second glass coverslip. The chamber was placed on a modified PL1 platform (Warner Instruments, Inc., Hamden, CT) which was then firmly sealed (with screws) and placed within a 37°C isotherm chamber (University of Rochester, NY). The isotherm chamber was warmed with a vibration free air pump (AirThem, WPI, Boca Raton, FL). The inflow catheter was connected to a calibrated pulsatile roller pump (Watson Marlow Model # 403U/VM2, Wilmington, MA) via Tygon® tubing and leuc lock connections. The pump was set to apply a low mean wall shear stress along the vessel wall. The mean wall shear stress was either 0.059-0.145 dyne/cm² (~0.1 dyne/cm², “Low”) or 0.298-1.60 dyne/cm² (~1 dyne/cm², “High”). Shear stress was calculated with the Hagen-Poiseuille approximation (Equation 2.2) with viscosity as 0.85cP (Frame and Sarelius, 1995a). The perfusate was a 1:1 mixture of McCoy’s 5A medium (supplemented with 10% FCS, 0.5U/mL Pen, and 0.5 μ g/mL Strep) and 10mM Hepes Buffered Saline (HBS, pH 7.4). McCoy’s medium is a CO₂ buffer and therefore it was supplemented with HBS to maintain a pH of 7.4 during the experiment. Perfusate was filtered through a 0.2 μ m filter before experiments and stored at 4°C for no more than 7 days before the experiment. The perfusate was warmed to 37°C within the isotherm chamber. Outflow was connected to a waste collection beaker via leuc locks.

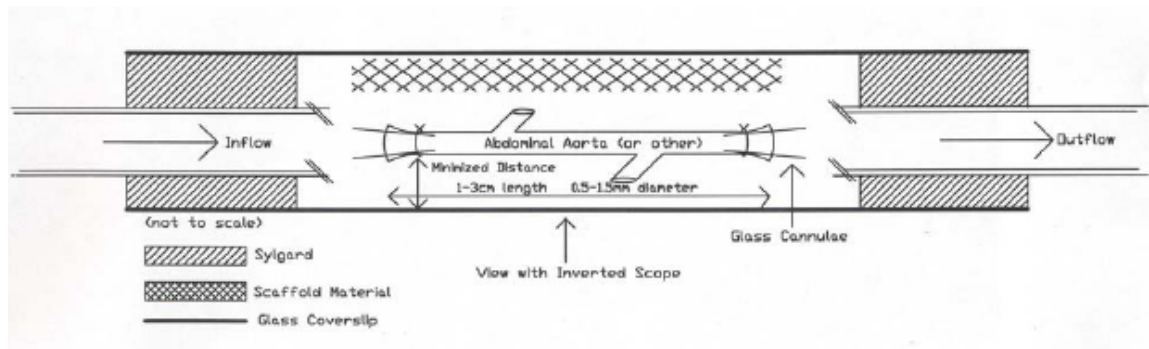


Figure 3.5: Schematic of the Bioassay Chamber with a Cannulated Aorta and Electrospun Scaffold. This image shows the fabricated bioassay chamber with a cannulated aorta and all parameters that have been optimized for this design. To note, if a different scaffold is used during the experiment the lay out would be slightly different, as described above (i.e. the glass coverslip may have been modified to be hydrophobic with or without microstamped ECM proteins). This schematic is not to scale. This figure has been taken from (Rubenstein et al., 2007).

3.3.3 Characterization of Flow within the Bioassay Chamber

Flow patterns were investigated in vessels not used to test EC viability, density and morphology within our scaffolds. Flow patterns were not verified in all experiments because the presence of flow markers (hamster red blood cells) has the potential to confound our results. Red blood cells were obtained from an institution endorsed tissue sharing protocol. RBCs were seeded into our perfusate and mechanically stirred every 10-15 minutes to prevent settling. Flow characteristics were obtained immediately after the onset of perfusion and ~4 hours later. This later time point was used to allow the flow to reach a steady state. Data was recorded with our imageacq.m MATLAB® m-file (Appendix A2). Entry flow was always sharply pulsatile and entirely into the cannulated vessel. Exit flow was likewise pulsatile, but to a lesser extent. Outflow exited either through the cannulae or via the outer catheter sheath (between the glass cannulae and the Teflon® IV needle). Flow was observed to exit some branches, enter other branches, but some branches were observed to have no flow. In some cases, the flow within branches could change over time. Flow through branches was not dependent on branch location (i.e. relative to the inflow). Digital images, taken at the end of our experiments, were taken without knowing the flow conditions of the side branches (Section 3.4.2.b).

3.4 Data Collection – Endothelial Cell Culture and Bioassay Chamber

3.4.1 Immunohistochemistry

3.4.1.a Live/Dead Viability Assay

HUVECs, hDMECs or cells originating from the perfused explanted (bioassay chamber) were stained with a live/dead cell viability and cytotoxicity assay (2 μ M calcein and 4 μ M ethidium in PBS, Molecular Probes, Carlsbad, CA) at the end of experiments. Calcein accumulates inside intact and viable cells, while ethidium only stains the DNA of compromised cells. Therefore, cells positive for calcein were considered live and cells positive for ethidium were considered dead. To stain HUVECs or hDMECs, culture media was removed from the well, taking effort to maintain the geometry between the scaffold and the cells. The glass coverslip and the scaffold were removed from the well and the bottom of the glass was dried and cleaned on sterile lens paper. To maintain the geometry of the scaffold/cells, 3-5 drops of the cytotoxicity assay was added to the scaffold/glass. A second cleaned coverslip was placed on top of the scaffold to prevent drying during imaging. The reagents were allowed to associate with the cells and the scaffold (at 37°C) for 15 minutes prior to imaging (optimized for our conditions).

For bioassay chamber experiments, 1mL of the cytotoxicity assay was infused slowly through the lumen of the explant via the inflow catheter. This was done to maintain the natural geometry of the vessel and the scaffold. The dye was allowed to associate with the vessel/scaffold for 15 minutes prior to imaging (optimized for our particular conditions).

3.4.1.b BS-1 Lectin

After some perfusion experiments, the *Bandeiraea simplicifolia*-1 (BS-1, 100 μ g/mL in PBS, Sigma) lectin was used to verify that cells found within the scaffold were endothelial. The BS-1 lectin was conjugated to fluorescein isothiocyanate (FITC) and is specific for endothelial cells. Staining was accomplished without altering the natural geometry of the vessel/scaffold complex by infusing 1mL slowly through the

inflow catheter. The lectin was allowed to associate with the explant and any cells within the scaffold for 15 minutes prior to imaging. Before imaging, the vessel and scaffold were washed with warmed PBS (3 times, 10 minutes each) to remove any unbound lectin from the scaffold (this was optimized for our conditions). This also minimizes the background fluorescent of the BS-1 lectin-FITC. Samples stained with the BS-1 lectin were not fixed because formaldehyde would dissolve the cellulose acetate scaffolds and the natural cell-scaffold interactions would not be retained.

3.4.1.c DAPI

After some perfusion experiments, 1 μ g/mL diamidinophenylindol (DAPI, Sigma) (in water) was used to identify the nucleus of endothelial cells within electrospun scaffolds (Eberl et al., 1999). Staining was accomplished without altering the natural geometry of the vessel/scaffold complex by infusing 0.5mL DAPI slowly through the inflow catheter. DAPI was allowed to associate with the cells for 5-10 minutes before imaging (Eberl et al., 1999). This staining was done in conjunction with the BS-1 lectin stain described in Section 3.4.1.b.

3.4.1.d Fibronectin Coating

The presence of fibronectin on CA180 scaffolds or on hydrophilic and hydrophobic glass coverslips was verified with a fluorescent antibody against fibronectin. 3.4 μ g/mm² Fn was allowed to dry on a CA180 scaffold, hydrophilic glass or hydrophobic glass for 30 minutes within a sterile laminar flow hood. The CA180 scaffold was previously sterilized under *uv* light for 15 minutes. Glass coverslips were cleaned as described in Section 3.1.3.b. Anti-fibronectin (100 μ g/mL, Sigma) was allowed to associate with the Fn coated scaffolds (electrospun or glass) for 45 minutes in our laminar flow hood. Excess antibody was then aspirated off. The sample was washed with PBS for 10 minutes (x3) to remove any unbound anti-Fn. Our secondary antibody, FITC conjugated anti-rabbit IgG (Sigma), was allowed to associate with the scaffold for 30 minutes. Excess secondary antibody was aspirated off and the scaffold was cleaned gently with a PBS solution (10 minutes, x3). After secondary antibody binding, scaffolds or microstamped glass coverslips were soaked in PBS for at least 4 hours to mimic conditions in experiments. The scaffold was then imaged using fluorescent microscopy (Section 3.4.2 for microscope equipment). Controls were conducted without the primary antibody staining and without fibronectin staining. To note, our scaffolds and glass coverslips do not autofluoresce (i.e. see Figure 4.8).

3.4.2 Imaging

3.4.2.a Imaging of Cultured Endothelial Cells

A Nikon (Japan) inverted E400 microscope connected to a Retiga digital camera (Media Cybernetics, USA) was used to image endothelial cells in culture. Q Imaging software (Q Imaging, Canada) was used as the interface between the computer and the camera. After the viability and cytotoxicity stains associated with the cells/scaffold for 15 minutes, 3 random locations were chosen to image. These sites were identified using phase-contrast microscopy (i.e. can not determine if cells are viable prior to fluorescent imaging) with a 10X (FLOR Nikon, 0.5, 160/0.17) objective. 2 other random locations were identified with transmitted light using a 20X (FLOR Nikon, 0.75, 160/0.17)

objective. With either objective, the image location was not altered when switching between phase-contrast and fluorescence. At each location, 4 images (1 fluorescent image each with green and blue excitation, 1 summated image and 1 transmitted light with phase-contrast) were taken to document the cells in this region. 2-3 locations on the glass coverslip were imaged at both 10X and 20X (4 images are obtained, as above). Images were only taken within 20 minutes after the dye has been allowed to associate with the cells and the scaffold. After this time, viable cells begin to uptake ethidium (false positive identification of dead cells) and the dye can begin to photobleach. This time frame was optimized for our conditions.

3.4.2.b Imaging in the Bioassay Chamber

Within the first 30 minute of perfusion, the vessel and scaffold were imaged with transmitted light to determine the initial geometry of the vessel. Our inverted Nikon microscope and Retiga Fast Cooled digital camera was used for all bioassay chamber imaging. Initial vessel maps were imaged with 4X (Nikon, 0.13DL, 160/-) and 10X objectives. These images were combined in a montage to obtain the initial geometry of the explant. In some experiments, a MATLab® program (Section 3.5.4.b/Appendix A2) was used to catalogue the pulsatile perfusion of the explant. Upon completion of the experiment, the vessel was imaged with transmitted light to obtain a post-perfusion map with 4X and 10X objectives. The vessel and scaffold were then stained with calcein and ethidium or BS-1 lectin (Section 3.4.1.b). To document positively stained cells for either reagents, 10X or 20X objective were used. Generally, 5-10 images were taken with the scaffold, “Near” each open branch point (within 100 μ m) and “Far” from each open branch point (between 400 and 500 μ m) using a well-defined imaging paradigm (Figure 3.6). Image locations were identified by phase-contrast microscopy prior to fluorescent imaging (the viability of cells was unknown). BS-1 lectin images were also identified under transmitted light. 100% of cells identified in this way (n=89) were BS-1 lectin positive and hence endothelial. With either dye (calcein/ethidium or BS-1 lectin) fluorescent images were only taken within 20 minutes after imaging began (i.e. after the 15 minutes allotted to allow the dye to associate with the cells). This is due to possible photobleaching and compromised cell viability (i.e. all cells uptake ethidium) for longer duration imaging. This time frame was optimized for our conditions.

3.5 Data Processing and Statistical Analysis

3.5.1 Cell Viability

Cell viability was obtained from digital images of calcein and ethidium stained cells. The total number of calcein positive cells (live cells) and ethidium positive cells (dead cells) were counted per image. Cell viability was defined as the total number of live cells divided by the total number of cells (live plus dead cells). This ratio helps to quantify the compatibility of the scaffold of interest with the cells.

3.5.2 Cell Density

Cell density was obtained from digital images of calcein and ethidium stained cells. Cell density is defined as total number of calcein positive cells, live cells, divided by the image area. Image area was calibrated for each objective and camera combination. For all experiments that were conducted with microstamped ECM proteins, the stamp

area was considered as the image area. Only calcein or ethidium positive cells within this region were counted. This ratio helps to quantify cell growth on the scaffold.

3.5.3 Percent Confluence

Percent confluence can be calculated from the cell density and cell area (Section 3.5.4.a) measurements. The percent confluence is defined as the average perimeter area multiplied by the cell density. This formulation approximates the percent of area with cells growing on it.

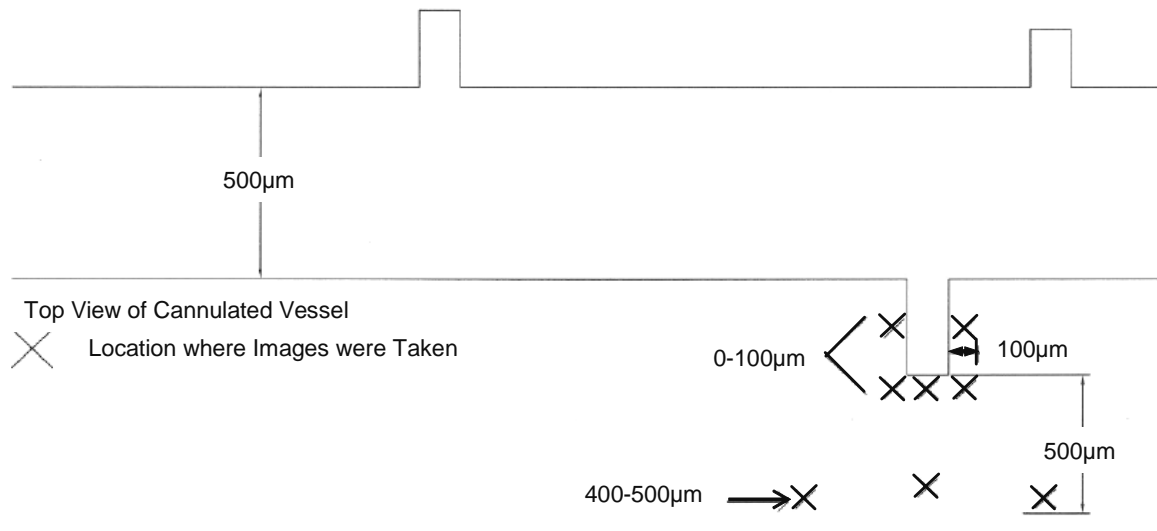


Figure 3.6: Schematic of Images Taken After Explant Perfusion in the Bioassay Chamber. This image shows the approximate locations of images taken after a perfusion experiment has been completed. Approximately 5 images were taken within 100µm from the explant. Approximately 3 images were taken between 400-500µm from the explant. The image shows the top view of a vessel with only the exterior wall depicted. This figure has been taken from (Rubenstein et al., 2007).

3.5.4 MATLAB® Programming

3.5.4.a Cell Morphology

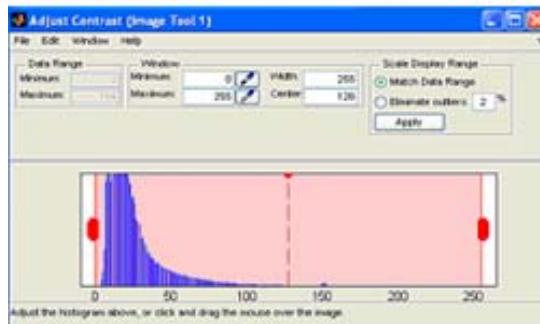
Two MATLAB® m-files were written by me to increase the accuracy and enhance the rate of data processing in Dr. Frame's laboratory (see Appendix A for source code). MATLAB® is a powerful mathematical software and was chosen because it uses matrix based computations and it incorporates a user-friendly interface for inputting and outputting data. The program can identify cells within a digital image, locate the cell boundary and calculate the cell area based on the perimeter measurements. The first portion of this program (Appendix A1 lines 1-80) inputs a digital image into a MATLAB® matrix, has users manually threshold the image and identifies the cells in the image. Images are manually thresholded in order to allow the user to determine if the cell perimeter is accurate when the color image is converted to a black and white image (black and white images are needed to locate the cell boundary). If the user defines a low threshold, then the cells will have an artificially high area. If the threshold is high, the cells have an artificially low area. All users were trained to threshold properly.

The second portion of this program (Appendix A1 lines 81-201) calculates the long and short axis of the cell, determines if the cell is circular or elongated and determines the area based on the axis measurements. A randomized grid is merged with the black and white image and only the cells within the grid were analyzed. Using the *bwselect* command, users identify cells by clicking on the long and short axis of each cell. From the long and short axis end points, the program measures the axes. The ratio of the short axis to the long axis is quantified determining if the cell is circular (the short axis is greater than or equal to 80% of the long axis) or elongated (the short axis is less than 80% of the long axis) (Uttayarat et al., 2005). The area measurement based on circular or elongated cells is an approximation to cell area. We defined circular cells to have an area that is equal to half of the long axis squared multiplied by π . Elongated cells have an area that is equal to the long axis multiplied by the short axis.

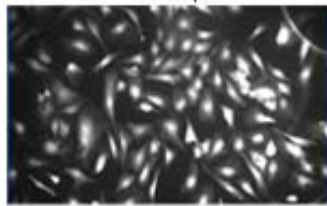
The last section of code (Appendix A1 lines 204-587) calculates the area of the cell based on the perimeter measurements. The boundary of selected cells is saved into a separate matrix which is modified to make calculations more efficiently. Modifications normalize each cell with regard to its location and then organize data sequential. Since cells can have irregular shapes, we decided to integrate the boundary measurements over the entire surface for the perimeter based area. No mathematical expression can describe the cell boundary, so the program uses the Boole's numerical integration technique (Equation 3.1) to quantify cell area. Boole's technique uses the five nearest data points to approximate an integral (Mathews and Fink, 2004) and is more accurate than using two points (Trapezoid Rule), three points (Simpson's Rule) or four points (Simpson's 3/8 rule) because the error term with these approximations converges slower than Boole's approximation (Mathews and Fink, 2004). Using more integration points (i.e. >5) increase the computing time and processor power needed while decreasing error convergence minimally. Boole's rule is applied to the upper and lower boundary. The approximation of the lower boundary is subtracted from the upper boundary to obtain an approximation of the cell area. Sample steps for this program are shown in Figure 3.7.

$$\int_{x_0}^{x_4} f(x)dx \approx \frac{2h}{45}(7f_0 + 32f_1 + 12f_2 + 32f_3 + 7f_4) \quad \text{Equation 3.1}$$

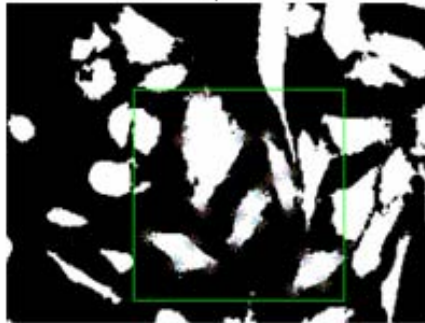
$$\text{where } h = \frac{x_4 - x_0}{4}$$



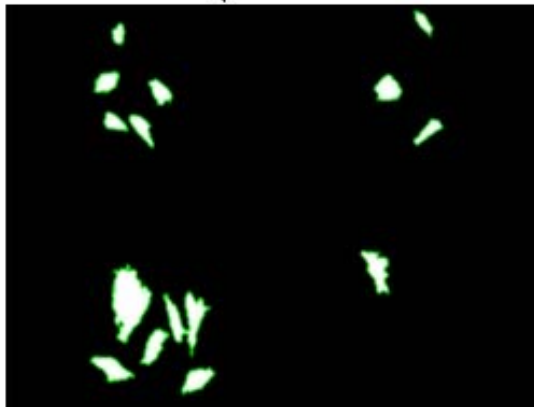
Manually Adjust the Contrast



Black and White
Image to Analyze



One Quadrant with
Selected Cells



All Cells Whose Areas will
be Calculated using
Boole's Numerical
Approximation, Giving the
Perimeter Based Area

Figure 3.7: Sample Steps Taken While Using Cellcounting.m Program. This figure illustrates the steps used during the cellcounting.m program. First, the image is manually thresholded (using *imtool* command), particular cells are selected within a randomized region (using *bwselect* command) and then the perimeter of these cells is located. The perimeter based area based is then calculated using Boole's Numerical Integration technique (equation 3.1).

3.5.4.b Video Image Acquisition

A second program (Appendix A2) was written utilizing many of the image acquisition functions in MATLAB®. This program was written in order to take time lapse video recordings during bioassay chamber perfusion and to verify and characterize the flow field in perfused vessels. The first portion of the program (Appendix A2 lines 1-60) prompts for acquisition commands to obtain individual time-lapsed images. The user defines how often to image, how long each exposure is and the acquisition time length. After this is determined the program triggers the camera to take snaps at the specified times. The second portion of the program (Appendix A2 lines 61-81) converts all snaps, which are saved in a three dimensional matrix, into a video file (extension .avi) so that it can be viewed elsewhere. Long term videos can not be obtained because the allocated storage space for these functions is minimal in MATLAB® and it is not possible to increase the allocation space to what would be required for these videos.

3.5.4.c Monte Carlo Simulation to Optimize Parameters

The cellcounting.m MATLAB® m-file was used to obtain the long and short axis of cells imaged in cell culture and in the bioassay chamber. It was also used to obtain a more accurate value for the cell area which was based on the perimeter of the cell. Before this program, values for the long and short axis were obtained from ProAnalyst (V1.1.9.0) and were recorded manually. Area measurements were then approximated from the axis measurements. This method for area calculation was inaccurate for randomly shaped cells and the entire process was laborious. The cellcounting.m program was used to quickly obtain axis measurements, record them and then calculate the more accurate perimeter based area of the cell. Axis measurements collected from the new program was compared to the old method to test the accuracy of the program. To test the accuracy of the perimeter based area measurements, the area of cells from high resolution printed images were measured with a calibrated map wheel. With the map wheel, a cell effective radius was obtained from the perimeter measurements; assuming cells were circular in shape. The area was then calculated from the radius, again using a circular approximation. These cell area measurements were used to calculate the accuracy of the perimeter based cell area measurement from the program. 72 individual cells were used to test the accuracy of the program (Table 3.2). The long and short axis varied by less than 5% between the two measurement methods. The perimeter based area measurements varied by ~6% between the two methods. This error is acceptable based on the assumption that cells are close to circular in shape, when calculating the area using a map-wheel.

We also investigated the accuracy of the cellcounting.m MATLAB® m-file at finding and accurately describing the perimeter of closely neighboring cells. To do this, 20X phase-contrast image of endothelial cells were obtained; to visually identify the cell boundary of individual endothelial cells. The program was then used to describe the perimeter of these cells (after thresholding). A comparison of these two images (Figure 3.8) shows that there is a high correlation between the perimeter of the cell seen with phase contrast and obtained from the cellcounting.m MATLAB® m-file.

Measurement	Average Percent Error \pm S.E.M.
72 Individual Cells were Analyzed for Comparison	
Long Axis	2.71 \pm 0.20%
Short Axis	1.94 \pm 0.18%
Perimeter Based Area	6.33 \pm 0.87%

Table 3.2: Average Percent Error between Two Methods of Analyzing Cell Morphology. The initial method to measure the cell axes was using ProAnalyst (V1.1.9.0) program. This method was time consuming. The cellcounting.m MATLAB® m-file was written to quicken the processing time. The perimeter based area is a more accurate method to calculate the cell area compared to our original method. A map wheel was used to test the accuracy of the coding.

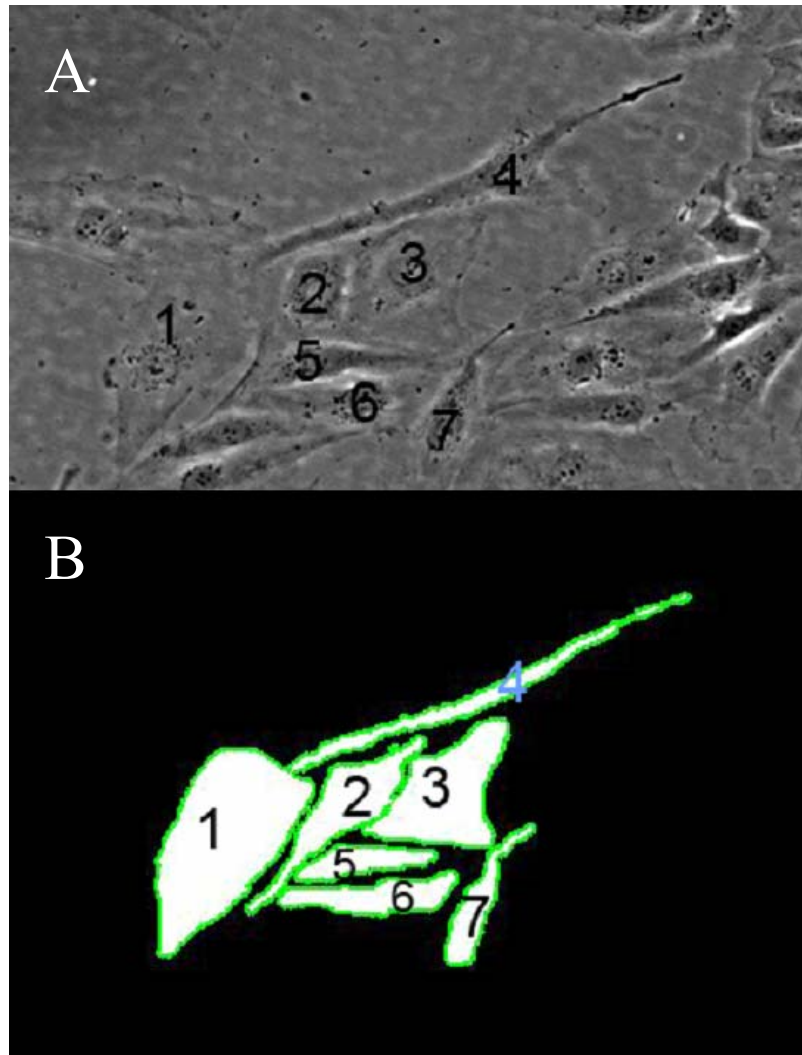


Figure 3.8: Endothelial Cell Boundary with Phase-Contrast and the Cellcounting.m MATLAB® Program. Phase-contrast microscopy was used to obtain the perimeter of individual endothelial cells in culture (A). Cell boundaries were then obtained with the cellcounting.m program (B) to determine the accuracy of the program at identifying cell boundaries. This is one sample of such a comparison, showing the high correlation between the two methods. Numbers identify the same cells in both images.

3.5.5 Statistical Analysis

3.5.5.a Cell Culture

Cell viability and cell density was obtained from all images. Cell morphology for 10-20 cells was also obtained from each image taken. Statistical analysis was performed using the Primer for Biostatistics (Glantz, 1996) or SAS V9.0 (with $\alpha = 0.05$) for all statistical tests. In most cases, 2-way, 3-way or 4-way ANOVA was used to analyze differences within the data. Possible input variables were cell passage, duration on scaffold, cell type (elongate vs. circular) and scaffold material. The Least Squares Means post-hoc test was used to analyze any differences found from the ANOVA. For experiments using the microstamp, data was paired based on the well and the stamped protein. This was taken into account when running the statistical analysis on the data.

3.5.5.b Bioassay Chamber

Cell viability and cell density was obtained from all images taken in the bioassay chamber. Cell morphology for 10-20 cells was also obtained from each image taken. Statistical analysis was performed using the Primer for Biostatistics (Glantz, 1996) or SAS V9.0 (with $\alpha = 0.05$) for all statistical tests. In most cases a 2-way or 3-way ANOVA was used to analyze differences within the data. Possible input variables were flow rate, distance from explant and scaffold material. The Least Squares Means post-hoc test was used to analyze any differences found from the ANOVA. In all experiments, the glass data was paired with the scaffold data. This was taken into account when running the statistical analysis on the data.

SECTION IV: RESULTS

4.1 Cell Culture

Cell culture studies were used as control studies for our bioassay chamber experiments (Section 4.2). These studies tested the effects of electrospun scaffold fiber diameter and composition on endothelial cell viability, density and morphology. Optimal scaffolds were then used in my bioassay chamber to test the combined effects of shear stress and scaffold composition on endothelial cells initiating from a perfused explanted murine abdominal aorta. Next, a microcontact printing method was used to direct the growth of endothelial cells onto ECM proteins patterned on hydrophilic or hydrophobic glass substrates. Our goal was to exclude endothelial cells from the non-patterned (glass) regions and rapidly approach cell confluence on the microstamped ECM proteins. We investigated endothelial cell viability, density, and morphology and percent confluence during the early phases of angiogenesis.

Initial studies conducted in Dr. Frame's laboratory investigated the effects of electrospun scaffolds on cell viability and density as well as characterizing the permeability of scaffolds. These experiments on CA scaffolds with added CNT or VEGF addition were conducted by M. Frame and S. Tonick. Initial studies have been combined with my work to make overall conclusions on the effects of cellulose acetate based electrospun scaffolds on ECs. S. Goldgraben characterized the effective porosity of scaffolds with an average fiber diameter range between 1-5 μ m (Section 2.5.1).

4.1.1 Effects of Electrospun Cellulose Acetate Scaffolds

4.1.1.a Effect of Electrospun Cellulose Acetate Fiber Diameter

Human umbilical vein endothelial cells (HUVECs) were used to study the biocompatibility of electrospun cellulose acetate on endothelial cells in culture. Three base cellulose acetate scaffolds with different characteristic fiber diameters (Table 3.1) were studied. Fiber diameters were obtained from SEM images of each scaffold configuration (Figure 4.1, images obtained by Dr. J. Quinn). Fibers were flattened with a ribbon-like morphology. CA40 showed the same morphology with nodule structures.

For some scaffold preparations, fibronectin was adsorbed onto CA180 scaffolds to verify the percent of the CA180 scaffold that was covered by Fn. Also we wanted to investigate if the morphology of the electrospun fibers changed with the addition of Fn. A fluorescent antibody against fibronectin (FITC-anti-Fn, Sigma) was used to stain these scaffolds. Before imaging, the scaffolds were soaked in PBS for ~4 hours. After PBS soaking, Fn remained adsorbed on CA180 scaffolds and it uniformly coated the entire electrospun fibers (Figure 4.2). The ribbon-like morphology of CA180 scaffolds was preserved with the addition of fibronectin to the scaffold. We confirmed the absence of non-specific binding of the secondary antibody to the scaffold (Figure 4.2 D); the scaffolds do not autofluoresce (i.e. Figure 4.8).

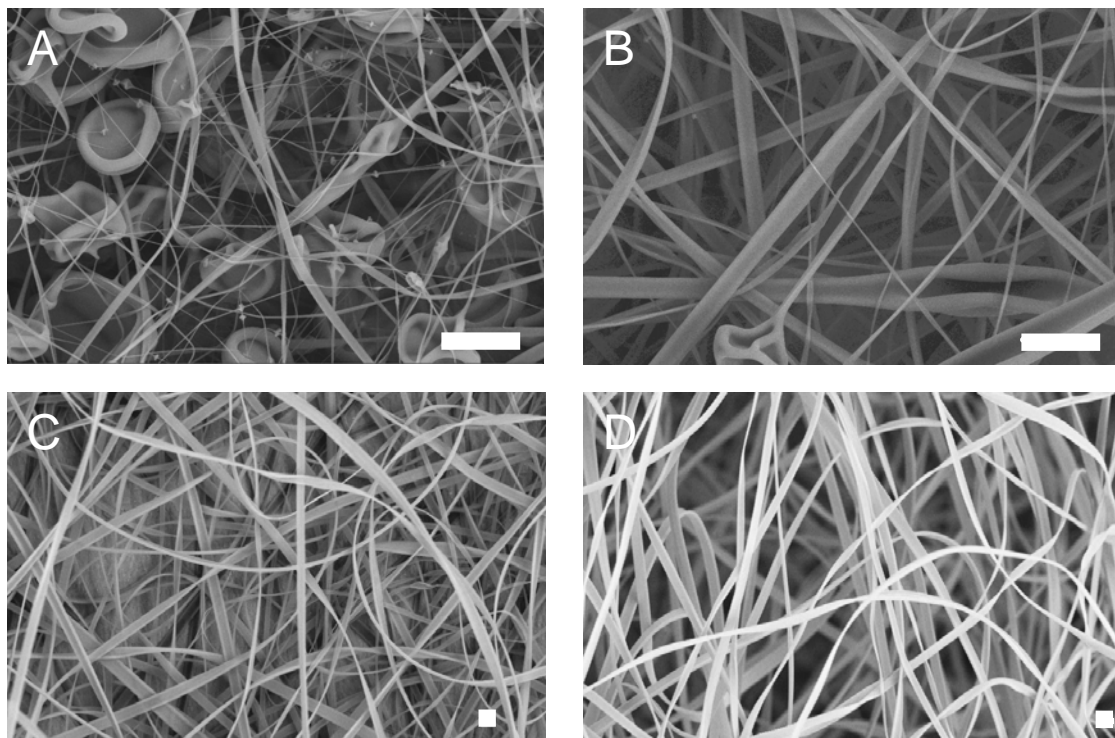


Figure 4.1: Representative Scanning Electron Microscope Images of Electrospun Scaffolds. These SEM images show the morphology of our electrospun CA40 (A), CA80 (B), CA180 (C) and CA + 1.6% chitosan (D) scaffolds. Fibers are elongated providing a directional cue for endothelial cell growth and culture. These images were used to obtain the characteristic fiber diameter for each scaffold. Scale bars are each 20 μ m. SEM images were taken by Dr. J. Quinn from the Department of Material Science and Engineering at Stony Brook University. This figure has been taken from (Rubenstein et al., 2007).

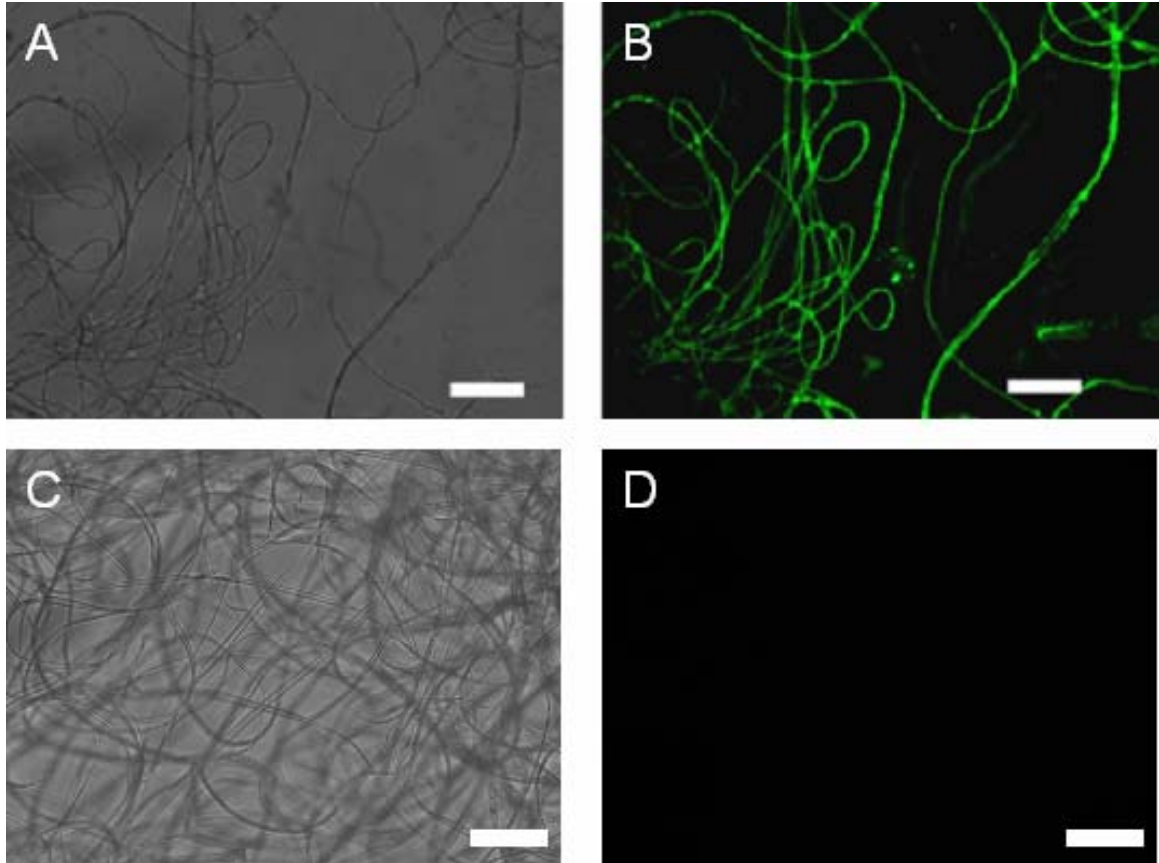


Figure 4.2: Verification of Fibronectin Coating of CA180 Scaffolds. Scaffolds were stained with an antibody against fibronectin to determine the percent of the scaffold coated by fibronectin. We can see uniform coating (B) of the entire scaffold and that the morphology of the scaffold does not change (compared with Figure 4.1). Panels A and C are 20X images with transmitted light and Panels B and C are the corresponding fluorescent images. We confirmed the absence of non-specific binding of the secondary antibody to the scaffold (D). All scale bars are 100 μ m. This figure has been modified from (Rubenstein et al., 2007).

The apparent void space and the surface area to volume ratio for our scaffolds have been calculated using formulas derived by G. Bowlin's group (Boland et al., 2004). These formulations are approximated using the scaffold density, material density, fiber radius and mass of the scaffold (Boland et al., 2004). Using these approximations, our CA180 and CA+ 1.6% chitosan scaffolds were approximately 75% and 95% void, respectively (Table 4.1). This is in comparison to other common electrospun scaffolds that are approximately 85-90% void. The surface area to volume ratio was also improved with addition of chitosan to the electrospun scaffold (Table 4.1).

The stiffness for CA180 and CA+1.6% chitosan scaffolds were obtained from compressive testing of the scaffolds done by IMR Test Labs. The stiffness, yield force, compressive modulus and yield stress for CA+1.6% chitosan scaffolds was significantly enhanced as compared to CA180 scaffolds (Figure 4.3). Nominal values for stiffness are -0.25N/m and -0.41N/m for CA180 and CA+1.6% chitosan, respectively. The yield force for CA180 and CA+1.6% chitosan are 0.0473N and 0.064N. The compressive modulus is 12.8kPa and 15.2kPa respectively for CA180 and CA+1.6% chitosan. The yield stress is 7.9kPa and 10.7kPa for CA180 and CA+1.6% chitosan respectively.

HUVECs were cultured on CA180 (1-5 μ m), CA80 (0.2-1 μ m) and CA40 (0.01-0.2 μ m) scaffolds for either "Short" (2-3 days) or "Long" (4-5 days) durations. These different growth durations were studied as a deliberate test for changes during initial growth periods versus longer growth periods where a confined/confluent morphology would be expected. "Early" (passage 2-3) or "Late" (passage 4-5) passage HUVECs were also investigated, due to the known changes in endothelial cell growth pattern with passage. Unmodified glass coverslips (hydrophilic) and Matrigel® were used as control scaffolds in these conditions. Cell density and viability was quantified for all conditions. Cell morphology was also quantified with our perimeter-based cell area measurement. Cell culture data was generated for 1) a means to test optimal growth conditions and 2) as a comparison to our bioassay chamber data (Section 4.2). Results from the bioassay chamber were expected to mimic Short duration and Early passage HUVECs.

Cell density and viability for Early and Late passage HUVECs on our control substrates and our three base cellulose acetate scaffolds is shown in Figure 4.4. These cells were cultured for Short or Long durations. As expected, cell density on the glass coverslips decreased for Late passage cells compared with Early passage cells (Figure 4.4 A vs. C). Matrigel® had a reduced cell density as compared to on glass. Cell density on CA40 and CA80 either remained low or decreased for longer growth durations and it was significantly lower than cell density on glass for Long growth durations. In contrast, HUVECs on glass coverslips, Matrigel® and CA180 had increases in cell density for Long growth durations. HUVEC density on CA180 was not different than on glass.

Cell viability for HUVECs on our control substrates and our three base scaffolds was also quantified (Figure 4.4 B and D). In general cell passage did not affect HUVEC viability. The viability of cells on CA40 and CA80 were significantly lower than on glass and Matrigel® controls. Interestingly, the viability of HUVECs on the CA180 scaffold was not significantly different from on glass or Matrigel®. Figure 4.4 illustrates that the diameter of cellulose acetate electrospun scaffolds (compare CA40 to CA80 to CA180) significantly effects cell density and cell viability; for both Short and Long durations of cell growth and Early and Late cell passage. CA180 (fiber diameter 1-5 μ m) provided the best growth template for endothelial cells in these conditions.

Electrospun Scaffold (fiber diameter; μm)	Void Space (%)	Surface Area to Volume Ratio (cm^2/cm^3)
Electrospun Scaffolds Fabricated Here and by Others		
CA180 (1-5)	74.0	1187
CA + 1.6% chitosan (1-5)	94.7	1858
Collagen (3.5)	83.3 (Barnes et al., 2006)	5000 (Barnes et al., 2006)
PLGA (0.5-0.8)	91.6 (Li et al., 2002b)	4300 (Lu et al., 1999)
PGA (0.22-0.88)	81.0 (Boland et al., 2004)	8100 (Boland et al., 2004)

Table 4.1: Void Space and Surface Area to Volume Ratio for CA180, CA + 1.6% Chitosan and Other Common Electrospun Scaffolds. Void space and surface area to volume ratio were calculated from the formulations derived in (Boland et al., 2004). The effective hydraulic radius and not the width of the fibers were used in this formulation. Scaffolds with a combination of a high void space and a large surface area to volume ratio should perform well in tissue engineering applications.

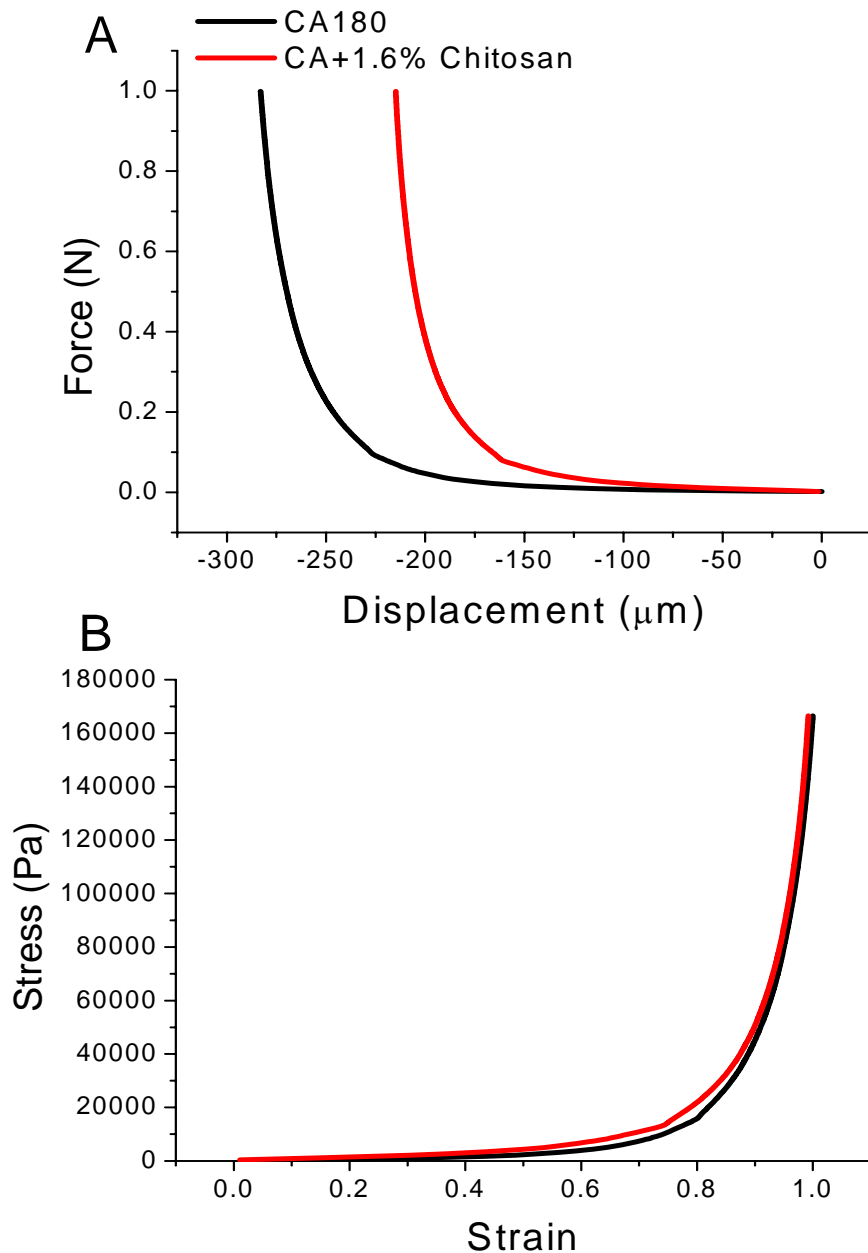


Figure 4.3: Force vs. Displacement and Stress vs. Strain Curve for CA180 and CA+1.6% Chitosan. Stiffness of electrospun scaffolds were tested using thermomechanical analysis by IMR Test Labs (Lansing, NY). A preload of 0.001N was applied to the scaffold and this was set to a zero displacement. Force was controlled at 0.1N/min and displacement was measured. Stiffness and yield force were calculated from the data using Hooke's Law (A). Stress vs. strain curve (B) was calculated with the force probe area ($\sim 6 \times 10^{-6} \text{ m}^2$) and the change in length normalized by the original length. Compressive modulus and yield stress were calculated from this curve.

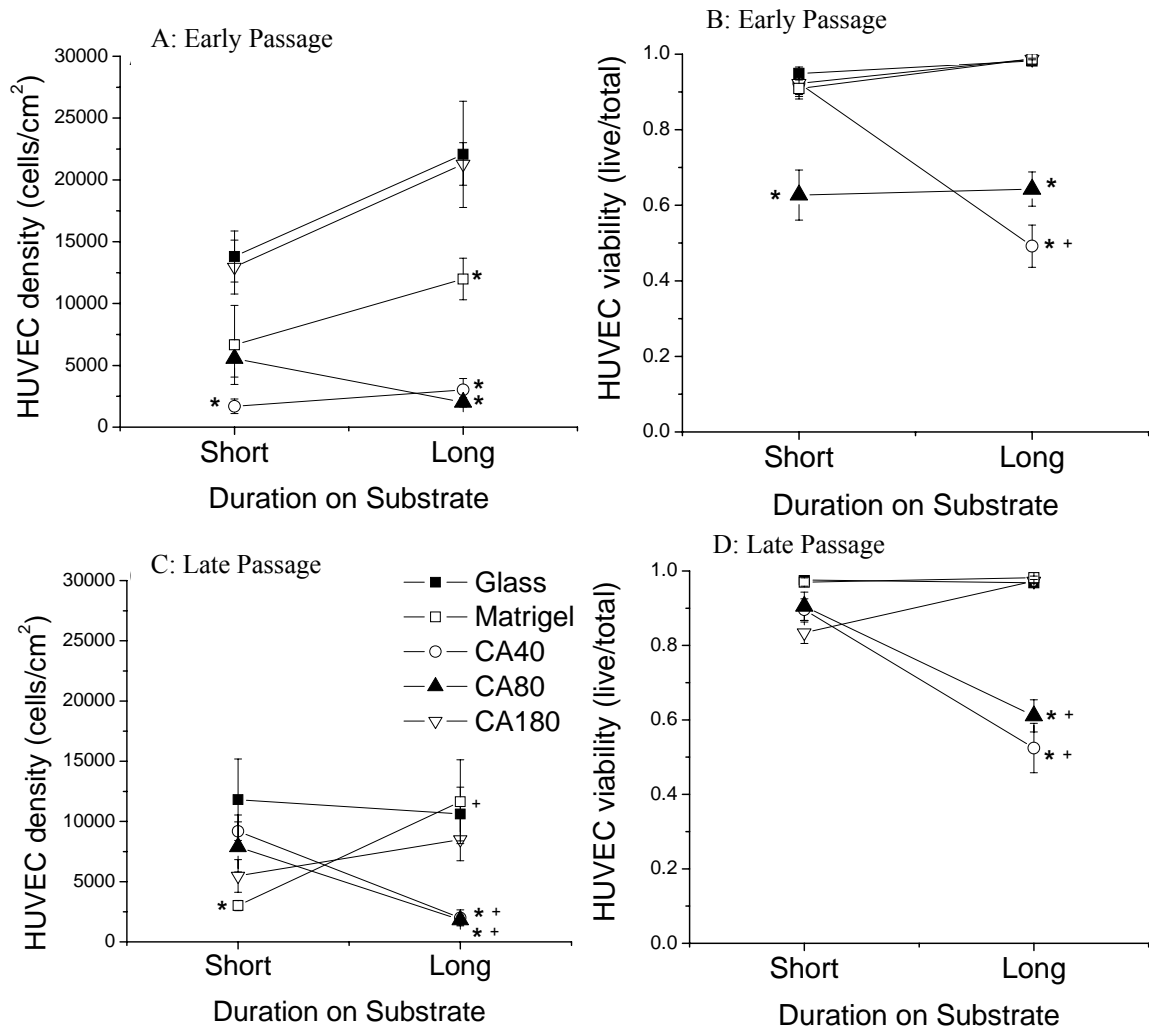


Figure 4.4: Endothelial Cell Density and Viability on our Base Cellulose Acetate Scaffolds. Scaffolds with a different characteristic fiber diameter (see Table 3.1) were compared to our control hydrophilic glass coverslips and Matrigel®. HUVECs were investigated at Early (A and B) or Late (C and D) passages and Short (2-3 days) or Long (4-5 days) growth durations. Values are mean±S.E.M. Each data point represents the average of all digital images in 2-8 independent experiments (>30 images with >100 cells). *differs from on glass (ANOVA, $P < 0.05$) and, +differs from Short duration (t -test, $P < 0.05$). This figure has been taken from (Rubenstein et al., 2007).

4.1.1.b Effects of Additives to the Electrospun Cellulose Acetate Scaffolds

HUVECs were used to study the effects of electrospun cellulose acetate modified with four additives (Table 3.1). Carbon nano-tubes (CNT), chitosan and vascular endothelial growth factor (VEGF) were added to the electrospinning solution prior to electrospinning. Fibronectin (Fn) was added to formed CA180 scaffolds (Figure 4.2). CNT and chitosan have been shown by other groups to increase the stiffness of electrospun scaffolds. VEGF was investigated to quantify the effects of a potent angiogenic growth factor. Fn was added to quantify the effects of adding an extra ligand binding site onto formed scaffolds. Only Early passage HUVECs were cultured on these scaffolds for Short durations to later make comparisons to data trends in the bioassay chamber. Unmodified glass coverslips (hydrophilic) and Matrigel® were used as control scaffolds in these conditions. Cell density, cell viability and cell morphology were quantified at the end of the culture period.

HUVEC cell density (Figure 4.5 A) did not differ significantly on either of our control substrates; glass and Matrigel® ($P = 0.13$ Matrigel® vs. glass, ANOVA, Least Square Means post-hoc test). HUVEC cell density for all scaffolds with a characteristic fiber diameter within the ranges of 0.01-0.2 μm or 0.2-1 μm was significantly reduced as compared to on glass. For the largest fiber diameter group (1-5 μm), the addition of 3.3% CNT significantly reduced cell density as compared to on hydrophilic glass. The addition of Fn or chitosan increased HUVEC cell density as compared to CA180 ($P = 0.42$, CA180 vs. CA180 + Fn; $P = 0.09$, CA180 vs. CA + chitosan 1.6%, ANOVA). In fact the cell density, on scaffolds with either Fn or chitosan, was higher than on our glass control. Thus, reduction of the fiber diameter to less than 1 μm significantly reduced cell density for HUVECs and the addition of Fn or chitosan improved cell density.

HUVEC cell viability did not change between our control substrates (Figure 4.5 B). Cell viability for all our electrospun scaffolds within the 1-5 μm diameter range did not differ from on the control substrates. Viability was significantly decreased for substrates within the 0.2-1 μm diameter range as compared to on glass, with no significant differences between scaffolds within that range (CA80 vs. CA + 1.7% CNT). Therefore, addition of CNT did not affect cell viability as compared to its corresponding base scaffold. Addition of VEGF (13ng/cm² in the fabricated scaffold area) decreased viability significantly over glass and CA40. This quantity of VEGF would be considered biologically relevant (Section 5.1.2) although we did not measure its bioactivity. Thus, Figure 4.5 illustrates again that fiber diameter affects endothelial culture conditions and that additives to the electrospun scaffold also affects culture conditions.

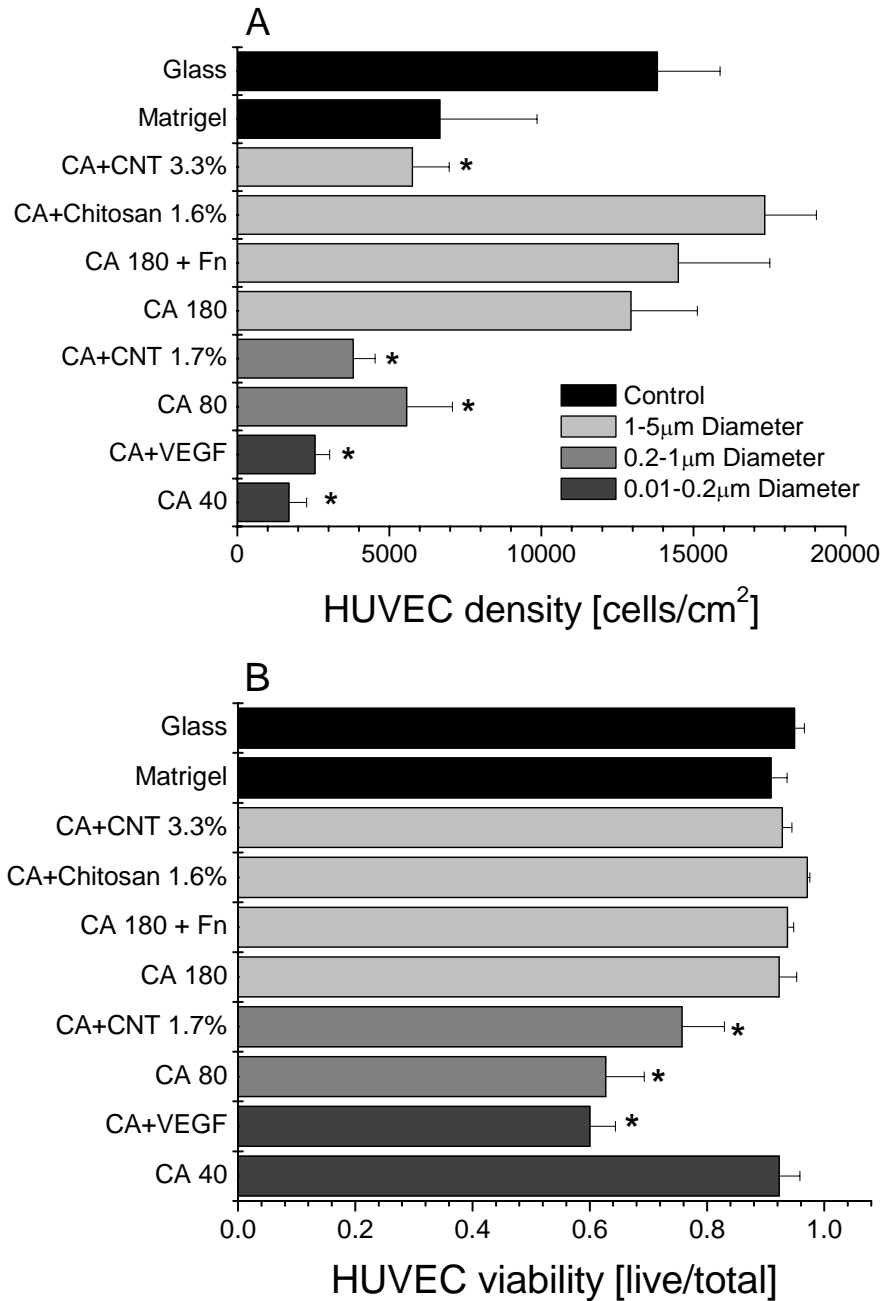


Figure 4.5: Endothelial Cell Density and Viability on Electrospun Scaffolds with Different Material Composition. Scaffolds with different material composition (Table 3.1) were compared to our control glass coverslips and Matrigel®. Short duration and Early passage HUVECs were investigated here. Values are mean+S.E.M. The data was obtained from digital images (>30 for each condition with >100 cells) from 2-8 independent cell culture experiments for all substrates.*differs from on glass (ANOVA, $P < 0.05$). This figure has been taken from (Rubenstein et al., 2007).

Overall, the addition of CNT did not improve HUVEC viability and decreased cell density in both fiber diameter ranges examined. Therefore, we conclude that CNT is an unsuitable additive in these conditions. VEGF showed a reduction in both cell viability and cell density within the 0.01-0.2 μ m fiber diameter range. It is also considered to be unsuitable in these conditions. The addition of fibronectin increased cell viability and cell density. While the addition of chitosan to cellulose acetate electrospun fibers appeared to maintain HUVEC viability and perhaps improve density (even as compared with the glass substrate). We conclude that the addition of 1.6% chitosan to the CA180 scaffolds is an improvement over the base scaffold. Therefore, to study the effects of shear stress and scaffold composition we chose to use CA180 with and without 1.6% chitosan in the bioassay chamber (Section 4.2).

Control experiments were conducted with the addition of 3.4 μ g/mm² fibronectin to 4 substrates to determine the effects of Fn addition on endothelial cell density and cell viability. Fn addition would provide an added specific ligand attachment point to ECs that was not provided by the base scaffolds. Paired samples of HUVECs were added to substrates with or without fibronectin. The addition of Fn to any substrate increased the cell density over the base substrate (Figure 4.6). Statistically significant increases were found upon addition of Fn to our electrospun scaffolds CA180 and CA + chitosan 1.6% electrospun scaffolds. Cell viability was not affected by the addition of fibronectin to the substrates, although for all cases (except for on glass) cell viability did increase marginally. PDMS substrates were studied here to test the biocompatibility of PDMS towards endothelial cells because it is a major constituent of the bioassay chamber. PDMS substrates were made with a grooved topology (Figure 3.1).

Cellulose acetate is the base material for our electrospun scaffolds. 15% cellulose acetate or 5% chitosan was allowed to dry on clean glass coverslips (hydrophilic), used to test the effect of these materials alone on HUVEC viability and density. Chitosan was the additive that improved endothelial cell culture parameters in electrospun scaffolding and was subsequently investigated with the bioassay chamber. Early passage HUVECs were seeded onto these coverslips for a Short duration. Cell density and cell viability for HUVECs grown on these substrates did not differ significantly from on glass or on CA180 electrospun scaffolds (Figure 4.7), although, the addition of cellulose acetate did increase cell density insignificantly ($P = 0.12$, ANOVA compared to on glass).

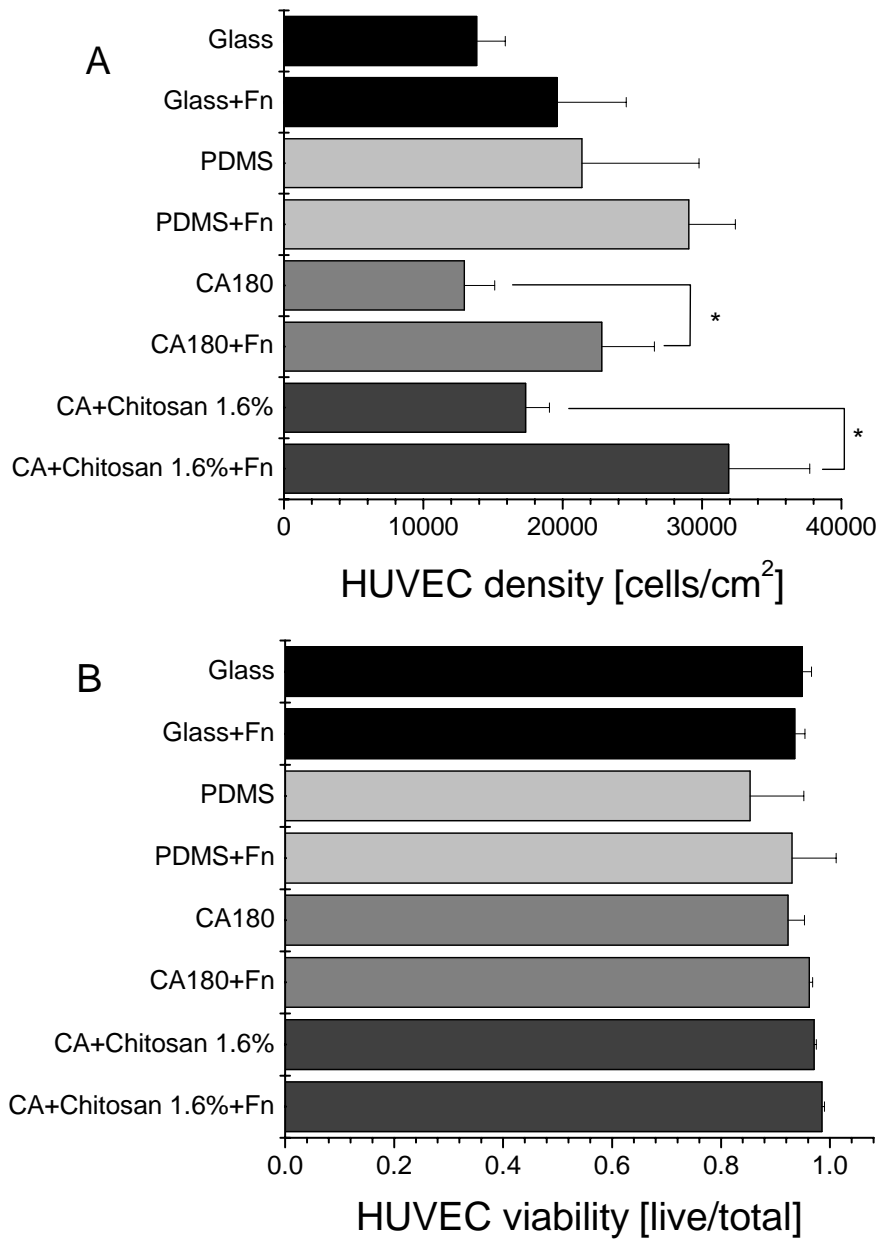


Figure 4.6: Endothelial Cell Density and Viability on Substrates With or Without 3.4µg/mm² Fibronectin. Paired experiments were conducted with Early passage HUVECs to test the effects of fibronectin addition. Cells were grown on the scaffolds for Short durations. Values are mean+S.E.M. Data was obtained from digital image (>30 for each substrate with >100 cells) from 2-8 independent experiments. *differs from paired base substrate (Paired *t*-test, *P* < 0.05).

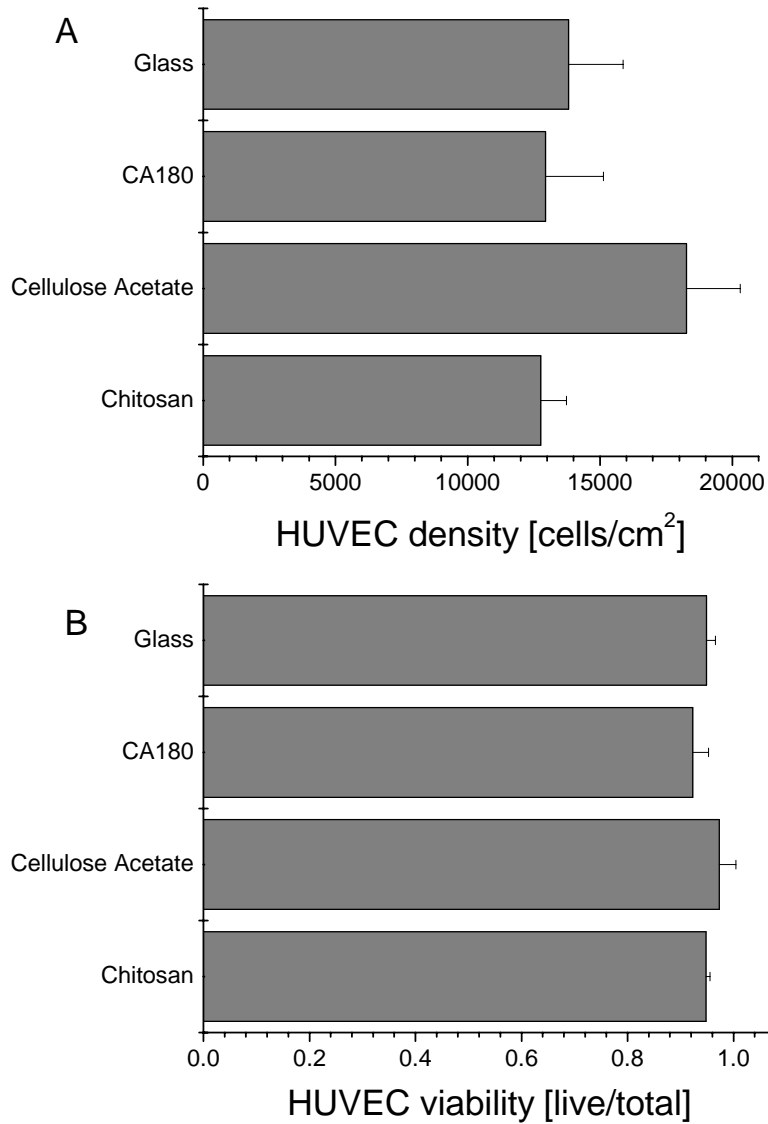


Figure 4.7: Control Experiments to Quantify the Effects of Cellulose Acetate or Chitosan Material on HUVECs. Experiments were conducted with Early passage HUVECs seeded on cellulose acetate or chitosan for a Short duration. This was done to test the base effects of these materials on HUVECs. CA180 and glass data are shown for comparison. Values are mean + S.E.M. Data was obtained from 4 independent experiments.

4.1.1.c HUVEC Morphology on Electrospun Scaffolds

HUVECs were grown on various electrospun substrates as described in Sections 4.1.1.a and 4.1.1.b. Perimeter based cell area was quantified from digital images. Morphology was also investigated visually from these images. Our custom built MATLAB® program, cellcounting.m (Appendix A1), was used to obtain the long and short axis of cells, determine if the cells were elongated or circular and calculate the perimeter based cell area. Of interest were the cell area for circular and elongated cells and the percentage of cells found to be growing in an elongated morphology on each scaffold. Changes in morphology based on the scaffold composition were investigated.

Cell area (Table 4.2) is shown for Short duration HUVECs at both Early and Late passages. There were no trends found in cell area based on, passage, scaffold, duration and cell type (elongated vs. circular). However, the fraction of elongated cells was different based on the substrate that the cells were cultured on. For Early passage cells, our control substrate Matrigel®, had the highest percentage of elongated cells, followed by 5% Chitosan, 15% Cellulose Acetate, CA180 + 3.4 $\mu\text{g}/\text{mm}^2$ Fn, CA + 1.6% chitosan, CA180, CA40, glass and CA80. Thus, smaller fiber scaffolds (CA40 and CA80) tended to have a lower percentage of cells in our preferential elongated morphology. The larger fiber scaffold (CA180) had the highest percentage of elongated cells for our base electrospun scaffolds. With the addition of fibronectin or chitosan to this diameter scaffold (CA180, 1-5 μm), the percentage of elongated cells increased. For Late passage HUVECs, the persistence of the elongated morphology was improved as compared to Early passage cells, but was similar on each substrate.

Cell morphology can also be investigated by visual inspection of digital images obtained after cell culture. The prevalence of the elongated morphology can be seen on both CA + 1.6% chitosan and CA180 scaffolds (Figure 4.8). Early passage HUVECs grown on CA + 1.6% chitosan for 2 days are seen to grow along particular fibers, forming distinct capillary-like structures (Figure 4.8 A), which was unexpected based on the normal *in vivo* timeline for angiogenesis. There are both circular and elongated cells present at this Short growth duration. As a comparison, Early HUVECs grown on CA180 for 3 days do not form those same capillary-like structures, but yet the elongated morphology was still prevalent (Figure 4.8 B). Matrigel® (Figure 4.8 D) induces a distinct capillary network-like morphology for culture endothelial cells. At Long growth durations CA + 1.6% chitosan was able to mimic this distinct morphology (Figure 4.8 C). Both the Matrigel® and the Long duration CA + 1.6% chitosan images were obtained from Early passage HUVECs seeded on the scaffolds for 4 days.

Cell Substrate Type		Elongated cells (n, cells)	Circular cells (n, cells)	Fraction of elongated cells
HUVEC in culture – 2-3 days growth (Short)				
Cell passage (N, experiments)				
Glass	Early (18)	4.99±0.42 (233)	5.56±1.14 (125)	65%
	Late (10)	6.12±1.18 (46)	4.79±0.63 (15)	90%
Matrigel®	Early (3)	4.61±1.52 (65)	---	100%
	Late (3)	4.85±1.84 (52)	6.90±1.49 (4)	89%
CA40	Early (5)	5.33±0.89 (56)	4.16±0.89 (24)	70%
	Late (2)	3.22±0.29 (112)	2.64±1.13 (19)	85%
CA80	Early (4)	5.39±1.20 (88)	4.60±0.87 (55)	61%
	Late (2)	5.00±0.19 (125)	6.21±1.55 (12)	91%
CA180	Early (6)	3.77±1.18 (147)	1.85±0.47 (46)	76%
	Late (3)	4.19±0.29 (85)	3.35±0.52 (10)	89%
CA + 1.6% chitosan	Early (2)	4.48±0.45 (99)	3.79±1.28 (17)	85%
	Late (2)	6.37±0.09 (86)	7.61±0.11 (9)	91%
CA180 + 3.4µg/mm ² Fn	Early (2)	4.14±0.36 (127)	3.14±0.65 (15)	89%
	Late (0)	---	---	---
15% Cellulose Acetate	Early (4)	3.47±0.16 (194)	3.12±0.78 (8)	96%
	Late (0)	---	---	---
5% Chitosan	Early (4)	4.02±0.18 (184)	4.11±1.30 (7)	96%
	Late (0)	---	---	---

Table 4.2: HUVEC Area and Fraction Elongated Cells for Short Growth Durations. Our Cellcounting.m program (Appendix A1) was used to determine the cell area of HUVECs. Entries are the mean±S.E.M. of the cell area [μm^2] (x1,000). For statistical analysis, the sample size for each experiment was considered as the N reported in this table. These were the individual independent experiments. Number of cells, n, is shown for calculation of elongated cell morphology. Statistics were performed on the mean±SD from the original independent experiments. Some data presented here was collected by H. El-Gendi. This table has been modified from (Rubenstein et al., 2007).

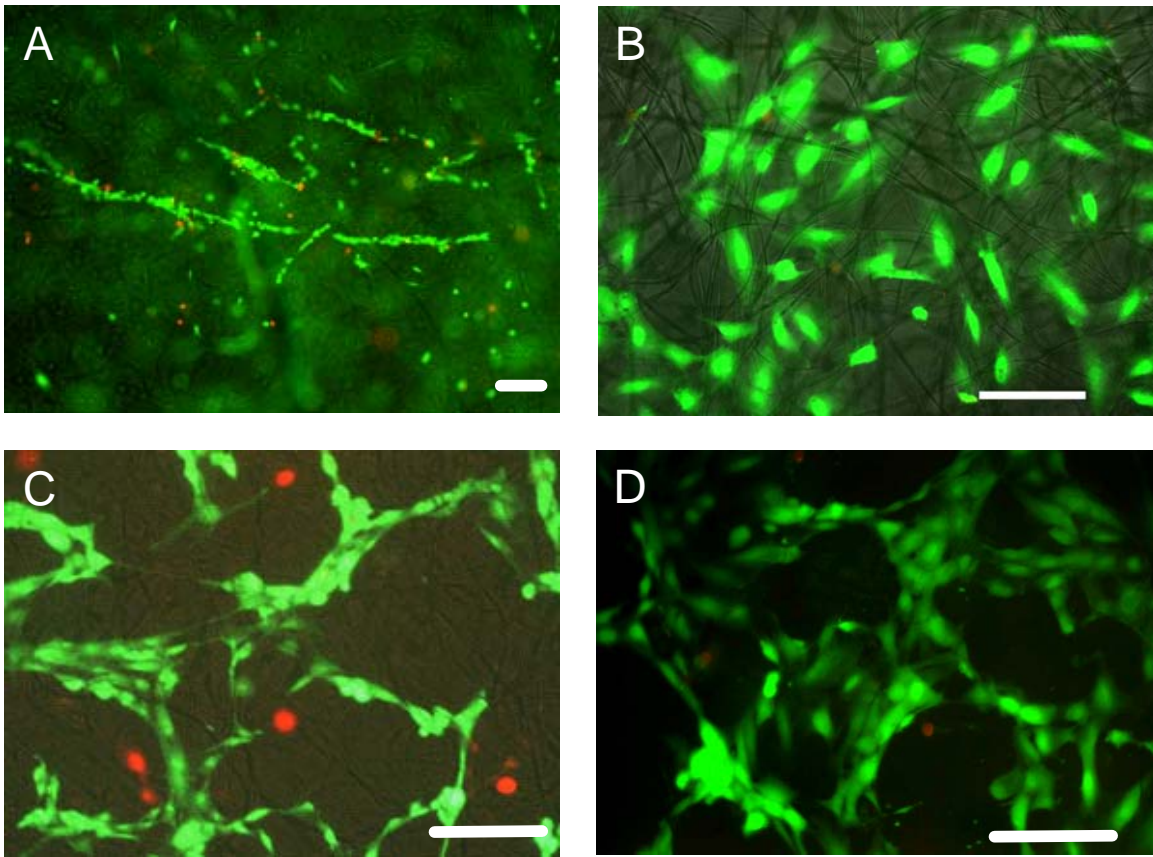


Figure 4.8: Digital Images of HUVECs Grown on Electrospun Scaffolds or Matrigel®. Early passage HUVECs were grown on CA + 1.6% Chitosan for 2 days (A) or 4 days (C), CA180 for 3 days (B) or Matrigel® for 4 days (D). Cells were stained with calcein (green, live) and ethidium (red, dead). The scale bar is 100µm (A) or 10µm (B,C,D). Both elongated and circular cells can be seen in these images. This figure has been taken from (Rubenstein et al., 2007).

4.1.1.d Migration onto Cellulose Acetate Scaffolds

Experiments were conducted to determine if endothelial cells had the ability to migrate onto our electrospun cellulose acetate scaffolds. To test this, early passage HUVECs were seeded onto glass coverslips in individual wells of an 8-well plate (day zero). When media was exchanged on the first day after cell seeding, a *uv* light sterilized CA180 scaffold ($\pm 3.4\mu\text{g}/\text{mm}^2$ Fn or $\pm 1.6\%$ chitosan) was placed into each well (day 1). Digital images of HUVECs were taken on subsequent days (day 2, 4, 7 and 10) examining cells both in the scaffold and on the associated glass $\sim 100\mu\text{m}$ from the scaffold. As a negative control, the contract transfer of ECs onto our scaffolds was investigated. 1 day after cell seeding, a *uv* light sterilized scaffold was placed on top of cells. Media was added to the well and then immediately removed. No live cells (calcein positive) were found in the scaffold indicating that contact transfer does not occur.

Endothelial cells were found on CA180 scaffolds on each imaging day (Figure 4.9). On day 4, cell density on CA180 reached a plateau that was approximately double that of the day 2 cell density. Days 2, 4, 7 and 10, all had a significant increase in cell density as compared with day 1 cell density (0 cells/cm²). Days 4, 7 and 10 had a significantly higher cell density than day 2. This trend was mimicked on the paired glass substrates, where by day 4 the cell population had reached a plateau that was approximately double that of the cell density on day 2. On glass, the cell density on day 2, 4, 7 and 10 was significantly larger than the initial seeding density (500 cells/cm²). The cell density on glass was significantly larger than on paired CA180 for all days.

Endothelial cells were found to be present on the CA180 scaffold with a high viability on all days (Figure 4.9 B). On day 2, the viability of HUVECs on the CA180 scaffold was significantly lower than on glass. However, with more time on the scaffold, cell viability improved and was equal to the viability on glass. At no other time points (other than day 2) was the cell viability on CA180 significantly different than on glass.

Perimeter based cell area (Table 4.3) is shown for HUVECs that had migrated onto a CA180 scaffold. There were no trends in cell area for HUVECs culture on glass substrates. However, location and culture duration did affect the fraction of elongated cells on CA180 scaffolds. HUVECs on the CA180 scaffold showed a preference towards an elongated morphology at all times but this percentage was low and significantly different than on glass for short durations. At longer growth durations HUVECs cultured on CA180 had a significant increase in the percent of elongated cells and this was not significantly different than the paired glass samples (compare day 2 vs. days 4, 7 and 10). HUVECs cultured on glass, maintained a high percentage of elongated cells throughout the culture period.

Digital images taken of HUVECs on the CA180 scaffold or on the paired glass substrates can confirm the morphology quantified in Table 4.3. After day 2, we can see a large increase in cell density and maintenance of the elongated morphology on glass substrates (Figure 4.10, Panels A-D). Comparing cells found on the CA180 scaffold, we see that the population has a large increase in density after day 2 and that HUVECs have an increased preference for the elongated morphology (Figure 4.10, Panels E-H). On day 4, endothelial cells cultured on CA180 began to form capillary-like structures that are commonly found on Matrigel®. This morphology became more prevalent with longer growth durations on the CA180 scaffold and reached a plateau after 7 days of culture (compare Figure 4.8 D with Figure 4.10 H).

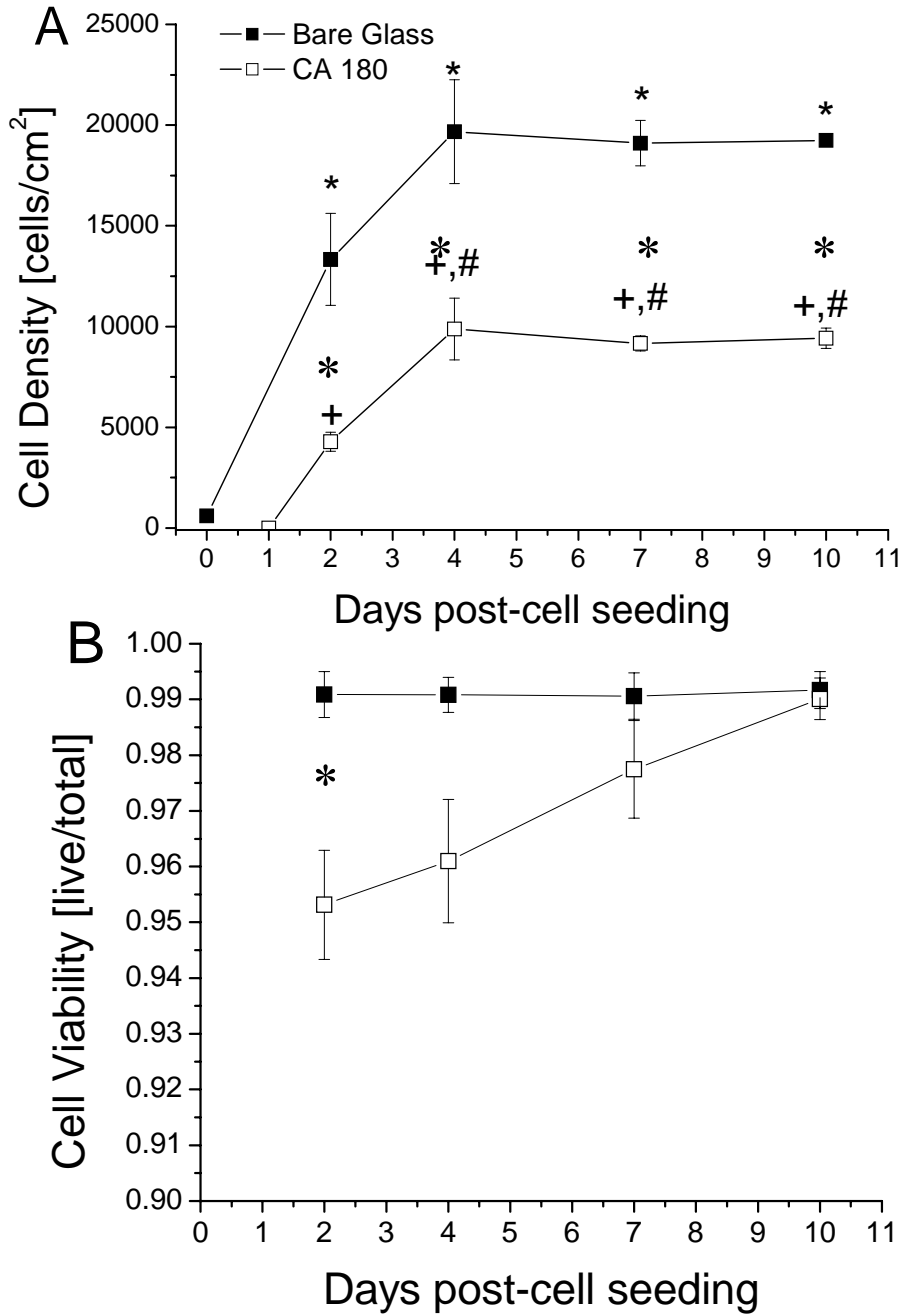


Figure 4.9: Cell Density and Viability for HUVECs that had Migrated onto CA180 Scaffolds. Early passage HUVECs were seeded onto glass coverslips on day zero. One day later, the media was removed from the cells, a sample of CA180 electrospun scaffold was placed into the well and the cells/scaffold were given fresh media. Digital images were taken on days 2, 4, 7 and 10 after cell seeding to determine if cells can migrate onto CA180 scaffolds. Values are mean \pm S.E.M. Data were obtained from 4 independent experiments. ★differs from day 0 (glass, ANOVA, $P < 0.05$), +differs from day 1 (HUVECs, ANOVA, $P < 0.05$), #differs from day 2 (glass or HUVECs, ANOVA, $P < 0.05$), *differs from glass (t -test, $P < 0.05$).

Cell Substrate Type	Elongated cells (n, cells)	Circular cells (n, cells)	Fraction of elongated cells	
HUVEC Migration onto Electrospun Scaffolds – Early Passage				
Days After Cell Seeding (N, experiments)				
2 Days	Glass (8)	3.16±0.26 (313)	3.16±0.55 (16)	95%
	Glass + Fn (4)	2.40±0.14 (241)	2.30±0.22 (26)	90%
	CA180 (4)	2.87±0.34 (128)	2.60±0.36 (73)	64% ^a
	CA180 + Fn (4)	1.89±0.07 (284)	2.03±0.06 (67)	81% ^b
	CA + 1.6% chitosan (4)	2.58±0.29 (268)	2.58±0.42 (42)	86% ^b
4 Days	Glass (8)	3.10±0.08 (323)	3.13±0.27 (30)	92%
	Glass + Fn (4)	2.67±0.33 (124)	2.98±0.50 (12)	91%
	CA180 (4)	2.38±0.13 (111)	2.12±0.25 (29)	79% ^{a,c}
	CA180 + Fn (4)	2.69±0.19 (176)	3.36±0.68 (26)	87% ^b
	CA + 1.6% chitosan (4)	2.42±0.16 (447)	2.69±0.24 (34)	93% ^{b,c}
7 Days	Glass (8)	2.98±0.09 (284)	2.12±0.21 (17)	94%
	Glass + Fn (4)	2.88±0.29 (127)	2.80±0.28 (14)	90%
	CA180 (4)	2.35±0.13 (75)	2.30±0.20 (11)	87% ^c
	CA180 + Fn (4)	2.97±0.21 (194)	2.35±0.34 (24)	89% ^c
	CA + 1.6% chitosan (4)	2.25±0.05 (600)	1.79±0.34 (20)	97% ^{b,c}
10 Days	Glass (8)	2.89±0.11 (219)	3.72±0.50 (19)	92%
	Glass + Fn (4)	2.84±0.02 (41)	2.30±0.28 (5)	89%
	CA180 (4)	2.10±0.02 (50)	1.84±0.17 (9)	85% ^c
	CA180 + Fn (4)	3.19±0.07 (133)	2.80±0.57 (13)	91% ^{b,c}
	CA + 1.6% chitosan (4)	3.22±0.47 (103)	3.23±0.12 (8)	93% ^{b,c}

Table 4.3: Cell Area and Fraction Elongated Cells for HUVECs that had Migrated onto Electrospun Scaffolds. Our Cellcounting.m program (Appendix A1) was used to determine the cell area of HUVECs on CA180 scaffolds and glass. Entries are the mean±S.E.M. of the cell area [μm^2] (x1,000). For statistical analysis, the sample size for each experiment was considered as the **N** reported in this table. These were the individual independent experiments. Number of cells, **n**, is shown for calculation of elongated cell morphology. ^adiffers from hydrophilic glass (*t*-test, $P < 0.05$). ^bdiffers from CA180 (grouped by day, *t*-test, $P < 0.05$). ^cdiffers from 2 day (grouped by scaffold, ANOVA, $P < 0.05$). Some data presented here was collected by D. Zamfir.

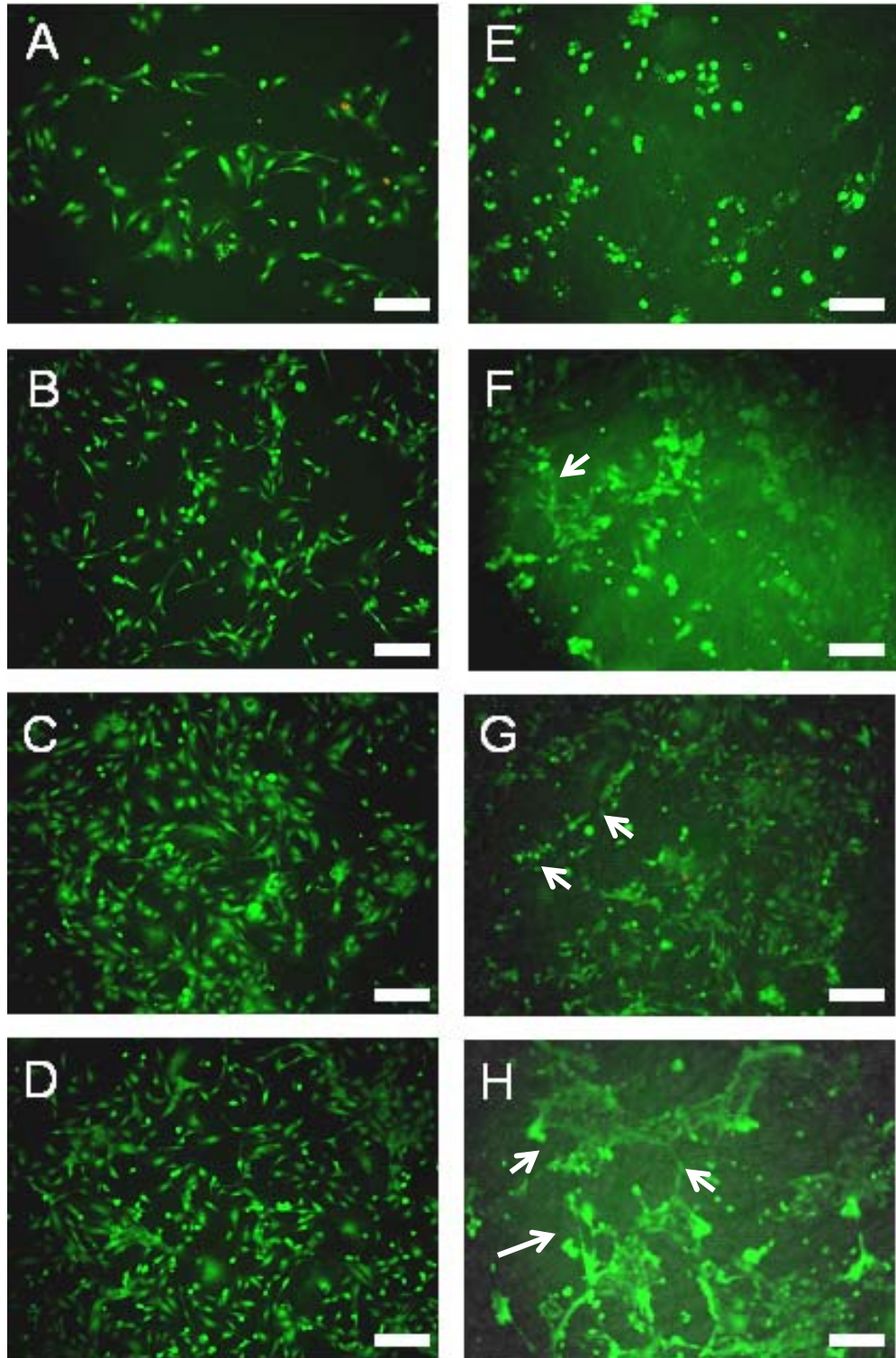


Figure 4.10: Digital Images of HUVECs that had Migrated onto CA180 Electrospun Scaffolds and Paired Bare Glass. HUVECs were found with a high density and viability on CA180 scaffolds 2 (E), 4 (F), 7 (G) and 10 (H) days after cells were seeded onto bare glass coverslips. Paired glass images after 2 (A), 4 (B), 7 (C) and 10 (D) days of culture. Scale bars are 100 μ m. Arrows point to spontaneous capillary-like structures.

Experiments were conducted to determine if endothelial cells had the ability to migrate onto our CA180 + 3.4 $\mu\text{g}/\text{mm}^2$ fibronectin electrospun scaffolds. When media was exchanged on the first day after cell seeding, a *uv* light sterilized CA180 + Fn scaffold was placed into each well (day 1). Endothelial cells were found to be present on the scaffold on each imaging day (Figure 4.11). For cells on the scaffold, the cell density was significantly greater than the initial density (0 cells/cm²) on all imaging days (days 2, 4, 7 and 10). On days 7 and 10, cells on the scaffold had a significantly higher cell density than on day 2. The cell density for longer durations approached and even surpassed that of the cell density on glass even though the early cell density was significantly lower than on glass. On our hydrophilic glass control substrate, the cell density on day 2, 4, 7 and 10 was significantly larger than the initial seeding density. On day 4, the density of cells on the glass reached a plateau (i.e. Figure 4.9). When comparing to base CA180 scaffolds the addition of 3.4 $\mu\text{g}/\text{mm}^2$ Fn increased the cell density for HUVECs within the electrospun scaffold (Table 4.4).

Endothelial cells were found to be present on the scaffold with a high viability on all days (Figure 4.11 B). On day 4, the viability of HUVECs on the CA180 + Fn scaffold was significantly lower than on glass. However, the trend in cell viability was mimicked on the glass (reduction on day 4). By day 10, the viability on both substrates improved and was equal. At no other time points (other than day 4) was the cell viability on CA180 + Fn significantly different than on glass. The addition of Fn did not have a significant effect on cell viability as compared to bare CA180 scaffolds (Table 4.4).

Perimeter based cell area (Table 4.3) is shown for HUVECs that were found on a CA180 + Fn scaffold after cells were seeded onto glass. There were no trends found in cell area for these HUVECs. The fraction elongated cells was dependent on scaffold type and the duration that the cells were on the scaffold. At all durations cells that had migrated onto a CA180 + Fn scaffold had a higher probability of growing with an elongated morphology than cells that had migrated onto a bare CA180 scaffold (significantly different on days 2, 4 and 10). With longer growth durations, the percent elongated cells were significantly increased over the day 2 percent elongated. Cells on the CA180 + Fn or the paired glass did not have a significantly different percent of elongated cells at all growth durations.

Digital images taken of HUVECs on the CA180 + Fn scaffold or the paired glass samples confirm the morphology quantified in Table 4.3. After day 2, we see a large increase in cell density and maintenance of the elongated morphology on glass substrates (Figure 4.12, Panels A-D). Comparing cells found on the CA180 + Fn scaffold, we see that the population increases in density after day 2 and an increased preference for the elongated morphology over the culture duration (Figure 4.12, Panels E-H). By day 7, there were distinct spontaneous capillary-like network forming on both the bare glass and the electrospun scaffold similar to what is commonly found on Matrigel®. This morphology persisted and by day 10 the cells were nearly confluent.

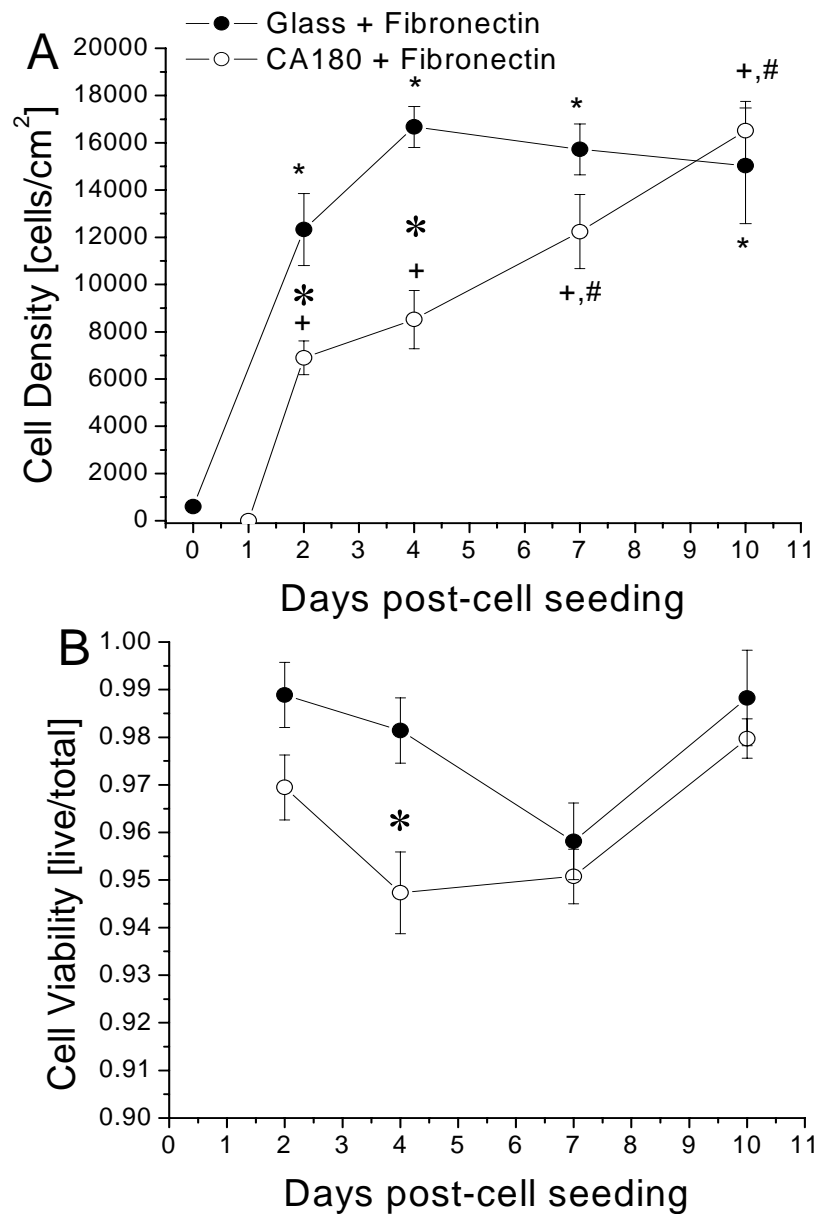


Figure 4.11: Cell Density and Viability for HUVECs that had Migrated onto CA180 Electrospun Scaffolds with the Addition of 3.4µg/mm² Fibronectin. Early passage HUVECs were seeded onto glass coverslips on day zero. One day later, the media was removed from the cells, a sample of CA180 + Fn electrospun scaffold was placed into the well and the cells were given fresh media. Digital images were taken on days 2, 4, 7 and 10 after cell seeding to quantify cell migration onto scaffolds. Values are mean±S.E.M. Data were obtained from 4 independent experiments. ★differs from day 0 (glass, ANOVA, $P < 0.05$), +differs from day 1 (HUVECs, ANOVA, $P < 0.05$), #differs from day 2 (glass or HUVECs, ANOVA, $P < 0.05$), *differs from glass (t -test, $P < 0.05$).

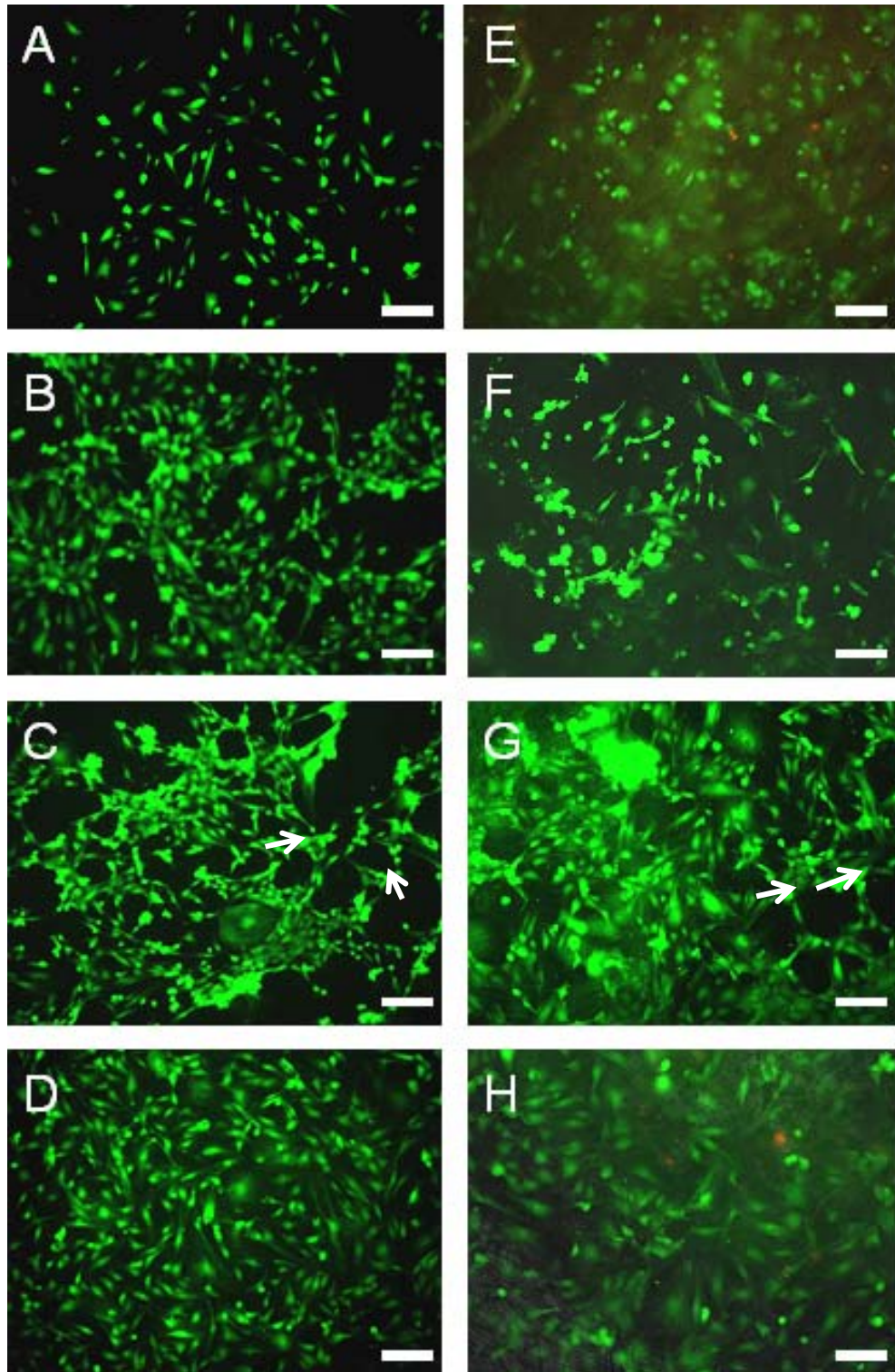


Figure 4.12: Digital Images of HUVECs that had Migrated onto CA180 Electrospun Scaffolds with $3.4\mu\text{g}/\text{mm}^2$ Fibronectin and Paired Bare Glass. HUVECs were found with a high density and viability on CA180 + Fn scaffolds 2 (E), 4 (F), 7 (G) and 10 (H) days after cells were seeded onto glass coverslips. Paired glass images after 2 (A), 4 (B), 7 (C) and 10 (D) days of culture. Scale bars are $100\mu\text{m}$. Arrows point to spontaneous capillary-like structures.

Experiments were conducted to determine if endothelial cells had the ability to migrate onto our electrospun cellulose acetate plus 1.6% chitosan scaffolds (Table 3.1). When media was exchanged on the first day after cell seeding, a *uv* light sterilized CA + 1.6% chitosan scaffold was placed into each well (day 1). Endothelial cells were found to be present on the scaffold on each imaging day (Figure 4.13 A). For cells on the scaffold, the cell density was significantly greater than the seeding density on all days (days 2, 4, 7 and 10). On days 4, 7 and 10 cells on the scaffold had a significantly higher cell density than on day 2. The cell density for longer growth durations approached and even surpassed that of on glass (cell density on days 2 and 4 were significantly lower than on glass). On glass, the cell density on day 2, 4, 7 and 10 was significantly higher than the initial seeding density. On day 4, the cell density on glass reached a plateau. The addition of chitosan to the electrospun scaffold increased HUVEC cell density at all culture times as compared to the base CA180 scaffold (Table 4.4).

Endothelial cells were found to be present on the scaffold with a high viability on all days (Figure 4.13 B). There were no significant differences in cell viability at any culture duration or compared between the paired two substrates. The addition of chitosan did not have a significant effect on cell viability as compared to bare CA180 scaffolds (Table 4.4).

Perimeter based cell area (Table 4.3) is shown for HUVECs that were found on a CA + 1.6% chitosan scaffold after cells were initial seeded onto bare glass coverslips. There were no trends in the perimeter based cell area for these cells. However, the fraction elongated cells was dependent on scaffold type and the duration that the cells were on the scaffold. At all durations the percentage of elongated endothelial cells on a CA + 1.6% chitosan scaffold was higher than cells on a base CA180 scaffold. Also, the fraction of elongated cells increased over time for cells that had migrated onto a CA + 1.6% chitosan scaffold (compared day 2 vs. all later days).

Digital images taken of HUVECs on the CA + 1.6% chitosan scaffold or the paired glass samples confirm cell density/viability (Figure 4.13) and morphology (Table 4.3). After day 2, we can see a large increase in cell density and maintenance of the elongated morphology on hydrophilic glass substrates (Figure 4.14, Panels A-D). Comparing cells found on the electrospun scaffold, we see that the population increases in density after day 2 and there is also an increased preference for the elongated morphology over the culture duration (Figure 4.10, Panels E-H). By day 7, HUVECs found on the electrospun CA + 1.6% chitosan scaffold and on the bare hydrophilic glass were nearly confluent. Spontaneous capillary-like structures were not as prevalent on these scaffolds but appeared by day 10.

HUVEC migration onto various electrospun scaffolds was investigated here. Cell density was significantly improved with the addition of $3.4\mu\text{g}/\text{mm}^2$ fibronectin or 1.6% chitosan to a base cellulose acetate scaffold (CA180) (Table 4.4). From this table we can see that cell density on scaffolds with fibronectin adsorbed approached and even surpassed that of bare hydrophilic glass. These scaffolds also surpassed the cell density found on glass with fibronectin. Chitosan addition increased cell density to levels higher than on bare hydrophilic glass. Viability was high and equal on all substrates and was independent of the substrate that the HUVECs were culture on. For pair-wise comparisons please refer to the individual experiments (Figures 4.8, 4.10 and 4.12). Table 4.4 is shown relative to bare hydrophilic glass for an easy comparison.

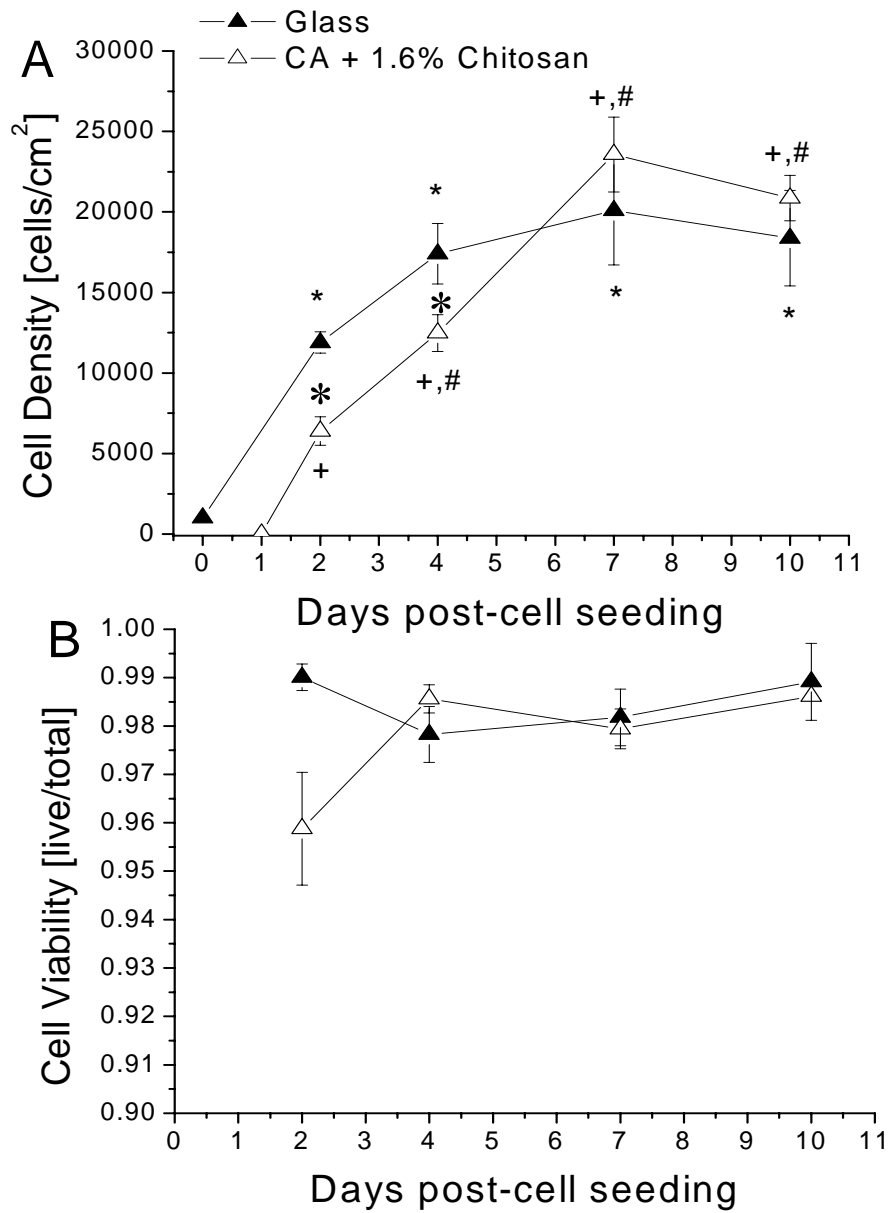


Figure 4.13: Cell Density and Viability for HUVECs that had Migrated onto CA180 + 1.6% Chitosan Electrospun Scaffold. Early passage HUVECs were seeded onto glass coverslips on day zero. One day later, the media was removed from the cells, a sample of CA + 1.6% chitosan electrospun scaffold was placed into the well and the cells/scaffold were given fresh media. Digital images were taken on days 2, 4, 7 and 10 after cell seeding to determine if cells can migrate onto the scaffolds. Values are mean \pm S.E.M. Data was obtained from 4 independent experiments. ★differs from day 0 (glass, ANOVA, $P < 0.05$), +differs from day 1 (HUVECs, ANOVA, $P < 0.05$), #differs from day 2 (glass or HUVECs, ANOVA, $P < 0.05$), *differs from glass (t -test, $P < 0.05$).

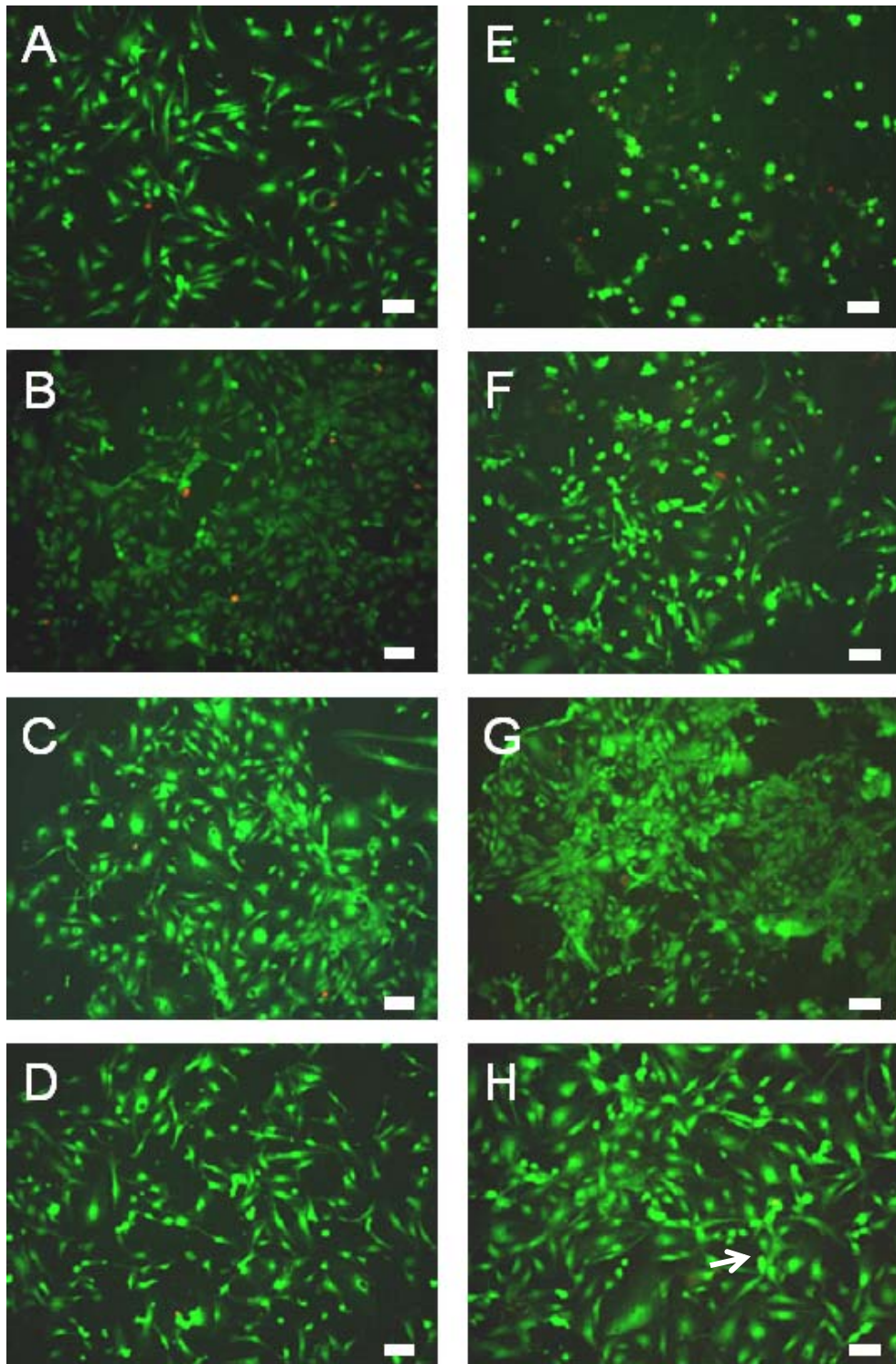


Figure 4.14: Digital Images of HUVECs that had Migrated onto CA + 1.6% Chitosan Electrospun Scaffold. HUVECs were found with a high density and viability on CA + 1.6% chitosan scaffolds 2 (E), 4 (F), 7 (G) and 10 (H) days after cells were seeded onto glass coverslips. Paired glass images after 2 (A), 4 (B), 7 (C) and 10 (D) days of culture. Scale bars are 100 μ m. Arrows point to spontaneous capillary-like structures.

		Bare Glass	Glass + Fn 3.4 μ g/mm ²	CA180	CA180 + Fn 3.4 μ g/mm ²	CA + 1.6% chitosan
HUVEC Cell Density and Cell Viability on CA180 Scaffolds Relative to Bare Glass						
Days After Cell Seeding						
2 Days	Cell Density	100%	97.7%	33.9%	54.7% ^a	50.7% ^a
	Cell Viability	100%	99.8%	96.2%	97.9%	96.8%
4 Days	Cell Density	100%	89.9%	53.5%	46.0%	67.3% ^a
	Cell Viability	100%	99.6%	97.6%	96.2%	100%
7 Days	Cell Density	100%	80.0%	46.3%	61.9% ^a	119.3% ^a
	Cell Viability	100%	98.3%	99.7%	96.6% ^a	99.5%
10 Days	Cell Density	100%	79.9%	50.0%	87.8% ^a	110.9% ^a
	Cell Viability	100%	99.8%	100.0%	98.9%	99.6%

Table 4.4: Cell Density and Viability Relative to Bare Glass for HUVEC Migration onto Cellulose Acetate Based Electrospun Scaffolds. This table allows for a comparison between endothelial cell migration onto a CA180 electrospun scaffold with or without fibronectin adsorbed onto it and a CA + 1.6% chitosan electrospun scaffolds. Bare glass scaffolds are used as the control scaffold for comparison. Electrospun scaffolds were added to individual wells, 1 day after HUVECs were seeded onto the glass substrates. Statistics were performed on the mean \pm SD from the original independent experiments. For more details on individual experiments see Section 4.1.1.d. ^adiffers from CA180 (ANOVA, $P < 0.05$).

4.1.2 Effects of Surface Modifications

Hydrophilic and hydrophobic glass coverslips were used to investigate the directed growth of endothelial cells onto microstamped ECM proteins. To determine the extent that microstamped fibronectin had adsorb onto hydrophilic or hydrophobic glass coverslips, a fluorescent antibody against Fn was used to stain the microstamp preparations. After the Fn had dried and the antibody staining, the coverslips were soaked in a PBS solution for at least 4 hours. The fibronectin remained adsorbed onto both the hydrophilic (Figure 4.15 A) and hydrophobic (Figure 4.15 C) glass coverslips after the wash. The microstamped Fn patterns retain the original stamp geometry after this time period as well. We confirmed the absence of non-specific binding to the glass substrates (Figure 4.15 B/D).

The contact angle for hydrophilic and hydrophobic glass coverslips was measured using KSV Instruments Software. These slides were prepared ~1 week before the contact angle measurement. This mimicked the fabrication procedure for experiments, where coverslips were prepared 1-2 weeks prior to the experiment. The average contact angle for 2 hydrophilic glass coverslips was measured as $28.18^{\circ} \pm 2.50^{\circ}$ (mean \pm SD, left and right angles were measured for one droplet per glass preparation). The average contact angle for 2 hydrophobic glass coverslips was measured as $127.20^{\circ} \pm 4.80^{\circ}$ (mean \pm SD, left and right angles were measured for one droplet per glass preparation). For comparison hydrophilic and hydrophobic glass coverslips were made and tested within 2 hours. The contact angles for these preparations were not significantly different than slides which had been coated for 1 week.

4.1.2.a Effects of Hydrophilic vs. Hydrophobic Surfaces

Control studies were conducted in order to determine the effect of surface modification on endothelial cell viability, density and morphology. Hydrophilic glass coverslips maintained a high density and viability during the culture period (Figure 4.16). However, by altering the glass surface from hydrophilic to hydrophobic there was a significant reduction in both endothelial cell density and viability. Morphology of endothelial cells was investigated. There was no significant trend in cell area (Table 4.5). However, there was a general decrease in the perimeter based area of viable cells on hydrophobic glass coverslips. The fraction of elongated cells was prominent on both substrates but was significantly reduced for endothelial cells on hydrophobic glass substrates. From the obtained cell density, we can calculate a percent confluence of cells grown on hydrophilic vs. hydrophobic glass. By day 3, endothelial cell confluence was 61% on hydrophilic glass and 4.0% on hydrophobic glass (Figure 4.17). Morphology was investigated visually by digital images of hDMECs grown on these substrates (Figure 4.18). Cells found on the hydrophilic glass coverslips were elongated, viable and found with a high density; unlike cells found on hydrophobic glass which had a low viability and density.

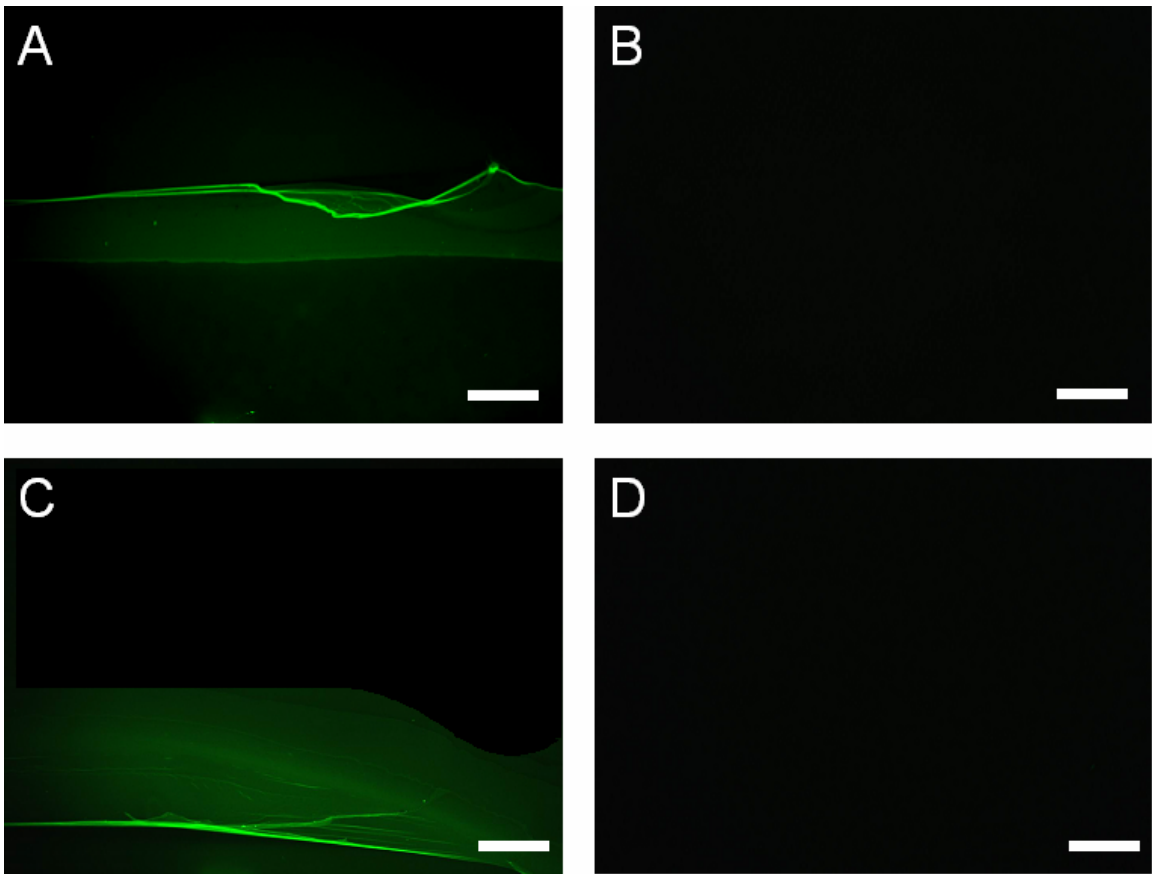


Figure 4.15: Verification of Fibronectin Coating of Hydrophilic and Hydrophobic Glass. Hydrophilic and hydrophobic glass coverslips were used as the base substrate to microstamp fibronectin onto. These coverslips were then stained with an antibody against fibronectin to determine if Fn would remain absorbed onto the glass after 4 hours of being in a PBS solution. We can see the fibronectin remains on both hydrophilic (A) and hydrophobic (C) glass. We confirm the absence of nonspecific binding of the secondary antibody to hydrophilic (B) or hydrophobic (D) glass. All scale bars are 100 μ m.

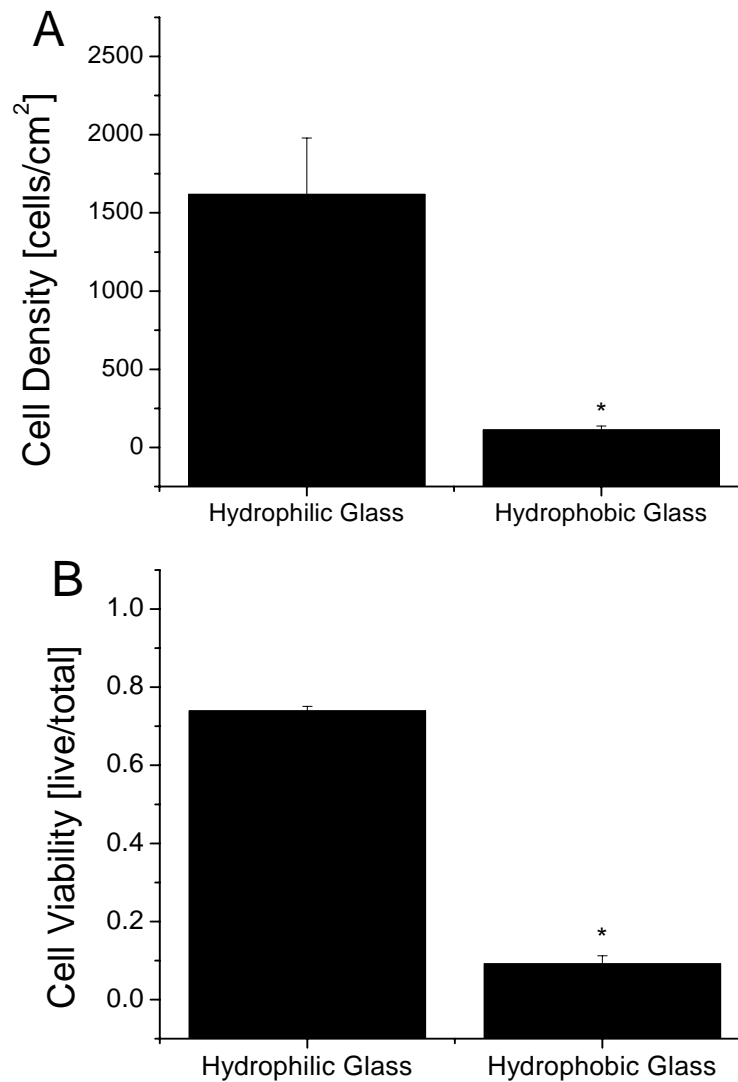


Figure 4.16: hDMEC Density and Viability on Bare Hydrophilic or Hydrophobic Glass. For these experiments, no ECM protein was microstamped onto the glass. The surface of the glass was either hydrophilic or hydrophobic. Values are mean + S.E.M. Data are obtained from 4 independent experiments. *differs from hydrophilic glass (*t*-test, $P < 0.05$).

Cell Substrate Type	Elongated cells (n, cells)	Circular cells (n, cells)	Fraction of elongated cells
hDMEC in culture – Short Duration, Early Passage			
Glass Substrate (N, experiments)			
Hydrophilic Glass (4)	4.15±0.47 (76)	4.51±1.09 (8)	91%
Hydrophobic Glass (4)	3.49±0.95 (18)	3.27±0.13 (5)	78% ^a

Table 4.5: hDMEC Area and Fraction Elongated Cells on Bare Hydrophilic or Hydrophobic Glass. Our cellcounting.m program (Appendix A1) was used to determine the cell area of hDMECs on bare hydrophilic or hydrophobic glass. Entries are the mean±S.E.M. of the cell area [μm^2] (x1,000). For statistical analysis, the sample size for each experiment was considered as the **N**, reported in this table. These were the individual independent experiments. Number of cells, **n**, is shown for comparison of elongated to circular cells. Statistics were performed on the mean±SD from the original independent experiments. ^adiffers from hydrophilic (*t*-test, $P < 0.05$)

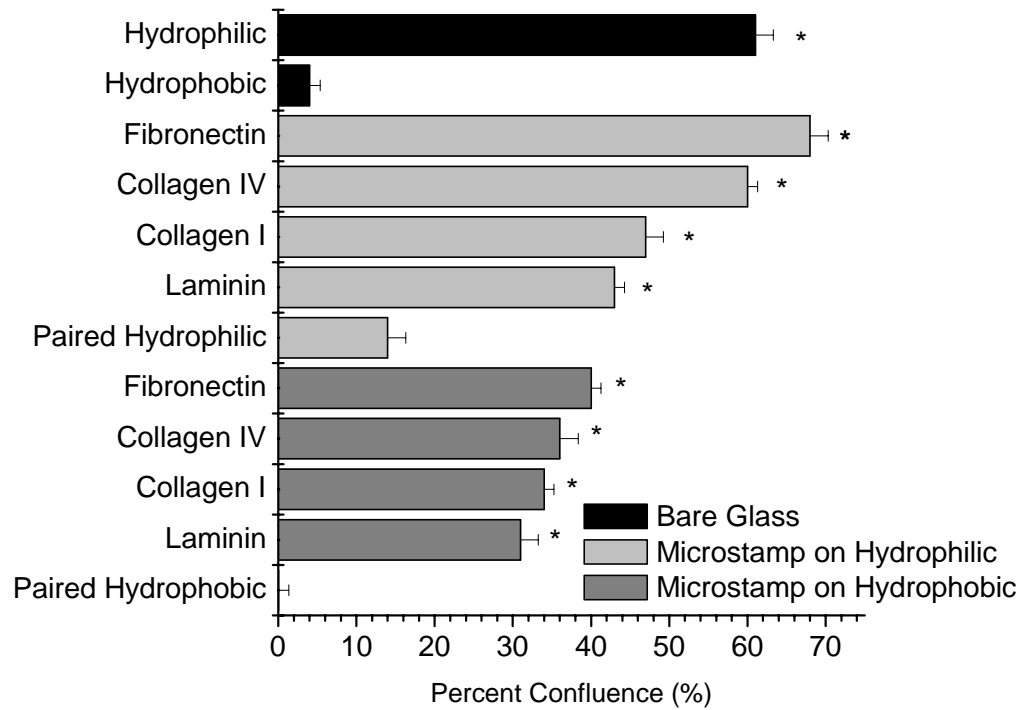


Figure 4.17: hDMEC Percent Confluence for all Microstamp Experiments. Percent confluence is a measure of the area coverage for each particular substrate. For all cell culture experiments, hDMECs were seeded at 800 cells/cm². Values are mean+S.E.M. Data are obtained from 4 independent experiments. *differs from control paired glass (bare samples, *t*-test, $P < 0.05$) or (microstamp samples, ANOVA, $P < 0.05$).

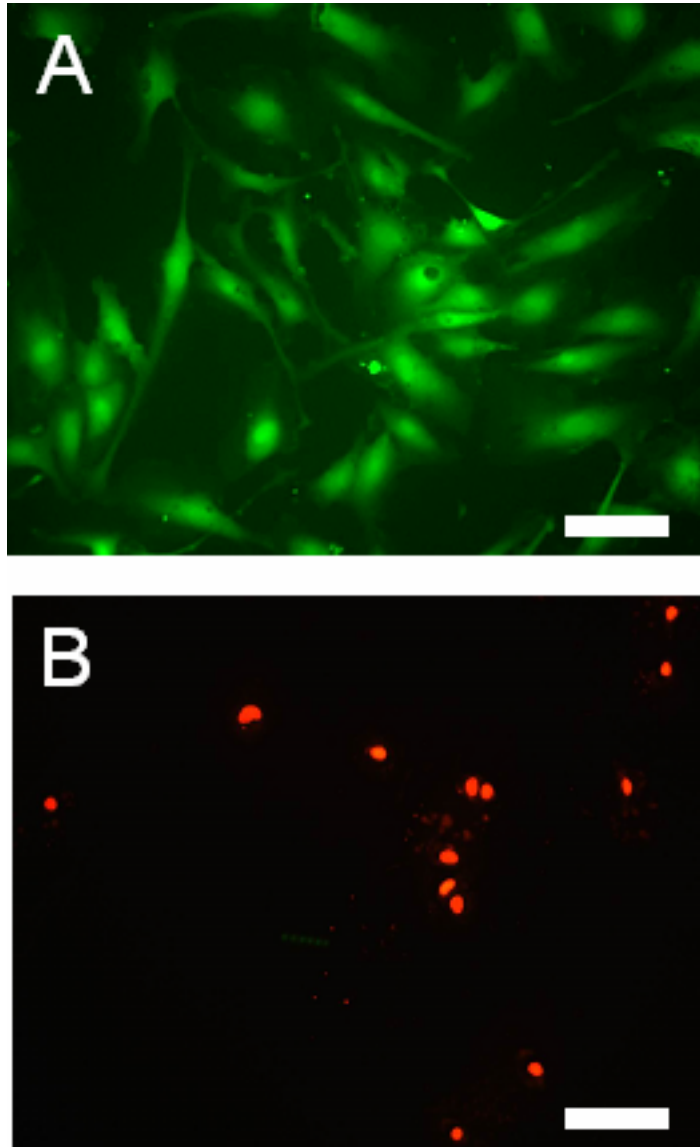


Figure 4.18: Digital Image of hDMECs on Bare Hydrophilic or Hydrophobic Glass. For these experiments, no ECM protein was microstamped onto the glass substrate. The surface of the glass was either hydrophilic (A) or hydrophobic (B). The viability and density for cells grown on hydrophobic glass coverslips was significantly lower than for cells on hydrophilic glass. Scale bars are 100 μ m.

4.1.2.b Effects of Microstamped ECM Proteins on Hydrophilic Surfaces

hDMECs were used to test the directed growth of endothelial cell using our microstamp technique. hDMEC initial seeding density for these experiments was 800 cells/cm². Early passage cells were cultured for Short durations to compare with bioassay chamber experiments (Section 4.2.2.b). Cell density (Figure 4.19 A) was significantly higher on the stamped ECM proteins vs. the bare glass (hydrophilic) for all microstamped ECM proteins. The density was approximately 4 fold higher on the stamped protein than on the bare hydrophilic glass. The cell density on hydrophilic glass was approximately 4 fold larger than the initial seeding density. From the obtained cell density (and perimeter areas), the percent confluence of endothelial cells cultured on the ECM microstamp and on the hydrophilic glass can be calculated. By day 3, endothelial cell confluence was significantly enhanced on each microstamped ECM protein as compared to on paired hydrophilic glass (Figure 4.17). Cell viability (Figure 4.19 B) was not dependent on whether or not the cells were within the stamped region or on the unstamped region for all ECM proteins. Stamp widths were obtained both before and after cell seeding to quantify how effective the stamp would be transferred and then maintain in the same geometry. These values did not vary significantly and were ~160µm (data not shown).

Morphology of hDMECs was also examined using our Cellcounting.m program (Table 4.6). There was no trend in cell area on microstamped ECM proteins on hydrophilic glass. However, the fraction of elongated cells was different based on the substrate that the cells were found on. Cells cultured on microstamped proteins generally had an increase in the percentage of elongated cells after the three day culture period. Stamped fibronectin had the largest percent elongated cells; although all of the substrates were similar and not statistically different.

Digital images of hDMECs were taken within the stamped region (Figure 4.20). A fluorescent marker was mixed with the protein before it was stamped onto glass (XRITC at 1_E-7 M) to determine where the protein had been stamped after culture time. The edges of the patterns were marked as a secondary means to detect the patterns after culture. Cells cultured on all microstamped proteins can be seen to have a preference to grow within the stamped region (Figure 4.20). They also follow the stamp geometry and are mostly excluded from the unstamped region (bare hydrophilic glass). Laminin and collagen I microstamped proteins were less able to exclude hDMECs from the glass than collagen IV and fibronectin. ECs on collagen IV and fibronectin have a higher affinity for the stamped protein and can exclude endothelial cells from the unstamped region better. Endothelial cell clusters were found on some microstamped ECM proteins. The increase in the preference to grown on ECM proteins was confirmed with the increased cell density on all microstamped proteins (Figure 4.19).

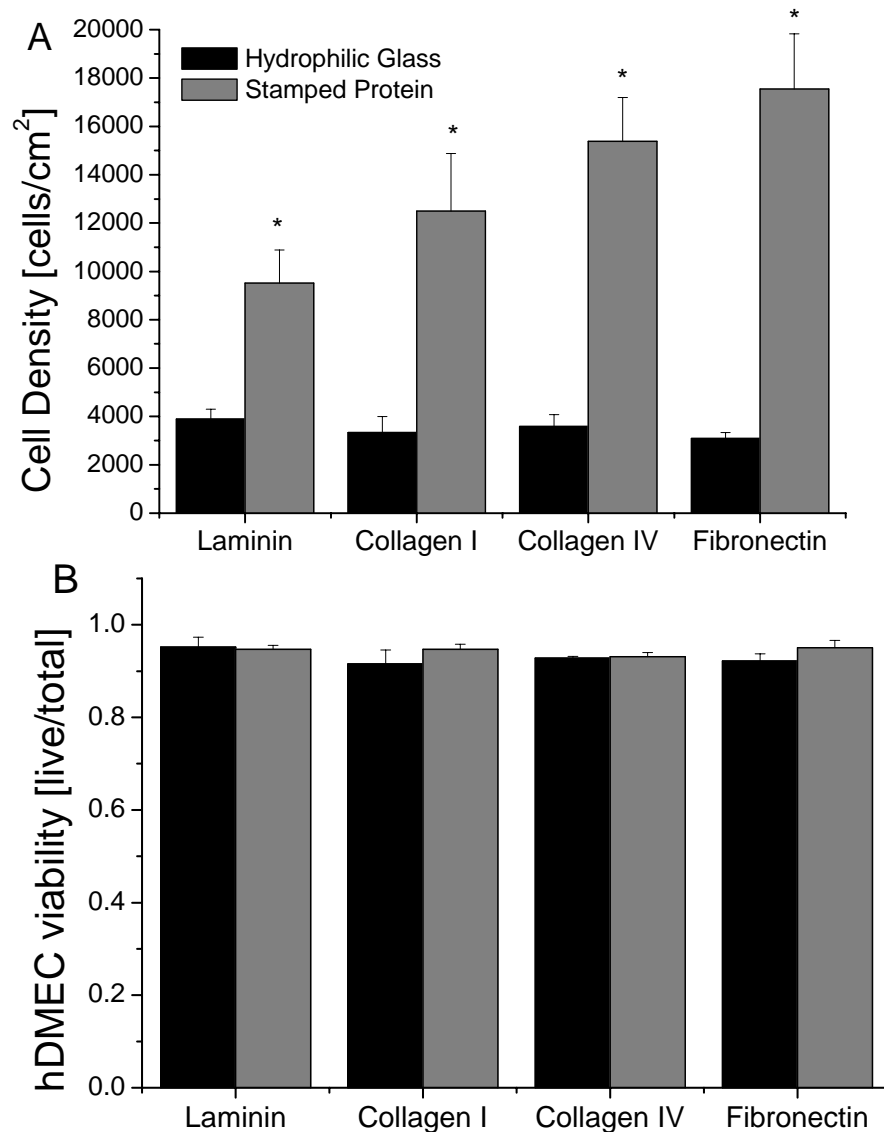


Figure 4.19: hDMEC Density and Viability on ECM Microstamped Proteins on Hydrophilic Glass. hDMECs were seeded onto hydrophilic glass coverslips with microstamped ECM proteins on the surface of the glass. Cell density and viability were calculated. Values are mean + S.E.M. Data is obtained from 4 independent experiments. *differs from hydrophilic glass substrate (Paired *t*-test, $P < 0.05$).

Cell Substrate Type		Elongated cells (n, cells)	Circular cells (n, cells)	Fraction of elongated cells
hDMEC in culture – Short Duration, Early Passage, Hydrophilic Glass				
ECM Protein	Location (N, experiments)			
Laminin	Glass (4)	4.04±0.41 (98)	4.42±0.56 (23)	79%
	Stamp (4)	4.54±0.35 (113)	5.18±0.46 (20)	85%
Collagen I	Glass (4)	4.31±0.66 (59)	3.75±0.25 (18)	77%
	Stamp (4)	3.62±0.15 (123)	4.54±0.14 (25)	86%
Collagen IV	Glass (4)	4.12±0.09 (62)	4.78±0.10 (11)	85%
	Stamp (4)	3.77±0.22 (127)	4.22±0.79 (28)	82%
Fibronectin	Glass (4)	3.87±0.39 (98)	4.52±0.41 (19)	80%
	Stamp (4)	3.71±0.48 (125)	3.91±0.43 (18)	88%

Table 4.6: hDMEC Area and Fraction Elongated Cells on Stamped Proteins on Hydrophilic Glass. Our cellcounting.m program (Appendix A1) was used to determine the cell area of hDMECs on ECM proteins microstamped on hydrophilic glass. Entries are the mean±S.E.M. of the cell area [μm^2] ($\times 1,000$). For statistical analysis, the sample size for each experiment was considered as the **N**, reported in this table. These were the individual independent experiments. Number of cells, **n**, is shown for comparison of elongated to circular cells. Statistics were performed on the mean±SD from the original independent experiments.

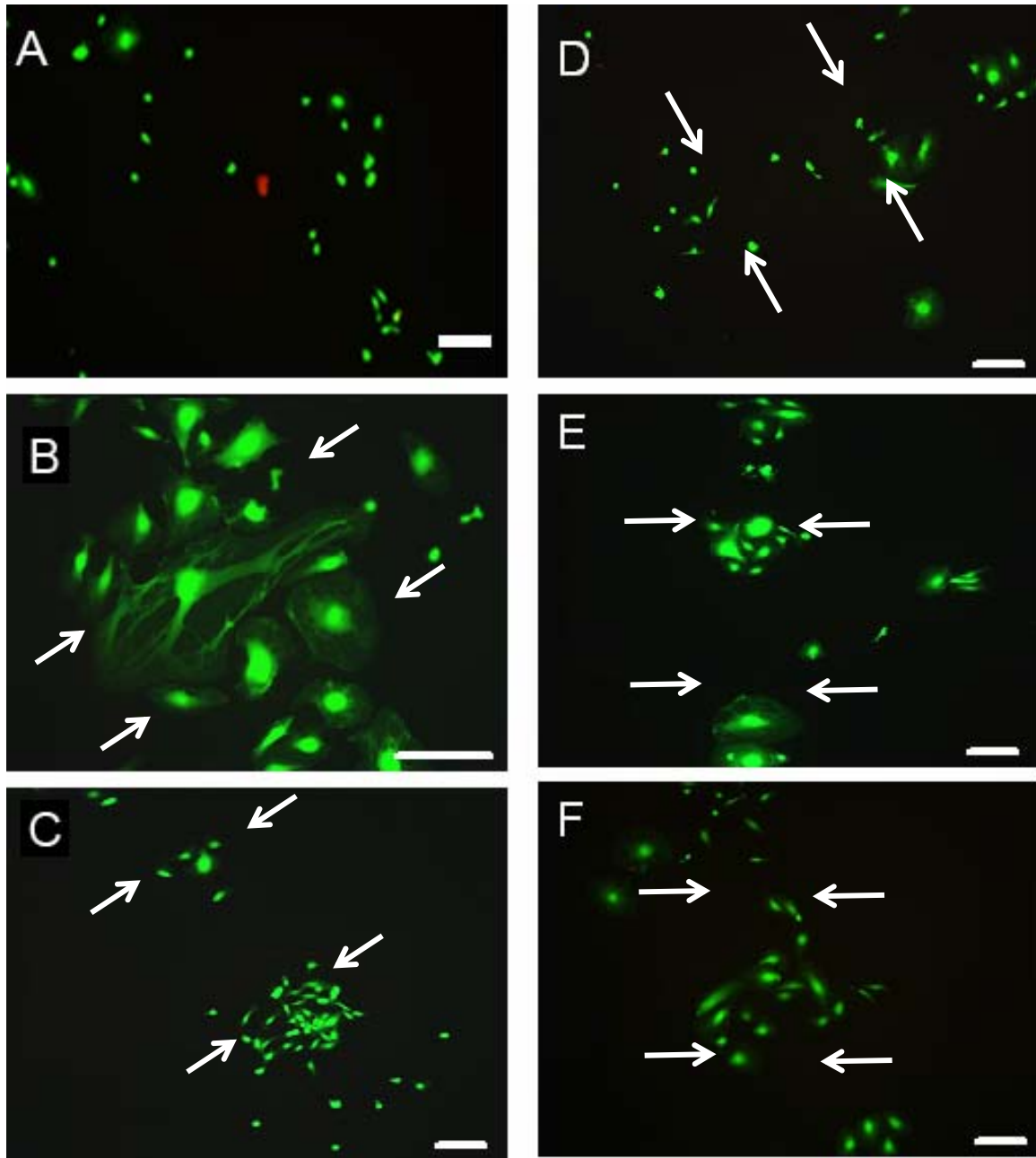


Figure 4.20: Digital Images of hDMECs Cultured on Microstamped ECM Proteins on Hydrophilic Glass. Early passage hDMECs were cultured on stamps for 3 days with an initial seeding density of 800 cells/cm². Cells were stained with calcein (green, live) and ethidium (red, dead). Samples were imaged on bare hydrophilic glass (A) or hydrophilic glass coverslips microstamped with Fn (B,C), laminin (D), collagen I (E) or collagen IV (F) to glass coverslips. All scale bars are 100μm. Arrows mark the boundary of the microstamped region.

4.1.2.c Effects of Microstamped ECM Proteins on Hydrophobic Surfaces

hDMECs were used to test the directed growth of endothelial cell using our microstamp technique onto hydrophobic glass coverslips. Early passage hDMECs were cultured for short durations at an initial seeding density of 800 cells/cm². Cell density (Figure 4.21 A) was significantly higher on the stamped proteins vs. the bare hydrophobic glass for all microstamped ECM proteins. Cell density did not differ between microstamped proteins. Cell density on the hydrophobic glass was lower than the initial seeding density. By day 3, endothelial cell confluence significantly enhanced on each microstamped ECM protein as compared to on hydrophobic glass (Figure 4.17). Cell viability (Figure 4.21 B) was significantly lower on the paired hydrophobic glass coverslips as compared to the microstamped ECM protein.

Morphology of hDMECs was also examined with the Cellcounting.m program (Table 4.7). Cells on microstamped fibronectin, collagen IV and collagen I had a significant increase in perimeter based cell area as compared with paired cells cultured on the non-patterned hydrophobic glass. Laminin did not induce a significant change in perimeter based cell area. Cell type (i.e. elongated vs. circular) did not affect cell area. Endothelial cells found on all of the microstamped ECM proteins showed a preference towards the elongated morphology which was significantly greater than the percent elongated on hydrophobic glass. Some populations of cells found on hydrophobic glass preferred a circular morphology. The quantity of viable cells on the hydrophobic surface was lower than the stamped protein.

Digital images of hDMECs were taken within the microstamped region (Figure 4.22) and can be used to visually inspect cell morphology, density and viability. Endothelial cells cultured on all microstamped proteins can be seen to have a preference to grow within the stamped region and are mostly excluded from the non-stamped region (Figure 4.22). Cells follow the pattern of the stamp geometry. During imaging, cells found within the unstamped region were mostly dead (ethidium positive). Again cells cultured on microstamped fibronectin and collagen IV had a higher affinity for the stamped region than cells cultured on laminin and collagen I. Although ECs were more easily excluded from the unstamped region on these proteins the cell density was not significantly different on any ECM microstamped protein (Figure 4.21).

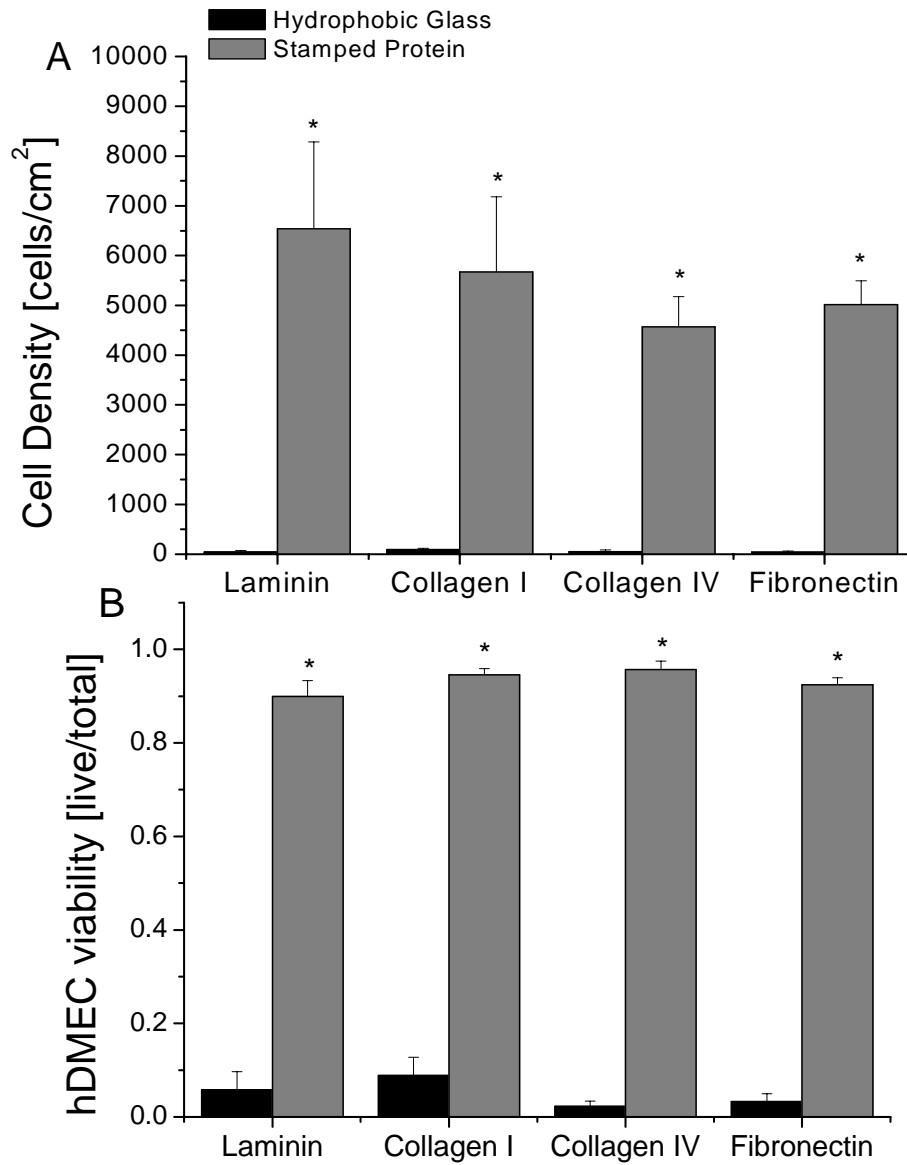


Figure 4.21: hDMEC Density and Viability on ECM Microstamped Proteins on Hydrophobic Glass. hDMECs were seeded onto hydrophobic glass coverslips that was microstamped with ECM proteins. Cell density and viability were calculated from digital images. Values are mean+S.E.M. Data were obtained from 4 independent experiments. *differs from hydrophobic glass (Paired *t*-test, $P < 0.05$).

Cell Substrate Type		Elongated cells (n, cells)	Circular cells (n, cells)	Fraction of elongated cells
hDMEC in culture – Short Duration, Early Passage, Hydrophilic Glass				
ECM Protein	Location (N, experiments)			
Laminin	Glass (4)	3.27±0.49 (13)	3.42±0.29 (5)	72%
	Stamp (4)	3.82±0.22 (121)	4.56±0.09 (11)	92% ^b
Collagen I	Glass (4)	2.86±0.24 (12)	1.99±0.37 (3)	80%
	Stamp (4)	4.32±0.55 ^a (99)	4.19±0.09 ^a (16)	86%
Collagen IV	Glass (4)	1.89±0.19 (5)	2.25±0.22 (11)	32%
	Stamp (4)	4.76±0.14 ^a (76)	3.81±0.18 ^a (7)	92% ^b
Fibronectin	Glass (4)	1.70±0.21 (4)	2.28±0.43 (9)	31%
	Stamp (4)	3.34±0.07 ^a (70)	3.09±0.08 ^a (12)	85% ^b

Table 4.7: hDMEC Area and Fraction Elongated Cells on Stamped Proteins on Hydrophobic Glass. Our Cellcounting.m program (Appendix A1) was used to determine the cell area of hDMECs found on ECM proteins microstamped on hydrophobic glass. Entries are the mean±S.E.M. of the cell area [μm^2] (x1,000). For statistical analysis, the sample size for each experiment was considered as the **N**, reported in this table. These were the individual independent experiments. Number of cells, **n**, is shown for comparison of elongated to circular cells. Statistics were performed on the mean±SD from the original independent experiments. ^adiffers from paired glass sample (ANOVA, $P < 0.05$). ^bdiffers from paired glass (t -test, $P < 0.05$)

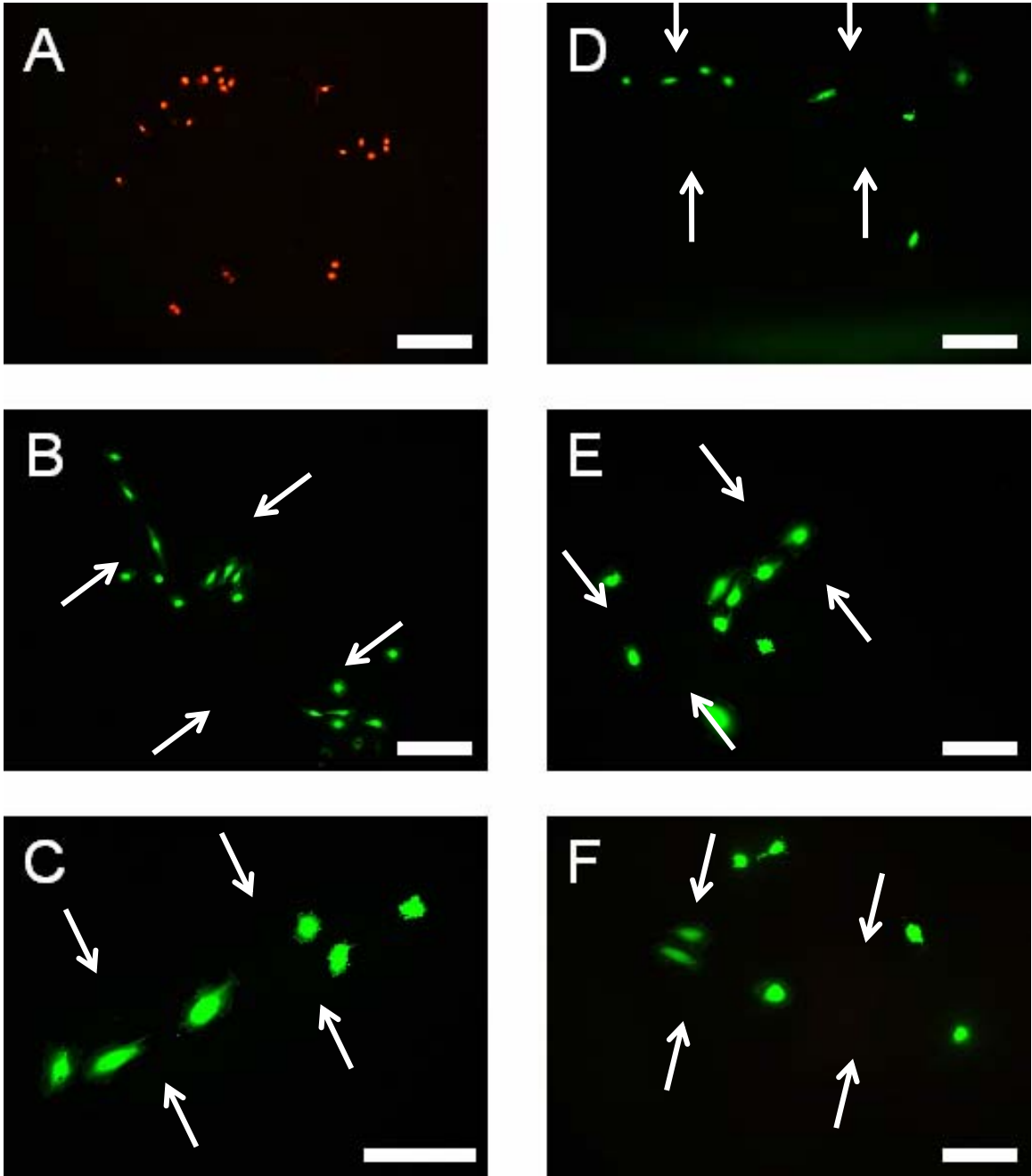


Figure 4.22: Digital Images of hDMECs Cultured on Microstamped ECM Proteins on Hydrophobic Glass. Early passage hDMECs were cultured on stamps for 3 days with an initial seeding density of 800 cells/cm². Cells were stained with calcein (green, live) and ethidium (red, dead). Paired samples were imaged bare hydrophilic glass (A) or hydrophobic glass microstamped with Fn (B,C), collagen IV (D), collagen I (E) or Laminin (F) to glass coverslips. All scale bars are 100µm. White arrows mark the microstamped region.

4.2 Bioassay Chamber

The bioassay chamber was used as a proof of principle that an explanted blood vessel can be used as the initial source of autologous endothelial cells and that these cells can be cultured on electrospun scaffolds in the bioassay chamber. Also, the bioassay chamber can be used to investigate the onset of angiogenesis by stimulating endothelial cells with topographical/topological cues provided by the scaffold and mechanical cues provided by the perfusate flow rate. We also have the ability to direct endothelial cell growth within the bioassay chamber. With the bioassay chamber we have the novel ability to investigate the combined effects of scaffold composition and applied flow rate on a small explanted perfused blood vessel.

Within 30 minutes of perfusion, a pre-map of the vessel (Figure 4.23) was obtained to determine the initial geometry of the cannulated vessel and the branches. A digital movie (obtained using the `imageacq.m` MATLAB® m-file, Appendix A2) was also collected within 30 minutes to verify that the explant was cannulated and was being perfused. One second time lapse frame shots (Figure 4.24) show the changes in the diameter of the blood vessel over time caused by pulsatile perfusion. The period of this flow cycle (perfused at 240 μ L/min) is approximately 4 seconds. (The blood vessel reaches its minimum diameter at time zero and time zero plus four seconds.) The maximum diameter of the blood vessel is reached at approximately time zero plus two seconds. Vessel diameter was measured using ProAnalyst (Version 1.1.9.0, Xcitex Inc., Cambridge, MA) and is shown here in millimeters as the average of 10 individual experiments. The nominal change in diameter is 26 μ m, which is an ~5% increase in vessel diameter. This accounts for an ~11% increase in area (assuming a circular vessel). The accuracy of the diameter measurements and the pulsatile perfusion was tested by performing a sinusoidal regression on the obtained diameter data (Figure 4.25). The best fit sinusoidal regression line was described by: $y = 0.0237\sin(1.579x + 4.6189) + 0.9704$, where x is the time (in seconds) and y is the diameter (in millimeters). The correlation coefficient for this fit was 0.9150. Sinusoidal regression was chosen due to the pulsatile nature of the flow. For some cannulated blood vessels, the vasoactive response was measured after perfusion. Dilation to 10^{-2} M adenosine was measured after perfusion to verify blood vessel tone (baseline $400\pm 60\mu$ m, mean \pm SD, $n=3$) and diameter change (peak-baseline, $45\pm 9\mu$ m, mean \pm SD). These vessels were stored overnight and were perfused for 24 hours (~42 hours after dissection). This indicates that the vessel was responsive and viable after the storage time and more importantly after the experiment.

After perfusion many cells were found within the *uv* light sterilized scaffold that initiated from the blood vessel. It was verified that the cells were endothelial cells and not other cells from the explant (i.e. VSMCs) with the BS-1 lectin staining. To image cells with the BS-1 lectin, transmitted light was used to identify cells within the scaffold. Without changing the focus, we switched to fluorescent light to determine if the cells were stained positively with the BS-1 lectin. All cells identified in this way were BS-1 lectin positive (Figure 4.26). Although cells were seen to undergo apoptosis during the BS-1 lectin staining, some cells remained in an elongated morphology attached to scaffold fibers. Cell death is a known side effect of the lectin imaging. Some cells appeared circular during imaging. Dual staining with DAPI identifies the nucleus of endothelial cells in scaffolds (Figure 4.26 C-E). These images were taken after a murine aorta was perfused for 24 hours at a flow rate of 240 μ L/min.

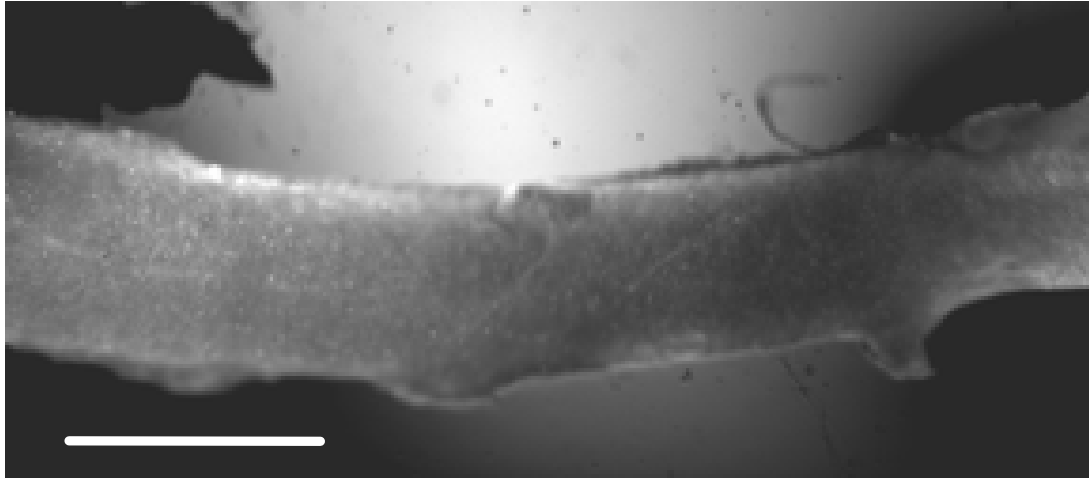


Figure 4.23: Cannulated Isolated Murine Aorta. This is a pre-map of a cannulated vessel, obtained within 30 minutes of initiating perfusion. The image was taken using a 4X objective. Open side branches can be seen in this image. Data would be obtained at the end of the experiment near this branch as dictated by Figure 3.6. The scale bar is 500 μ m. This figure has been taken from (Rubenstein et al., 2007).

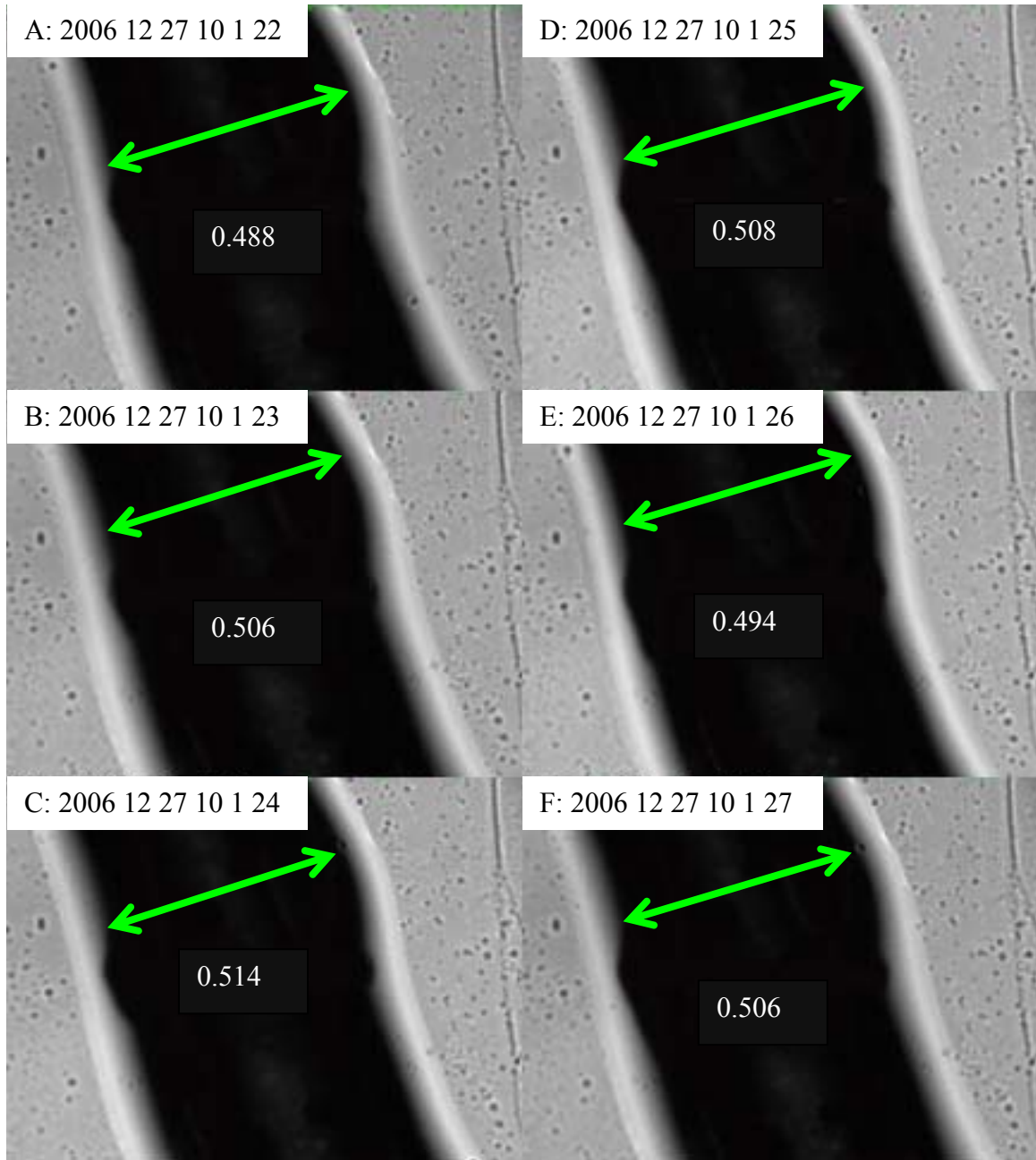


Figure 4.24: Time Lapse Images of a Perfused Murine Aorta. An explanted murine aorta was perfused at a flow rate of $240\mu\text{L}/\text{min}$. A movie of vessel perfusion was obtained using the imageacq.m program (Appendix A2). These images progress at 1 second interval; the time stamp is year, month, day, hour, min, second (the stamp is for 1 individual perfusion video). The diameter of the vessel was measured at each time point and is shown in millimeters as the average of 10 independent experiments.

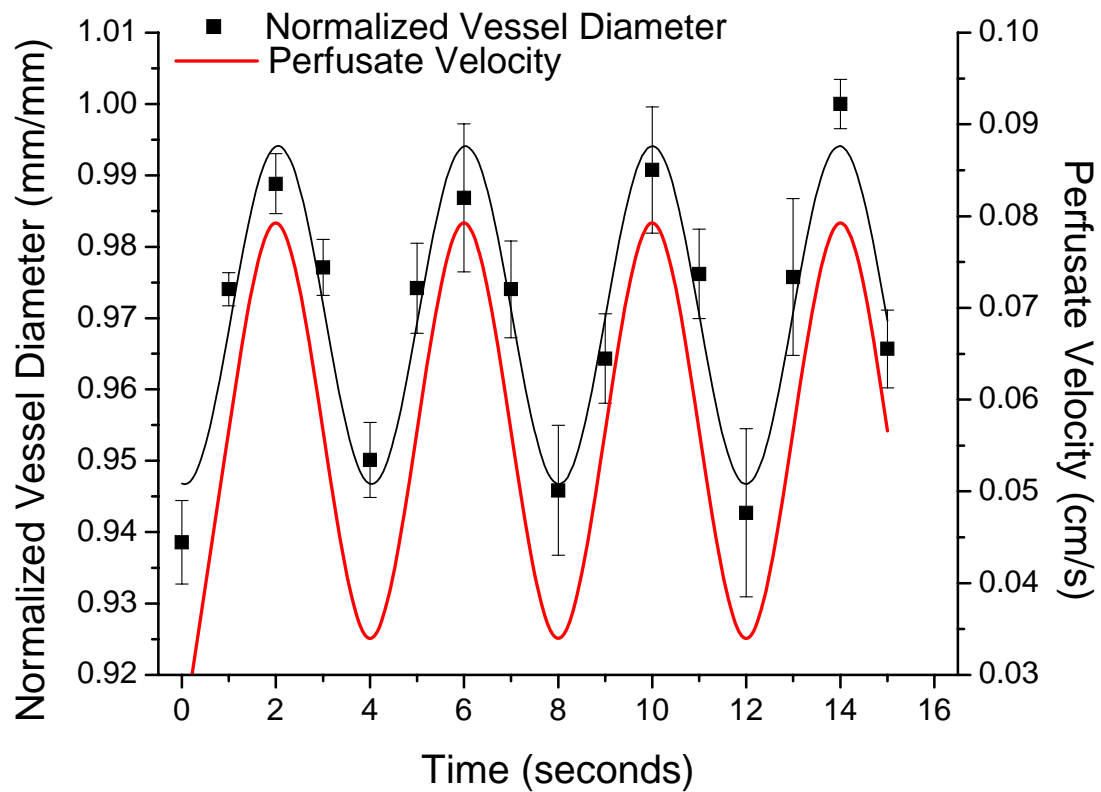


Figure 4.25: Sinusoidal Waveform Approximation of Perfused Vessel Diameter. Using a sinusoidal regression, the best fit line was obtained for the diameter data measured in Figure 4.23. The pulsatile perfusate velocity waveform is a sine wave (red), calculated from the input flow rate. The data is the means \pm S.E.M. of 10 vessels normalized to the maximum value for diameter. Sinusoidal best-fit regression line for normalized vessel diameter is $y = 0.0237 \sin(1.579x + 4.6189) + 0.9704$, with $r^2 = 0.9150$.

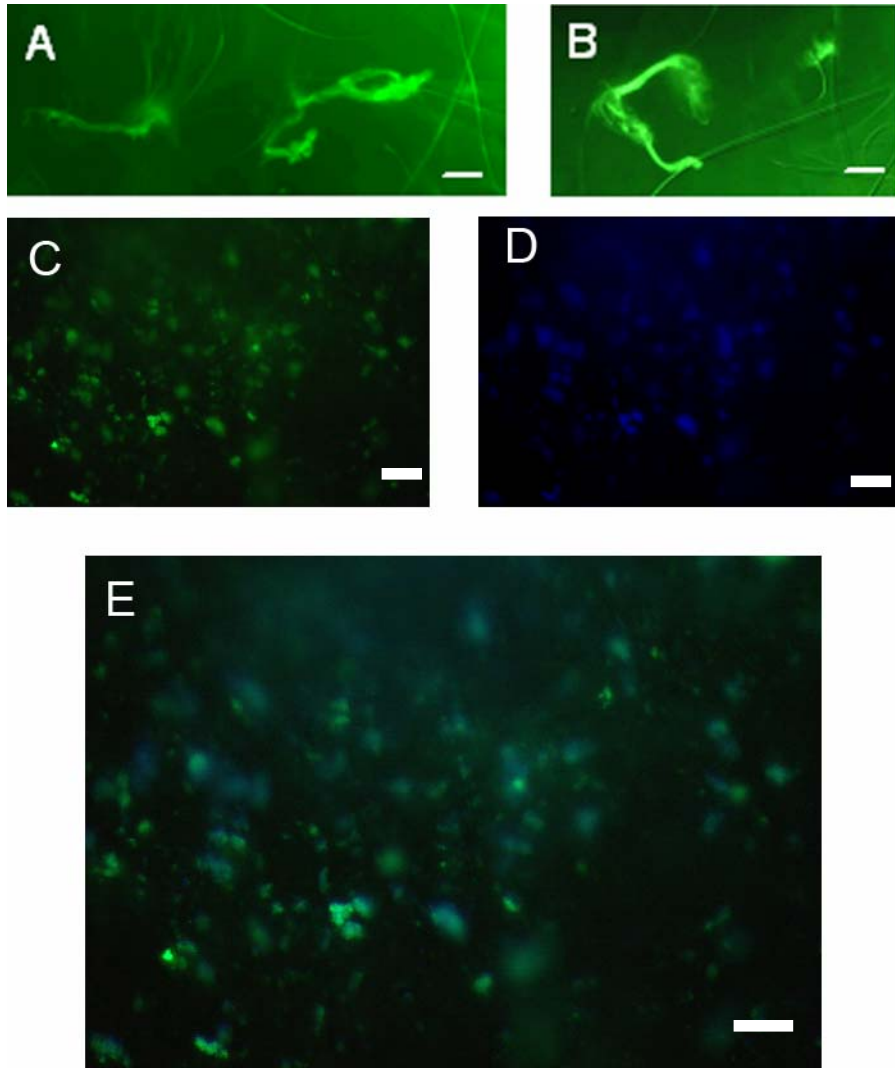


Figure 4.26: Digital Images of Endothelial Cells Stained with the BS-1 Lectin and DAPI. These images were taken without fixation because the cellulose acetate scaffold would dissolve. These representative cells were found between 400 and 500 μm from the explanted blood vessel. Cells are seen with a circular (A) or elongated (B) morphology after the BS-1 lectin staining. Dual staining of the BS-1 lectin (C) and DAPI (D) identifies endothelial cells and their nuclei. Merged image shows the co-localization of BS-1 lectin and DAPI (E). Scale bars are 100 μm . These cells were found in a CA180 scaffold after 24 hours of perfusion at 240 $\mu\text{L}/\text{min}$. This figure has been modified from (Rubenstein et al., 2007).

4.2.1 Electrospun Cellulose Acetate Scaffolds

4.2.1.a Effects of Scaffold Composition and Flow Rate

Cell culture experiments were used as initial studies to examine the effects of scaffold fiber diameter and composition on endothelial cell density, viability and morphology. From these experiments, we concluded that endothelial cells preferred electrospun cellulose acetate with larger fiber diameters than the characteristic ECM fiber diameter (CA180). Also, there was an enhancement in this preference with the addition of chitosan to the electrospun scaffold. Both of these scaffolds provided a growth template to support high density and viability of HUVECs with an elongated morphology. Therefore, we chose to examine these two scaffolds in the bioassay chamber. Matrigel® was used as the controls scaffold in these studies. In all studies, a murine aorta was used as the explanted cannulated blood vessel. During perfusion, the explant and perfusate was warmed to 37°C with room air (partial pressures/humidity).

Figure 4.27 shows cell density (A, C) and viability (B, D) as a function of scaffold type, flow rate and distance from the open side branch. Examining Low flow, both density and viability were improved by the addition of chitosan to the CA180 electrospun scaffold. Matrigel® did not show improved density or viability over CA180 Near the side branch, but viability Far from the branch was significantly enhanced. With High flow, cells found within the CA180 electrospun scaffold had an increased cell density Far from the side branch. Viability was high for all scaffolds and imaging locations, with High flow, except for a diminished viability on Matrigel® Far from the branch.

Comparing Low vs. High flow conditions, neither density nor viability on CA + 1.6% chitosan was affected by flow state, suggesting that flow rate was not an indicator of a growth limiting condition (e.g., low oxygen delivery). However, with a higher flow rate the cell viability improved on CA180 and Matrigel®. Matrigel® showed higher density and improved viability near the side branch with High flow, but decreased density and viability far from the side branch. Overall, the addition of chitosan enhanced the culture conditions of CA180 scaffolds and provided the most stable endothelial cell growth scaffolding.

Control experiments were conducted without subjecting murine aortas to a low pulsatile flow. These aortas were kept in our normal perfusate surrounded by a CA180 electrospun scaffold, testing if endothelial cells would migrate out of the blood vessel into the surrounding scaffold. After 24-48 hours, endothelial cells were found in the scaffold Near the explanted blood vessel but not Far from the blood vessel, indicating that without flow cells can enter the electrospun scaffold. Cell density was approximately 200 cell/cm² (range was ~100-500 cells/cm²) Near the vessel. Cell viability was >90% without perfusion. Cell density but not viability was significantly higher in the presence of flow (i.e. Figure 4.27) showing that there is an extra stimulus for migration in the presence of a low pulsatile flow rate.

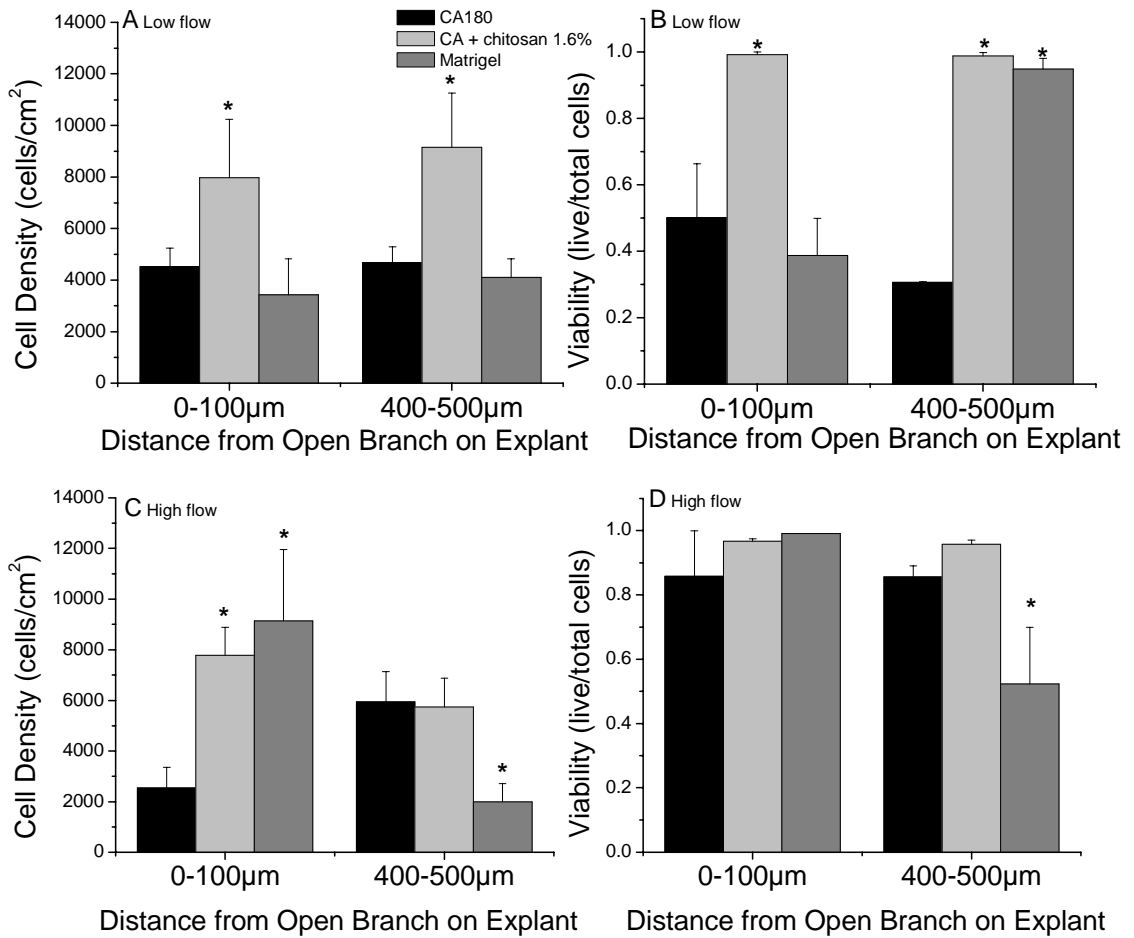


Figure 4.27: Endothelial Cell Density and Viability in our Bioassay Chamber after Perfusion of the Explanted Artery. The x-axis shows the distance from the open side branch where the images were taken (refer to Figure 3.6). The explanted aortas were perfused with pulsatile flow at 100µL/min (Low Flow, A, B) or 240µL/min (High Flow, C, D). Values are mean+S.E.M. Data were obtained from 4-6 independent experiments. *differs from on CA180 (ANOVA, $P < 0.05$). This figure has been taken from (Rubenstein et al., 2007).

4.2.1.b Cell Morphology on Electrospun Scaffolds

Perimeter based cell area for elongated and circular cells exposed to High flow did not differ significantly (Table 4.8). There were no trends found in cell area. The majority of cells were found with an elongated morphology but to a lesser extent than endothelial cells in cell culture (compare Table 4.8 with Tables 4.1 and 4.3). However, cells that had apparently migrated onto electrospun scaffolds had a lower percentage of elongated cells, one day after cell seeding. Similar to cell culture results, endothelial cells within Matrigel® scaffolds were found only to be in the elongated morphology. The addition of chitosan enhanced the elongated morphology as compared to the CA180 scaffolds. Cell area was unrelated to flow rate (data not shown).

Endothelial cell morphology in the bioassay chamber was visually inspected from digital images obtained after perfusion (Figure 4.28). This figure illustrates the prevalence of both elongated and circular morphologies within the scaffold for this Short growth duration. Both Near (Figure 4.28 A) and Far (Figure 4.28 B) from the blood vessel a high density of viable cells were found within CA180 scaffold. Endothelial cells found within the CA + 1.6% chitosan (Figure 4.28 C) and Matrigel® scaffolds (Figure 4.28 D) had a high density and viability as well. Endothelial cells cultured in Matrigel® were seen to initiate spontaneous capillary-like structures that were common in cell culture experiments (Figure 4.8 D). At this Early growth duration spontaneous capillary-like networks were not seen in the electrospun scaffolds.

Cell substrate type		Elongated cells (n, cells)	Circular cells (n, cells)	Fraction of elongated cells
Endothelial Cells in the Bioassay Chamber – High Flow				
Proximity to explant				
Matrigel® (4)	0-150µm	8.22±0.44 (207)	---	100%
	400-500µm	4.08±1.16 (205)	---	100%
CA180 (6)	0-150µm	4.62±0.89 (35)	2.91±0.85 (15)	70%
	400-500µm	4.18±1.18 (175)	3.32±1.60 (161)	52%
CA + 1.6% chitosan (4)	0-150µm	4.18±1.36 (117)	3.20±0.45 (68)	63%
	400-500µm	8.51±2.24 (144)	5.75±2.48 (77)	65%

Table 4.8: Endothelial Cell Area and Fraction Elongated Cells in the Bioassay Chamber After Perfusion. Our Cellcounting.m program (Appendix A1) was used to determine the cell area of endothelial cells within the bioassay chamber. Entries are the mean±S.E.M. of the cell area [μm^2] (x1,000). For statistical analysis, the sample size for each experiment was considered as the **N**, reported in this table. These were the individual independent experiments. Number of cells, **n**, is shown for comparison of elongated to circular cells. Statistics were performed on the mean±SD from the original independent experiments. This table has been taken from (Rubenstein et al., 2007).

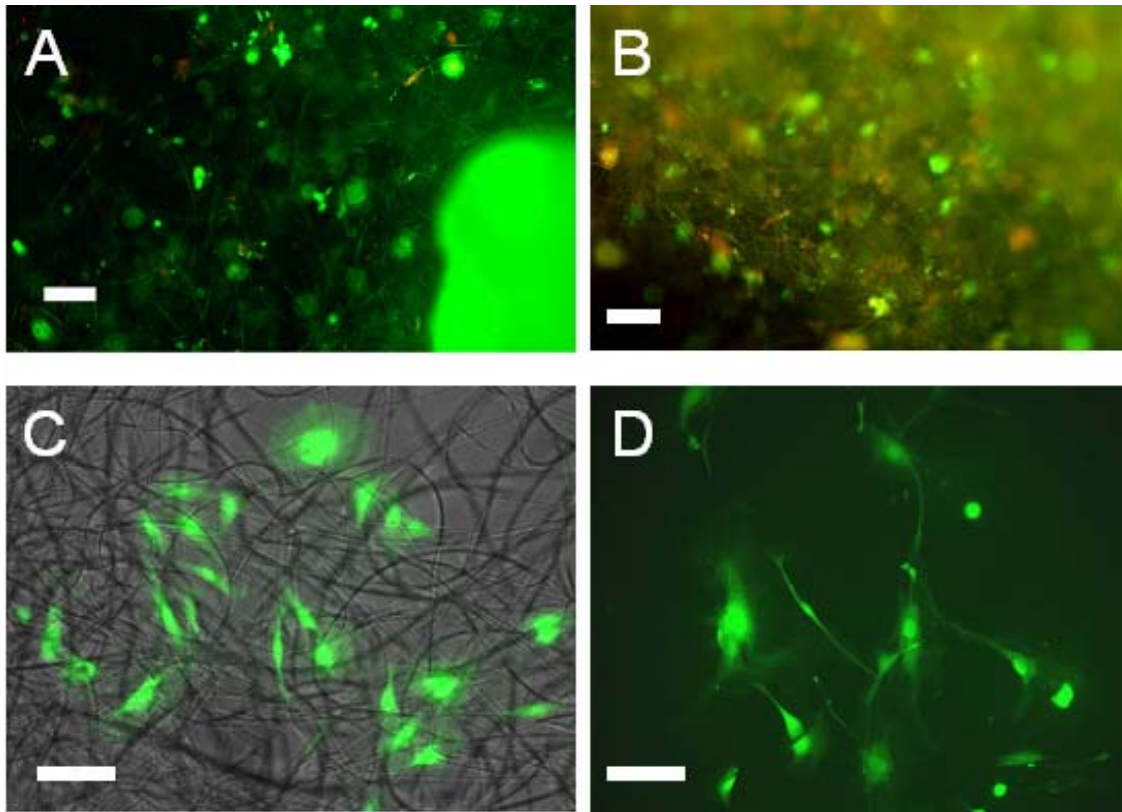


Figure 4.28: Digital Images of Endothelial Cells within Scaffolds after Perfusion in the Bioassay Chamber. CA180 Near (A) and Far (B) from the explant, CA + 1.6% chitosan Far (C) and Matrigel® Far (D) scaffolds all supported the culture of endothelial cells with a high density and viability. These endothelial cells originated from an explanted aorta that was perfused for 24 hours at 240 μ L/min. Cells were stained with calcein (green, live) and ethidium (red, dead). These images were used for visual inspection of cell morphology. Scale bars are 100 μ m. This figure has been modified from (Rubenstein et al., 2007).

4.2.1.c Long Term Culture of Murine Aortas in Electrospun Scaffolds

The long-term culture of an explanted murine aorta was studied in the bioassay chamber. These experiments were conducted as a proof-of-principle that an autologous endothelial cell source can be kept viable over a 7 day perfusion period and that endothelial cells can be maintained in an electrospun scaffold over this culture period. Aortas were perfused at 240 μ L/min over the entire culture period. Endothelial cells from the explant were found within a cellulose acetate electrospun scaffold (CA180) at all time points after perfusion (Figure 4.29). The cell density was highest Far from the explant on day 1 but at all other locations and times cell density was equal. Cell viability was low on day 1 both Near and Far from the explant and increased significantly with longer perfusion. The cell viability significantly improved and reached the highest value after seven days of perfusion.

Perimeter based cell area was measured for endothelial cells that had originated from an explanted perfused murine aorta over long culture times. No trends were found in the perimeter based cell area for these cells. However, the percent of elongated cells was affected by the perfusion duration. After 1 day of perfusion, the elongated morphology was prominent Near the explant, but is not as prominent Far from the explant. For longer perfusion times, the percent of elongated cells significantly increases both Near and Far from the explant. The largest percentage of elongated cells is found with the longest perfusion time. This mimics the morphology data that was collected to test migration into our electrospun scaffolds (Section 4.1.1.d).

Morphology was visually inspected from digital images taken after perfusion. Endothelial cells imaged Near and Far from the branch were found with a high cell density and viability (Figure 4.30). Comparing cells found after 1 day of perfusion (Figure 4.28 A/B), the percentage of elongated cells increased with an increased perfusion time. Digital images obtained Near the blood vessel after 7 days of perfusion were similar to the representative images shown here.

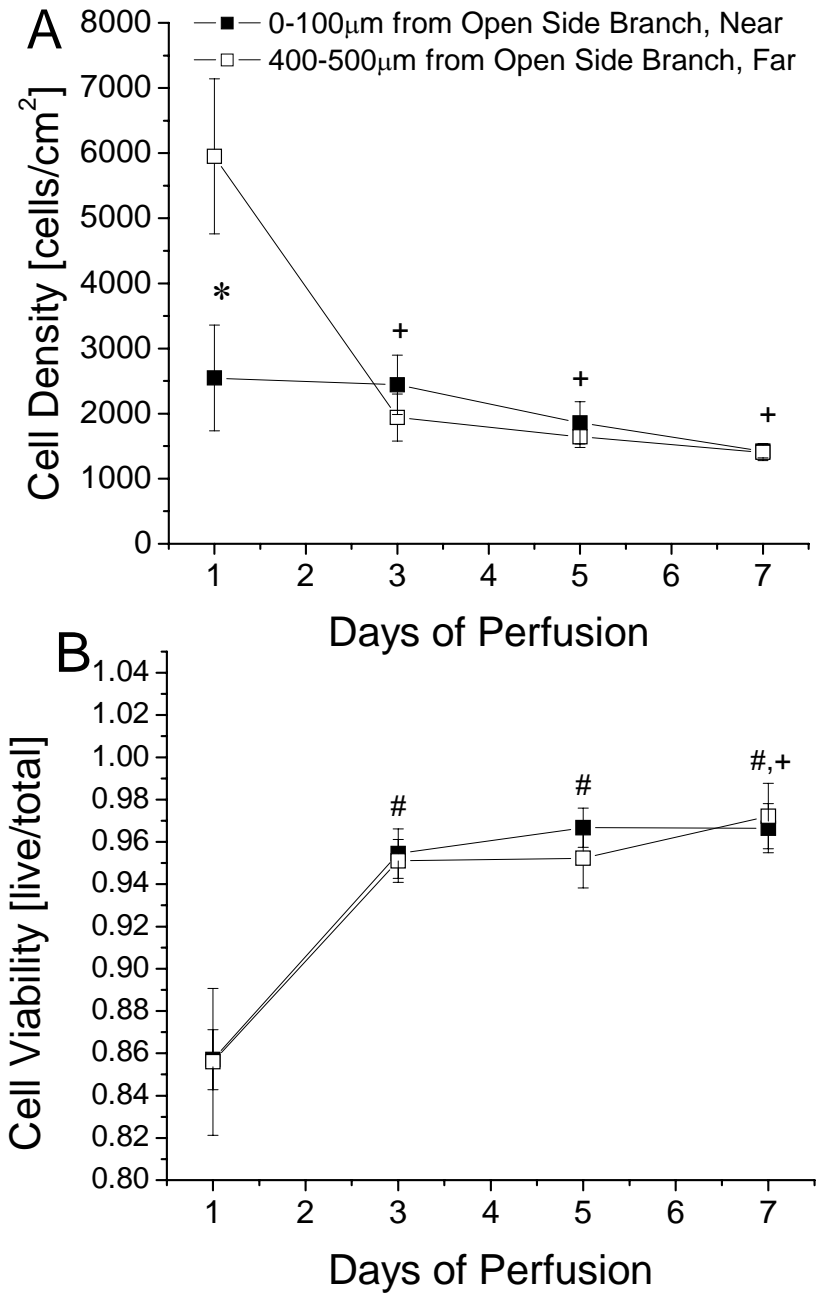


Figure 4.29: Endothelial Cell Density and Viability after Long-Term Perfusion of an Explanted Murine Aorta in our Bioassay Chamber. Mouse aortas were cannulated and perfused at 240µL/min for up to 7 days in the bioassay chamber. Explants were surrounded by a CA180 scaffold. Viability and density was measured both Near (0-100µm) and Far (400-500µm) from open side branches. Values are mean± S.E.M. #differs from day 1 (Near explant, ANOVA, $P < 0.05$), *differs from Near (Paired t -test, $P < 0.05$), +differs from day 1 (Far from explant, ANOVA, $P < 0.05$).

Cell substrate type		Elongated cells (n, cells)	Circular cells (n, cells)	Fraction of elongated cells
Endothelial Cells in the Bioassay Chamber – High Flow, Long-Term Perfusion				
Proximity to explant				
1 Day (6)	0-150 μ m	4.62 \pm 0.89 (35)	2.91 \pm 0.85 (15)	70%
	400-500 μ m	4.18 \pm 1.18 (175)	3.32 \pm 1.60 (161)	52%
3 Day (4)	0-150 μ m	3.19 \pm 0.73 (69)	3.62 \pm 1.84 (15)	82% ^a
	400-500 μ m	3.42 \pm 1.00 (57)	3.01 \pm 0.81 (17)	77% ^a
5 Day (4)	0-150 μ m	3.24 \pm 0.79 (56)	3.34 \pm 1.40 (12)	82% ^a
	400-500 μ m	3.45 \pm 0.41 (46)	3.99 \pm 1.44 (17)	73% ^a
7 Day (4)	0-150 μ m	4.60 \pm 0.53 (60)	4.34 \pm 0.71 (13)	82% ^a
	400-500 μ m	3.31 \pm 0.72 (65)	3.79 \pm 0.54 (9)	88% ^a

Table 4.9: Endothelial Cell Area and Fraction Elongated Cells in the Bioassay Chamber After Long-Term Perfusion. Our Cellcounting.m program (Appendix A1) was used to determine the cell area of endothelial cells within the bioassay chamber. Entries are the mean \pm S.E.M. of the cell area [μm^2] (x1,000). For statistical analysis, the sample size for each experiment was considered as the **N**, reported in this table. These were the individual independent experiments. Number of cells, **n**, is shown for comparison of elongated to circular cells. Statistics were performed on the mean \pm SD from the original independent experiments. ^adiffers from day 1 (grouped by proximity to explant, ANOVA, $P < 0.05$).

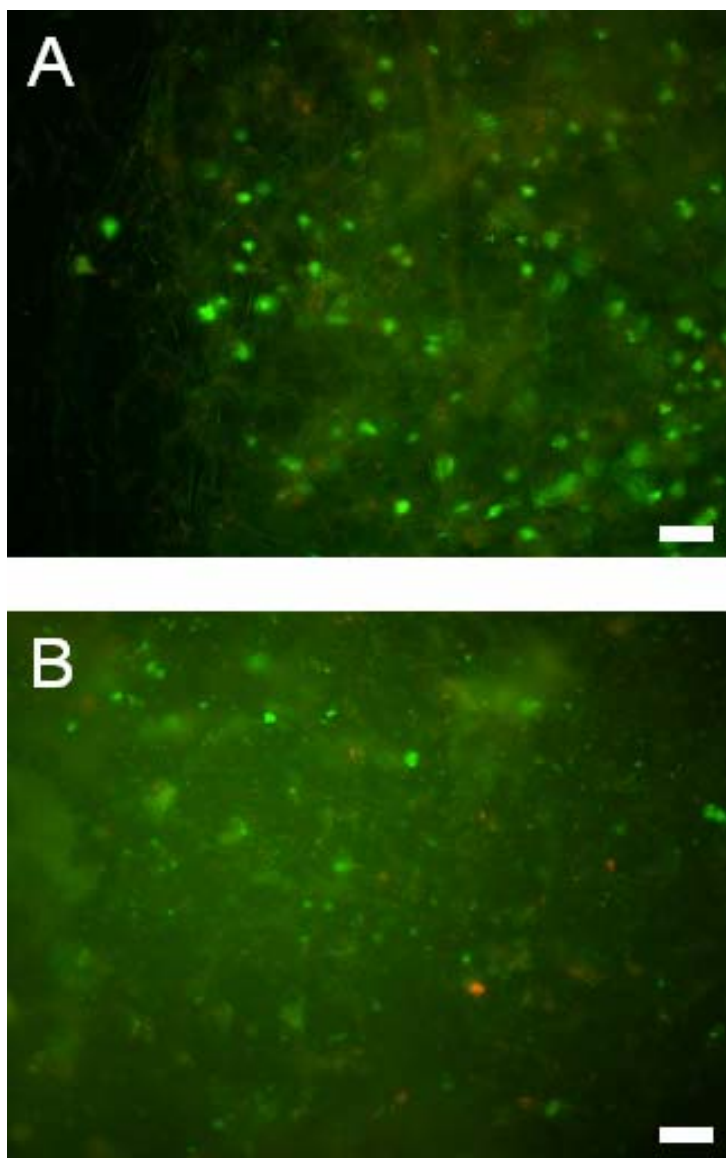


Figure 4.30: Digital Images of Endothelial Cells within CA180 Electrospun Scaffolds after Long-Term Perfusion in the Bioassay Chamber. Endothelial cells were found with high cell density and viability Far from the explant 3 days (A) and 5 days (B) after perfusion. Cells were stained with calcein (green, live) and ethidium (red, dead). See Figure 4.28 B for density and viability comparisons after 1 day of perfusion. Digital images collected after 7 days of perfusion were similar to the representative images shown here. Scale bars are 100 μ m.

4.2.2 Effects of Surface Modifications

4.2.2.a Effects of Hydrophilic vs. Hydrophobic Surfaces

Control studies were conducted in order to determine the combined effects of our glass surface modification and a low pulsatile flow on endothelial cell viability, density and morphology in the bioassay chamber. Endothelial cells that had originated from a perfused murine aorta were found with a significantly higher cell density and cell viability both Near and Far from an open side branch on hydrophilic glass as compared to on hydrophobic glass (Figure 4.31). Morphology of endothelial cells was also investigated for these two substrates. Cell area was not significantly different for elongated or circular cells on hydrophilic vs. hydrophobic glass (Table 4.10). This was true both Near and Far from the blood vessel. The fraction of elongated cells was prominent on both substrates but was significantly enhanced for endothelial cells on hydrophilic glass substrates. After one day of perfusion, endothelial cell confluence was significantly higher on hydrophilic glass as compared with hydrophobic glass (Figure 4.32). Morphology can also be investigated visually from digital images of endothelial cells found on the glass substrates (Figure 4.33). These images confirm our findings of a low viability/density on hydrophobic glass. The cell density, in these experiments, was generally lower than most other bioassay chamber experiments (Section 5.2.2).

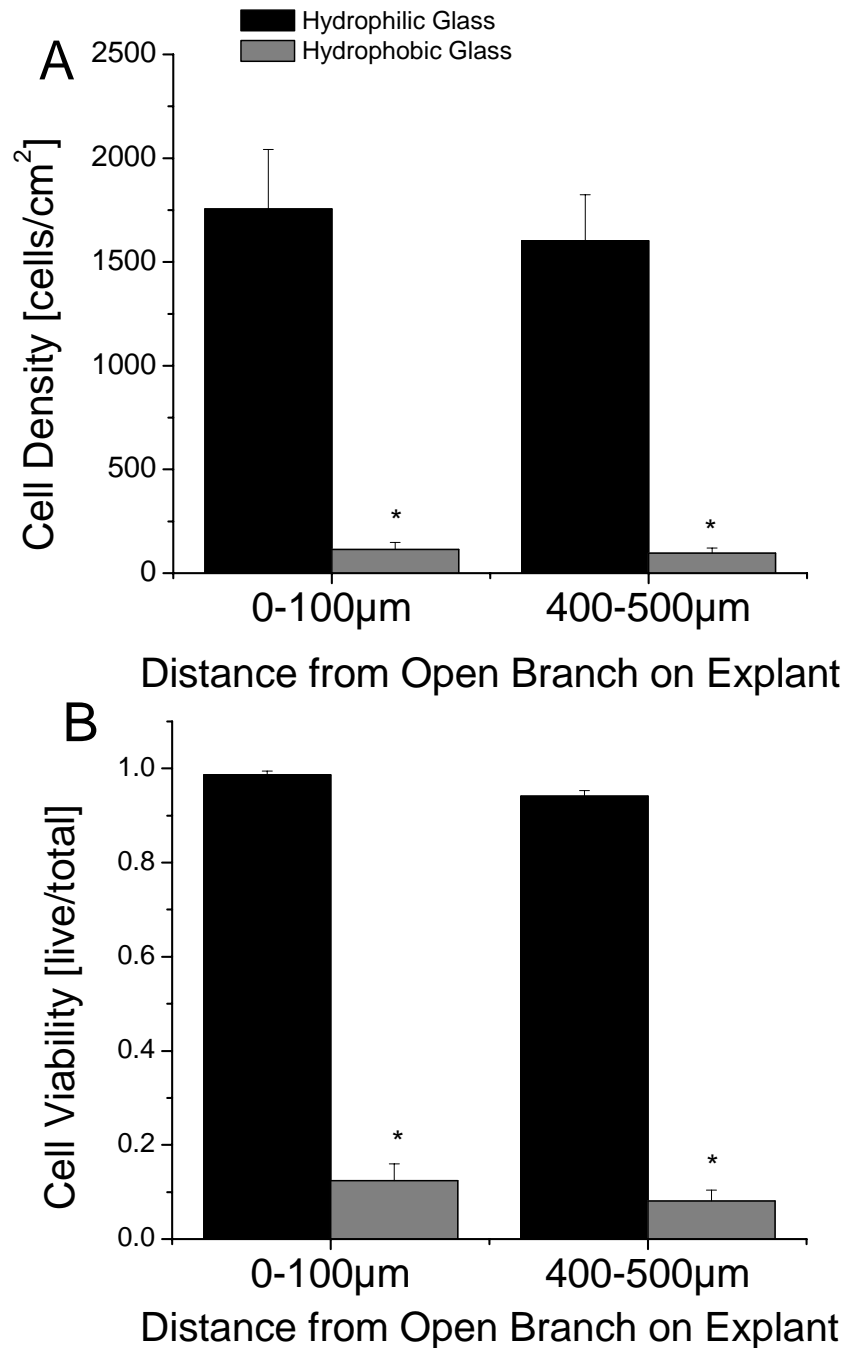


Figure 4.31: Endothelial Cell Density and Viability on Bare Hydrophilic or Hydrophobic Glass in the Bioassay Chamber. For these experiments, no ECM protein was microstamped onto either glass substrate. The surface of the glass was either hydrophilic or hydrophobic. Murine aortas were perfused at 240μL/min (High flow) for 24 hours. Values are mean+S.E.M. Data were obtained from 4 independent experiments. *differs from hydrophilic glass (*t*-test, *P* < 0.05).

Cell Substrate Type		Elongated cells (n, cells)	Circular cells (n, cells)	Fraction of elongated cells
Endothelial Cells in the Bioassay Chamber – High Flow				
Proximity to explant				
Hydrophilic	0-150 μ m	3.03 \pm 0.20 (50)	2.50 \pm 0.60 (8)	86%
Glass (4)	400-500 μ m	3.17 \pm 0.24 (60)	3.84 \pm 0.79 (11)	85%
Hydrophobic	0-150 μ m	3.09 \pm 0.40 (27)	2.10 \pm 0.23 (13)	68% ^a
Glass (4)	400-500 μ m	2.14 \pm 0.36 (34)	2.52 \pm 0.11 (22)	61% ^a

Table 4.10: Perimeter Based Cell Area and Fraction Elongated Cells on Bare Hydrophilic or Hydrophobic Glass in the Bioassay Chamber. Our Cellcounting.m program (Appendix A1) was used to determine the cell area of endothelial cells on hydrophilic or hydrophobic glass. Entries are the mean \pm S.E.M. of the cell area [μm^2] (x1,000). For statistical analysis, the sample size for each experiment was considered as the **N**, reported in this table. These were the individual independent experiments. Number of cells, **n**, is shown for comparison of elongated to circular cells. Statistics were performed on the mean \pm SD from the original independent experiments. ^adiffers from hydrophilic (grouped by proximity, *t*-test, $P < 0.05$)

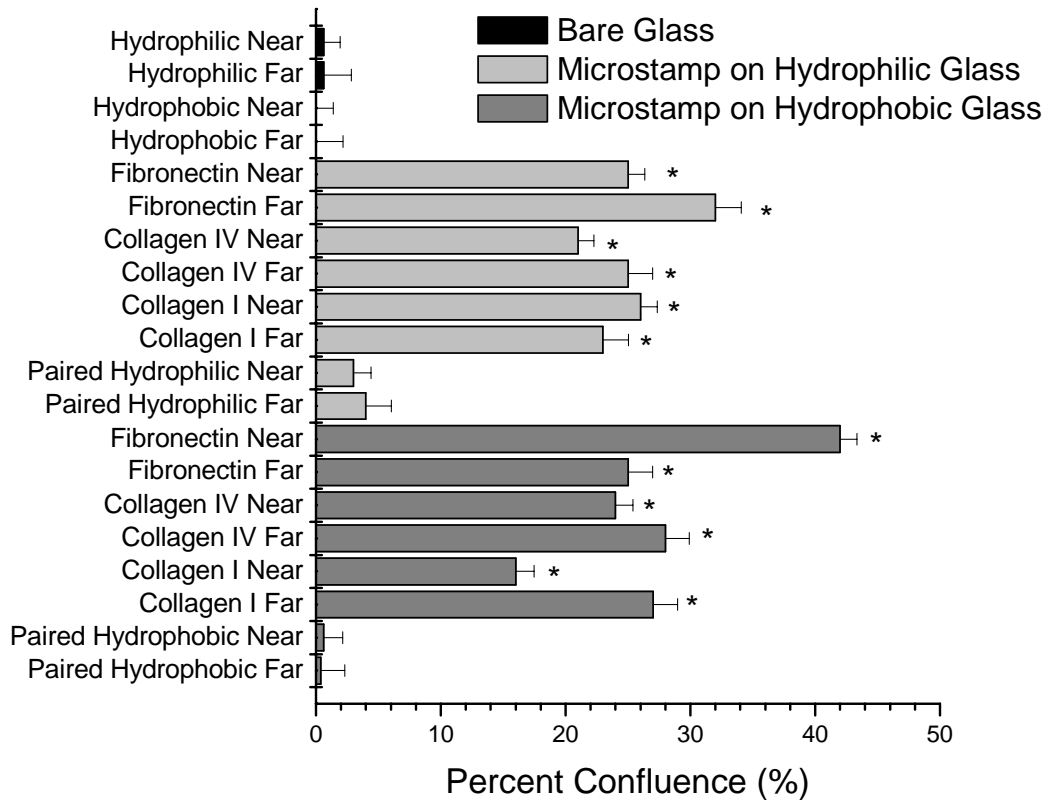


Figure 4.32: Endothelial Cell Percent Confluence for all Microstamp Experiments in the Bioassay Chamber. Percent confluence is a measure of the area coverage for each particular substrate. For all experiments, explanted murine abdominal aortas were perfused for 24 hours at 240 μ L/min. Values are mean+S.E.M. Data are obtained from 4 independent experiments. Near is 0-100 μ m from the open side branch, Far is 400-500 μ m from the open side branch. *differs from control paired glass (bare samples, *t*-test, $P < 0.05$) or (microstamp samples, ANOVA, $P < 0.05$).

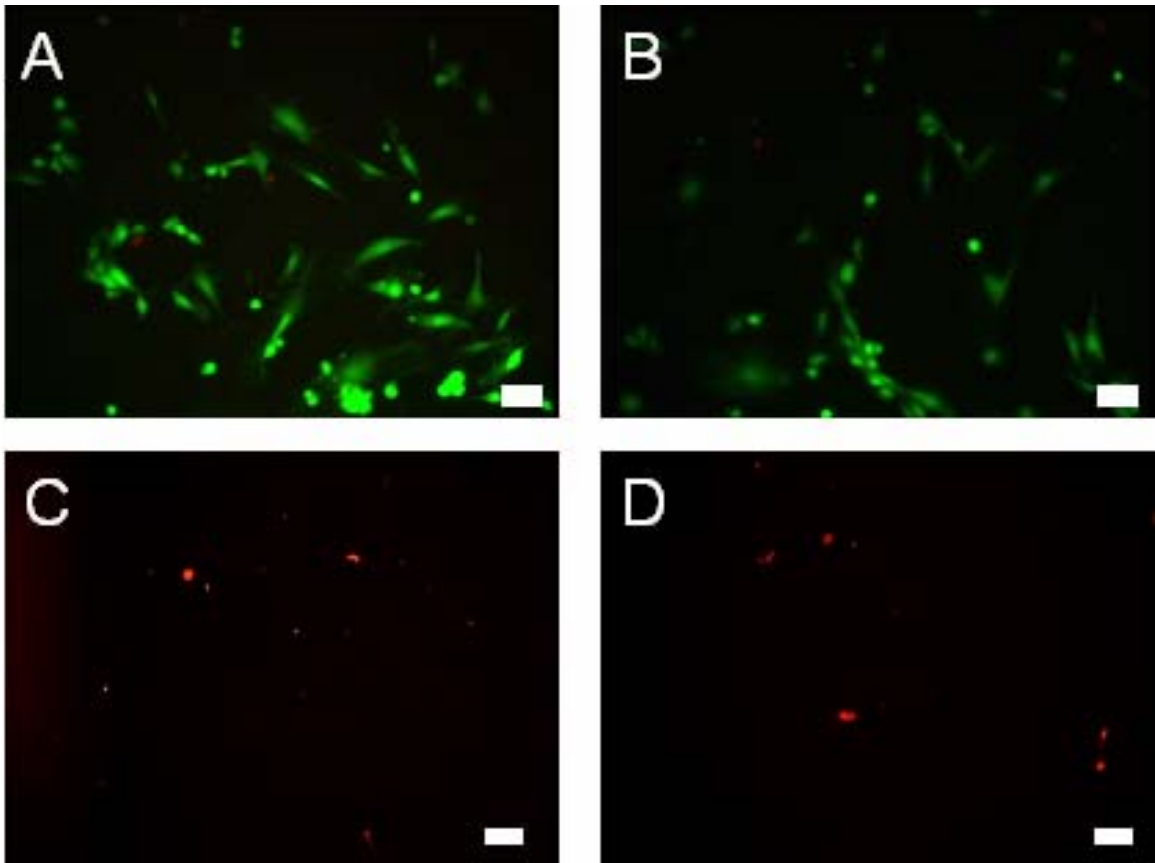


Figure 4.33: Digital Image of Endothelial on Bare Hydrophilic or Hydrophobic Glass in the Bioassay Chamber. For these experiments, no ECM protein was microstamped onto the glass substrate. The surface of the glass was either hydrophilic (A, B) or hydrophobic (C, D). ECs were found Near (A,C) or Far (B,D) from the open side branch. Cells were stained with calcein (green, live) and ethidium (red, dead). Mouse aortas were perfused for 24 hours at 240 μ L/min (High) flow. The viability and density for cells grown on hydrophobic glass coverslips were significantly lower than for cells on hydrophilic glass. Scale bars are 100 μ m.

4.2.2.b Effects of Microstamped ECM Proteins on Hydrophilic Surfaces

From cell culture experiments we saw that endothelial cell density was enhanced on the microstamped ECM protein as compared with bare hydrophilic glass. Fibronectin, collagen IV and collagen I all had a large significant increase in cell density and percent confluence after the culture time. Laminin increased density to a lesser extent in cell culture; and therefore, we only examined fibronectin (Fn), collagen IV and collagen I within the bioassay chamber. Cell density was significantly higher on the microstamped ECM protein both Near and Far from the open side branch as compared to hydrophilic glass (Figure 4.34). Cell viability was also significantly enhanced on some microstamped proteins Near but not Far from the explant. However, cell viability was high for all conditions. EC confluence after one day of perfusion significantly enhanced on the microstamped ECM proteins as compared with the bare hydrophilic glass (Figure 4.32).

Cell morphology was investigated for endothelial cells found on microstamped proteins on hydrophilic glass in the bioassay chamber (Table 4.11). There were no trends found in the perimeter based cell area. Endothelial cells showed a preference to grow in an elongated morphology on all substrates. Percent elongated was independent of where the cells were found within the bioassay chamber and the substrate (hydrophilic glass vs. microstamped protein). ECs had a higher tendency to be elongated Far from the open side branch and on the microstamped protein.

Morphology of endothelial cells found on ECM proteins microstamped on hydrophilic glass can also be investigated from digital images obtained after perfusion (Figure 4.35). Cells found on the bare hydrophilic glass Near the open perfused side branch were not organized. These cells adhered to the hydrophilic glass at any location, and were cultured with a lower density. However, cells found on a Fn stamp, both Near and Far from the explant, were more organized and concentrated within the microstamped protein region becoming partially excluded from the bare hydrophilic glass. At neither location, was the microstamped protein able to completely exclude cells from the bare hydrophilic glass. ECs found on other microstamped proteins were similar to the representative digital images shown here.

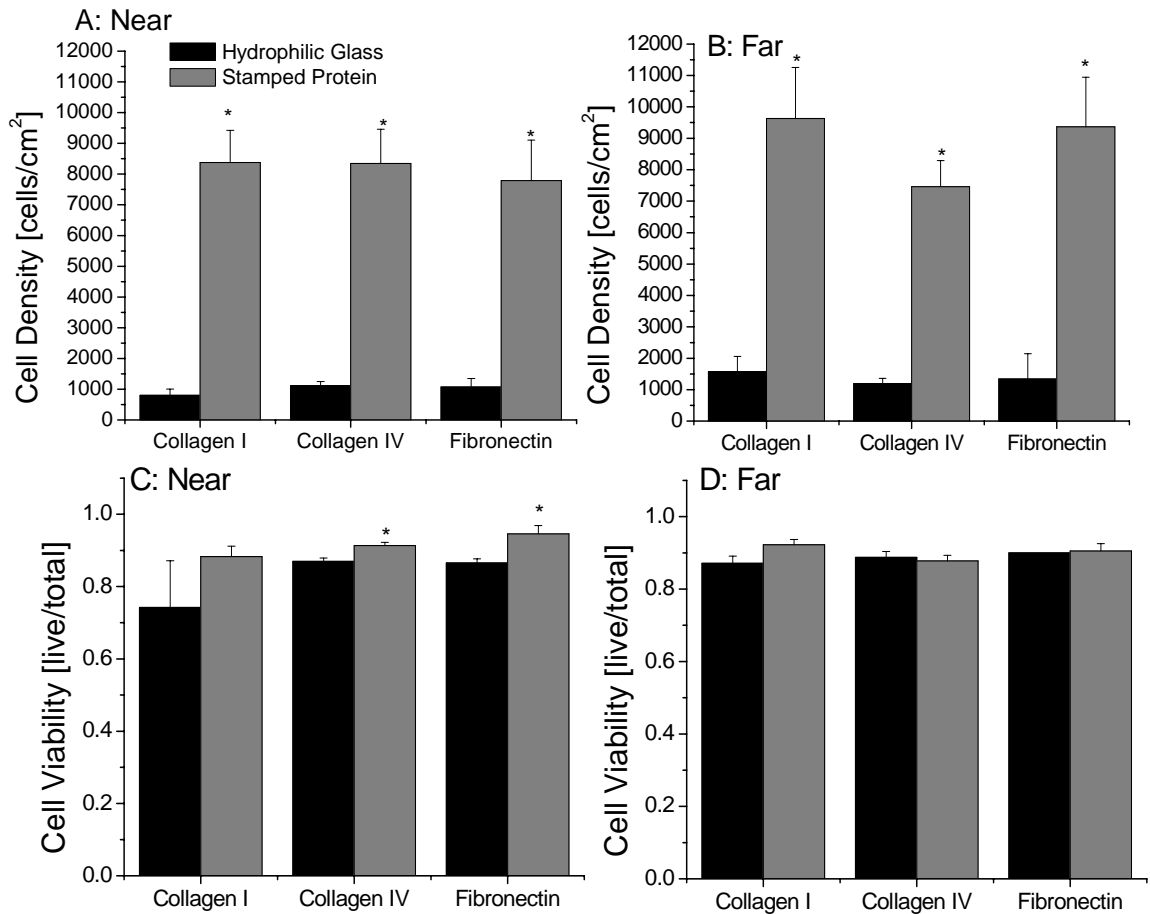


Figure 4.34: Cell Density and Viability in the Bioassay Chamber on Microstamped ECM Proteins on Hydrophilic Glass. Cell viability and density were measured both Near (A, C) and Far (B, D) from the open side branch of the cannulated blood vessel. Cells were either on the microstamped protein or on the hydrophilic glass substrate. Mouse aortas were perfused at 240 μ L/min (High flow) for 24 hours. Data are mean+S.E.M. Data here were obtained from 4 independent experiments. *differs from hydrophilic glass (*t*-test, $P < 0.05$).

Cell Substrate Type		Elongated cells (n, cells)	Circular cells (n, cells)	Fraction of elongated cells
Endothelial Cells in Bioassay Chamber on the Microstamp – High Flow				
ECM Protein	Proximity to Explant (N, experiments)			
Collagen I	Near (4)	2.68±0.43 (43)	1.94±0.14 (41)	75%
	Far (4)	2.75±0.62 (14)	2.37±0.72 (10)	80%
Collagen IV	Near (4)	3.00±0.40 (47)	3.08±0.16 (48)	67%
	Far (4)	3.13±0.57 (23)	3.06±0.28 (19)	71%
Fibronectin	Near (4)	3.28±0.46 (50)	3.23±0.90 (49)	72%
	Far (4)	3.22±0.50 (19)	2.84±0.55 (18)	73%
Endothelial Cells in Bioassay Chamber on Hydrophilic Glass – High Flow				
Collagen I – Glass	Near (4)	2.30±0.23 (30)	2.21±0.61 (22)	77%
	Far (4)	3.21±0.26 (9)	2.63±0.28 (5)	82%
Collagen IV – Glass	Near (4)	3.68±0.58 (38)	3.26±0.15 (29)	82%
	Far (4)	3.02±0.58 (8)	2.91±0.33 (13)	69%
Fibronectin – Glass	Near (4)	3.22±0.49 (34)	2.72±0.16 (10)	81%
	Far (4)	3.07±0.93 (8)	3.35±0.19 (7)	71%

Table 4.11: Perimeter Based Cell Area and Fraction Elongated Cells on Stamped ECM Proteins on Hydrophilic Glass within the Bioassay Chamber. Our Cellcounting.m program (Appendix A1) was used to determine the cell area of endothelial cells within the bioassay chamber. Entries are the mean±S.E.M. of the cell area [μm^2] (x1,000). For statistical analysis, the sample size for each experiment was considered as the **N**, reported in this table. These were the individual independent experiments. Number of cells, **n**, is shown for comparison of elongated to circular cells. Statistics were performed on the mean±SD from the original independent experiments. Near is 0-100 μm from the open side branch, Far is 400-500 μm from the open side branch.

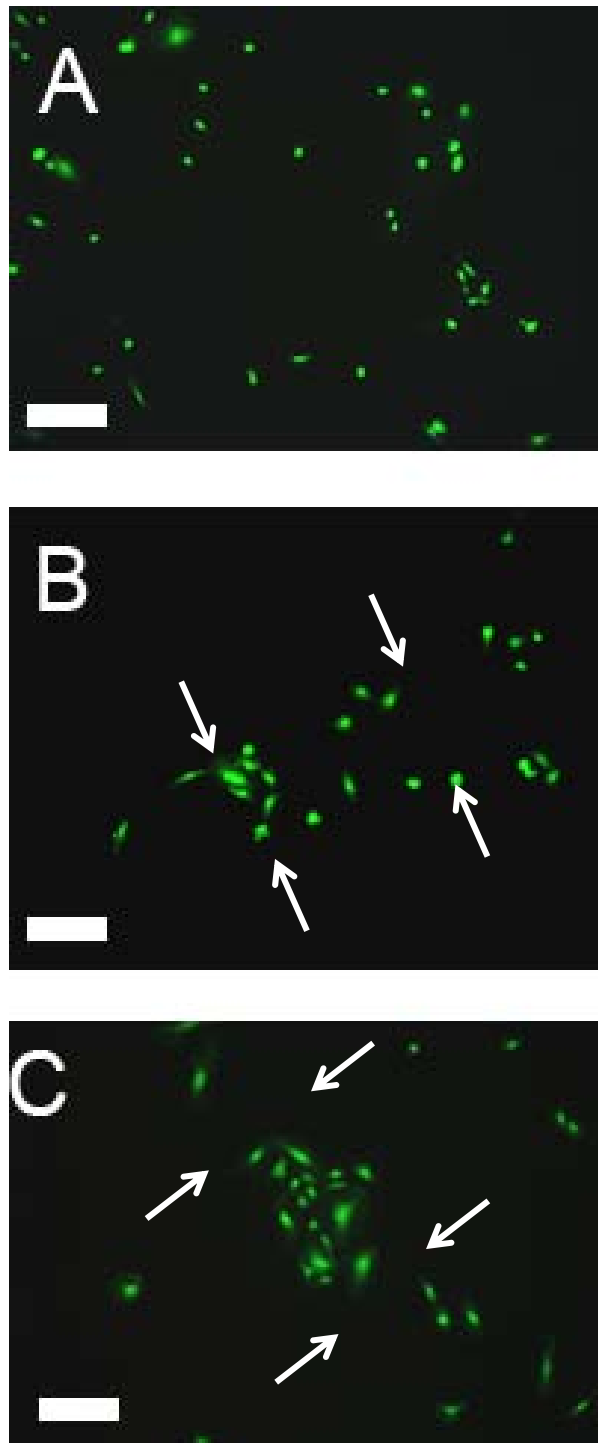


Figure 4.35: Digital Images of Endothelial Cells Grown on ECM Microstamped Proteins on Hydrophilic Glass in the Bioassay Chamber. An explanted mouse aorta was perfused in the bioassay chamber for 24 hours at $240\mu\text{L}/\text{min}$. Cells were stained with calcein (green, live) and ethidium (red, dead). Endothelial cells found Near the open side branch on hydrophilic glass (A), Near the open side branch on a $150\mu\text{m}$ Fn stamp (B) and Far from the open side branch on a $150\mu\text{m}$ Fn stamp (C). All scale bars are $100\mu\text{m}$. White arrows mark the microstamped region.

4.2.2.c Effects of Microstamped ECM Proteins on Hydrophobic Surfaces

Cell culture studies showed that endothelial cells cultured on microstamped proteins on hydrophobic glass coverslips had an enhanced cell viability and density as compared to the non-pattered region. The percent confluence and percent elongated was enhanced also. In the bioassay chamber, there was a significant increase in cell density and cell viability on microstamped fibronectin, collagen IV and collagen I both Near and Far from the side branch as compared to the paired hydrophobic glass substrates (Figure 4.36). EC confluence after one day of perfusion significantly enhanced on the microstamped ECM proteins as compared with the bare hydrophobic glass (Figure 4.32).

Cell morphology was investigated for endothelial cells originating from an explanted blood vessel found on microstamped proteins on hydrophobic glass (Table 4.12). There were no significant differences in cell area based on the microstamped ECM protein, the distance from the open side branch or the cell type (elongated vs. circular). All endothelial cells showed a preference towards an elongated morphology. Cells cultured on collagen IV and fibronectin had a significantly higher percentage of cells with an elongated morphology.

Morphology of endothelial cells found on ECM proteins microstamped onto hydrophobic glass can also be investigated from digital images obtained after perfusion (Figure 4.37). Nearly all cells found on hydrophobic glass Near (and Far from) the open perfused side branch were not organized and were largely dead (ethidium positive) (Figure 4.37 A). These cells were found with a significantly lower cell density and viability than cells on the microstamped ECM protein (Figure 4.37 B and C). Cells found on the Fn microstamp, both Near and Far from the explant, were more organized and somewhat restricted to the microstamped protein region. Furthermore, the cells that were found on the hydrophobic glass had a low viability, density and percent confluence.

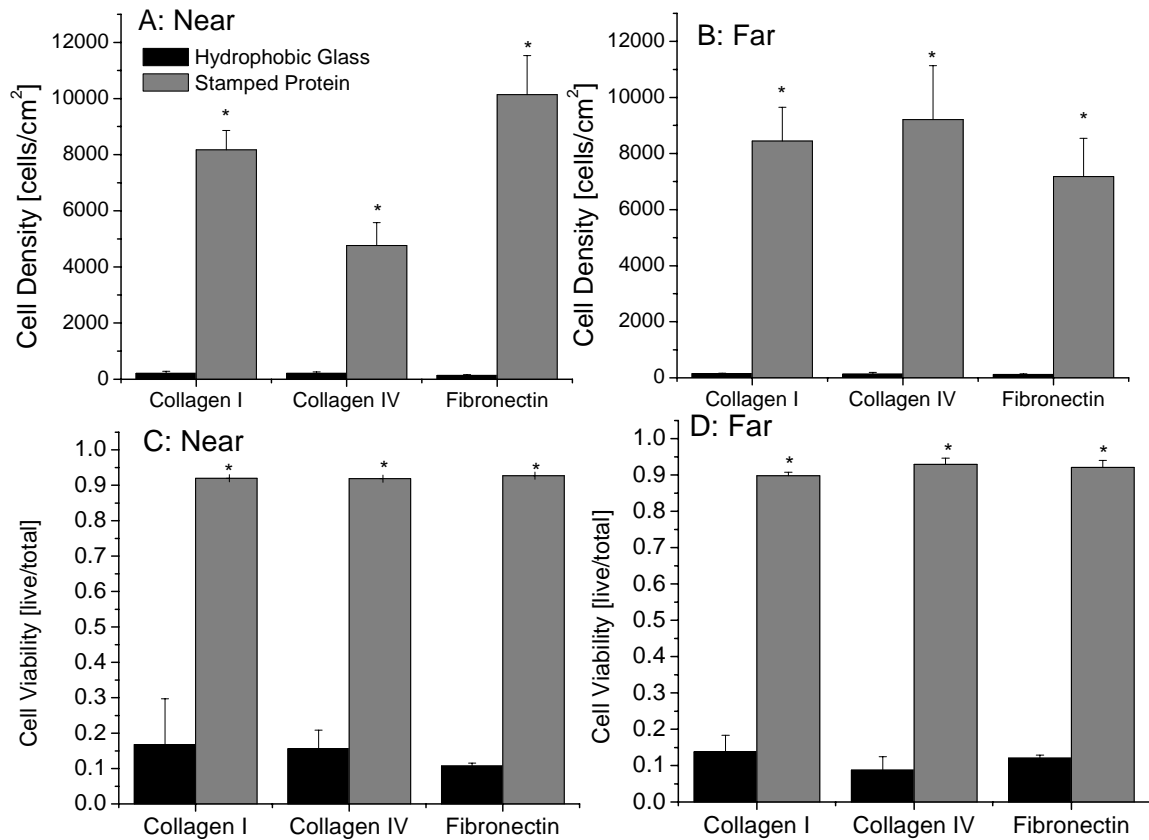


Figure 4.36: Cell Density and Viability in the Bioassay Chamber on Microstamped ECM Proteins on Hydrophobic Glass. Cell viability and density were measured both near (A, C) and far (B, D) from the open side branch of the cannulated blood vessel. Cells were either on the stamped protein or on the bare hydrophobic glass substrate. Mouse aortas were perfused at 240 μ L/min (High flow). Data are mean+S.E.M. Data were obtained from 4 independent experiments. *differs from hydrophobic glass (*t*-test, $P < 0.05$).

Cell Substrate Type		Elongated cells (n, cells)	Circular cells (n, cells)	Fraction of elongated cells
Endothelial cells in Bioassay Chamber on the Microstamp– High Flow				
ECM Protein	Proximity to Explant (N, experiments)			
Collagen I	Near (4)	2.95±0.38 (46)	2.96±0.42 (12)	79%
	Far (4)	3.34±0.51 (44)	4.84±0.18 (8)	85%
Collagen IV	Near (4)	3.47±0.29 (44)	2.50±0.17 (5)	90% ^a
	Far (4)	3.22±0.21 (56)	2.65±0.12 (17)	77% ^a
Fibronectin	Near (4)	4.10±0.80 (42)	4.25±0.75 (7)	86% ^a
	Far (4)	3.41±0.37 (52)	3.03±0.15 (8)	87%
Endothelial cells in Bioassay Chamber on Hydrophobic Glass – High Flow				
Collagen I – Glass	Near (4)	3.02±0.34 (19)	3.30±0.13 (5)	79%
	Far (4)	3.15±0.52 (34)	2.31±0.63 (7)	83%
Collagen IV – Glass	Near (4)	3.69±0.48 (23)	5.62±0.59 (8)	74%
	Far (4)	3.40±0.29 (23)	4.15±0.46 (12)	66%
Fibronectin – Glass	Near (4)	3.79±0.30 (35)	3.40±0.46 (13)	73%
	Far (4)	2.67±0.26 (31)	2.54±0.15 (3)	91%

Table 4.12: Perimeter Based Cell Area and Fraction Elongated Cells on Stamped ECM Proteins on Hydrophobic Glass within the Bioassay Chamber. Our Cellcounting.m program (Appendix A1) was used to determine the cell area of endothelial cells within the bioassay chamber. Entries are the mean±S.E.M. of the cell area [μm^2] (x1,000). For statistical analysis, the sample size for each experiment was considered as the **N**, reported in this table. These were the individual independent experiments. Number of cells, **n**, is shown for comparison of elongated to circular cells. Near is 0-100 μm from the open side branch, Far is 400-500 μm from the open side branch. Statistics were performed on the mean±SD from the original independent experiments. ^adiffers from paired hydrophobic glass (paired *t*-test, $P < 0.05$).

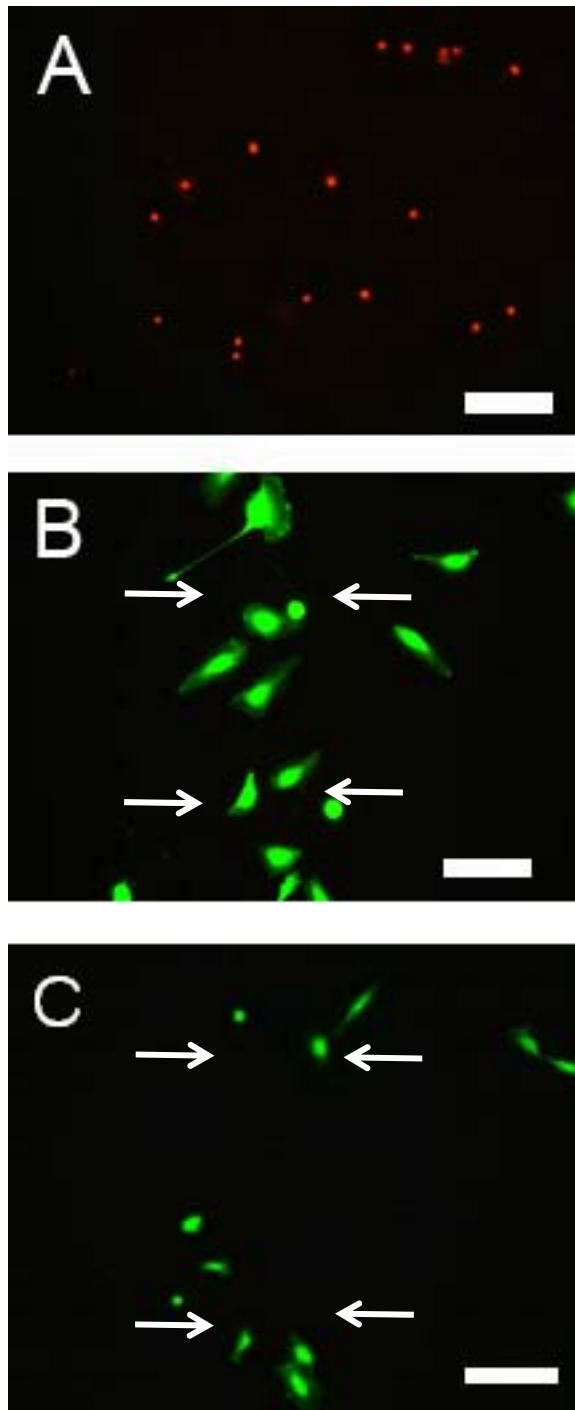


Figure 4.37: Digital Images of Endothelial Cells Grown on ECM Microstamped Proteins on Hydrophobic Glass in the Bioassay Chamber. An explanted murine aorta was perfused in the bioassay chamber for 24 hours at $240\mu\text{L}/\text{min}$. Cells were stained with calcein (green, live) and ethidium (red, dead). Endothelial cells found Near the open side branch on the hydrophobic glass (A), Near the open side branch on a $150\mu\text{m}$ Fn stamp (B) and Far from the open side branch on a $150\mu\text{m}$ Fn stamp (C). All scale bars are $100\mu\text{m}$. White arrows mark the microstamped region.

4.2.2.d Effects of Microstamped Fibronectin onto CA180 Scaffolds

To investigate the combination of topographical and topological cues, fibronectin ($3.4\mu\text{g}/\text{mm}^2$) was microstamped onto CA180 electrospun scaffolds. Murine aortas were perfused for 24 hours in the bioassay chamber. Density and viability on the microstamped protein as compared to the bare scaffold was investigated after perfusion. Cell density and cell viability was not significantly different on the microstamped Fn as compared to the bare electrospun scaffold (Figure 4.38). In general the cell density was greater Far from the vessel as compared to Near the vessel. There were no trends found in cell viability.

Cell morphology was also investigated both Near and Far from the open side branch on microstamped Fn or on the bare electrospun scaffold (Table 4.13). There were no trends in perimeter based cell area for cells that were on the microstamped Fn or the bare CA180 scaffolds. Also, there were no trends in the percent of elongated cells, although there were a high percentage of elongated cells found under these conditions, then as bioassay chamber experiments described in Section 4.2.1. Digital images taken during experiments show that ECs did not prefer particular fibers and did not form spontaneous capillary-like structures (data not shown).

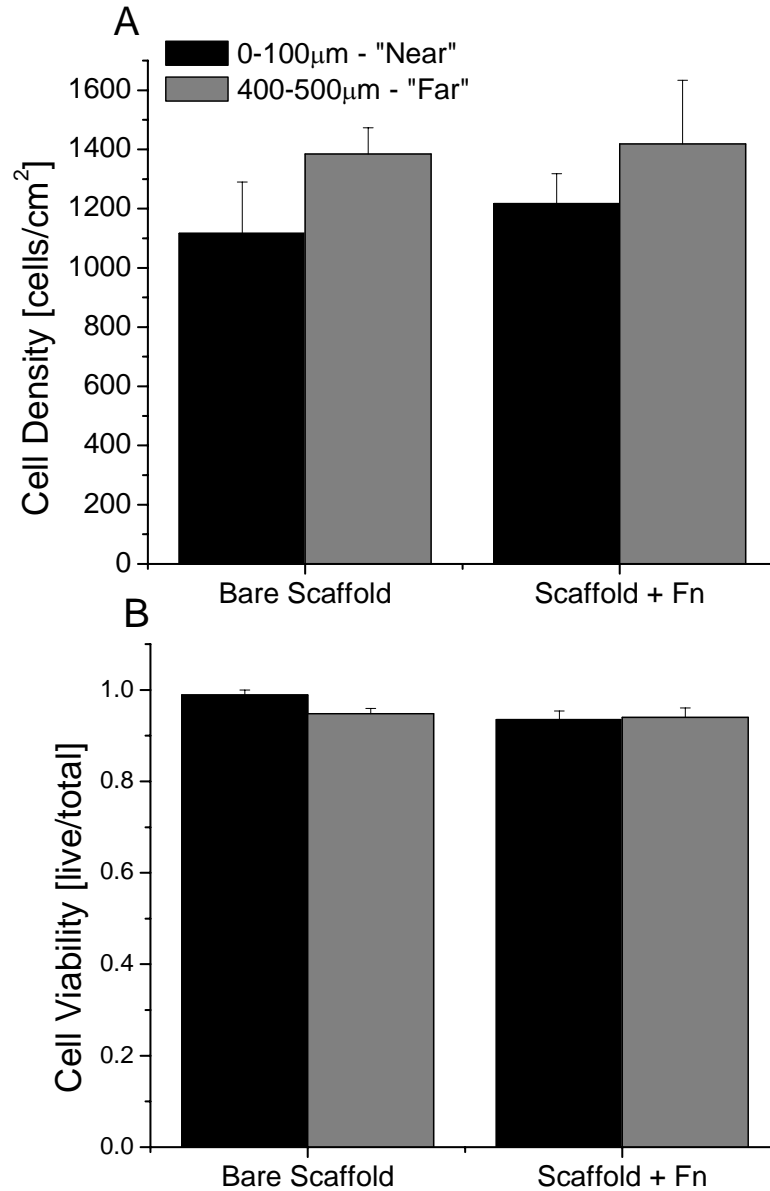


Figure 4.38: Cell Density and Viability in the Bioassay Chamber on Microstamped Fibronectin onto CA180 Electrospun Scaffolds. Cell density (A) and cell viability (B) were measured both Near and Far from the open side branch of the cannulated blood vessel. Cells were either on the bare scaffold or on the scaffold which had microstamped fibronectin ($3.4\mu\text{g}/\text{mm}^2$). Mouse aortas were perfused at $240\mu\text{L}/\text{min}$ (High flow) for 24 hours. Data are mean+S.E.M. Data were obtained from 4 independent experiments.

Cell Substrate Type		Elongated cells (n, cells)	Circular cells (n, cells)	Fraction of elongated cells
Endothelial cells in Bioassay Chamber on the Microstamp on CA180 – High Flow				
ECM Protein	Proximity to Explant (N, experiments)			
Fibronectin	Near (4)	4.06±0.34 (60)	4.91±1.47 (8)	88%
	Far (4)	4.83±0.42 (47)	5.63±1.41 (8)	85%
Endothelial cells in Bioassay Chamber on Bare CA180 – High Flow				
Scaffold	Near (4)	3.48±0.39 (31)	2.29±1.27 (2)	94%
	Far (4)	4.83±0.57 (27)	4.63±0.99 (7)	79%

Table 4.13: Perimeter Based Cell Area and Fraction Elongated Cells on Stamped Fibronectin onto CA180 within the Bioassay Chamber. Our Cellcounting.m program (Appendix A1) was used to determine the cell area of endothelial cells within the bioassay chamber. Entries are the mean±S.E.M. of the cell area [μm^2] (x1,000). For statistical analysis, the sample size for each experiment was considered as the N, reported in this table. These were the individual independent experiments. Number of cells, n, is shown for comparison of elongated to circular cells. Near is 0-100 μm from the open side branch, Far is 400-500 μm from the open side branch. Statistics were performed on the mean±SD from the original independent experiments.

SECTION V: DISCUSSION

The effects of tissue scaffold fiber diameter and composition on endothelial cell viability, density and morphology were investigated to determine the optimal scaffold for use in a bioassay chamber. In the bioassay chamber, electrospun scaffolds can support the growth of endothelial cells that have originated from an isolated artery perfused with a low mean wall shear stress. The data indicate that the CA180 material with a fiber diameter of 1-5 μ m was the best base material and that addition of 1.6% chitosan enhanced cell density, viability and our preferential elongated morphology both using HUVECs as a model, and in the bioassay chamber. The effects of microstamped ECM proteins onto hydrophilic and hydrophobic glass coverslips on endothelial cell viability, density, percent confluence and morphology was investigated to determine if ECs can be excluded from non-patterned regions. We also investigated if shear stress effects this exclusion in the bioassay chamber. The data indicate that endothelial cells preferred to be culture on microstamped ECM proteins on hydrophilic or hydrophobic surfaces both in cell culture and the bioassay chamber.

5.1 Cell Culture

Early and Late passage HUVECs were studied because of the known transformation of these cells with continued passaging (Hayashi et al., 1995; Jersmann et al., 2001). Prior studies have shown that cell density is dependent on passage number, culture duration and endothelial cell type (Craig et al., 1998). Our data agree with this finding in general, for HUVECs. For all conditions and materials tested, the cells showed a preference towards an elongated morphology (except for on hydrophobic glass), which is the preferential morphology we sought to duplicate (Phongkitkarun et al., 2004).

5.1.1 Electrospun Cellulose Acetate

5.1.1.a Effects of Scaffold Fiber Diameter on Viability and Density

Normal *in vivo* extracellular matrix fiber diameters are in the range of 20-80nm (Fawcett, 1986). Previous studies have suggested that various cell types show a characteristic fiber diameter preference and perhaps even a material preference (Ayutsede et al., 2006; Baker et al., 2006; He et al., 2005b; He et al., 2005a; Li et al., 2006; Matthews et al., 2002; Park et al., 2006; Xu et al., 2004a). For one particular cell type, by changing the material of the scaffold, the preferential fiber diameter can change as well. Therefore, we chose to test a range of fibers (and additives, Section 5.1.1.b) with diameters that mimic the characteristic fiber diameter found in the normal ECM, and those with larger mean fiber diameters. This was used as a test to determine which fiber diameter size was preferred by ECs in our culture conditions.

Our electrospun scaffolds were flat, with a ribbon-like morphology (Figure 4.1). CA40 scaffolds (fiber diameter was similar to native ECM fiber diameter) were flattened

and ribbon-like with nodule structures interspersed throughout the scaffold. In general, a flattened structure would provide a larger surface area to which the cells could attach; possibly mimicking a two-dimensional surface (such as glass). This structure can direct the growth of cells by providing one surface to which ECs are more likely to adhere (the flattened portion vs. the edge). The void space and the surface area to volume ratio for electrospun scaffolds are important parameters for tissue engineering applications. Scaffolds with a high void space combined with a large surface area to volume ratio are good candidates for tissue engineering purposes (Boland et al., 2004). Using these guidelines, our CA + 1.6% chitosan electrospun scaffolds would be a better choice for tissue engineering purposes. The mechanical properties of electrospun cellulose acetate with or without added chitosan were measured using thermomechanical analysis (Figure 4.3). With the addition of chitosan to scaffolds, the stiffness, yield force, compressive modulus and yield stress all increased by approximately 50%. These measurements obtained material properties for the bulk scaffold and not individual fibers, which are what endothelial cells, would most likely interact with.

At both Early and Late passages and Short and Long growth durations, endothelial cells cultured on CA180 (1-5 μ m, Figure 4.4) consistently had a high cell density and viability. This was comparable to cells cultured on glass coverslips. Cells cultured on smaller fiber diameter scaffolds (CA40 and CA80) consistently had a lower density and viability. For these scaffolds, when the cell viability was high for Short growth durations (see Figure 4.4 D, \circ and \blacktriangle), it significantly reduced for our Long growth duration. These Long growth durations are more critical in tissue engineering where initial estimates are that it would take weeks to months in order to fully engineer a patent tissue with a patent vasculature (Bianchi et al., 2006). Others have shown that endothelial cells will grow preferentially on small diameter electrospun fibers (400nm, PLLA coated with collagen I) (He et al., 2005b; He et al., 2005a). Using electrospun CA, we found that ECs will grow on smaller diameter fibers, but HUVECs showed a preference towards larger fiber diameters (1-5 μ m) in our conditions. This may be due to an increase in overall surface area for cells to interact with or from changes in the material (as compared with previous studies). Others have shown that with increases in surface area, ECs adhere better and grow with a higher density (Nair et al., 2004). Our data supports this finding. The nodule structures that appeared in the CA40 scaffold, despite that the fiber diameter was representative of the native ECM, may have played a role in the reduced cell viability and cell density reported here. Material composition plays an important role in the preferential fiber diameter of the scaffold (He et al., 2005b; He et al., 2005a). On electrospun CA scaffolds, we show that ECs prefer larger diameter scaffolds that are not representative of the characteristic ECM fiber diameter.

5.1.1.b Effects of Scaffold Additives on Viability and Density

Additives to the electrospun solution were tested to determine whether they could enhance EC culture parameters. Two compounds reported to increase the strength of fibers or films (single walled carbon nanotubes, CNT (Mahfuz et al., 2006; Moore et al., 2004) and chitosan (Khan et al., 2000)) were added to the electrospinning solution. The addition of CNT or chitosan decreased scaffold permeability significantly (Rubenstein et al., 2007). Others show heightened flow through scaffolds with the addition of organized parallel CNT arrays (Kalra et al., 2003). The CNTs in our scaffolds were not organized

and the decrease in permeability was attributed to an uneven distribution of CNT within the scaffold (Rubenstein et al., 2007). A potent angiogenic growth factor (VEGF (Favot et al., 2003; Herve et al., 2005; Koolwijk et al., 1996)) was also added to the electrospinning solution prior to fabrication. These scaffolds were fabricated with process parameters that were expected to provide larger diameter fibers (Table 3.1), within the 0.2-1 μ m range. Instead, the fibers were an order of magnitude smaller in diameter than expected, possibly from changes in other process parameters. The amount of VEGF incorporated into the scaffolds was 13ng/cm² (per area of fabricated scaffold); this would have been equivalent to 6.6ng/mL if all the VEGF had leached from the electrospun material into the media (this concentration is considered biologically active (Tille et al., 2001)). Lastly, fibronectin (an integrin binding glycoprotein (Heilshorn et al., 2003)) was added to the formed electrospun scaffold. Addition of Fn to pre-formed electrospun scaffolds did not change the characteristic fiber diameter size but added an extra initial ligand binding site for ECs for at least four hours (Figure 4.2).

Within the smallest fiber diameter group (characteristic of the native ECM fiber diameter range), we saw that the addition of VEGF significantly reduced cell viability (over CA40 and our glass control) (Figure 4.5). Cell density was significantly reduced as compared to on glass. In these preparations, VEGF is an unsuitable additive to the scaffold due to the reduced EC viability and density. It is known that VEGF is difficult to incorporate into fabricated scaffolds (Young et al., 2005) and in order to retain its activity the electrospinning process parameters must be carefully optimized. VEGF data is included as a negative finding for these scaffolds preparations and culture conditions.

CNT addition within any fiber diameter range did not affect cell viability over the base CA electrospun scaffold in the same diameter range (Figure 4.5). The addition of CNT (0.2-1 μ m, CA + 1.7% CNT) caused a significant reduction in cell viability as compared to on our control substrates (i.e. glass). With CNT addition within any fiber diameter range, cell density was significantly reduced. Others have shown that CNTs in a HUVEC media were not cytotoxic towards endothelial cells in culture (Flahaut et al., 2006). The cytotoxicity of our fibers may arise from the reduction in permeability of the scaffolds, causing a decrease in oxygen/nutrient delivery to cells that have invaded the scaffold. This would effectively reduce the density/viability of cells in the scaffold. CNT is thus an unsuitable additive in these conditions. Therefore, we conclude that carbon nanotubes and vascular endothelial growth factor were not suitable additives to the electrospun cellulose acetate scaffolds.

The addition of fibronectin significantly increased HUVEC density within the largest fiber diameter cellulose acetate scaffolds in paired experiments (Figure 4.6). The addition of fibronectin to any substrate did not affect cell viability; all substrates had a high viability. Fibronectin addition can increase cell density by providing endothelial cells with an extra initial specific ligand binding point not provided by the scaffolds (Heilshorn et al., 2003; Wittmer et al., 2007).

With the addition of 1.6% chitosan to CA180, we saw improved cell viability and density (Figure 4.5). Based on the nano-scale porosity of electrospun chitosan (Li, 2005; Li and Hsieh, 2006), this improved viability and density may be a direct result of an increased ability of cells to attach to the scaffold. Others have seen enhanced fibroblast attachment to electrospun chitin (Park et al., 2006), a precursor of chitosan. Increased attachment can lead to increased proliferation due to enhanced cell stability on the

scaffold (Salacinski et al., 2001), or increased ability to migrate, as found for fibroblasts (Doherty et al., 1990). Also, the mechanical properties enhanced with the addition of chitosan; this may make a more suitable culture substrate for endothelial cells. Since the addition of chitosan increased the viability and density to levels greater than on glass, we conclude that this is an optimal scaffold for our culture conditions. Therefore, this scaffold was investigated in the bioassay chamber to study the combined effects of flow rate and scaffold morphology (Section 5.2).

To study the base effects of our electrospun materials on endothelial cells, experiments were conducted in which chitosan or cellulose acetate were allowed to dry onto glass coverslips. The viability and density of HUVECs on these scaffolds did not differ from on glass or on CA180 (Figure 4.7). This indicates that the materials themselves do not induce significant changes to the EC culture parameters. Others have shown that cellulose acetate (Sugiu et al., 1995) and chitosan (Lohbach et al., 2006) do not affect culture parameters. Our findings agree with these results. Improvements in culture parameters that were seen with electrospun scaffolds are most likely from the topology and/or morphology of the scaffolds themselves and not necessarily due to changes in the additives to the electrospun solution.

5.1.1.c Effects of Scaffolds on Cell Morphology

Elongated ECs are necessary for the progression of angiogenesis *in vivo* (Phongkitkarun et al., 2004) and therefore, this was the morphology that we sought to obtain on our scaffolds. Perimeter based cell area was quantified for Early and Late passage cells cultured on electrospun scaffolds (Table 4.2). There was no trend in perimeter based cell area. The majority of cells were found to be growing with an elongated morphology on all scaffolds (Table 4.2). Percent of elongated cells increased as the passage of the cells increased; except for cells on Matrigel® (100% elongated for Early passage). This agrees with others, where the circularity of HUVECs decreases with time (Wittmer et al., 2007). Overall the percent elongated was greatest for cells grown on the largest fiber diameter scaffolds (i.e. CA180, 1-5 μ m, comparing base scaffolds without additives). The addition of chitosan to these fibers further increased the percentage of ECs found with an elongated morphology. These results agree with others that showed, different materials do not elicit changes in cell area, but they can effect the percent of elongated cells grown on the material (Palmaz et al., 1999). On glass coverslips, the addition of cellulose acetate or chitosan to glass coverslips did not affect cell area, but it did increase the percent of elongated cells. This can be attributed to an increase in the attachment and spreading of cells on these materials as others have seen compared with the bare glass substrate (Liu et al., 2005; Lohbach et al., 2006).

There was a notable association of HUVECs with individual fibers on the CA + 1.6% chitosan scaffolds. This may be caused by an increase in non-specific attachment to chitosan (Park et al., 2006) as compared with the base cellulose acetate scaffolds. On CA180 cells were not seen to associate with individual fibers, instead cells were associated with many fibers via individual tethers. An unexpected finding was that cells cultured on CA + 1.6% chitosan scaffolds showed evidence of spontaneous capillary-like structures within four days of culture (Figure 4.8 A, C). This was similar to network structures that we (Figure 4.8 D) and others (Ouellette et al., 2000) have found with Matrigel®. No other scaffolds supported the formation of spontaneous capillary-like

structures. The addition of Fn did not further enhance spontaneous capillary-like structures. With the heightened cell density and viability (Sections 5.1.1.a and 5.1.1.b) and the enhancement of our preferential elongated morphology on large diameter fibers, we studied CA180 with or without chitosan (1.6%) in the bioassay chamber.

5.1.1.d Migration onto Cellulose Acetate Scaffolds

HUVECs were used to test whether or not endothelial cells seeded onto glass substrates could migrate onto an electrospun cellulose acetate scaffold. To study this, the scaffold was placed over ECs that had already adhered to a glass coverslip (1 day after cell seeding). A significant number of cells were found within a CA180, CA180 + Fn and CA + 1.6% chitosan electrospun scaffold (Figures 4.8, 4.10, 4.12). We verified that ECs do not infiltrate electrospun scaffolds via initial contact of the dry scaffold with the wet cell surface. Therefore, cells that were found in the scaffold on subsequent imaging days would have migrated into the scaffold. Others have seen the rapid (within 3 days) infiltration of ECs into an electrospun collagen scaffold (Telemeco et al., 2005). Our cell culture studies agree with this finding and show that ECs can infiltrate electrospun CA180 scaffolds rapidly. The trend in HUVEC cell density on CA180 scaffold mimicked the cell density trend on bare hydrophilic glass substrates (Figure 4.9). To explain the density trend, HUVECs may have continually infiltrated the scaffold until day 4 and then maintained their culture. Another explanation is that cells infiltrated the scaffold by day 2 remained on the scaffold and proliferated at a similar rate to cells on bare glass. A combination of these two can also explain the data. Others showed that HUVECs can have different proliferation rates on different materials (Xu et al., 2004b), but we see similar cell density rate changes on glass and on CA180 (where we use cell density as a measure of proliferation). This shows that the electrospun CA scaffolds can maintain EC culture and that ECs can infiltrate a CA180 scaffold within 1 day and maintain a high viability and density.

Likewise, we saw a rapid increase in cell density on a CA180 scaffold with $3.4\mu\text{g}/\text{mm}^2$ Fn within 1 day (Figure 4.11). HUVEC cell density increased with time and was equal to the cell density on glass with longer growth times. Compared to bare CA180, cell density was higher on all days on CA180 with Fn; this is attributed to increased specific ligand binding provided by Fn (Heilshorn et al., 2003; Koenig et al., 2003). We and others see increased cell adhesion to Fn coated substrates as compared to their base substrates (Koenig et al., 2003). Others have seen different proliferation rates on different electrospun PLLA scaffolds (Xu et al., 2004a) and this can explain why the cell density on glass/CA180 plateaus on day 4 and continues to increase on CA180 + Fn.

HUVEC infiltration into a CA + 1.6% chitosan electrospun occurred rapidly and cell density of HUVECs on scaffolds surpassed that of on glass (Figure 4.13). Cells can have different proliferation rates on different scaffolds (Xu et al., 2004a) and we attribute our steady proliferation rate on glass (after day 4) and our increase in proliferation on CA + 1.6% chitosan to this. Others have seen an increased attachment of cells to chitosan based scaffolds (Khan et al., 2000; Li, 2005) and this can explain why the cell density is greater on CA + 1.6% chitosan as compared with CA180.

Perimeter based cell area for ECs that had infiltrated a CA180, CA180 + Fn or CA + 1.6% chitosan scaffold were not significantly different for any condition (Table 4.3). However, the percent of elongated cells was variable over the culture period. For

shorter durations on the scaffold, cells showed a slight preference for an elongated morphology. This preference increased significantly over the culture time and was not different from the percent of elongated cells on glass. This agrees with the decrease of EC circularity over time which was attributed to an increase in cell attachment (Wittmer et al., 2007). HUVECs that had migrated onto a Fn coated or a chitosan scaffold had significantly more cells with an elongated morphology (than CA180). We attribute this to more cells adhering and spreading on scaffolds with Fn or chitosan addition as compared with the bare scaffolds. Digital images of HUVECs confirm cell density, viability and area measurements (Figures 4.9, 4.11 and 4.13). On CA180, we see an approximate population doubling (on day 4) that is maintained throughout the rest of the culture time, leading us to conclude that the culture had reached confluence on the scaffolding. This further supports the use of CA180 scaffolds for EC culture. Digital images of HUVECs on the CA180 + Fn and CA + 1.6% chitosan scaffold show a continual increase in cell density and a heightened elongated morphology.

With the addition of $3.4\mu\text{g}/\text{mm}^2$ fibronectin or 1.6% chitosan to a CA180 scaffold, there was a significant increase in HUVEC cell density on the electrospun scaffold (Table 4.4). Others have seen increased cell density on fibronectin adsorbed polymers over the bare polymer substrates (Heilshorn et al., 2003; Koenig et al., 2003). They and we attributed this finding to the increased likelihood for cells to interact, adhere and spread on fibronectin coated substrates as compared to the base substrate. Others have also seen an increased attachment and cell spreading on chitosan based scaffolds (Khan et al., 2000). Our data support this finding; that cells can interact with electrospun scaffolds with added chitosan better than the base scaffold. Cell density was significantly improved on the chitosan scaffold. This improvement can also be attributed to the enhancement of mechanical properties, upon addition of chitosan to the electrospinning solution measured by us and others (Khan et al., 2000).

HUVECs that had infiltrated our electrospun scaffolds migrated against gravity. Neutrophils have been seen to migrate against gravity in response to a chemotactic gradient (Park, 1975; Park, 1980). While this phenomenon has not been studied extensively, our results show that it is possible for HUVECs to release from glass coverslips in favor for electrospun cellulose acetate scaffolds migrating against gravity. HUVECs may show a preference for the three-dimensional topology of the electrospun scaffolds over the two-dimensional glass.

5.1.2 Effects of Surface Modifications

The hydrophobicity of glass substrates was altered to determine if endothelial cells can be directed onto microstamped patterns on each substrate and excluded from the non-patterned region. Our surfaces are clearly hydrophilic or hydrophobic after our cleaning technique as determined by the contact angle measurements. In some preparations, the extent to which Fn had adsorbed onto glass substrates was investigated. After 4 hours in a PBS solution, Fn remained on both hydrophilic and hydrophobic glass substrates (Figure 4.15) and the stamp geometry was preserved. Other groups have reported that Fn can be adsorb onto hydrophobic polymer surfaces (Osaki et al., 2006). Although we did not investigate Fn adsorption over longer periods, at least within 4 hours, the adsorbed proteins would provide a specific ligand binding site for ECs. Although we did not measure the extent to which the other ECM proteins are adsorbed

onto glass substrates, we assume similar results would be obtained. These proteins would at least provide an initial attachment point for ECs in culture.

5.1.2.a Effects of Hydrophilic vs. Hydrophobic Surfaces on Viability and Density

The effects of bare hydrophilic and hydrophobic glass substrates on hDMEC culture parameters were investigated. There was a reduction in cell viability, density and percent confluence on hydrophobic substrates as compared to hydrophilic substrates (Figures 4.15, 4.16). Others have seen similar results where ECs were partially excluded from hydrophobic surfaces in favor of hydrophilic surfaces (Iuliano et al., 1993). This is attributed to the ease with which cells can adhere to hydrophilic surfaces as compared with hydrophobic surfaces; cells do not adhere well to hydrophobic surfaces (Patrino et al., 2007). EC area was not different based on the substrate that the cells were culture on but the fraction of elongated cells was significantly reduced on hydrophobic substrates (Table 4.5). Reduced ability for ECs to spread on hydrophobic substrates vs. hydrophilic surfaces has been previously reported (Iuliano et al., 1993). Digital images of hDMECs confirm these findings, showing a lack of viable cells on hydrophobic surfaces as compared to on hydrophilic surfaces (Figure 4.17).

5.1.2.b Effects of Microstamped ECM Proteins on Hydrophilic Surfaces on Viability, Density and Morphology

Microstamped ECM proteins onto hydrophilic glass surfaces were investigated to determine if ECs can be directed to preferentially grow on patterned surfaces. Others have found that with micro-scale features of ECM proteins ECs can be restricted to particular regions within a substrate (Falconnet et al., 2006; Jiang et al., 2002; Uttayarat et al., 2005). Using a microcontact printing approach we saw that EC viability was independent of where the cells were cultured (unstamped hydrophilic glass vs. microstamped ECM proteins) (Figure 4.19). Cell density (and percent confluence), however, was approximately 4 fold higher within the stamped region as compared to on hydrophilic glass (Figures 4.16 and 4.18). Cells found on the glass had a density approximately 4 fold larger than the initial seeding density (therefore cells on the stamped region had an approximate 16 time increase in density within 3 days; cells on the stamped ECM proteins were proliferating at a higher rate and were approaching confluence at the end of three days in culture). This increase in cell density can directly be caused by a preferential increase in EC attachment to the ECM proteins (Jiang et al., 2002; Kubota et al., 1988; Moon et al., 2005) or to an increase in proliferation of adherent cells (Schneider et al., 1997). This preferential accelerated growth on ECM patterns was found even though ECs adhere well to hydrophilic glass substrates.

The morphology of cells on microstamped ECM proteins was also investigated. The cell area was independent of conditions (Table 4.6). However, our preferential elongated morphology was found to be enhanced on the stamped proteins. Enhanced elongated morphology on ECM proteins can be attributed to increased adhesion and spreading to the ECM proteins and could account for cell groupings (He et al., 2004; He et al., 2005b; He et al., 2005a; He et al., 2006). Microstamped Fn had the highest percentage of elongated cells, which is attributed to the normal *in vivo* function of Fn. Fn plays an important role in EC migration during angiogenesis (Moon et al., 2005;

Tonnesen et al., 2000). Digital images of cells cultured on microstamped proteins (Figure 4.20) showed the preference for ECs to grow within the stamped region and they are somewhat excluded from the neighboring non-stamped region. This exclusion was variable based on the ECM protein. Laminin, the ECM protein with the lowest exclusion ability, is prevalent in the basal lamina but not during angiogenesis (Kleinman et al., 1986). Cells cultured on collagen IV or fibronectin were excluded from the neighboring unstamped region to a larger extent. These proteins make up a large part of the basal lamina and play important roles in EC migration/adhesion (Alberts et al., 2001) leading to an increased exclusion ability. On the glass substrate, we see that cells were not organized and grew in any region.

5.1.2.c Effects of Microstamped ECM Proteins on Hydrophobic Surfaces on Viability, Density and Morphology

Microstamped ECM proteins on hydrophobic glass surfaces were investigated to determine if endothelial cells can be directed to grow onto patterned surfaces and be excluded from the hydrophobic non-patterned surface. ECs can be restricted to particular regions within a substrate coated with ECM proteins (Falconnet et al., 2006; Jiang et al., 2002; Uttayarat et al., 2005). Using a microcontact printing approach we saw that EC viability and density was significantly higher on the microstamped ECM protein as compared to on the hydrophobic glass (Figure 4.21). Cells did proliferate on the microstamped protein; there was an approximate 10 fold increase in cell density over the initial seeding density. Increased density can directly be caused by increase in EC attachment (Jiang et al., 2002; Kubota et al., 1988; Moon et al., 2005) or proliferation (Schneider et al., 1997). Reduction of density and viability on hydrophobic glass is attributed to the inability for cells to adhere to hydrophobic surfaces (Patrino et al., 2007). Exclusion from the non-patterned region has been partially quantified with the percent confluence; there was a significant decrease in percent confluence on hydrophobic glass as compared with the microstamped ECM proteins (Figure 4.17). With the drastic reduction in cell density, viability and percent confluence on hydrophobic glass, we therefore had the ability to exclude ECs from the non-patterned region.

The morphology of cells on microstamped ECM proteins was also investigated. Cell area *was* dependent on whether the cell was cultured on hydrophobic glass or on the microstamped ECM protein (Table 4.7). This was true for hDMECs seeded onto microstamped Fn, collagen IV and collagen I but not laminin. The independence for laminin is attributed to its normal *in vivo* function. Laminin plays an important role in defining the structure of the basal lamina but has minimal effects on cell migration (Alberts et al., 2001). The preferential elongated morphology was significantly enhanced on microstamped ECM proteins and is attributed to the increased adhesion and spreading of cells to ECM proteins (He et al., 2004; He et al., 2005b; He et al., 2005a; He et al., 2006). Digital images of cells cultured on microstamped proteins (Figure 4.22) showed the preference for ECs to align and grow within the stamped region for all proteins investigated. On the hydrophobic glass substrate, cells were not organized and mostly dead (ethidium positive). Comparing the stamped proteins, we see that the exclusion of ECs from the non-patterned region was variable. Again, the substrate with the lowest exclusion was laminin which is prevalent in the basement membrane but not during angiogenesis (Kleinman et al., 1986). Collagen IV and fibronectin, which had a greater

ability to exclude cells, make up a large part of the basal lamina and play an important role in EC migration (Alberts et al., 2001).

Comparing the results found between microstamped proteins on hydrophilic vs. hydrophobic glass substrates, we see that cell viability was independent of the same microstamped proteins on different glass surfaces. The density was lower on the ECM proteins stamped onto hydrophobic glass surfaces; this is attributed to the detrimental effects in general for ECs cultured on bare hydrophobic surfaces. However, ECM proteins that were stamped onto hydrophobic glass had a greater ability to exclude cells from the non-patterned region (compare ratio changes in percent confluence). Also, the cells that were on the unstamped hydrophobic region were not viable and had a decrease in cell density as compared to the initial seeding density. Therefore, we have the ability to direct the growth of endothelial cells onto microstamped ECM proteins.

5.2 Bioassay Chamber

5.2.1 Electrospun Cellulose Acetate Scaffolds

My bioassay chamber was developed to evaluate the behavior of cells originating from an explanted perfused small artery. A calibrated flow rate was applied to explants in order to subject ECs along the blood vessel wall to a low pulsatile shear stress not to mimic *in vivo* flow conditions, but as a mechanical stimulus to promote proliferation and migration (flow was not calibrated in each branch). Low pulsatile shear stress enhances EC migration, proliferation and growth factor production (Ando et al., 1987; Frame and Sarelius, 2000; Mitsumata et al., 1993). We investigated the effects of a pulsatile flow, electrospun scaffold composition and substrate hydrophobicity with ECM proteins on the viability, density and morphology of ECs originating from an explanted aorta.

Vessels were dissected and cannulated with open side branches to allow for cell migration into our scaffolds (Figure 4.22). Inflow was verified to be pulsatile using aortas that were not used for viability/density experiments since flow verification could not be performed in those experiments without compromising the experiment because red blood cells would alter the flow profile (Section 3.3.3). A defined pulsatile inflow waveform was found in the main branch of the aorta (Figures 4.23, 4.24). Others have seen that low flow rates ($\tau_w = 1.4$ dynes/cm²) can increase angiogenesis in cell culture studies (Cullen et al., 2002). This shear stress is equivalent to our High flow rate. A sinusoidal regression analysis was performed to determine the propagation of the perfusate velocity waveform through the explant (Figure 4.25). Others have shown that with a low correlation coefficient for the best fit regression line, there is an energy loss between the calibrated pump and the explant (Demiray, 1997; Marchais et al., 1993). They claim, it is possible that the explant would not experience a truly pulsatile flow (Demiray, 1997; Marchais et al., 1993). However, a pulsatile inflow waveform was verified in 10 aortas with a high correlation for the best fit regression line.

When investigating the flow through explants, flow was into, out of or bypassing the branch completely. Further the flow direction changed over time for some branches (i.e. branches with outflow changed to inflow). For the experiments in which we tested EC growth from the explant, digital images were taken at each branch location without knowing the direction of flow through the branch.

ECs originating from explants were found within our scaffolds (Figure 4.26). The BS-1 lectin was used to verify that cells found within the electrospun scaffold are

endothelial (Hayes and Goldstein, 1974) and not other vascular cells. All cells investigated with the BS-1 lectin fluoresced positively, identifying them as endothelial cells. Cells were seen to release from the scaffold during BS-1 lectin staining but others elongated along the electrospun scaffold during staining. Dual staining with DAPI confirmed the presence of nuclei within endothelial cells (Figure 4.26 C-E). Cells in this preparation seem to be clustered and round as compared to cells identified in the scaffold with just the BS-1 lectin (Figure 4.26 A-B). This is most likely from the water (pH 7.0) that was required to dilute the DAPI.

5.2.1.a Effects of Scaffold Composition and Flow Rate

Endothelial cells originating from the perfused artery were found in high density with high viability on the CA180, CA + 1.6% chitosan and Matrigel® scaffolds (Figure 4.27). Two low pulsatile flow rates were used to provide oxygen and nutrients to the explanted vessel, and perhaps provide a stimulus for EC growth and migration (Cullen et al., 2002). The mean shear stress was $\sim 0.1 \text{ dynes/cm}^2$ for the Low flow rate and $\sim 1 \text{ dyne/cm}^2$ for the High flow rate. These flow rates (and corresponding τ_w) are low compared to studies done on the macrocirculation (Warabi et al., 2007) but are more appropriate for microcirculation studies examining EC proliferation and migration (Cullen et al., 2002; Hong et al., 2006). Cell viability improved with High flow (Figure 4.27). This enhanced viability may have been due to increased oxygen delivery to the cells within the scaffold, as measured by others (Nguyen et al., 2005). ECs found within the CA + 1.6% chitosan scaffold showed an enhanced viability under either flow rate as compared to the CA180 scaffold. Density was high and unrelated to flow for all scaffolds. The cell density approached that of HUVECs cultured on glass and other substrates in cell culture experiments even though the culture conditions and cell types were different (Section 4.1 and 5.1).

One might consider that an increased flow rate could cause increases in cell density by convective drag of cell with the flow. However, flow was not uniformly outflow for all branches (Section 3.3.3). There were not distinct populations showing high vs. low cell density, which would have suggested convective drag had artificially increased the EC population. Further, as Figure 4.27 shows, cell density was not statistically different between High and Low flow conditions, suggesting that EC migration and not convective flow was the means by which cells traveled through the scaffold. Migration, per se, was not quantified in the bioassay chamber because the logistics of opening a chamber to add a second scaffold would compromise the experiment. Migration of ECs onto CA180, CA180 + Fn and CA + 1.6% chitosan electrospun scaffolds were investigated in cell culture (Sections 4.1.1.d and 5.1.1.d). Also, in the absence of flow, endothelial cells were still found in the electrospun scaffold Near the explanted blood vessel. This indicates that cells originating from the blood vessel have the potential to migrate into the CA180 scaffold without the mechanical shear stress stimulus.

5.2.1.b Cell Morphology on Electrospun Scaffolds

As for the cell culture studies, there were no trends in perimeter based cell area for cells in the bioassay chamber. Our preferential elongated morphology for ECs was prominent in the bioassay chamber (Table 4.8), but to a lesser extent than HUVECs under

cell culture conditions. This may be consistent with the known differences in morphologies between HUVECs (Zhu et al., 2004) vs. aortic endothelial cells (Suda et al., 2000). Furthermore, ECs in the bioassay chamber would have only been in contact with the electrospun scaffold for a maximum of 24 hours. From infiltration studies (Sections 4.1.1.d and 5.1.1.d) we saw that although ECs showed a preference towards an elongated morphology at short duration, this preference was low and increased with longer durations. With the addition of 1.6% chitosan to a CA180 scaffold we saw an enhanced percentage of elongated cells (consistent with cell culture). The increased cell density, viability and elongated morphology for cells found on the CA + 1.6% chitosan scaffold can be attributed to the increased attachment of cells to chitosan mimicking ours and other groups (Li and Hsieh, 2006; Park et al., 2006) cell culture results.

Digital images of ECs show a preference towards the elongated morphology (Figure 4.28). Panels A and B in Figure 4.28 illustrate that after the culture period there is a high density and viability of cells found both Near and Far from the open side branch. The addition of chitosan showed an increase in the elongated morphology (Figure 4.28 C). Matrigel® induced the beginnings of spontaneous capillary-like structures (Figure 4.28 D) and all cells were elongated at this Short growth duration. We conclude that within the novel bioassay chamber, a perfused explanted vessel can serve as the initial source for ECs and that base cellulose acetate electrospun scaffolds, with a fiber diameter range of 1-5 μ m, support these cells. The addition of chitosan supported the culture of ECs initiating from a perfused explant better than the CA180 scaffolds.

5.2.1.c Long Term Culture of Murine Aortas in Electrospun Scaffold

These experiments were conducted as proof-of-principle studies towards the long term culture of autologous endothelial cells within our bioassay chamber. Dilation to 10^{-2} adenosine was verified after some perfusion experiments to verify tone. After adenosine exposure, aortas dilated approximately 15% of their resting value. In the hamster cheek pouch microvascular preparation, blood vessels can dilate as much as 20% of their baseline diameter (Fox and Frame, 2002b). Our vessels are responsive after the perfusion time. High flow (240 μ L/min, ~ 1 dyne/cm²) was investigated due to the increased viability for shorter culture periods (Figure 4.27). ECs were found with a high cell density and high cell viability over 7 days of culture (Figure 4.29, 4.28). With longer shear stress exposure, ECs align and elongated in the direction of flow (Li et al., 2005; Ohashi and Sato, 2005; Ueda et al., 2004). The increase in our preferential elongated morphology both Near and Far from the explant supports that cells which initially leave the explant enter the scaffold and stay there during perfusion. They are therefore exposed to shear stresses for longer durations, which would increase the number of elongated cells. Due to the increased viability/preferential morphology with perfusion time, our data supports migration of ECs into the electrospun cellulose acetate scaffold.

5.2.2 Effects of Surface Modifications

5.2.2.a Effects of Hydrophilic vs. Hydrophobic Surfaces

The effects of hydrophilic vs. hydrophobic glass substrates on endothelial cell density and viability in the bioassay chamber were investigated. There was a significant reduction in cell viability and density on hydrophobic substrates as compared with the hydrophilic substrates (Figure 4.31). Others have seen similar results where ECs were

partially excluded from hydrophobic surfaces in favor of hydrophilic surfaces (Iuliano et al., 1993), although the effects of shear stress on this exclusion were not investigated. EC density on hydrophobic surfaces was low and this was attributed to the ease of which cells can adhere to hydrophobic surfaces (Iuliano et al., 1993; Patrino et al., 2007). Our cell density was lower here than other bioassay chamber experiments because the scaffolds in these experiments did not surround the vessel, whereas electrospun scaffolds and Matrigel® did surround the vessel. These scaffolds come into contact with the open side branch, possibly provide a stimulus for infiltration and/or migration.

The percent confluence of cells is also relatively low on hydrophobic and hydrophilic surfaces in the bioassay chamber. We attribute this to the lack of a direct contact point for cells from the open side branch (Figure 4.32). However, the percent confluence is still three orders of magnitude larger on the hydrophilic surface as compared to on the hydrophobic surface. EC area was not different based on the glass substrate but the fraction of elongated cells was significantly higher on hydrophilic substrates (Table 4.10). Previous groups have seen that the extent that cells were able to spread on hydrophobic substrates was reduced as compared with hydrophilic surfaces (Iuliano et al., 1993). Digital images of ECs confirm this; viable cells do not appear with high density on hydrophobic surfaces and adhered cells do not elongated (Figure 4.33).

5.2.2.b Effects of Microstamped ECM Proteins on Hydrophilic Surfaces

ECM proteins microstamped onto hydrophilic glass substrates were investigated in order to direct the growth of endothelial cells. The aim was to investigate the exclusion of ECs, originating from a perfused aorta, from non-patterned regions in favor of the patterned ECM proteins. Others have restricted cells to particular regions within a substrate (Falconnet et al., 2006; Jiang et al., 2002; Uttayarat et al., 2005). However, the combination of flow, surface topology and topography were not combined in these studies. Here, EC density was approximately 8 fold higher within the microstamped protein as compared to on the hydrophilic glass (Figure 4.34). This increase in cell density is attributed to increases in cell attachment to the ECM proteins (Jiang et al., 2002; Kubota et al., 1988; Moon et al., 2005) or to an increase in proliferation of attached ECs (Schneider et al., 1997). The microstamped protein did not affect viability as compared to hydrophilic glass substrates. The high percent confluence on microstamped proteins confirms that ECs show a preference for the microstamped ECM protein over the hydrophilic glass (Figure 4.32). Here, the percent confluence was lower than cell culture because these cells were only cultured for one day, whereas hDMECs were cultured for three days. However, the trend in percent confluence is the same for both microstamp experiments.

The morphology of cells on microstamped ECM proteins was also investigated (Table 4.11). No trend in cell area was found under these conditions. All cells were found to grow in our preferential elongated morphology but this was unrelated to the culture substrate (hydrophilic glass vs. ECM protein). Digital images (Figure 4.35) confirmed the EC preference to grow within the microstamped ECM protein (only Fn is shown). These results are similar to our cell culture studies, the microstamped ECM protein did *not* completely exclude cells from the bare hydrophilic glass but there was a preference for EC growth within the microstamped proteins.

5.2.2.c Effects of Microstamped ECM Proteins on Hydrophobic Surfaces

Using hydrophobic glass as our base substrate to microstamp ECM proteins onto, we found that we were able to direct the growth of ECs onto microstamped proteins and largely exclude cells from the hydrophobic substrate (Figure 4.36). Other groups have seen similar results in cell culture where they had the ability to direct cells onto collagen IV which had been patterned onto hydrophobic glass coverslips (Ludwig et al., 2006). Increases in cell density in the patterned region were attributed to an increased ability for cells to initiate an attachment to collagen IV vs. the hydrophobic glass (Ludwig et al., 2006). Others have shown a drastic decrease in cell viability on hydrophobic glass and attributed this to the inability of cells to adhere to hydrophobic substrates (Iuliano et al., 1993). We confirm these findings and with the addition of the mechanical stimulus of low flow, the results do not change. We saw a significantly lower viability and density on the hydrophobic surfaces as compared to on the microstamped ECM proteins. In the bioassay chamber, the ability to exclude ECs from the non-patterned hydrophobic region with the addition of fluid forces was maintained. This was confirmed with the large increase in percent confluence on the microstamped proteins (Figure 4.32). The increase in percent confluence can also be attributed to the known preference for ECs to interact with ECM proteins vs. hydrophobic substrates (Armulik et al., 2005; Iuliano et al., 1993).

Cell morphology of ECs on ECM microstamped proteins on hydrophobic glass showed a preference for our preferential elongated morphology (Table 4.12, Figure 4.37). Cell area was independent of all conditions. Heightened elongated morphology can be caused by the combined effects of fluid forces and spreading on ECM proteins (Ando et al., 1987; Frame and Sarelius, 2000; McCue et al., 2004). These results are similar to our cell culture studies, the microstamped ECM protein did *not* completely exclude cells from the bare hydrophobic glass but there was a preference for EC growth within the microstamped proteins.

In conjunction with our cell culture results, we see an enhancement of integrin mediated binding to ECM proteins which had been patterned onto hydrophobic or hydrophilic glass coverslips. Although we did not quantify if integrins were causing the enhancement, it is well documented that Fn and collagen interact with EC integrins (i.e. $\alpha_5\beta_1$ interacts with Fn, $\alpha_1\beta_1/\alpha_2\beta_1$ interacts with collagens) (Alberts et al., 2001; Davis and Camarillo, 1995; Stupack and Cheresch, 2004; Tuckwell and Humphries, 1996). In cell culture, laminin did not provide a good template for cell exclusion (therefore laminin was not studied in the bioassay chamber). ECM proteins microstamped onto hydrophobic coverslips provided a better patterning substrate than hydrophilic glass for ECs that had originated from a small explanted perfused artery. Therefore, we have the ability to exclude endothelial cells exposed to a low pulsatile shear stress from the non-patterned region on hydrophobic glass surfaces, in favor of the patterned ECM proteins.

5.2.2.d Effects of Microstamped Fibronectin onto CA180 Scaffolds

Cell density and viability was not improved on microstamped Fn onto an electrospun cellulose acetate scaffold (CA180, Figure 4.38). Perimeter based cell area and fraction of elongated cells was also not different for cells on the microstamped Fn as compared with the bare CA180 scaffold (Table 4.13). In control cell culture studies, cell density, viability and morphology was not significantly improved on CA180+Fn

scaffolds as compared with CA180 scaffolds (Figure 4.5, Table 4.2). In cell culture experiments, the scaffolds were 100% coated with fibronectin (Figure 4.2). In these microstamp experiments, fibronectin coated CA180 accounted for less than 5% of the entire scaffold. It was therefore not unexpected that microstamped Fn onto CA180 did not elicit significant changes in cell density, viability and morphology. Also, electrospun scaffolds are three dimensional structures and with this method, only a two dimensional surface can be coated with fibronectin. We have some evidence that endothelial cells prefer three dimensional scaffolds over two dimension scaffolds (Section 4.1.1.d). In these studies, cells originating from an explanted aorta would presumably prefer the three dimensional scaffold non-coated regions over the two dimension coated region.

5.3 MATLAB® Programs Used to Facilitate Data Collection or Analysis

A program was written using MATLAB® in order to obtain reliable measurements of perimeter based cell area. The accuracy of this program needed to be high. To validate the long and short axis measurements obtained from the cellcounting.m MATLAB® program, we used ProAnalyst as the control in a Monte Carlo simulation (Section 3.6.3.c). Axes of the same cells were quantified with both methods and the percent error between the readings was less than 3% (Table 3.2). We therefore conclude that our cellcounting.m program can accurately measure the long and short axis of cells.

To validate the perimeter based area, we compared results obtained with a map wheel and our program. Both methods allow us to obtain the perimeter of a randomly shaped object and then calculate the area based on this perimeter. By assuming that the object was circular (map wheel method), a radius can be calculated and from that radius an area can be obtained; this method is somewhat inaccurate for objects that are not close to circular in shape. My program does not assume the object is circular and calculates the perimeter based area on a numerical approximation for an integral (the integral is calculated from the perimeter). This method is more accurate for objects that are not circular but has an intrinsic error, which converges to zero quickly with 5 overlapping points (a point is equivalent to a pixel). The percent error between these two methods was small (Table 3.2). Although the error was greater than 5%, we still consider the program acceptable because the methods used to test the accuracy are different and for cells that are not close to circular, the calculated areas have a large variation, justifying the acceptance of this error rate.

The ability of the cellcounting.m program to locate and identify cell boundaries was also investigated. There was a very high correlation by visual inspection between perimeters identified by phase-contrast microscopy (Figure 3.8 A) and the cellcounting.m program (Figure 3.8 B). This combined with the accurate calculations for cell axes and the perimeter based cell area, justifies the use of this program to rapidly obtain a more accurate perimeter based cell area to quantify cell morphology.

SECTION VI: SUMMARY AND FUTURE WORK

The major aim of this thesis was to optimize the growth of endothelial cells through a combination of mechanical, topological and chemical growth cues. Initial studies were conducted in cell culture to determine the optimal scaffold for the use in a novel bioassay chamber. Using a cellulose acetate based electrospun scaffold, we found that endothelial cells prefer scaffolds with a larger fiber diameter as compared to what is common within the native extracellular matrix (1-5 μ m vs. <100nm) (Figures 4.3, 4.7, 4.8, 4.9 and Tables 4.1, 4.2, 4.3). On these scaffolds endothelial cells maintained a high cell viability and cell density under all tested conditions. We also saw that these scaffolds enhanced the percentage of endothelial cells in our preferential elongated morphology. Next, the effects of material composition of a cellulose acetate based electrospun scaffold were investigated. Material strengthening compounds, ECM proteins and a potent angiogenic growth factor were added to the electrospun scaffolds, either prior to electrospinning or to the formed scaffold. The addition of chitosan to the large fiber diameter CA180 scaffolds enhanced endothelial cell viability and density and increased the percentage of elongated cells found within the scaffold (supports Hypothesis 2.1, Figures 4.4, 4.7, 4.12, 4.13 and Tables 4.2, 4.3). Carbon nano-tubes and vascular endothelial growth factor were unsuitable additives in these conditions. Fibronectin as an additive did not significantly change the culture conditions (although cell density was enhanced) (supports Hypothesis 2.2, Figures 4.5, 4.10, 4.11 and Tables 4.2, 4.3). For these preparations, we therefore concluded that the large fiber diameter scaffolds (1-5 μ m), especially with the addition of 1.6% chitosan, were optimal for the culture of endothelial cells. We therefore, chose the scaffolds to investigate within the bioassay chamber.

The bioassay chamber was designed to investigate if an explanted perfused artery can serve as the initial source of endothelial cells (Aim 1.1, Figures 4.24, 4.25). These endothelial cells can then be used to investigate the onset of angiogenesis or be used to design autologous tissue engineered products. We found that, endothelial cells were present with a high density and viability within the CA180 electrospun scaffolds (supports Aim 1.2, Figures 4.25, 4.26, 4.27 and Table 4.8). With the addition of chitosan to these scaffolds, we saw an improvement in culture conditions (supports Hypothesis 2.1, Figure 4.27, 4.27). Elongated morphology was prominent within both scaffolds. The viability of cells improved with higher flow rates and time, whereas the density was independent of flow rate (supports Aim 1.3, Figures 4.28, 4.29 and Table 4.9). These combined findings allude to the migration of cells throughout the scaffold instead of the convective flow of cells. This provides a proof of principle for the possibility of co-culture tissue engineering vascular networks from an autologous perfused explant. Long-term culture of endothelial cells was also investigated within the bioassay chamber. We saw that ECs maintained their culture parameters over the entire perfusion time.

In order to further investigate the possibility for tissue engineering blood vessels, the directed growth of endothelial cells was investigated. First in cell culture studies, the

exclusion of ECs from particular regions using microstamped patterns of ECM proteins on hydrophilic or hydrophobic glass substrates was investigated. Endothelial cells were found with a significantly higher density within the stamped region (supports Hypothesis 2.3 and Aim 2.3.a and refutes Aim 2.3.b, Figures 4.15, 4.16, 4.17, 4.18, 4.19 and Tables 4.4, 4.5). On hydrophobic substrates, the cells were almost completely excluded from the non-patterned region (supports Hypothesis 2.4 and Aim 2.4.a and refutes Aim 2.4.b, Figures 4.16, 4.20, 4.21 and Table 4.7). Cell viability and cell density was significantly enhanced on the patterned ECM protein surface. Similarly, in the bioassay chamber, the addition of shear stress to patterned hydrophilic or hydrophobic substrates was investigated. The cell density was enhanced on the microstamped ECM protein for both hydrophilic and hydrophobic surfaces (Figures 4.15, 4.16, 4.17, 4.30, 4.31, 4.32, 4.35, 4.36 and Tables 4.4., 4.6, 4.9, 4.11). Cell viability was low on hydrophobic surfaces and we had the ability to exclude ECs from the non-patterned region on hydrophobic surfaces.

Future studies will investigate the complete exclusion of cells from the non-patterned region while fabricating patent vascular networks on the patterned substrate. To accomplish this task, a combination of electrospun scaffolds (or other topological structures) and surface modified substrates will be combined. This will provide ECs with both topological and topographical cues during their culture period. Within the bioassay chamber, shear stress can be applied to autologous endothelial cells that also have topological and topographical cues. Once patent vessels can be formed within these substrates, a pattern which resembles anatomical networks will be applied to the glass substrate. The initial goals for this project will be the formation of patent networks with highly organized geometries in cell culture and the bioassay chamber.

The next step would address tissue engineering problems via investigating whether or not the fabricated patent vascular networks are biocompatible and can be incorporated into an animal model. The effects of the scaffold *in vivo* would also need to be investigated at this time. If the scaffold is biocompatible and biodegradable and a fully patent vascular network can be formed within this scaffold, the effects of the entire product would be investigated in animal wound healing models. Using a dorsal window preparation, this vascular patch can be applied to see if angiogenesis can be enhanced *in vivo* or if a network fabricated *ex vivo* can be applied into the wound to enhance the healing process.

SECTION VII: REFERENCE LIST

1. Aguzzi,M.S., Facchiano,F., Ribatti,D., Gaeta,R., Casadio,R., Rossi,I., Capogrossi,M.C., and Facchiano,A. (2004). A novel RGDS-analog inhibits angiogenesis in vitro and in vivo. *Biochemical and Biophysical Research Communications* 321, 809-814.
2. Alberts,B., Johnson,A., Lewis,J., Raff,M., Roberts,K., and Walter,P. (2001). *Molecular Biology of the Cell*. (New York: Garland Science).
3. Albini,A. (1998). Tumor and Endothelial cell invasion of basement membranes. *Pathology Oncology Research* 4, 230-241.
4. Albini,A., Benelli,R., Noonan,D.M., and Brigati,C. (2004). The "chemoinvasion assay": a tool to study tumor and endothelial cell invasion of basement membranes. *International Journal of Developmental Biology* 48, 563-571.
5. Ando,J., Nomura,H., and Kamiya,A. (1987). The Effect of Fluid Shear-Stress on the Migration and Proliferation of Cultured Endothelial-Cells. *Microvascular Research* 33, 62-70.
6. Arbisser,J.L. (1996). Angiogenesis and the skin: A primer. *Journal of the American Academy of Dermatology* 34, 486-497.
7. Arenberg,D.A. and Strieter,R.M. (1999). Angiogenesis. In *Inflammation: Basic Principles and Clinical Correlates*, J.I.Gallin and R.Snyderman, eds. (Philadelphia: Lippincott Williams and Wilkins), pp. 851-864.
8. Armulik,A., Abramsson,A., and Betsholtz,C. (2005). Endothelial/pericyte interactions. *Circulation Research* 97, 512-523.
9. Asahara,T., Bauters,C., Zheng,L.P., Takeshita,S., Bunting,S., Ferrara,N., Symes,J.F., and Isner,J.M. (1995). Synergistic Effect of Vascular Endothelial Growth-Factor and Basic Fibroblast Growth-Factor on Angiogenesis In-Vivo. *Circulation* 92, 365-371.
10. Ausprunk,D.H. and Folkman,J. (1977). Migration and Proliferation of Endothelial Cells in Preformed and Newly Formed Blood-Vessels During Tumor Angiogenesis. *Microvascular Research* 14, 53-65.
11. Ayutsede,J., Gandhi,M., Sukigara,S., Ye,H.H., Hsu,C.M., Gogotsi,Y., and Ko,F. (2006). Carbon nanotube reinforced Bombyx mori silk nanofibers by the electrospinning process. *Biomacromolecules* 7, 208-214.
12. Baker,S.C., Atkin,N., Gunning,P.A., Granville,N., Wilson,K., Wilson,D., and Southgate,J. (2006). Characterisation of electrospun polystyrene scaffolds for three-dimensional in vitro biological studies. *Biomaterials* 27, 3136-3146.

13. Barnes,C.P., Smith,M.J., Bowlin,G.L., Sell,S.A., Tang,T., Matthews,J.A., Simpson,D.G., and Nimitz,J.C. (2006). Feasibility of Electrospinning the Globular Proteins Hemoglobin and Myoglobin. *Journal of Engineered Fibers and Fabrics 1*, 16.
14. Bates,D.O. and Jones,R.O. (2003). The role of vascular endothelial growth factor in wound healing. *Int. J Low Extrem. Wounds 2*, 107-120.
15. Battegay,E.J., Rupp,J., Iruelaarispe,L., Sage,E.H., and Pech,M. (1994). PDGF-BB Modulates Endothelial Proliferation and Angiogenesis In-Vitro Via PDGF Beta-Receptors. *Journal of Cell Biology 125*, 917-928.
16. Bauer,S.M., Bauer,R.J., Liu,Z.J., Chen,H., Goldstein,L., and Velazquez,O.C. (2005). Vascular endothelial growth factor-C promotes vasculogenesis, angiogenesis, and collagen constriction in three-dimensional collagen gels. *Journal of Vascular Surgery 41*, 699-707.
17. Becker,D., Meier,C.B., and Herlyn,M. (1989). Proliferation of Human-Malignant Melanomas Is Inhibited by Antisense Oligodeoxynucleotides Targeted Against Basic Fibroblast Growth-Factor. *Embo Journal 8*, 3685-3691.
18. Benelli,R. and Albini,A. (1999). In vitro models of angiogenesis: the use of matrigel. *The International Journal of Biological Markers 14*, 243-246.
19. Berg,B.R. and Sarelius,I.H. (1995). Functional Capillary Organization in Striated-Muscle. *American Journal of Physiology-Heart and Circulatory Physiology 37*, H1215-H1222.
20. Bianchi,F., Vassalle,C., Simonetti,M., Vozzi,G., Domenici,C., and Ahluwalia,A. (2006). Endothelial cell function on 2D and 3D micro-fabricated polymer scaffolds: applications in cardiovascular tissue engineering. *Journal of Biomaterials Science-Polymer Edition 17*, 37-51.
21. Board,R. and Jayson,G.C. (2005). Platelet-derived growth factor receptor (PDGFR): A target for anticancer therapeutics. *Drug Resistance Updates 8*, 75-83.
22. Boland,E.D., Telemeco,T.A., Simpson,D.G., Wnek,G.E., and Bowlin,G.L. (2004). Utilizing acid pretreatment and electrospinning to improve biocompatibility of poly(glycolic acid) for tissue engineering. *Journal of Biomedical Materials Research Part B-Applied Biomaterials 71B*, 144-152.
23. Britland,S., Morgan,H., WojakStodart,B., Riehle,M., Curtis,A., and Wilkinson,C. (1996). Synergistic and hierarchical adhesive and topographic guidance of BHK cells. *Experimental Cell Research 228*, 313-325.
24. Brooks,P.C., Clark,R.A.F., and Cheresch,D.A. (1994). Requirement of Vascular Integrin Alpha(V)Beta(3) for Angiogenesis. *Science 264*, 569-571.

25. Brown,X.Q., Ookawa,K., and Wong,J.Y. (2005). Evaluation of polydimethylsiloxane scaffolds with physiologically-relevant elastic moduli: interplay of substrate mechanics and surface chemistry effects on vascular smooth muscle cell response. *Biomaterials* 26, 3123-3129.
26. Buijtenhuijs,P., Buttafoco,L., Poot,A.A., Daamen,W.F., van Kuppevelt,T.H., Dijkstra,P.J., De Vos,R.A.I., Sterk,L.M.T., Geelkerken,B.R.H., Feijen,J., and Vermes,I. (2004). Tissue engineering of blood vessels: characterization of smooth-muscle cells for culturing on collagen-and-elastin-based scaffolds. *Biotechnology and Applied Biochemistry* 39, 141-149.
27. Burns,A.R., Smith,C.W., and Walker,D.C. (2003). Unique structural features that influence neutrophil emigration into the lung. *Physiological Reviews* 83, 309-336.
28. Carmeliet,P. (2005). Angiogenesis in life, disease and medicine. *Nature* 438, 932-936.
29. Chapeau,C. and Gagnon,C. (1987). Nitrocellulose and Polyvinyl Coatings Prevent Sperm Adhesion to Glass Without Affecting the Motility of Intact and Demembrated Human-Spermatozoa. *Journal of Andrology* 8, 34-40.
30. Chen,C.S., Alonso,J.L., Ostuni,E., Whitesides,G.M., and Ingber,D.E. (2003). Cell shape provides global control of focal adhesion assembly. *Biochemical and Biophysical Research Communications* 307, 355-361.
31. Chen,C.S., Mrksich,M., Huang,S., Whitesides,G.M., and Ingber,D.E. (1997). Geometric control of cell life and death. *Science* 276, 1425-1428.
32. Chen,I.I.H. (1983). A Mathematical Representation for Vessel Networks .2. *Journal of Theoretical Biology* 104, 647-654.
33. Chen,I.I.H., Fleming,B.P., and Prewitt,R.L. (1983). Mathematical Representation for the Microvascular Network in the Bats Wing. *Microvascular Research* 25, 227.
34. Chen,K.D., Li,Y.S., Kim,M., Li,S., Yuan,S., Chien,S., and Shyy,J.Y.J. (1999). Mechanotransduction in response to shear stress - Roles of receptor tyrosine kinases, integrins, and Shc. *Journal of Biological Chemistry* 274, 18393-18400.
35. Chettibi,S. and Ferguson,M.W.J. (1999). Wound Repair: An Overview. In *Inflammation: Basic Principles and Clinical Correlates*, J.I.Gallin and R.Snyderman, eds. (Philadelphia: Lippincott Williams and Wilkins), pp. 865-882.
36. Chien,S. (2007). Mechanotransduction and endothelial cell homeostasis: the wisdom of the cell. *American Journal of Physiology-Heart and Circulatory Physiology* 292, H1209-H1224.

37. Clark,P., Connolly,P., Curtis,A.S.G., Dow,J.A.T., and Wilkinson,C.D.W. (1987). Topographical Control of Cell Behavior .1. Simple Step Cues. *Development* 99, 439-448.
38. Clark,P., Connolly,P., Curtis,A.S.G., Dow,J.A.T., and Wilkinson,C.D.W. (1990). Topographical Control of Cell Behavior .2. Multiple Grooved Substrata. *Development* 108, 635-644.
39. Clark,R.A.F. (1985). Cutaneous Tissue-Repair - Basic Biologic Considerations .1. *Journal of the American Academy of Dermatology* 13, 701-725.
40. Craig,L.E., Spelman,J.P., Strandberg,J.D., and Zink,M.C. (1998). Endothelial Cells from Diverse Tissues Exhibit Differences in Growth and Morphology. *Microvascular Research* 55, 65-76.
41. Craighead,H.G., James,C.D., and Turner,A.M.P. (2001). Chemical and topographical patterning for directed cell attachment. *Current Opinion in Solid State & Materials Science* 5, 177-184.
42. Cullen,J.P., Sayeed,S., Sawai,R.S., Theodorakis,N.G., Cahill,P.A., Sitzmann,J.V., and Redmond,E.M. (2002). Pulsatile flow-induced angiogenesis - Role of G(i) Subunits. *Arteriosclerosis Thrombosis and Vascular Biology* 22, 1610-1616.
43. Curtis,A. and Wilkinson,C. (1997). Topographical control of cells. *Biomaterials* 18, 1573-1583.
44. Dardik,A., Yamashita,A., Aziz,F., Paszkowiak,J., Asada,H., and Sumpio,B.E. (2003). Shear stress stimulated endothelial cell derived PDGF and IL-1 alpha both stimulate SMC chemotaxis via the MAPK pathway. *Journal of Surgical Research* 114, 249.
45. Dardik,A., Yamashita,A., Aziz,F., Asada,H., and Sumpio,B.E. (2005). Shear stress-stimulated endothelial cells induce smooth muscle cell chemotaxis via platelet-derived growth factor-BB and interleukin-1[alpha]. *Journal of Vascular Surgery* 41, 321-331.
46. Davis,G.E., Bayless,K.J., and Mavila,A. (2002). Molecular basis of endothelial cell morphogenesis in three-dimensional extracellular matrices. *Anatomical Record* 268, 252-275.
47. Davis,G.E. and Senger,D.R. (2005). Endothelial extracellular matrix - Biosynthesis, remodeling, and functions during vascular morphogenesis and neovessel stabilization. *Circulation Research* 97, 1093-1107.
48. Davis,G.E. and Camarillo,C.W. (1995). Regulation of Endothelial Cell Morphogenesis by Integrins, Mechanical Forces, and Matrix Guidance Pathways. *Experimental Cell Research* 216, 113-123.

49. De Coensel,N., Desmet,K., Gorecki,T., and Sandra,P. (2006). Determination of polydimethylsiloxane-air partition coefficients using headspace sorptive extraction. *Journal of Chromatography A*.
50. De Marchis,F., Ribatti,D., Giampietri,C., Lentini,A., Faraone,D., Scoccianti,M., Capogrossi,M.C., and Facchiano,A. (2002). Platelet-derived growth factor inhibits basic fibroblast growth factor angiogenic properties in vitro and in vivo through its alpha receptor. *Blood* 99, 2045-2053.
51. Defouw,D.O., Rizzo,V.J., Steinfeld,R., and Feinberg,R.N. (1989). Mapping of the Microcirculation in the Chick Chorioallantoic Membrane During Normal Angiogenesis. *Microvascular Research* 38, 136-147.
52. Demiray,H. (1997). Waves in initially stressed fluid-filled thick tubes. *Journal of Biomechanics* 30, 273-276.
53. den Braber,E.T., de Ruijter,J.E., Ginsel,L.A., von Recum,A.F., and Jansen,J.A. (1998). Orientation of ECM protein deposition, fibroblast cytoskeleton, and attachment complex components on silicone microgrooved surfaces. *Journal of Biomedical Materials Research* 40, 291-300.
54. Dewey,C.F., Bussolari,S.R., Gimbrone,M.A., and Davies,P.F. (1981). The Dynamic-Response of Vascular Endothelial-Cells to Fluid Shear-Stress. *Journal of Biomechanical Engineering-Transactions of the Asme* 103, 177-185.
55. Doherty,D.E., Henson,P.M., and Clark,R.A.F. (1990). Fibronectin Fragments Containing the Rgds Cell-Binding Domain Mediate Monocyte Migration Into the Rabbit Lung - A Potential Mechanism for C5 Fragment-Induced Monocyte Lung Accumulation. *Journal of Clinical Investigation* 86, 1065-1075.
56. Donose,B.C., Taran,E., Vakarelski,I.U., Shinto,H., and Higashitani,K. (2006). Effects of cleaning procedures of silica wafers on their friction characteristics. *Journal of Colloid and Interface Science* 299, 233-237.
57. Dye,J.F., Lawrence,L., Linge,C., Leach,L., Firth,J.A., and Clark,P. (2004). Distinct patterns of microvascular endothelial cell morphology are determined by extracellular matrix composition. *Endothelium-Journal of Endothelial Cell Research* 11, 151-167.
58. Eberl,T., Salvenmoser,W., Rieger,G., Gorny,I., Heiss,V., Kumpitsch,B., Gnaiger,E., and Margreiter,R. (1999). Ultrastructural analysis of human endothelial cells after hypothermic storage in organ preservation solutions. *Journal of Surgical Research* 82, 253-260.
59. Elena Diaz,M. and Cerro,R.L. (2004). Transition from split streamlines to dip-coating during Langmuir-Blodgett film deposition. *Thin Solid Films* 460, 274-278.

60. Entcheva,E., Bien,H., Yin,L., Chung,C.Y., Farrell,M., and Kostov,Y. (2004). Functional cardiac cell constructs on cellulose-based scaffolding. *Biomaterials* 25, 5753-5762.
 61. Falconnet,D., Csucs,G., Grandin,H.M., and Textor,M. (2006). Surface engineering approaches to micropattern surfaces for cell-based assays. *Biomaterials* 27, 3044-3063.
 62. Fang,S., Sharma,R.V., and Bhalla,R.C. (1997). Endothelial Nitric Oxide Synthase Gene Transfer Inhibits Platelet-Derived Growth Factor-BB Stimulated Focal Adhesion Kinase and Paxillin Phosphorylation in Vascular Smooth Muscle Cells. *Biochemical and Biophysical Research Communications* 236, 706-711.
 63. Favot,L., Keravis,T., Holl,V., Le Bec,A., and Lugnier,C. (2003). VEGF-induced HUVEC migration and proliferation are decreased by PDE2 and PDE4 inhibitors. *Thrombosis and Haemostasis* 90, 334-343.
 64. Fawcett,D.W. (1986). *A Textbook of Histology*. (Philadelphia: W.B. Saunders Company).
 65. Flahaut,E., Durrieu,M.C., Remy-Zolghadri,M., Bareille,R., and Baquey,C. (2006). Investigation of the cytotoxicity of CCVD carbon nanotubes towards human umbilical vein endothelial cells. *Carbon* 44, 1093-1099.
 66. Flemming,R.G., Murphy,C.J., Abrams,G.A., Goodman,S.L., and Nealey,P.F. (1999). Effects of synthetic micro- and nano-structured surfaces on cell behavior. *Biomaterials* 20, 573-588.
 67. Folkman,J., Haudenschild,C.C., and Zetter,B.R. (1979). Long-Term Culture of Capillary Endothelial-Cells. *Proceedings of the National Academy of Sciences of the United States of America* 76, 5217-5221.
 68. Folkman,J. and Klagsbrun,M. (1987). Angiogenic Factors. *Science* 235, 442-447.
 69. Folkman,J., Klagsbrun,M., Sasse,J., Wadzinski,M., Ingber,D., and Vlodavsky,I. (1988). A Heparin-Binding Angiogenic Protein - Basic Fibroblast Growth-Factor - Is Stored Within Basement-Membrane. *American Journal of Pathology* 130, 393-400.
 70. Folkman,J. and Shing,Y. (1992). Angiogenesis. *J Biol. Chem.* 267, 10931-10934.
 71. Form,D.M., Pratt,B.M., and Madri,J.A. (1986). Endothelial-Cell Proliferation During Angiogenesis - In vitro Modulation by Basement-Membrane Components. *Laboratory Investigation* 55, 521-530.
 72. Formhals, A. Process and apparatus for preparing artificial threads. [1,975,504]. 10-2-1934.
- Ref Type: Patent

73. Formhals, A. Method and apparatus for spinning. [2,160,962]. 6-6-1939.
Ref Type: Patent
74. Fox,R.J. and Frame,M.D. (2002a). Arteriolar flow recruitment with vitronectin receptor stimulation linked to remote wall shear stress. *Microvascular Research* 64, 414-424.
75. Fox,R.J. and Frame,M.D. (2002b). Regulation of flow and wall shear stress in arteriolar networks of the hamster cheek pouch. *Journal of Applied Physiology* 92, 2080-2088.
76. Frame,M.D. and Sarelius,I.H. (1995a). A system for culture of endothelial cells in 20-50-microns branching tubes. *Microcirculation* 2, 377-385.
77. Frame,M.D. and Sarelius,I.H. (2000). Flow-induced cytoskeletal changes in endothelial cells growing on curved surfaces. *Microcirculation* 7, 419-427.
78. Frame,M.D.S. and Sarelius,I.H. (1993). Arteriolar Bifurcation Angles Vary with Position and When Flow Is Changed. *Microvascular Research* 46, 190-205.
79. Frame,M.D.S. and Sarelius,I.H. (1995b). Energy Optimization and Bifurcation Angles in the Microcirculation. *Microvascular Research* 50, 301-310.
80. Friedman,M.H., Himburg,H.A., and Lamack,J.A. (2006). Statistical hemodynamics: A tool for evaluating the effect of fluid dynamic forces on vascular biology in vivo. *Journal of Biomechanical Engineering-Transactions of the Asme* 128, 965-968.
81. Fung,Y.C. (1997). *Biomechanics: Circulation*. (New York: Springer Verlag).
82. Furie,M.B., Raffanello,J.A., Gergel,E.I., Lisinski,T.J., and Horb,L.D. (2000). Extracts of smokeless tobacco induce pro-inflammatory changes in cultured human vascular endothelial cells. *Immunopharmacology* 47, 13-23.
83. Gamperl,A.K., Hein,T.W., Kuo,L., and Cason,B.A. (2002). Isoflurane-induced dilation of porcine coronary microvessels is endothelium dependent and inhibited by glibenclamide. *Anesthesiology* 96, 1465-1471.
84. Gan,L.m., Miocic,M., Doroudi,R., Selin-Sjogren,L., and Jern,S. (2000). Distinct Regulation of Vascular Endothelial Growth Factor in Intact Human Conduit Vessels Exposed to Laminar Fluid Shear Stress and Pressure. *Biochemical and Biophysical Research Communications* 272, 490-496.
85. Gelaw,B. and Levin,S. (2001). Wound-induced angiogenesis and its pharmacologic inhibition in a murine model. *Surgery* 130, 497-501.
86. Giancoli,D.C. (2000). *Physics for Scientists and Engineers*. (Upper Saddle River: Prentice Hall).

87. Giavaresi,G., Tschon,M., Borsari,V., Daly,J.H., Liggat,J.J., Fini,M., Bonazzi,V., Nicolini,A., Carpi,A., and Morra,M. (2004). New polymers for drug delivery systems in orthopaedics: in vivo biocompatibility evaluation. *Biomedicine & Pharmacotherapy* 58, 411-417.
88. Gimbrone,M.A., Cotran,R.S., and Folkman,J. (1974). Human Vascular Endothelial Cells in Culture - Growth and DNA-Synthesis. *Journal of Cell Biology* 60, 673-684.
89. Glantz, Stanton A. *Primer for Biostatistics V. 4.02.* [4.02]. 1996. McGraw Hill.
Ref Type: Computer Program
90. Gospodarowicz,D. (1990). Fibroblast Growth-Factor - Chemical-Structure and Biologic Function. *Clinical Orthopaedics and Related Research* 231-248.
91. Goto,F., Goto,K., Weindel,K., and Folkman,J. (1993). Synergistic Effects of Vascular Endothelial Growth-Factor and Basic Fibroblast Growth-Factor on the Proliferation and Cord Formation of Bovine Capillary Endothelial-Cells Within Collagen Gels. *Laboratory Investigation* 69, 508-517.
92. Grant,D.S., Tashiro,K.I., Segulreal,B., Yamada,Y., Martin,G.R., and Kleinman,H.K. (1989). 2 Different Laminin Domains Mediate the Differentiation of Human-Endothelial Cells Into Capillary-Like Structures In vitro. *Cell* 58, 933-943.
93. Guyton,A.C. and Hall,J.E. (2000). *Textbook of Medical Physiology.* Elsevier Science).
94. Han,D. and Gouma,P.I. (2006). Electrospun bioscaffolds that mimic the topology of extracellular matrix. *Nanomedicine: Nanotechnology, Biology and Medicine* 2, 37-41.
95. Hayashi,T., Yamada,K., Esaki,T., Kuzuya,M., Satake,S., Ishikawa,T., Hidaka,H., and Iguchi,A. (1995). Estrogen Increases Endothelial Nitric-Oxide by A Receptor-Mediated System. *Biochemical and Biophysical Research Communications* 214, 847-855.
96. Hayes,C.E. and Goldstein,I.J. (1974). An alpha-D-Galactosyl-binding Lectin from *Bandeiraea simplicifolia* Seeds. *Journal of Biological Chemistry* 249, 1904-1914.
97. He,W., Halberstadt,C.R., and Gonsalves,K.E. (2004). Lithography application of a novel photoresist for patterning of cells. *Biomaterials* 25, 2055-2063.
98. He,W., Ma,Z.W., Yong,T., Teo,W.E., and Ramakrishna,S. (2005a). Fabrication of collagen-coated biodegradable polymer nanofiber mesh and its potential for endothelial cells growth. *Biomaterials* 26, 7606-7615.

99. He,W., Yong,T., Ma,Z.W., Inai,R., Teo,W.E., and Ramakrishna,S. (2006). Biodegradable polymer nanofiber mesh to maintain functions of endothelial cells. *Tissue Engineering 12*, 2457-2466.
100. He,W., Yong,T., Teo,W.E., Ma,Z.W., and Ramakrishna,S. (2005b). Fabrication and endothelialization of collagen-blended biodegradable polymer nanofibers: Potential vascular graft for blood vessel tissue engineering. *Tissue Engineering 11*, 1574-1588.
101. Heilshorn,S.C., DiZio,K.A., Welsh,E.R., and Tirrell,D.A. (2003). Endothelial cell adhesion to the fibronectin CS5 domain in artificial extracellular matrix proteins. *Biomaterials 24*, 4245-4252.
102. Herbst,T.J., Mccarthy,J.B., Tsilibary,E.C., and Furcht,L.T. (1988). Differential-Effects of Laminin, Intact Type-Iv Collagen, and Specific Domains of Type-Iv Collagen on Endothelial-Cell Adhesion and Migration. *Journal of Cell Biology 106*, 1365-1373.
103. Herve,M.A., Buteau-Lozano,H., Mourah,S., Calvo,F., and Perrot-Applanat,M. (2005). VEGF189 stimulates endothelial cells proliferation and migration in vitro and up-regulates the expression of Flk-1/KDR mRNA. *Experimental Cell Research 309*, 24-31.
104. Hisamoto,H., Nakashima,Y., Kitamura,C., Funano,S., Yasuoka,M., Morishima,K., Kikutani,Y., Kitamori,T., and Terabe,S. (2004). Capillary-assembled microchip for universal integration of various chemical functions onto a single microfluidic device. *Analytical Chemistry 76*, 3222-3228.
105. Hong,D., Jaron,D., Buerk,D.G., and Barbee,K.A. (2006). Heterogeneous response of microvascular endothelial cells to shear stress. *American Journal of Physiology-Heart and Circulatory Physiology 290*, H2498-H2508.
106. Hong,Z., Zhang,P., He,C., Qiu,X., Liu,A., Chen,L., Chen,X., and Jing,X. (2005). Nano-composite of poly(l-lactide) and surface grafted hydroxyapatite: Mechanical properties and biocompatibility. *Biomaterials 26*, 6296-6304.
107. Hotchkiss,K.A., Basile,C.M., Spring,S.C., Bonuccelli,G., Lisanti,M.P., and Terman,B.I. (2005). TEM8 expression stimulates endothelial cell adhesion and migration by regulating cell-matrix interactions on collagen. *Experimental Cell Research 305*, 133-144.
108. Huang,M.T., Mason,J.C., Birdsey,G.M., Amsellem,V., Gerwin,N., Haskard,D.O., Ridley,A.J., and Randi,A.M. (2005). Endothelial intercellular adhesion molecule (ICAM)-2 regulates angiogenesis. *Blood 106*, 1636-1643.
109. Hughes,G.C., Biswas,S.S., Yin,B., Coleman,R.E., DeGrado,T.R., Landolfo,C.K., Lowe,J.E., Annex,B.H., and Landolfo,K.P. (2004). Therapeutic angiogenesis in

- chronically ischemic porcine myocardium: comparative effects of bFGF and VEGF. *The Annals of Thoracic Surgery* 77, 812-818.
110. Hunt,S. (2001). Technology evaluation: IMC-1C11, ImClone Systems. *Current Opinion in Molecular Therapeutics* 3, 418-424.
 111. Ichioka,S., Shibata,M., Kosaki,K., Sato,Y., Harii,K., and Kamiya,M.D. (1997). Effects of Shear Stress on Wound-Healing Angiogenesis in the Rabbit Ear Chamber. *Journal of Surgical Research* 72, 29-35.
 112. Ingber,D.E. (1990). Fibronectin Controls Capillary Endothelial-Cell Growth by Modulating Cell-Shape. *Proceedings of the National Academy of Sciences of the United States of America* 87, 3579-3583.
 113. Ingber,D.E. and Folkman,J. (1989). Mechanochemical Switching Between Growth and Differentiation During Fibroblast Growth Factor-Stimulated Angiogenesis In vitro - Role of Extracellular-Matrix. *Journal of Cell Biology* 109, 317-330.
 114. Ishii,O., Shin,M., Sueda,T., and Vacanti,J.P. (2005). In vitro tissue engineering of a cardiac graft using a degradable scaffold with an extracellular matrix-like topography. *Journal of Thoracic and Cardiovascular Surgery* 130, 1358-1363.
 115. Iuliano,D.J., Saavedra,S.S., and Truskey,G.A. (1993). Effect of the Conformation and Orientation of Adsorbed Fibronectin on Endothelial-Cell Spreading and the Strength of Adhesion. *Journal of Biomedical Materials Research* 27, 1103-1113.
 116. Iwai,S., Sawa,Y., Taketani,S., Torikai,K., Hirakawa,K., and Matsuda,H. (2005). Novel Tissue-Engineered Biodegradable Material for Reconstruction of Vascular Wall. *The Annals of Thoracic Surgery* 80, 1821-1827.
 117. Jersmann,H.P.A., Hii,C.S.T., Hodge,G.L., and Ferrante,A. (2001). Synthesis and surface expression of CD14 by human endothelial cells. *Infection and Immunity* 69, 479-485.
 118. Ji,Y., Ghosh,K., Shu,X.Z., Li,B.Q., Sokolov,J.C., Prestwich,G.D., Clark,R.A.F., and Rafailovich,M.H. (2006). Electrospun three-dimensional hyaluronic acid nanofibrous scaffolds. *Biomaterials* 27, 3782-3792.
 119. Jiang,X., Takayama,S., Qian,X., Ostuni,E., Wu,H., Bowden,N., LeDuc,P., Ingber,D., and Whitesides,G.M. (2002). Controlling mammalian cell spreading and cytoskeletal arrangement with conveniently fabricated continuous wavy features on Poly(dimethylsiloxane). *Langmuir* 18, 3273-3280.
 120. Jonca,F., Ortega,N., Gleizes,P.E., Bertrand,N., and Plouet,J. (1997). Cell release of bioactive fibroblast growth factor 2 by exon 6-encoded sequence of vascular endothelial growth factor. *Journal of Biological Chemistry* 272, 24203-24209.

121. Jung,K.S., Ahn,M.J., Lee,Y.D., Go,G.M., and Shin,T.K. (2002). Histochemistry of six lectins in the tissues of the flat fish *Paralichthys olivaceus*. *J Vet. Sci* 3, 293-301.
122. Kalebic,T., Garbisa,S., Glaser,B., and Liotta,L.A. (1983). Basement-Membrane Collagen - Degradation by Migrating Endothelial-Cells. *Science* 221, 281-283.
123. Kalra,A., Garde,S., and Hummer,G. (2003). Osmotic water transport through carbon nanotube membranes. *Proceedings of the National Academy of Sciences of the United States of America* 100, 10175-10180.
124. Khademhosseini,A., Suh,K.Y., Jon,S., Eng,G., Yeh,J., Chen,G.J., and Langer,R. (2004). A soft lithographic approach to fabricate patterned microfluidic channels. *Analytical Chemistry* 76, 3675-3681.
125. Khan,T.A., Peh,K.K., and Ch'Ng,H.S. (2000). Mechanical, bioadhesive strength and biological evaluations of Chitosan films for wound dressing. *Journal of Pharmacy and Pharmaceutical Sciences* 3, 303-311.
126. Kim,D.S., Lee,S.H., Ahn,C.H., Lee,J.Y., and Kwon,T.H. (2006). Disposable integrated microfluidic biochip for blood typing by plastic microinjection moulding. *Lab on A Chip* 6, 794-802.
127. Kleinman,H.K., McGarvey,M.L., Hassell,J.R., Star,V.L., Cannon,F.B., Laurie,G.W., and Martin,G.R. (1986). Basement membrane complexes with biological activity. *Biochemistry* 25, 312-318.
128. Koenig,A.L., Gambillara,V., and Grainger,D.W. (2003). Correlating fibronectin adsorption with endothelial cell adhesion and signaling on polymer substrates. *Journal of Biomedical Materials Research Part A* 64A, 20-37.
129. Koolwijk,P., vanErck,M.G.M., deVree,W.J.A., Vermeer,M.A., Weich,H.A., Hanemaaijer,R., and vanHinsbergh,V.W.M. (1996). Cooperative effect of TNF alpha, bFGF, and VEGF on the formation of tubular structures of human microvascular endothelial cells in a fibrin matrix. Role of urokinase activity. *Journal of Cell Biology* 132, 1177-1188.
130. Kovarik,M.L. and Jacobson,S.C. (2006). Fabrication of three-dimensional micro- and nanoscale features with single-exposure photolithography. *Analytical Chemistry* 78, 5214-5217.
131. Krylov,S.N. and Dovichi,N.J. (2000). Single-cell analysis using capillary electrophoresis: Influence of surface support properties on cell injection into the capillary. *Electrophoresis* 21, 767-773.
132. Kubota,Y., Kleinman,H.K., Martin,G.R., and Lawley,T.J. (1988). Role of Laminin and Basement-Membrane in the Morphological-Differentiation of

Human-Endothelial Cells Into Capillary-Like Structures. *Journal of Cell Biology* 107, 1589-1598.

133. Kulkarni,S.S., Orth,R., Ferrari,M., and Moldovan,N.I. (2004). Micropatterning of endothelial cells by guided stimulation with angiogenic factors. *Biosensors and Bioelectronics* 19, 1401-1407.
134. Kumar,R., Yoneda,J., Bucana,C.D., and Fidler,I.J. (1998). Regulation of distinct steps of angiogenesis by different angiogenic molecules. *Int. J Oncol.* 12, 749-757.
135. L'Heureux,N., Paquet,S., Labbe,R., Germain,L., and Auger,F.A. (1998). A completely biological tissue-engineered human blood vessel. *Faseb Journal* 12, 47-56.
136. Langille,B.L. and Adamson,S.L. (1981). Relationship Between Blood-Flow Direction and Endothelial-Cell Orientation at Arterial Branch Sites in Rabbits and Mice. *Circulation Research* 48, 481-488.
137. Lee,J.Y., Kang,T.Y., Lee,Y.D., and Shin,T.K. (2003). Histochemical characterization of the lectin-binding sites in the equine vomeronasal organ. *J Vet. Sci* 4, 15-19.
138. Li,C.M., Vepari,C., Jin,H.J., Kim,H.J., and Kaplan,D.L. (2006). Electrospun silk-BMP-2 scaffolds for bone tissue engineering. *Biomaterials* 27, 3115-3124.
139. Li,L. (2005). Chitosan/poly(vinyl alcohol) nanofibers. *Abstracts of Papers of the American Chemical Society* 229, U938.
140. Li,L. and Hsieh,Y.L. (2006). Chitosan bicomponent nanofibers and nanoporous fibers. *Carbohydrate Research* 341, 374-381.
141. Li,S., Butler,P., Wang,Y.X., Hu,Y.L., Han,D.C., Usami,S., Guan,J.L., and Chien,S. (2002a). The role of the dynamics of focal adhesion kinase in the mechanotaxis of endothelial cells. *Proceedings of the National Academy of Sciences of the United States of America* 99, 3546-3551.
142. Li,W.J., Laurencin,C.T., Caterson,E.J., Tuan,R.S., and Ko,F.K. (2002b). Electrospun nanofibrous structure: A novel scaffold for tissue engineering. *Journal of Biomedical Materials Research* 60, 613-621.
143. Li,Y.S., Haga,J.H., and Chien,S. (2005). Molecular basis of the effects of shear stress on vascular endothelial cells. *Journal of Biomechanics* 38, 1949-1971.
144. Lipowsky,H.H., Usami,S., and Chien,S. (1980). In vivo measurements of "apparent viscosity" and microvessel hematocrit in the mesentery of the cat. *Microvascular Research* 19, 297-319.

145. Lipowsky,H.H. and Zweifach,B.W. (1977). Methods for the simultaneous measurement of pressure differentials and flow in single unbranched vessels of the microcirculation for rheological studies. *Microvascular Research* 14, 345-361.
146. Liu,H.Q. and Hsieh,Y.L. (2002). Ultrafine fibrous cellulose membranes from electrospinning of cellulose acetate. *Journal of Polymer Science Part B-Polymer Physics* 40, 2119-2129.
147. Liu,Y., Chen,B.P.C., Lu,M., Zhu,Y., Stemerman,M.B., Chien,S., and Shyy,J.Y.J. (2002). Shear stress activation of SREBP1 in endothelial cells is mediated by Integrins. *Arteriosclerosis Thrombosis and Vascular Biology* 22, 76-81.
148. Liu,Y.X., He,T., and Gao,C.Y. (2005). Surface modification of poly(ethylene terephthalate) via hydrolysis and layer-by-layer assembly of chitosan and chondroitin sulfate to construct cytocompatible layer for human endothelial cells. *Colloids and Surfaces B-Biointerfaces* 46, 117-126.
149. Liu,Z.J., Snyder,R., Soma,A., Shirakawa,T., Ziober,B.L., Fairman,R.M., Herlyn,M., and Velazquez,O.C. (2003). VEGF-A and alpha(V)beta(3) integrin synergistically rescue angiogenesis via N-Ras and PI3-K signaling in human microvascular endothelial cells. *Faseb Journal* 17.
150. Loesberg,W.A., Walboomers,X.F., van Loon,J.J.W.A., and Jansen,J.A. (2005). The effect of combined cyclic mechanical stretching and microgrooved surface topography on the behavior of fibroblasts. *Journal of Biomedical Material Research* 75A, 723-732.
151. Lohbach,C., Neumann,D., Lehr,C.M., and Lamprecht,A. (2006). Human vascular endothelial cells in primary cell culture for the evaluation of nanoparticle bioadhesion. *Journal of Nanoscience and Nanotechnology* 6, 3303-3309.
152. Lu,L., Garcia,C.A., and Mikos,A.G. (1999). In vitro degradation of thin poly(DL-lactic-co-glycolic acid) films. *Journal of Biomedical Materials Research* 46, 236-244.
153. Ludwig,N.S., Yoder,C., McConney,M., Vargo,T.G., and Kader,K.N. (2006). Directed Type IV collagen self-assembly on hydroxylated PTFE. *Journal of Biomedical Materials Research Part A* 78A, 615-619.
154. Lusinskas,F.W. and Lawler,J. (1994). Integrins As Dynamic Regulators of Vascular Function. *Faseb Journal* 8, 929-938.
155. Ma,Z., Gao,C., Gong,Y., and Shen,J. (2005a). Cartilage tissue engineering PLLA scaffold with surface immobilized collagen and basic fibroblast growth factor. *Biomaterials* 26, 1253-1259.
156. Ma,Z., Kotaki,M., and Ramakrishna,S. (2005b). Electrospun cellulose nanofiber as affinity membrane. *Journal of Membrane Science* 265, 115-123.

157. Madri, J.A. and Williams, S.K. (1983). Capillary Endothelial Cell-Cultures - Phenotypic Modulation by Matrix Components. *Journal of Cell Biology* 97, 153-165.
158. Mangelakis, S.A. (2003). A mathematical model of tissue replacement during epidermal wound healing. *Applied Mathematical Modelling* 27, 189-196.
159. Mahfuz, H., Adnan, A., Rangari, V.K., Hasan, M.M., Jeelani, S., Wright, W.J., and DeTeresa, S.J. (2006). Enhancement of strength and stiffness of Nylon 6 filaments through carbon nanotubes reinforcement. *Applied Physics Letters* 88.
160. Marchais, S.J., Guerin, A.P., Pannier, B., Delavaud, G., and London, G.M. (1993). Arterial compliance and blood pressure. *Drugs* 46, 82-87.
161. Mathews, J.H. and Fink, K.D. (2004). *Numerical Methods Using MATLAB*. (Upper Saddle River, NJ: Prentice Hall).
162. Matsuzawa, M., Liesi, P., and Knoll, W. (1996). Chemically modifying glass surfaces to study substratum-guided neurite outgrowth in culture. *Journal of Neuroscience Methods* 69, 189-196.
163. Matthews, J.A., Wnek, G.E., Simpson, D.G., and Bowlin, G.L. (2002). Electrospinning of collagen nanofibers. *Biomacromolecules* 3, 232-238.
164. Mayrovitz, H.N., Tuma, R.F., and Wiedeman, M.P. (1977). Relationship Between Microvascular Blood Velocity and Pressure Distribution. *American Journal of Physiology* 232, H400-H405.
165. McCue, S., Noria, S., and Langille, B.L. (2004). Shear-induced reorganization of endothelial cell cytoskeleton and adhesion complexes. *Trends Cardiovasc. Med.* 14, 143-151.
166. Menger, M.D., Laschke, M.W., and Vollmar, B. (2002). Viewing the microcirculation through the window: Some twenty years experience with the hamster dorsal skinfold chamber. *European Surgical Research* 34, 83-91.
167. Microchem Corp. (2002). *Nano SU-8 2000: Negative Tone Photoresist Formulations 2035-2100*. (Newton, MA: Microchem Corp).
168. Mignatti, P., Tsuboi, R., Robbins, E., and Rifkin, D.B. (1989). In vitro Angiogenesis on the Human Amniotic Membrane - Requirement for Basic Fibroblast Growth-Factor Induced Proteinases. *Journal of Cell Biology* 108, 671-682.
169. Milkiewicz, M., Brown, M.D., Egginton, S., and Hudlicka, O. (2001). Association between shear stress, angiogenesis, and VEGF in skeletal muscles in vivo. *Microcirculation* 8, 229-241.

170. Millauer,B., Wizigmannvoos,S., Schnurch,H., Martinez,R., Moller,N.P.H., Risau,W., and Ullrich,A. (1993). High-Affinity Vegf Binding and Developmental Expression Suggest Flk-1 As A Major Regulator of Vasculogenesis and Angiogenesis. *Cell* 72, 835-846.
171. Mitsumata,M., Fishel,R.S., Nerem,R.M., Alexander,R.W., and Berk,B.C. (1993). Fluid Shear-Stress Stimulates Platelet-Derived Growth-Factor Expression in Endothelial-Cells. *American Journal of Physiology* 265, H3-H8.
172. Mo,X.M., Xu,C.Y., Kotaki,M., and Ramakrishna,S. (2004). Electrospun P(LLA-CL) nanofiber: a biomimetic extracellular matrix for smooth muscle cell and endothelial cell proliferation. *Biomaterials* 25, 1883-1890.
173. Montesano,R. and Orci,L. (1985). Tumor-Promoting Phorbol Esters Induce Angiogenesis In vitro. *Cell* 42, 469-477.
174. Montesano,R., Orci,L., and Vassalli,P. (1983). In vitro Rapid Organization of Endothelial-Cells Into Capillary-Like Networks Is Promoted by Collagen Matrices. *Journal of Cell Biology* 97, 1648-1652.
175. Montesano,R., Pepper,M.S., Vassalli,J.D., and Orci,L. (1987). Phorbol Ester Induces Cultured Endothelial-Cells to Invade A Fibrin Matrix in the Presence of Fibrinolytic Inhibitors. *Journal of Cellular Physiology* 132, 509-516.
176. Montesano,R., Vassalli,J.D., Baird,A., Guillemin,R., and Orci,L. (1986). Basic Fibroblast Growth-Factor Induces Angiogenesis In vitro. *Proceedings of the National Academy of Sciences of the United States of America* 83, 7297-7301.
177. Moon,J.J., Matsumoto,M., Patel,S., Lee,L., Guan,J.L., and Li,S. (2005). Role of cell surface heparan sulfate proteoglycans in endothelial cell migration and mechanotransduction. *Journal of Cellular Physiology* 203, 166-176.
178. Moore,E.M., Ortiz,D.L., Marla,V.T., Shambaugh,R.L., and Grady,B.P. (2004). Enhancing the strength of polypropylene fibers with carbon nanotubes. *Journal of Applied Polymer Science* 93, 2926-2933.
179. Mrksich,M., Chen,C.S., Xia,Y.N., Dike,L.E., Ingber,D.E., and Whitesides,G.M. (1996). Controlling cell attachment on contoured surfaces with self-assembled monolayers of alkanethiolates on gold. *Proceedings of the National Academy of Sciences of the United States of America* 93, 10775-10778.
180. Nagaoka,T., Takahashi,A., Sato,E., Izumi,N., Hein,T.W., Kuo,L., and Yoshida,A. (2006). Effect of systemic administration of simvastatin on retinal circulation. *Archives of Ophthalmology* 124, 665-670.
181. Nair,L.S., Bhattacharyya,S., Bender,J.D., Greish,Y.E., Brown,P.W., Allcock,H.R., and Laurencin,C.T. (2004). Fabrication and optimization of

- methylphenoxy substituted polyphosphazene nanofibers for biomedical applications. *Biomacromolecules* 5, 2212-2220.
182. Nalla,R.K., Balooch,M., Ager,J.W., Kruzic,J.J., Kinney,J.H., and Ritchie,R.O. (2005). Effects of polar solvents on the fracture resistance of dentin: role of water hydration. *Acta Biomaterialia* 1, 31-43.
 183. Neumann,T., Hauschka,S.D., and Sanders,J.E. (2003). Tissue engineering of skeletal muscle using polymer fiber arrays. *Tissue Engineering* 9, 995-1003.
 184. Nguyen,D.T., Brotherton,J.D., and Chau,P.C. (2005). Enhancing cell viability with pulsating flow in a hollow fiber bioartificial liver. *Biotechnology Letters* 27, 1511-1516.
 185. Nichol,J.W., Petko,M., Myung,R.J., Gaynor,J.W., and Gooch,K.J. (2005). Hemodynamic conditions alter axial and circumferential remodeling of arteries engineered ex vivo. *Ann Biomed. Eng* 33, 721-732.
 186. Nicosia,R.F., Nicosia,S.V., and Smith,M. (1994). Vascular Endothelial Growth-Factor, Platelet-Derived Growth-Factor, and Insulin-Like Growth-Factor-I Promote Rat Aortic Angiogenesis In-Vitro. *American Journal of Pathology* 145, 1023-1029.
 187. Nissen,N.N., Polverini,P.J., Gamelli,R.L., and DiPietro,L.A. (1996). Basic fibroblast growth factor mediates angiogenic activity in early surgical wounds. *Surgery* 119, 457-465.
 188. Nissen,N.N., Polverini,P.J., Koch,A.E., Volin,M.V., Gamelli,R.L., and DiPietro,L.A. (1998). Vascular endothelial growth factor mediates angiogenic activity during the proliferative phase of wound healing. *American Journal of Pathology* 152, 1445-1452.
 189. Offenberg Sweeney,N., Cummins,P.M., Cotter,E.J., Fitzpatrick,P.A., Birney,Y.A., Redmond,E.M., and Cahill,P.A. (2005). Cyclic strain-mediated regulation of vascular endothelial cell migration and tube formation. *Biochemical and Biophysical Research Communications* 329, 573-582.
 190. Ohashi,T. and Sato,M. (2005). Remodeling of vascular endothelial cells exposed to fluid shear stress: experimental and numerical approach. *Fluid Dynamics Research* 37, 40-59.
 191. Olesen,S.P., Clapham,D.E., and Davies,P.F. (1988). Hemodynamic Shear-Stress Activates A K⁺ Current in Vascular Endothelial-Cells. *Nature* 331, 168-170.
 192. Osaki,T., Renner,L., Herklotz,M., and Werner,C. (2006). Hydrophobic and electrostatic interactions in the adsorption of fibronectin at maleic acid copolymer films. *Journal of Physical Chemistry B* 110, 12119-12124.

193. Ouellette, Y., Lidington, D., Naus, C.G., and Tymk, K. (2000). A new in vitro model for agonist-induced communication between microvascular endothelial cells. *Microvascular Research* 60, 222-231.
194. Pahakis, M.Y., Kosky, J.R., Dull, R.O., and Tarbell, J.M. (2007). The role of endothelial glycocalyx components in mechanotransduction of fluid shear stress. *Biochemical and Biophysical Research Communications* 355, 228-233.
195. Palmaz, J.C., Benson, A., and Sprague, E.A. (1999). Influence of surface topography on endothelialization of intravascular metallic material. *Journal of Vascular and Interventional Radiology* 10, 439-444.
196. Papetti, M. and Herman, I.M. (2002). Mechanisms of normal and tumor-derived angiogenesis. *American Journal of Physiology-Cell Physiology* 282, C947-C970.
197. Pappenheimer, J.R. (1953). Passage of molecules through capillary walls. *Physiological Reviews* 33, 387.
198. Park, B.H. (1975). Migration of Human Neutrophils Against Gravity - New Method of Chemotaxis Assay. *Pediatric Research* 9, 333.
199. Park, B.H. (1980). Chemotaxis of Human-Neutrophils Against Gravity - A New Method. *Experientia* 36, 473-474.
200. Park, K.E., Kang, H.K., Lee, S.J., Min, B.M., and Park, W.H. (2006). Biomimetic nanofibrous scaffolds: Preparation and characterization of PGA/chitin blend nanofibers. *Biomacromolecules* 7, 635-643.
201. Patrito, N., McCague, C., Norton, P.R., and Petersen, N.O. (2007). Spatially controlled cell adhesion via micropatterned surface modification of poly(dimethylsiloxane). *Langmuir* 23, 715-719.
202. Peirce, S.M., Price, R.J., and Skalak, T.C. (2004). Spatial and temporal control of angiogenesis and arterialization using focal applications of VEGF(164) and Ang-1. *American Journal of Physiology-Heart and Circulatory Physiology* 286, H918-H925.
203. Pepper, M.S., Ferrara, N., Orci, L., and Montesano, R. (1992). Potent synergism between vascular endothelial growth factor and basic fibroblast growth factor in the induction of angiogenesis in vitro. *Biochemical and Biophysical Research Communications* 189, 824-831.
204. Peters, M.C., Polverini, P.J., and Mooney, D.J. (2002). Engineering vascular networks in porous polymer matrices. *Journal of Biomedical Materials Research* 60, 668-678.

205. Phongkitkarun,S., Kobayashi,S., Kan,Z., Lee,T.Y., and Charnsangavej,C. (2004). Quantification of angiogenesis by functional computed tomography in a matrigel model in rats. *Academic Radiology* *11*, 573-582.
206. Qin,K.D. and Li,Y.C. (2003). Mechanisms of particle removal from silicon wafer surface in wet chemical cleaning process. *Journal of Colloid and Interface Science* *261*, 569-574.
207. Ramos,O.H., Terruggi,C.H., Ribeiro,J.U., Cominetti,M.R., Figueiredo,C.C., Bernard,M., Crepin,M., Morandi,V., and Selistre-de-Araujo,H.S. (2007). Modulation of in vitro and in vivo angiogenesis by alternagin-C, a disintegrin-like protein from *Bothrops alternatus* snake venom and by a peptide derived from its sequence. *Arch Biochem Biophys*.
208. Resnick,N., Collins,T., Atkinson,W., Bonthron,D.T., Dewey,C.F., and Gimbrone,M.A. (1993). Platelet-Derived Growth Factor-B Chain Promoter Contains A Cis-Acting Fluid Shear-Stress-Responsive Element. *Proceedings of the National Academy of Sciences of the United States of America* *90*, 4591-4595.
209. Risau,W. (1997). Mechanisms of angiogenesis. *Nature* *386*, 671-674.
210. Roberts,M.S., Cross,S.E., and Anissimov,Y.G. (2004). Factors affecting the formation of a skin reservoir for topically applied solutes. *Skin Pharmacology & Physiology* *17*, 3-16.
211. Rozkiewicz,D.I., Kraan,Y., Werten,M.W.T., de Wolf,F.A., Subramaniam,V., Ravoo,B.J., and Reinhoudt,D.N. (2006). Covalent microcontact printing of proteins for cell patterning. *Chemistry-A European Journal* *12*, 6290-6297.
212. Rubenstein,D., Han,D., Goldgraben,S., El-Gendi,H., Gouma,P.I., and Frame,M.D. (2007). Bioassay chamber for angiogenesis with perfused explanted arteries and electrospun scaffolding. *Microcirculation In Press*.
213. Ruoslahti,E. (1999). Extracellular Matrix Proteins and Proteoglycans. In *Inflammation: Basic Principles and Clinical Correlates*, J.I.Gallin and R.Snyderman, eds. (Philadelphia: Lippincott Williams and Wilkins), pp. 259-263.
214. Salacinski,H.J., Tiwari,A., Hamilton,G., and Seifalian,A.M. (2001). Cellular engineering of vascular bypass grafts: role of chemical coatings for enhancing endothelial cell attachments. *Medical & Biological Engineering & Computing* *39*, 609-618.
215. Salathe,E.P. (1977). Analysis of Interstitial Fluid Pressure in Web of Bat Wing. *American Journal of Physiology* *232*, H297-H304.

216. Schmalenberg, K.E., Buettner, H.M., and Uhrich, K.E. (2004). Microcontact printing of proteins on oxygen plasma-activated poly(methyl methacrylate). *Biomaterials* 25, 1851-1857.
217. Schneider, A., Chandra, M., Lazarovici, G., Vlodaysky, I., Merin, G., Uretzky, G., Borman, J.B., and Schwalb, H. (1997). Naturally produced extracellular matrix is an excellent substrate for canine endothelial cell proliferation and resistance to shear stress on PTFE vascular grafts. *Thrombosis and Haemostasis* 78, 1392-1398.
218. Schober, A. and Weber, C. (2005). Mechanisms of monocyte recruitment in vascular repair after injury. *Antioxidants & Redox Signaling* 7, 1249-1257.
219. Seghezzi, G., Patel, S., Ren, C.J., Gualandris, A., Pintucci, G., Robbins, E.S., Shapiro, R.L., Galloway, A.C., Rifkin, D.B., and Mignatti, P. (1998). Fibroblast growth factor-2 (FGF-2) induces vascular endothelial growth factor (VEGF) expression in the endothelial cells of forming capillaries: An autocrine mechanism contributing to angiogenesis. *Journal of Cell Biology* 141, 1659-1673.
220. Sellati, T.J., Abrescia, L.D., Radolf, J.D., and Furie, M.B. (1996). Outer surface lipoproteins of *Borrelia burgdorferi* activate vascular endothelium in vitro. *Infection and Immunity* 64, 3180-3187.
221. Sephel, G.C., Kennedy, R., and Kudravi, S. (1996). Expression of capillary basement membrane components during sequential phases of wound angiogenesis. *Matrix Biology* 15, 263-279.
222. Shan, S.Q., Robson, N.D., Cao, Y.T., Qiao, T., Li, C.Y., Kontos, C.D., Garcia-Blanco, M., and Dewhirst, M.W. (2003). Responses of vascular endothelial cells to angiogenic signaling are important for tumor cell survival. *Faseb Journal* 17, 326-+.
223. Sharpe, R.B.A., Burdinski, D., van der Marel, C., Jansen, J.A.J., Huskens, J., Zandvliet, H.J.W., Reinhoudt, D.N., and Poelsema, B. (2006). Ink dependence of poly(dimethylsiloxane) contamination in microcontact printing. *Langmuir* 22, 5945-5951.
224. Shin, M., Matsuda, K., Ishii, O., Terai, H., Kaazempur-Mofrad, M., Borenstein, J., Detmar, M., and Vacanti, J.P. (2004). Endothelialized networks with a vascular geometry in microfabricated poly(dimethyl siloxane). *Biomedical Microdevices* 6, 269-278.
225. Sido, B., Teklote, J.R., Hartel, M., Friess, H., and Buchler, M.W. (2004). Inflammatory response after abdominal surgery. *Best Practice & Research Clinical Anaesthesiology* 18, 439-454.
226. Silva-Azevedo, L., Baum, O., Zakrzewicz, A., and Pries, A.R. (2002). Vascular endothelial growth factor is expressed in endothelial cells isolated from skeletal

- muscles of nitric oxide synthase knockout mice during prazosin-induced angiogenesis. *Biochemical and Biophysical Research Communications* 297, 1270-1276.
227. Silverstein,R.L. (1999). The Vascular Endothelium. In *Inflammation: Basic Principles and Clinical Correlates*, J.I.Gallin and R.Snyderman, eds. (Philadelphia: Lippincott Williams and Wilkins), pp. 207-226.
 228. Simionescu,D.T., Lu,Q., Song,Y., Lee,J.S., Rosenbalm,T.N., Kelley,C., and Vyavahare,N.R. (2006). Biocompatibility and remodeling potential of pure arterial elastin and collagen scaffolds. *Biomaterials* 27, 702-713.
 229. Sohl,G. and Willecke,K. (2004). Gap junctions and the connexin protein family. *Cardiovascular Research* 62, 228-232.
 230. Somasundaram,R. and Schuppan,D. (1996). Type I, II, III, IV, V, and VI collagens serve as extracellular ligands for the isoforms of platelet-derived growth factor (AA, BB, and AB). *Journal of Biological Chemistry* 271, 26884-26891.
 231. Son,W.K., Youk,J.H., and Park,W.H. (2004). Preparation of ultrafine oxidized cellulose mats via electrospinning. *Biomacromolecules* 5, 197-201.
 232. Stacker,S.A. and Achen,M.G. (1999). The vascular endothelial growth factor family: Signalling for vascular development. *Growth Factors* 17, 1-+.
 233. Sterpetti,A.V., Cucina,A., Fragale,A., Lepidi,S., Cavallaro,A., and Santorodangelo,L. (1994). Shear-Stress Influences the Release of Platelet-Derived Growth-Factor and Basic Fibroblast Growth-Factor by Arterial Smooth-Muscle Cells. *European Journal of Vascular Surgery* 8, 138-142.
 234. Stupack,D.G. and Cheresh,D.A. (2004). Integrins and angiogenesis. *Current Topics in Developmental Biology* , Vol 64 64, 207-238.
 235. Suda,T., Takakura,N., and Oike,Y. (2000). Hematopoiesis and angiogenesis. *International Journal of Hematology* 71, 99-107.
 236. Sugiu,K., Kinugasa,K., Mandai,S., Tokunaga,K., and Ohmoto,T. (1995). Direct Thrombosis of Experimental Aneurysms with Cellulose-Acetate Polymer (Cap) - Technical Aspects, Angiographic Follow-Up, and Histological Study. *Journal of Neurosurgery* 83, 531-538.
 237. Sung,H.J., Meredith,C., Johnson,C., and Galis,Z.S. (2004). The effect of scaffold degradation rate on three-dimensional cell growth and angiogenesis. *Biomaterials* 25, 5735-5742.
 238. Takano,H., Dora,K.A., and Garland,C.J. (2005). Spreading vasodilatation in resistance arteries. *J Smooth Muscle Res* 41, 303-311.

239. Takayama,S., McDonald,J.C., Ostuni,E., Liang,M.N., Kenis,P.J.A., Ismagilov,R.F., and Whitesides,G.M. (1999). Patterning cells and their environments using multiple laminar fluid flows in capillary networks. *Proceedings of the National Academy of Sciences of the United States of America* 96, 5545-5548.
240. Telemeco,T.A., Ayres,C., Bowlin,G.L., Wnek,G.E., Boland,E.D., Cohen,N., Baumgarten,C.M., Mathews,J., and Simpson,D.G. (2005). Regulation of cellular infiltration into tissue engineering scaffolds composed of submicron diameter fibrils produced by electrospinning. *Acta Biomaterialia* 1, 377-385.
241. Thiebaud,P., Lauer,L., Knoll,W., and Offenhausser,A. (2002). PDMS device for patterned application of microfluids to neuronal cells arranged by microcontact printing. *Biosensors & Bioelectronics* 17, 87-93.
242. Tille,J.C., Wood,J., Mandriota,S.J., Schnell,C., Ferrari,S., Mestan,J., Zhu,Z., Witte,L., and Pepper,M.S. (2001). Vascular endothelial growth factor (VEGF) receptor-2 antagonists inhibit VEGF- and basic fibroblast growth factor-induced angiogenesis in vivo and in vitro. *Journal of Pharmacology and Experimental Therapeutics* 299, 1073-1085.
243. Tonnesen,M.G., Feng,X.D., and Clark,R.A.F. (2000). Angiogenesis in wound healing. *Journal of Investigative Dermatology Symposium Proceedings* 5, 40-46.
244. Truskett,V.N. and Watts,M.P.C. (2006). Trends in imprint lithography for biological applications. *Trends in Biotechnology* 24, 312-317.
245. Tuckwell,D. and Humphries,M. (1996). Integrin-collagen binding. *Seminars in Cell & Developmental Biology* 7, 649-657.
246. Ueda,A., Koga,M., Ikeda,M., Kudo,S., and Tanishita,K. (2004). Effect of shear stress on microvessel network formation of endothelial cells with in vitro three-dimensional model. *American Journal of Physiology-Heart and Circulatory Physiology* 287, H994-H1002.
247. Uttayarat,P., Toworfe,G.K., Dietrich,F., Lelkes,P.I., and Composto,RJ. (2005). Topographical guidance of endothelial cells on silicone surfaces with micro- to nanogrooves: Orientation of actin filaments and focal adhesions. *Journal of Biomedical Material Research* 75A, 668-680.
248. Vazquez,R., Nogueira,R., Orfao,M., Mata,J.L., and Saramago,B. (2006). Stability of triglyceride liquid films on hydrophilic and hydrophobic glasses. *Journal of Colloid and Interface Science* 299, 274-282.
249. Velazquez,O.C., Snyder,R., Liu,Z.J., Fairman,R.M., and Herlyn,M. (2002). Fibroblast-dependent differentiation of human microvascular endothelial cells into capillary-like, three-dimensional networks. *Faseb Journal* 16.

250. Wang,B., Feng,J., and Gao,C.Y. (2005). Printing biomacromolecules on a bovine serum albumin precursor layer. *Macromolecular Bioscience* 5, 767-774.
251. Warabi,E., Takabe,W., Minami,T., Inoue,K., Itoh,K., Yamamoto,M., Ishii,T., Kodama,T., and Noguchi,N. (2007). Shear stress stabilizes NF-E2-related factor 2 and induces antioxidant genes in endothelial cells: Role of reactive oxygen/nitrogen species. *Free Radical Biology and Medicine* 42, 260-269.
252. Westerband,A., Crouse,D., Richter,L.C., Aguirre,M.L., Wixon,C.C., James,D.C., Mills,J.L., Hunter,G.C., and Heimark,R.L. (2001). Vein adaptation to arterialization in an experimental model. *Journal of Vascular Surgery* 33, 561-569.
253. Widmer,R.J., Laurinec,J.E., Young,M.F., Laine,G.A., and Quick,C.M. (2006). Local heat produces a shear-mediated biphasic response in the thermoregulatory microcirculation of the Pallid bat wing. *American Journal of Physiology-Regulatory Integrative and Comparative Physiology* 291, R625-R632.
254. Wiedeman,M.P. (1968). Blood Flow Through Terminal Arterial Vessels After Denervation of Bat Wing. *Circulation Research* 22, 83-&.
255. Williams,D.A. and Huxley,V.H. (1993). Bradykinin-Induced Elevations of Hydraulic Conductivity Display Spatial and Temporal Variations in Frog Capillaries. *American Journal of Physiology* 264, H1575-H1581.
256. Wittmer,C.R., Phelps,J.A., Saltzman,W.M., and Van Tassel,P.R. (2007). Fibronectin terminated multilayer films: Protein adsorption and cell attachment studies. *Biomaterials* 28, 851-860.
257. Wu,A.M., Song,A., Tsai,M., and Herp,A. (2001). A guide to the carbohydrate specificities of applied lectins-2. *Advances in experimental medicine and biology* 491, 551-585.
258. Wu,M.H., Cai,H.Y., Xu,X., Urban,J.P.G., Cui,Z.F., and Cui,Z. (2005). A SU-8/PDMS hybrid microfluidic device with integrated optical fibers for online monitoring of lactate. *Biomedical Microdevices* 7, 323-329.
259. Xu,C., Inai,R., Kotaki,M., and Ramakrishna,S. (2004a). Electrospun nanofiber fabrication as synthetic extracellular matrix and its potential for vascular tissue engineering. *Tissue Eng* 10, 1160-1168.
260. Xu,C., Yang,F., Wang,S., and Ramakrishna,S. (2004b). In vitro study of human vascular endothelial cell function on materials with various surface roughness. *J Biomed. Mater. Res. A* 71, 154-161.
261. Xu,C.Y., Inai,R., Kotaki,M., and Ramakrishna,S. (2004c). Aligned biodegradable nanofibrous structure: a potential scaffold for blood vessel engineering. *Biomaterials* 25, 877-886.

262. Yamaguchi,T., Yamamoto,Y., and Liu,H. (2000). Computational mechanical model studies on the spontaneous emergent morphogenesis of the cultured endothelial cells. *Journal of Biomechanics* 33, 115-126.
263. Yamamoto,K., Takahashi,T., Asahara,T., Ohura,N., Sokabe,T., Kamiya,A., and Ando,J. (2003). Proliferation, differentiation, and tube formation by endothelial progenitor cells in response to shear stress. *Journal of Applied Physiology* 95, 2081-2088.
264. Yang,C., Sodian,R., Fu,P., Luders,C., Lemke,T., Du,J., Hubler,M., Weng,Y., Meyer,R., and Hetzer,R. (2006). In Vitro Fabrication of a Tissue Engineered Human Cardiovascular Patch for Future Use in Cardiovascular Surgery. *The Annals of Thoracic Surgery* 81, 57-63.
265. Yayapour,N. and Nygren,H. (1999). Interactions between whole blood and hydrophilic or hydrophobic glass surfaces: kinetics of cell adhesion. *Colloids and Surfaces B-Biointerfaces* 15, 127-138.
266. Yin,L.H., Bien,H., and Entcheva,E. (2004). Scaffold topography alters intracellular calcium dynamics in cultured cardiomyocyte networks. *American Journal of Physiology-Heart and Circulatory Physiology* 287, H1276-H1285.
267. Young,S., Wong,M., Tabata,Y., and Mikos,A.G. (2005). Gelatin as a delivery vehicle for the controlled release of bioactive molecules. *Journal of Controlled Release* 109, 256-274.
268. Yuan,F., Chen,Y., Dellian,M., Safabakhsh,N., Ferrara,N., and Jain,R.K. (1996). Time-dependent vascular regression and permeability changes in established human tumor xenografts induced by an anti-vascular endothelial growth factor vascular permeability factor antibody. *Proceedings of the National Academy of Sciences of the United States of America* 93, 14765-14770.
269. Zhu,Y.B., Gao,C.Y., Liu,Y.X., and Shen,J.C. (2004). Endothelial cell functions in vitro cultured on poly(L-lactic acid) membranes modified with different methods. *Journal of Biomedical Materials Research Part A* 69A, 436-443.
270. Ziegler,T., Bouzourene,K., Harrison,V.J., Brunner,H.R., and Hayoz,D. (1998). Influence of oscillatory and unidirectional flow environments on the expression of endothelin and nitric oxide synthase in cultured endothelial cells. *Arteriosclerosis Thrombosis and Vascular Biology* 18, 686-692.
271. Zisch,A.H., Zeisberger,S.M., Ehrbar,M., Djonov,V., Weber,C.C., Ziemiecki,A., Pasquale,E.B., and Hubbell,J.A. (2004). Engineered fibrin matrices for functional display of cell membrane-bound growth factor-like activities: Study of angiogenic signaling by ephrin-B2. *Biomaterials* 25, 3245-3257.

Appendix A: MATLAB® m.files

```

1 Appendix A1: Program Used to Measure Cell Axes and Cell Area
2
3 % -----
4 % |This is used to calculate the long and short axis for cells and exact
5 % |areas for cells in tissue culture or the bioassay chamber
6 % |Make sure that this program is in the same directory of the images that
7 % |are being analyzed
8 % |Input is the file name and the magnification of the image
9 % |There are some questions during the course of the program
10 % |Also there are some pauses and some info is displayed
11 % |Therefore, beware of the command line for any help if you get stuck
12 % |This program needs some user-interface and make sure you understand what
13 % |is being asked before you use the program
14 % |Output is data.txt with first columns as follows:
15 % |1: Quad number 2: cell number, 3: long axis, 4: short axis, 5: ratio
16 % |short/long, 6: area, 7: mag, 8: approx. perimeter area
17 % |Second output is area.txt which has the exact areas for the cells
18 % |First thing is to rename the txt file before analyzing a second image
19 % |cellcounting Version 1
20 % |Programmed by David A. Rubenstein, May 2006, for Dr. Molly Frame
21 % |cellcounting and all modifications are only to be used by the Frame
22 % |laboratory and D. Rubenstein unless permission is granted otherwise by
23 % |D. Rubenstein or M. Frame
24 % -----
25
26 % input for the file that you want to analyze
27 A = input('What is the name of the file you want to analyze? (input with single
28 quotes) ');
29 % A is the file name
30
31 % Ask for magnification of image in order to convert pixel to micron
32 mag=input('What is the magnification of the image? ');
33
34 % reads the file as an image
35 B = imread(A);
36 % B is now the color image that MATLAB can work with
37
38 %Sets the image to a binary image so that we can work with it
39 level = graythresh(B); %thresholds the image
40 bw = im2bw(B,level); %converts to black and white for cell counting
41 bw2 = rgb2gray(B); %converts to gray with that threshold for axis measurement
42 figure, imshow(bw2) %shows the image
43 % now bw2 is the image to work with
44
45 % asks if you want to equilibrate the image and performs the equilibration
46 C = input('Do you want to contrast the image? (1 for yes, 2 for no) ');

```

```

47 disp('Contrast the image and then file-->print to figure and then hit enter')
48 if C==1
49     imtool(bw2);
50     pause
51     imtool close all
52     saveas(gcf, 'fig.jpg')
53 else
54     saveas(gcf, 'fig.jpg')
55 end
56
57 E=imread('fig.jpg');
58 a = size(E);
59 G=zeros(a(1),a(2));
60 for i=1:a(1)
61     for j=1:a(2)
62         if E(i,j)>45
63             G(i,j)=255;
64         else
65             G(i,j)=0;
66         end
67     end
68 end
69 figure, imshow(G)
70 quad=a(1)*a(2)/4;
71 length1=sqrt(0.3*quad);
72 xlength=a(2)/2-length1;
73 ylength=a(1)/2-length1;
74 % asks if the new image is ok and continues if is
75 D = input('Is the contrasted image ok? (1 for yes, 2 for no) ');
76 if D==1
77     % Determines the number of cells in the image
78     % Saved as num
79     [labeled, num] = bwlabel(bw,8); %8 sets the size of objects counted
80     disp(num)
81
82     hold;
83     %Randomizes the grid for choosing cells
84     for i=1:4
85         rx=rand;
86         ry=rand;
87         x1=rand*xlength;
88         y1=rand*ylength;
89         if i==1
90             plot([x1,x1+length1,x1+length1,x1,x1],[y1,y1,y1+length1,y1+length1,y1],'g')
91         elseif i==2

```

```

92
93 plot([x1+a(2)/2,x1+a(2)/2+length1,x1+a(2)/2+length1,x1+a(2)/2,x1+a(2)/2],[y1,y1,
94 y1+length1,y1+length1,y1],'g')
95     elseif i==3
96
97 plot([x1,x1+length1,x1+length1,x1,x1],[y1+a(1)/2,y1+a(1)/2,y1+a(1)/2+length1,y1
98 +a(1)/2+length1,y1+a(1)/2],'g')
99     else
100
101 plot([x1+a(2)/2,x1+a(2)/2+length1,x1+a(2)/2+length1,x1+a(2)/2,x1+a(2)/2],[y1+a(1
102 )/2,y1+a(1)/2,y1+a(1)/2+length1,y1+a(1)/2+length1,y1+a(1)/2],'g')
103     end
104 end
105
106 %Sets the grid on the image
107 plot([a(2)/2,a(2)/2],[0,a(1)],'r',[0,a(2)],[a(1)/2,a(1)/2],'r')
108 text(-100,10,'Quad 1')
109 text(a(2)+30,10,'Quad 2')
110 text(10,a(1)+40,'Quad 3')
111 text(a(2)+30,a(1)+40,'Quad 4')
112 title('Only choose cells within the green boxes')
113
114 % Program to allow the x and y coordinates of each image to be calculated
115 % Xi and Yi are the points of interest
116 [X,Y,bw3,IDX,xi,Yi]=bwselect;
117
118 %Combines the X and Y coordinates into one matrix
119 coor=[xi,Yi];
120
121 % Code to determine which quadrant the cell lies within
122 l=length(coor);
123
124 % Makes a new matrix, coor1, which will calculate the difference between
125 % the x and y coordinates (column 1 and 2 respectively for each axis)
126 % Also the third row of the coor1 matrix is the linear distance between
127 % consecutive points (ie the axes)
128 coor1=zeros(l/2,4);
129 for j=1:l/2
130     coor1(j,1)=abs(coor(2*j-1,1)-coor(2*j,1));
131     coor1(j,2)=abs(coor(2*j-1,2)-coor(2*j,2));
132     coor1(j,3)=sqrt(coor1(j,1)^2+coor1(j,2)^2);
133 end
134
135 % Converts the distances from coor1 column 3 into microns and inputs it
136 % into column 4 of coor1
137 if mag==10

```

```

138     coor1(:,4)=coor1(:,3)*100/(a(2)*93/1392);
139 elseif mag==20
140     coor1(:,4)=coor1(:,3)*100/(a(2)*93*2/1392);
141 else
142     coor1(:,4)=coor1(:,3)*100/(a(2)*93*4/1392);
143 end
144
145 p=length(coor1);
146 area=zeros(p/2,8);
147
148 % Code to determine which quadrant the cell lies within
149
150 ll=l/4;
151 for m=1:ll
152     g=[coor(4*m-3,1),coor(4*m-3,2)];
153     if g(1)<= a(2)/2
154         if g(2)<= a(1)/2
155             area(m,1)=1;
156         else
157             area(m,1)=3;
158         end
159     else
160         if g(2)<= a(1)/2
161             area(m,1)=2;
162         else
163             area(m,1)=4;
164         end
165     end
166 end
167
168 % Makes a matrix that will calculate the area and tell if circular or
169 % elongated and fills in the values
170
171 for k=1:p/2
172     area(k,2)=k;
173     h=0;
174     if coor1(k*2-1,4)>coor1(k*2,4)
175         area(k,3)=coor1(k*2-1,4);
176         area(k,4)=coor1(k*2,4);
177         area(k,5)=coor1(k*2,4)/coor1(k*2-1,4);
178         area(k,7)=mag;
179         h=1;
180     else
181         area(k,3)=coor1(k*2,4);
182         area(k,4)=coor1(k*2-1,4);
183         area(k,5)=coor1(k*2-1,4)/coor1(k*2,4);

```

```

184     area(k,7)=mag;
185 end
186
187 if h==1
188     if area(k,5)>0.8
189         area(k,6)= pi*(coor1(k*2-1,4)/2)^2;
190     else
191         area(k,6)=(coor1(k*2,4))*(coor1(k*2-1,4));
192     end
193 else
194     if area(k,5)>0.8
195         area(k,6)=pi*(coor1(k*2,4)/2)^2;
196     else
197         area(k,6)=(coor1(k*2,4))*(coor1(k*2-1,4));
198     end
199 end
200 end
201 % export the file for excel
202
203
204 %This part of the program is used to calculate the exact area of each cell
205 %in the image.
206 %Inputs are: the same from the above program
207 %Outputs are: the areas of the cells
208 %Programmed by David A. Rubenstein May, 2006 for Dr. Mary D. Frame
209
210 figure, imshow(bw3)
211
212 %calculates the boundaries on the image
213 bound=bwboundaries(bw3);
214 hold
215
216 %plots the boundary and calculates the area of each object
217 lb=length(bound);
218 uuuuu=0; %dummy for area
219 for nn=1:lb
220     bb=bound(Baker et al., 2006);
221     lbbb=length(bb);
222     if (lbbb>50) && (lbbb<10000)
223         uuuuu=uuuuu+1;
224     end
225 end
226
227 w=0; %dummy
228
229 for n=1:lb

```

```

230 b=bound(n); %takes the boundary information and makes a lbbx2 vector
231 % the x info is in the 2nd column and the y info is in the 1st
232 b1=bound(n);
233 xmin=min(b(:,2));
234 ymin=min(b(:,1));
235 lbb=length(b);
236 %sets a limit on how large or small the cell can be
237 if (lbb>50) && (lbb<10000)
238     w=w+1;
239     %moves the cells so that when calculating the area they are along the
240     %x and y axis
241     b(:,2)=b(:,2)-xmin;
242     b(:,1)=b(:,1)-ymin;
243     xmax=max(b(:,2));
244     ymax=max(b(:,1));
245
246     %creates 4 dummy variables
247     u=0;
248     uu=0;
249     tot=0;
250     tot2=0;
251
252     %calculates the average y-value at the xmin and xmax
253     for nn=1:lbb
254         if b(nn,2)==0
255             u=u+1;
256             tot=b(nn,1)+tot;
257         end
258         if b(nn,2)==xmax
259             uu=uu+1;
260             tot2=tot2+b(nn,1);
261         end
262     end
263     avgymn=tot/u;
264     avgymax=tot2/uu;
265
266     %recreates the dummy variables
267     v=0;
268     vv=0;
269     tot3=0;
270     tot4=0;
271
272     %calculates the average x-value at the xmin and xmax
273     for nnn=1:lbb
274         if b(nnn,1)==0
275             v=v+1;

```

```

276         tot3=b(nnnn,2)+tot3;
277     end
278     if b(nnnn,1)==ymax
279         vv=vv+1;
280         tot4=tot4+b(nnnn,2);
281     end
282 end
283 avgxmin=tot3/v;
284 avgxmax=tot4/vv;
285
286 %sorts the b vector into an upper and lower function
287 uuu=1; %dummy upper
288 uuuu=1; %dummy lower
289 for nnn=1:lbb
290     if b(nnn,2)==xmin
291         if b(nnn,1)>avgymn
292             upper(uuu,:)=b(nnn,:);
293             uuu=uuu+1;
294         else
295             lower(uuuu,:)=b(nnn,:);
296             uuuu=uuuu+1;
297         end
298     elseif b(nnn,2)==xmax
299         if b(nnn,1)>avgymn
300             upper(uuu,:)=b(nnn,:);
301             uuu=uuu+1;
302         else
303             lower(uuuu,:)=b(nnn,:);
304             uuuu=uuuu+1;
305         end
306     else
307         if b(nnn,1)>avgymn
308             upper(uuu,:)=b(nnn,:);
309             uuu=uuu+1;
310         else
311             lower(uuuu,:)=b(nnn,:);
312             uuuu=uuuu+1;
313         end
314     end
315 end
316
317 %sorts the upper and lower vectors into 2 vectors which contain
318 %information about the 4 quadrants of the area
319 lbbb=length(upper);
320 lbbbb=length(lower);
321 uuu=1; %dummy for upper2

```

```

322     uuuu=1; %dummy for upper1
323
324     for nnnnn=1:lbbb
325         if upper(nnnnn,2)>avgxmax
326             upper2(uuu,:)=upper(nnnnn,:);
327             uuu=uuu+1;
328         else
329             upper1(uuuu,:)=upper(nnnnn,:);
330             uuuu=uuuu+1;
331         end
332     end
333
334     uuu=1; %dummy for lower1
335     uuuu=1; %dummy for lower2
336
337     for nnnnnn=1:lbbbb
338         if lower(nnnnnn,2)<avgxmin
339             lower1(uuu,:)=lower(nnnnnn,:);
340             uuu=uuu+1;
341         else
342             lower2(uuuu,:)=lower(nnnnnn,:);
343             uuuu=uuuu+1;
344         end
345     end
346
347     %sort the upper 1/2 and lower 1/2 vectors so that we can take
348     %the integral of each vector
349     upper1=sortrows(upper1,[2,1]);
350     upper2=sortrows(upper2,[2,-1]);
351     lower1=sortrows(lower1,[2,-1]);
352     lower2=sortrows(lower2,[2,1]);
353
354     %get the lengths of the upper 1/2 and lower 1/2 vectors
355     lup1=length(upper1);
356     lup2=length(upper2);
357     llo1=length(lower1);
358     llo2=length(lower2);
359
360     %Get the remainders of division by 5 and then do the division
361     %by 5
362     lup1r=rem(lup1,5);
363     lup2r=rem(lup2,5);
364     llo1r=rem(llo1,5);
365     llo2r=rem(llo2,5);
366     lup1=floor(lup1/5);
367     lup2=floor(lup2/5);

```

```

368     llo1=floor(llo1/5);
369     llo2=floor(llo2/5);
370
371     %dummy variables for the integral
372     intup1=0;
373     intup2=0;
374     intlo1=0;
375     intlo2=0;
376
377     %integer for upper 1
378     if lup1r==0
379         for pp=1:lup1
380             intup1=(2/45)*(upper1(pp*5,2)-upper1(pp*5-
381 4,2))*(7*upper1(pp*5,1)+7*upper1(pp*5-4,1)+32*upper1(pp*5-
382 1,1)+32*upper1(pp*5-3,1)+12*upper1(pp*5-2,1))+intup1;
383         end
384     elseif lup1r==1
385         for pp2=1:lup1-1
386             intup1=(2/45)*(upper1(pp2*5,2)-upper1(pp2*5-
387 4,2))*(7*upper1(pp2*5,1)+7*upper1(pp2*5-4,1)+32*upper1(pp2*5-
388 1,1)+32*upper1(pp2*5-3,1)+12*upper1(pp2*5-2,1))+intup1;
389         end
390         intup1=intup1+(1/3)*(upper1(lup1*5-2,2)-upper1(lup1*5-
391 4,2))*(upper1(lup1*5-4,1)+upper1(lup1*5-2,1)+4*upper1(lup1*5-
392 3,1)))+(1/3)*(upper1(lup1*5+1,2)-upper1(lup1*5-1,2))*(upper1(lup1*5-
393 1,1)+upper1(lup1*5+1,1)+4*upper1(lup1*5,1));
394     elseif lup1r==2
395         for pp3=1:lup1
396             intup1=(2/45)*(upper1(pp3*5,2)-upper1(pp3*5-
397 4,2))*(7*upper1(pp3*5,1)+7*upper1(pp3*5-4,1)+32*upper1(pp3*5-
398 1,1)+32*upper1(pp3*5-3,1)+12*upper1(pp3*5-2,1))+intup1;
399         end
400         intup1=intup1+0.5*(upper1(lup1*5+2,2)-
401 upper1(lup1*5+1,2))*(upper1(lup1*5+1,1)+upper1(lup1*5+2,1));
402     elseif lup1r==3
403         for pp4=1:lup1
404             intup1=(2/45)*(upper1(pp4*5,2)-upper1(pp4*5-
405 4,2))*(7*upper1(pp4*5,1)+7*upper1(pp4*5-4,1)+32*upper1(pp4*5-
406 1,1)+32*upper1(pp4*5-3,1)+12*upper1(pp4*5-2,1))+intup1;
407         end
408         intup1=intup1+(1/3)*(upper1(lup1*5+3,2)-
409 upper1(lup1*5+1,2))*(upper1(lup1*5+1,1)+4*upper1(lup1*5+2,1)+upper1(lup1*5+
410 3,1));
411     else
412         for pp5=1:lup1

```

```

413         intup1=(2/45)*(upper1(pp5*5,2)-upper1(pp5*5-
414 4,2))*(7*upper1(pp5*5,1)+7*upper1(pp5*5-4,1)+32*upper1(pp5*5-
415 1,1)+32*upper1(pp5*5-3,1)+12*upper1(pp5*5-2,1))+intup1;
416         end
417         intup1=intup1+(3/8)*(upper1(lup1*5+4,2)-
418 upper1(lup1*5+1,2))*(upper1(lup1*5+1,1)+upper1(lup1*5+4,1)+3*upper1(lup1*5+
419 2,1)+3*upper1(lup1*5+3,1));
420         end
421
422         %integer for upper 2
423         if lup2r==0
424             for pp=1:lup2
425                 intup2=(2/45)*(upper2(pp*5,2)-upper2(pp*5-
426 4,2))*(7*upper2(pp*5,1)+7*upper2(pp*5-4,1)+32*upper2(pp*5-
427 1,1)+32*upper2(pp*5-3,1)+12*upper2(pp*5-2,1))+intup2;
428                 end
429             elseif lup2r==1
430                 for pp2=1:lup2-1
431                     intup2=(2/45)*(upper2(pp2*5,2)-upper2(pp2*5-
432 4,2))*(7*upper2(pp2*5,1)+7*upper2(pp2*5-4,1)+32*upper2(pp2*5-
433 1,1)+32*upper2(pp2*5-3,1)+12*upper2(pp2*5-2,1))+intup2;
434                     end
435                     intup2=intup2+(1/3)*(upper2(lup2*5-2,2)-upper2(lup2*5-
436 4,2))*(upper2(lup2*5-4,1)+upper2(lup2*5-2,1)+4*upper2(lup2*5-
437 3,1)))+(1/3)*(upper2(lup2*5+1,2)-upper2(lup2*5-1,2))*(upper2(lup2*5-
438 1,1)+upper2(lup2*5+1,1)+4*upper2(lup2*5,1));
439                 elseif lup2r==2
440                     for pp3=1:lup2
441                         intup2=(2/45)*(upper2(pp3*5,2)-upper2(pp3*5-
442 4,2))*(7*upper2(pp3*5,1)+7*upper2(pp3*5-4,1)+32*upper2(pp3*5-
443 1,1)+32*upper2(pp3*5-3,1)+12*upper2(pp3*5-2,1))+intup2;
444                         end
445                         intup2=intup2+0.5*(upper2(lup2*5+2,2)-
446 upper2(lup2*5+1,2))*(upper2(lup2*5+1,1)+upper2(lup2*5+2,1));
447                     elseif lup2r==3
448                         for pp4=1:lup2
449                             intup2=(2/45)*(upper2(pp4*5,2)-upper2(pp4*5-
450 4,2))*(7*upper2(pp4*5,1)+7*upper2(pp4*5-4,1)+32*upper2(pp4*5-
451 1,1)+32*upper2(pp4*5-3,1)+12*upper2(pp4*5-2,1))+intup2;
452                             end
453                             intup2=intup2+(1/3)*(upper2(lup2*5+3,2)-
454 upper2(lup2*5+1,2))*(upper2(lup2*5+1,1)+4*upper2(lup2*5+2,1)+upper2(lup2*5+
455 3,1));
456                         else
457                             for pp5=1:lup2

```

```

458         intup2=(2/45)*(upper2(pp5*5,2)-upper2(pp5*5-
459 4,2))*(7*upper2(pp5*5,1)+7*upper2(pp5*5-4,1)+32*upper2(pp5*5-
460 1,1)+32*upper2(pp5*5-3,1)+12*upper2(pp5*5-2,1))+intup2;
461         end
462         intup2=intup2+(3/8)*(upper2(lup2*5+4,2)-
463 upper2(lup2*5+1,2))*(upper2(lup2*5+1,1)+upper2(lup2*5+4,1)+3*upper2(lup2*5+
464 2,1)+3*upper2(lup2*5+3,1));
465         end
466
467         %integer for lower 1
468         if llo1r==0
469             for pp=1:llo1
470                 intlo1=(2/45)*(lower1(pp*5,2)-lower1(pp*5-
471 4,2))*(7*lower1(pp*5,1)+7*lower1(pp*5-4,1)+32*lower1(pp*5-
472 1,1)+32*lower1(pp*5-3,1)+12*lower1(pp*5-2,1))+intlo1;
473                 end
474             elseif llo1r==1
475                 for pp2=1:llo1-1
476                     intlo1=(2/45)*(lower1(pp2*5,2)-lower1(pp2*5-
477 4,2))*(7*lower1(pp2*5,1)+7*lower1(pp2*5-4,1)+32*lower1(pp2*5-
478 1,1)+32*lower1(pp2*5-3,1)+12*lower1(pp2*5-2,1))+intlo1;
479                     end
480                 intlo1=intlo1+(1/3)*(lower1(llo1*5-2,2)-lower1(llo1*5-
481 4,2))*(lower1(llo1*5-4,1)+lower1(llo1*5-2,1)+4*lower1(llo1*5-
482 3,1))+1/3*(lower1(llo1*5+1,2)-lower1(llo1*5-1,2))*(lower1(llo1*5-
483 1,1)+lower1(llo1*5+1,1)+4*lower1(llo1*5,1));
484             elseif llo1r==2
485                 for pp3=1:llo1
486                     intlo1=(2/45)*(lower1(pp3*5,2)-lower1(pp3*5-
487 4,2))*(7*lower1(pp3*5,1)+7*lower1(pp3*5-4,1)+32*lower1(pp3*5-
488 1,1)+32*lower1(pp3*5-3,1)+12*lower1(pp3*5-2,1))+intlo1;
489                     end
490                 intlo1=intlo1+0.5*(lower1(llo1*5+2,2)-
491 lower1(llo1*5+1,2))*(lower1(llo1*5+1,1)+lower1(llo1*5+2,1));
492             elseif llo1r==3
493                 for pp4=1:llo1
494                     intlo1=(2/45)*(lower1(pp4*5,2)-lower1(pp4*5-
495 4,2))*(7*lower1(pp4*5,1)+7*lower1(pp4*5-4,1)+32*lower1(pp4*5-
496 1,1)+32*lower1(pp4*5-3,1)+12*lower1(pp4*5-2,1))+intlo1;
497                     end
498                 intlo1=intlo1+(1/3)*(lower1(llo1*5+3,2)-
499 lower1(llo1*5+1,2))*(lower1(llo1*5+1,1)+4*lower1(llo1*5+2,1)+lower1(llo1*5+3,
500 1));
501             else
502                 for pp5=1:llo1

```

```

503         intlo1=(2/45)*(lower1(pp5*5,2)-lower1(pp5*5-
504 4,2))*(7*lower1(pp5*5,1)+7*lower1(pp5*5-4,1)+32*lower1(pp5*5-
505 1,1)+32*lower1(pp5*5-3,1)+12*lower1(pp5*5-2,1))+intlo1;
506         end
507         intlo1=intlo1+(3/8)*(lower1(llo1*5+4,2)-
508 lower1(llo1*5+1,2))*(lower1(llo1*5+1,1)+lower1(llo1*5+4,1)+3*lower1(llo1*5+2,
509 1)+3*lower1(llo1*5+3,1));
510         end
511
512         %integer for lower 2
513         if llo2r==0
514             for pp=1:llo2
515                 intlo2=(2/45)*(lower2(pp*5,2)-lower2(pp*5-
516 4,2))*(7*lower2(pp*5,1)+7*lower2(pp*5-4,1)+32*lower2(pp*5-
517 1,1)+32*lower2(pp*5-3,1)+12*lower2(pp*5-2,1))+intlo2;
518                 end
519             elseif llo2r==1
520                 for pp2=1:llo2-1
521                     intlo2=(2/45)*(lower2(pp2*5,2)-lower2(pp2*5-
522 4,2))*(7*lower2(pp2*5,1)+7*lower2(pp2*5-4,1)+32*lower2(pp2*5-
523 1,1)+32*lower2(pp2*5-3,1)+12*lower2(pp2*5-2,1))+intlo2;
524                     end
525                 intlo2=intlo2+(1/3)*(lower2(llo2*5-2,2)-lower2(llo2*5-
526 4,2))*(lower2(llo2*5-4,1)+lower2(llo2*5-2,1)+4*lower2(llo2*5-
527 3,1))+(1/3)*(lower2(llo2*5+1,2)-lower2(llo2*5-1,2))*(lower2(llo2*5-
528 1,1)+lower2(llo2*5+1,1)+4*lower2(llo2*5,1));
529             elseif llo2r==2
530                 for pp3=1:llo2
531                     intlo2=(2/45)*(lower2(pp3*5,2)-lower2(pp3*5-
532 4,2))*(7*lower2(pp3*5,1)+7*lower2(pp3*5-4,1)+32*lower2(pp3*5-
533 1,1)+32*lower2(pp3*5-3,1)+12*lower2(pp3*5-2,1))+intlo2;
534                     end
535                 intlo2=intlo2+0.5*(lower2(llo2*5+2,2)-
536 lower2(llo2*5+1,2))*(lower2(llo2*5+1,1)+lower2(llo2*5+2,1));
537             elseif llo2r==3
538                 for pp4=1:llo2
539                     intlo2=(2/45)*(lower2(pp4*5,2)-lower2(pp4*5-
540 4,2))*(7*lower2(pp4*5,1)+7*lower2(pp4*5-4,1)+32*lower2(pp4*5-
541 1,1)+32*lower2(pp4*5-3,1)+12*lower2(pp4*5-2,1))+intlo2;
542                     end
543                 intlo2=intlo2+(1/3)*(lower2(llo2*5+3,2)-
544 lower2(llo2*5+1,2))*(lower2(llo2*5+1,1)+4*lower2(llo2*5+2,1)+lower2(llo2*5+3,
545 1));
546             else
547                 for pp5=1:llo2

```

```

548         intlo2=(2/45)*(lower2(pp5*5,2)-lower2(pp5*5-
549 4,2))*(7*lower2(pp5*5,1)+7*lower2(pp5*5-4,1)+32*lower2(pp5*5-
550 1,1)+32*lower2(pp5*5-3,1)+12*lower2(pp5*5-2,1))+intlo2;
551         end
552         intlo2=intlo2+(3/8)*(lower2(llo2*5+4,2)-
553 lower2(llo2*5+1,2))*(lower2(llo2*5+1,1)+lower2(llo2*5+4,1)+3*lower2(llo2*5+2,
554 1)+3*lower2(llo2*5+3,1));
555         end
556         integer=intup1+intup2-intlo1-intlo2;
557
558         %change the integer from pixels to microns
559         if mag==10
560             area(w,8)=abs(integer*(100/(a(2)*93/1392))^2);
561         elseif mag==20
562             area(w,8)=abs(integer*(100/(a(2)*93*2/1392))^2);
563         else
564             area(w,8)=abs(integer*(100/(a(2)*93*4/1392))^2);
565         end
566     else
567         w=w+0;
568     end
569     %plots the edges
570     plot(b1(:,2),b1(:,1),'g','LineWidth',2)
571 end
572
573 save data.txt area -ASCII
574 clear A B C D E F G IDX X Xi Y Yi a area area1 avgxmax avgxmin
575 clear avgymax avgymmin b b1 bb bound bw bw2 bw3 bw4 bw5
576 clear coor coor1 g h i integer intlo1 intlo2 intup1 intup2
577 clear j k l ll labeled lb lbb lbbb lbbbb length1 level level_1 llo1
578 clear llo1r llo2 llo2r lower lower1 lower2 lup1 lup1r lup2
579 clear lup2r m mag n nn nnn nnnn nnnnn nnnnnn num quad p pp pp2 pp3
580 clear pp4 pp5 rx ry t tot tot2 tot3 tot4 u upper upper1
581 clear upper2 uu uuu uuuu uuuuu v vv w x1 xmax xmin y1 ymax ymin
582 clear xlength ylength
583 close(1,2,3)
584
585 else
586     ...
587 end

```

```

1  Appendix A2: Program Used to Acquire Video Images
2
3  % -----
4  % |This program is used to take images during perfusion and make a video
5  % |file for the acquired images
6  % |Add more here
7  % |Programmed by David A. Rubenstein, May 2006, for Dr. Molly Frame
8  % |imageacq and all modifications are only to be used by the Frame
9  % |laboratory and D. Rubenstein unless permission is granted otherwise by
10 % |D. Rubenstein or M. Frame
11 % -----
12 % Initates a video input for our Retiga Camera
13 vid = videoinput('qimaging',1);
14
15 % Sets the memory allocation to infinity
16 imaqmem(Inf);
17
18 % Asks questions in order to determine camera settings
19 disp('Answer this question with hours!!!')
20 hr = input('What is the length of time to take images for? ');
21 disp('Answer this question in seconds!!!')
22 exp = input('What is the exposure time you want? ');
23 disp('Answer this question in minutes!!!')
24 often = input('How often do you want a picture taken? ');
25 set(vid.source,'Exposure',exp);
26
27 preview(vid)
28
29 % This loop sets the exposure be careful not to set the exposure to high
30 disp('1 is for yes, 2 is for no')
31 q = input('Is the exposure ok? ');
32 while q==2
33     closepreview(vid)
34     exp = input('What is the exposure time you want? ');
35     set(vid.source,'Exposure',exp);
36     preview(vid)
37     disp('1 is for yes, 2 is for no')
38     q = input('Is the exposure ok? ');
39 end
40 closepreview(vid)
41
42 % Calculates the FrameGrabInterval and the trigger internal
43 FPT=(hr*360)/exp;
44 FGI=(often*6)/exp;
45 TR=(hr*60)/often;
46

```

```

47 % Opens a file to store the data that can be read later
48 %my_log = 'mydatalog.avi';
49 aviobj = avifile('mydatalog.avi');
50
51 % Sets various parameters of the acquisition
52 set(vid, 'FrameGrabInterval', FGI)
53 set(vid, 'FramesPerTrigger',FPT)
54 set(vid, 'TriggerRepeat', TR)
55 set(vid, 'Timeout', 6000)
56
57 % Starts the video recording and waits until it has finished
58 start(vid)
59 wait(vid)
60
61 % Makes the movie file and exports it to the working directory
62 g=get(vid, 'FramesAvailable');
63 for i=1:g
64     frame=getdata(vid,1);
65     a=min(frame);
66     a=min(a);
67     b=max(frame);
68     b=max(b);
69     imshow(frame,[a b])
70     [data, time, meta] = getdata(vid,1,'double');
71     stamp = int2str(meta(1).AbsTime);
72     text(20,20,stamp, 'FontSize', 18)
73     frame=getframe(gca);
74     aviobj=addframe(aviobj,frame);
75 end
76
77 aviobj = close(aviobj);
78 close all
79 delete(vid)
80 clear FGI FPT TR a b exp g hr i often q vid
81 clear frame aviobj data time meta stamp

```